Malaysian Journal of Analytical Sciences, Vol.9, No. 3 (2005)

TABLE OF CONTENTS

Malaysian Journal of Analytical Sciences, Vol. 9, No. 3 (2005): 388 - 395

KAJIAN KUALITI AIR 'ALUR ILMU' DI KAMPUS UKM, BANGI: KE ARAH PENDEKATAN PENGURUSAN SUMBER AIR BERSEPADU

Mazlin Bin Mokhtar*, Chee Fong Hoe,
Chong Wai Leng, Ooi Yih Yong & Tan Bee Heong

**Institut Alam Sekitar dan Pembangunan (LESTARI), &*
Fakulti Sains dan Teknologi, Universiti Kebangsaan Malaysia
43600 UKM BANGI, Selangor Darul Ehsan, Malaysia

Abstrak. Kajian kualiti air sistem saliran 'Alur Ilmu' di dalam Kampus Universiti Kebangsaan Malaysia (UKM) telah dijalankan dari September 1999 hingga April 2004. Kajian ini melibatkan lima buah stesen, iaitu S1, S2, S3, S4 dan S5, yang terletak di hulu ke hilir saliran tersebut. 'Alur Ilmu' adalah saluran yang mengalirkan air hujan dan air bawah tanah dari kawasan sekitaran lingkungan utama di dalam kampus UKM, Bangi. Saliran ini bermula di kawasan berbukit di hadapan bangunan Program Sains Nuklear, dan mengalir bersebelahan dengan bangunan Kolej Ungku Omar, PUSANIKA, Perpustakaan Tun Sri Lanang, Fakulti Sains dan Teknologi, Fakulti Ekonomi dan Perniagaan, Fakulti Sains Sosial dan Kemanusiaan, Fakulti Pengajian Islam dan akhirnya diluahkan ke Sungai Langat. Objektif kajian ini adalah untuk menentukan 21 parameter kualiti air dan membandingkannya dengan nilai yang disarankan oleh Piawai Kualiti Air Kebangsaan Interim Malaysia (INWQS), dan dikelaskan menurut Indeks Kualiti Air (IKA) Malaysia. Parameter yang telah dikaji adalah DO, BOD, TDS, TSS, COD, O&G, ammonia, warna, fosfat, suhu, pH, kekonduksian, nitrat, sulfat, koliform jumlah, koliform najis, Pb, Cu, Fe, Mn dan Cd. Kaedah persampelan dan analisis dilakukan mengikut garis panduan yang dicadangkan oleh *American Public Health Association* (APHA). Hasil kajian menunjukkan bahawa parameter yang telah melangkau Kelas II (INWQS) adalah Pb, sulfat, nitrat, COD, koliform jumlah, koliform najis, Fe, dan Mn.

Kata kunci: kualiti air, Alur Ilmu, UKM, pengurusan, bersepadu

Abstract. Water quality study of the storm water channel called 'Alur Ilmu' within the campus of Universiti Kebangsaan Malaysia (UKM) in Bangi, was carried out from September 1999 until April 2004. Measurements and samples were collected at five stations, namely S1, S2, S3, S4 and S5. This is a channel for rain, storm and ground waters flowing towards the main discharge point which meets the Langat River. Alur Ilmu originated from a hilly, jungle area in front of the Nuclear Science Building, and flows nearby the buildings and compounds of the Ungku Omar Residential College, PUSANIKA, Tun Sri Lanang Library, Faculty of Science and Technology, Faculty of Economics and Business, Faculty of Social Sciences and Humanities, Faculty of Islamic Studies and finally ends up in Langat River. Measurements of 21 water quality parameters were performed and compared with values of the Interim National Water Quality Standards (INWQS). The Water Quality Index (WQI) values based on six of the parameters were calculated. The 21 parameters were DO, BOD, TDS, TSS, COD, O&G, ammonia, colour, phosphate, temperature, pH, conductivity, nitrate, sulphate, total and faecal coliforms, Pb, Cu, Fe, Mn and Cd. Methods of sampling and analyses were based on recommendations by the *American Public Health Association* (APHA). Overall, the water quality parameters which had exceeded the Class II (INWQS) sub values were Pb, sulphate, nitrate, COD, total and faecal coliforms, Fe and Mn.

Keywords: water quality, Alur Ilmu, UKM, management, integrated

Pengenalan

Pendekatan yang disarankan untuk pengurusan kualiti air adalah Pengurusan Sumber Air Bersepadu (Integrated Water Resources Management, IWRM). Konsep IWRM merangkumi aspek pengurusan dan kerjasama yang diperlukan daripada pelbagai pihak berkepentingan yang terdiri daripada sector kerajaan, swasta, academia, penyelidik, NGO dan masyarakat umum dalam menguruskan isu sumber air dalam sesebuah kawasan geografi atau sempadan. Skala pada mana konsep IWRM boleh dilaksanakan juga pelbagai iaitu dari peringkat kebangsaan hinggalah ke peringkat tempatan. Aspek kewangan, sumber manusia, infrastruktur, kebolehan dan keupayaan adalah penting dalam menjayakan konsep IWRM dalam pengurusan sumber air. Sumber air tanah dan permukaan dan semua jenis air juga perlu diambil kira. Pada skala dalam sesebuah universiti konsep IWRM seharusnya melibatkan pihak pengurusan tertinggi, pertengahan, sokongan dan masyarakat umum kampus seperti pelajar dan penghuni lain. Proses penjagaan kualiti air juga sama pentingnya dengan aspek menjamin kuantiti sumber air yang mencukupi untuk kegunaan para penghuni kampus pada setiap masa, untuk jangka masa pendek dan

panjang. Konsep IWRM meletakkan kepentingan manusia di tengah-tengah dan kesihatan ekosistem sekitaran manusia juga perlu dijaga untuk menjamin kelestarian penggunaan ekosistem tersebut sebagai sumber perkhidmatan dan hasilan yang berkaitan. Kajian ini telah dilakukan berdasarkan kesedaran konsep IWRM untuk menjaga kualiti Alur Ilmu untuk tujuan asasnya, juga untuk tujuan nilai astetiknya sejajar dengan tema 'Universiti Dalam Taman'.

'Alur Ilmu' adalah suatu saluran air yang telah dibina dengan simen konkrit berasaskan saliran semulajadi sejak pembinaan kompleks bangunan kampus UKM Bangi pada awal tahun 1970-an, dengan tujuan untuk mengalirkan air hujan dan air tanah dari kampus UKM Bangi dari lingkungan pertama ke Sungai Langat. Panjang alur ini adalah lebihkurang 1000 meter dan had aliran puratanya pada hari kering adalah lebihkurang 0.011 m/s. Air buangan dan luahan dari tandas dan makmal bangunan UKM adalah disalurkan ke dalam sistem saliran yang berasingan dan tidak bersambung dengan Alur Ilmu. Sistem air luahan kumbahan ini dialirkan ke kolam pengoksidaan kumbahan UKM untuk proses perawatan sebelum ia dialirkan ke Sungai Langat.

Air 'Alur Ilmu' kelihatan berpunca daripada kawasan bukit di hadapan bangunan Program Sains Nuklear. Air hujan dan air tanah ini mangalir melalui bangunan seperti Perpustakaan Tun Sri Lanang, PUSANIKA, Kolej Ungku Omar, Kolej Aminuddin Baki serta Fakulti di sekitar Alur Ilmu. Di samping itu, air larian permukaan sewaktu hujan dari jalanraya, tempat letak kereta, bumbung bangunan juga mengalir kedalamnya. Oleh kerana air di dalam saliran ini akhirnya akan dialirkan ke Sungai Langat, maka persampelan juga dijalankan untuk mengkaji kualiti air yang mengalir ke Sungai Langat.
Kajian ini telah dijalankan sejak 1999 oleh penyelidik peringkat tahun akhir program ijazah sarjanamuda sains dengan kepujian UKM di bawah penyeliaan Profesor Madya Dr Mazlin Mokhtar (Chong 1999; Tan 2003; Ooi 2003; dan Chee 2004).

Lokasi Kajian
Stesen-stesen persampelan ditetapkan di sepanjang 'Alur Ilmu' yang mengalir ke Sungai Langat iaitu S1, S2, S3, S4 dan S5. Chong (1999) telah melakukan kajian di dua stesen sahaja iaitu S1 dan S5. Ooi (2003) telah melakukan kajian di S5 sahaja, manakala Tan (2003) dan Chee (2004) melakukan persampelan di S1 hingga S5 di sepanjang 'Alur Ilmu'. Lokasi persampelan ditunjukkan dalam Rajah 1.

Hasil dan Perbincangan

Oksigen terlarut (DO)
Sepanjang tempoh kajian kepekatan DO bagi semua stesen berada pada julat 1.03 ± 0.03mg/L (Kelas IV) hingga 7.98 ± 1.81mg/L (Kelas I) dan purata pada 5.00mg/L (Kelas IIA). ANOVA menunjukkan tiada perbezaan DO yang beerti ($p>0.05$) di antara stesen-stesen kajian tetapi terdapat perbezaan antara hari kering dan hari hujan ($p<0.05$). Kandungan bahan organic dalam air yang tinggi boleh merendahkan kepekatan DO (Mazlin et al. 2001).

Ammonia (AN)
Kandungan ammonia-nitrogen pada tahun 1999 (S1 dan S5) berada dalam julat 0.12 ± 0.12mg/L (Kelas IIA) hingga 1.14 ± 0.5 mg/L (melebihi Kelas III). ANOVA menunjukkan tiada perbezaan antara stesen kajian dan antara hari kering dengan hari basah ($p>0.05$). Ammonia adalah hasil primer dalam penguraian bahan organik yang diluahkan oleh haiwan dan tumbuhan. Kepekatan ammonia yang tinggi boleh wujud dalam kumbahan dan bahan buangan hasil pertanian (T$_0$lgyessy 1993). Nitrat mungkin berasal dari baja yang diberikan kepada tumbuhan dalam kawasan taman berhampiran Alur Ilmu. Bakteria dan fungi yang terlibat dalam proses pereputan boleh meningkatkan kepekatan ammonia (Hammer 1986).

***Jumlah pepejal terampai* (TSS)**
Secara keseluruhannya purata TSS adalah 38.50 mg/L. ANOVA menunjukkan tiada perbezaan beerti ($p>0.05$) di antara stesen dan antara hari kering dan hujan. Kandungan TSS adalah relative lebih tinggi pada hari hujan disebabkan air hujan membawa air larian tanah ke dalam saliran tersebut.

Permintaan oksigen kimia (COD)

COD telah melebihi Kelas IIA INWQS untuk setiap stesen dari tahun 1999 ke 2004. Julat COD adalah 9.43 ± 9.17mg/L hingga 41.30 ± 4.35mg/L. ANOVA menunjukkan tiada perbezaan beerti di antara stesen dan antara hari kering dengan hari hujan.

Ferum (Fe)

Sepanjang tempoh kajian kandungan Fe di semua stesen berada dalam julat 1.34 ± 0.03 mg/L hingga 4.36 ± 0.05 mg/L (Kelas IV). ANOVA menunjukkan tiada perbezaan yang bererti di antara stesen dan antara hari kering dengan hari hujan. S3 adalah lokasi pemerangkap lumpur dan kandungan Fe di sini adalah relatif tinggi.

Mangan (Mn)

Sepanjang tempoh kajian kepekatan Mn berada dalam julat 0.07 ± 0.04 mg/L (Kelas IIA) hingga 0.23 ± 0.02 mg/L (Kelas IV). Nilai puratanya adalah 0.15 mg/L, melebihi nilai Kelas III. ANOVA menunjukkan tiada perbezaan bererti ($p>0.05$) di antara stesen dan antara hari kering dan hari hujan. Mangan pada lazimnya dijumpai bersama ferum.

Fosfat

Kepekatan Fosfat pada tahun 1999 berada dalam julat 0.02 ± 0.01 mg/L (Kelas I) hingga 0.10 ± 0.12 mg/L (Kelas IIA). Fosforus adalah suatu komponen najis dan ia merupakan unsur penting dalam metabolisme tubuh badan hidupan (Hem 1983). Fosfat adalah hasil penguraian protein, dan hasil penguraian polifosfat dalam detergen yang digunakan untuk meningkatkan kekuatan cucian (Best & Ross 1977). Terdapat luahan air buangan hasil cucian kantin dan restoran yang dialirkan terus ke dalam 'Alur Ilmu' di lokasi tertentu, walaupun hal ini sepatutnya tidak berlaku.

Nitrat

Pemantauan kepekatan nitrat hanya dijalankan pada tahun 2003. Nilai purata kepekatan nitrat berada dalam julat 0.52 mg/L hingga 0.92 mg/L. Nilai maksimum nitrat dicerap di stesen S5 manakala nilai minimum dicerap di S1. Perbandingan dengan nilai sub indeks INWQS untuk nitrat mengelaskan semua stesen persampelan dalam Sub Kelas 1. Nitrat ialah produk terakhir pengoksidaan ammonia. Nitrat dijumpai dalam air tabii pada kepekatan antara 1 dan 10 mg/L. Ion nitrat kurang diserap oleh tanah dan mudah sampai ke air bawah tanah, dan kepekatan yang relatif lebih tinggi mungkin disebabkan baja yang mengandungi nitrogen. Kepekatan nitrat adalah parameter yang penting untuk penilaian ciri swa-pembersihan sesuatu jasad air dan keseimbangan nutrien di dalam air permukaan dan tanah (Rump 1999).

Koliform Jumlah dan Koliform Najis

Dalam kajian Tan (2003), koliform jumlah berada dalam julat dari di bawah had pengesanan hingga 360,000 MPN/100ml (sub kelas 5). Hanya koliform jumlah pada Stesen 1 berada di bawah had pengesanan. Stesen lain telah melebihi kelas IIA INWQS. Stesen 3 dan 4 mempunyai kepekatan koliform jumlah sebanyak 350,000 MPN/100ml dan 360,000 MPN/100ml, masing-masing, iaitu dalam sub kelas V. Bacaan yang tinggi ini mungkin disebabkan proses penguraian bangkai ikan semasa persampelan dijalankan. Koliform najis sepanjang kajian ini berada dalam julat di bawah had pengesanan hingga 320,000 MPN/100ml (Sub Kelas V). Stesen 1 dan Stesen 5 mempunyai kepekatan koliform najis di bawah had pengesanan; manakala Stesen 2 hingga 4 berjulat 10,000 MPN/100ml (sub kelas III) – 320,000 MPN/100ml (sub kelas V).

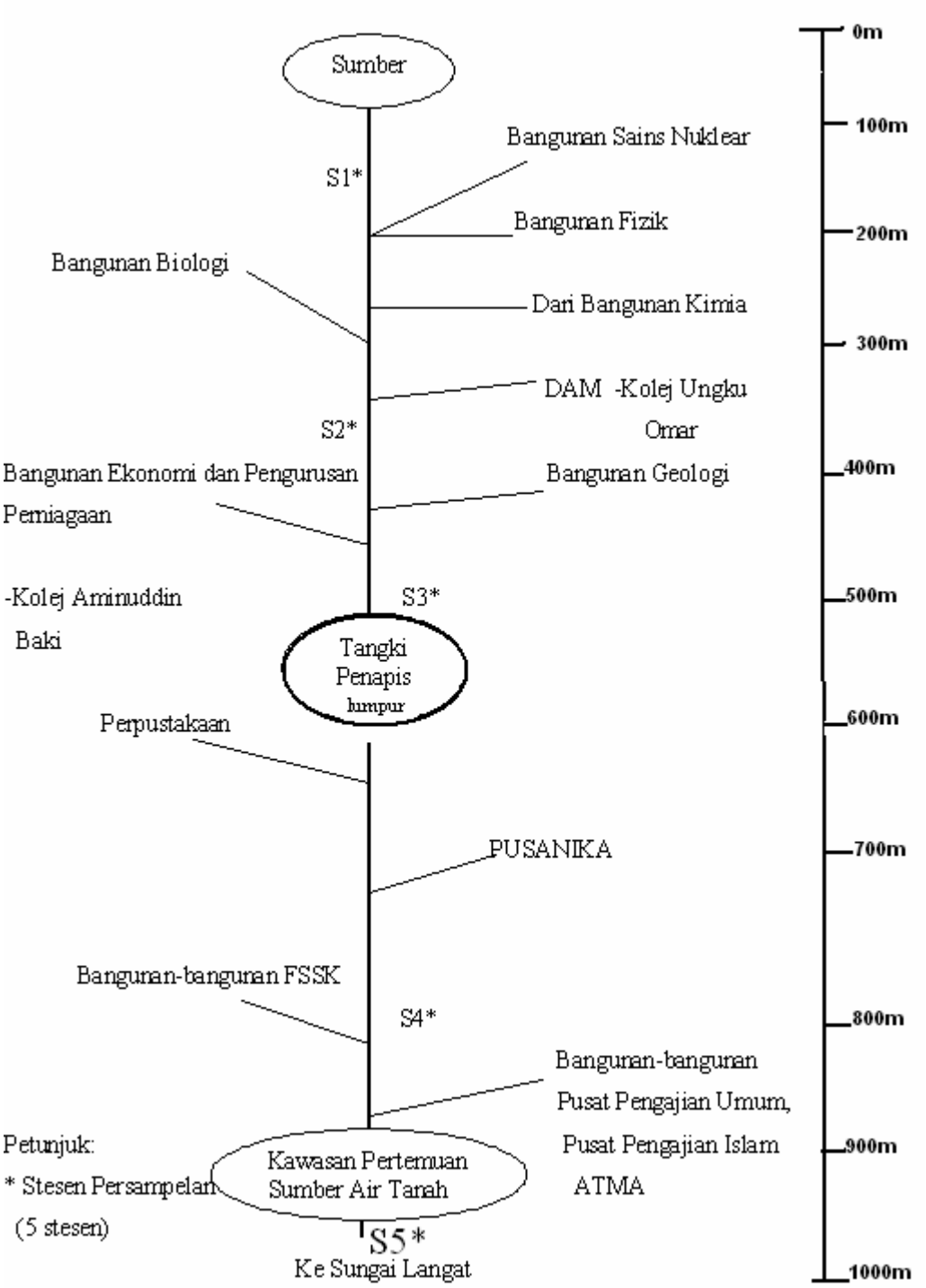

Rajah 2: Carta alir di sepanjang sistem perairan 'Alur Ilmu' dari kawasan UKM Bangi ke Sungai Langat.

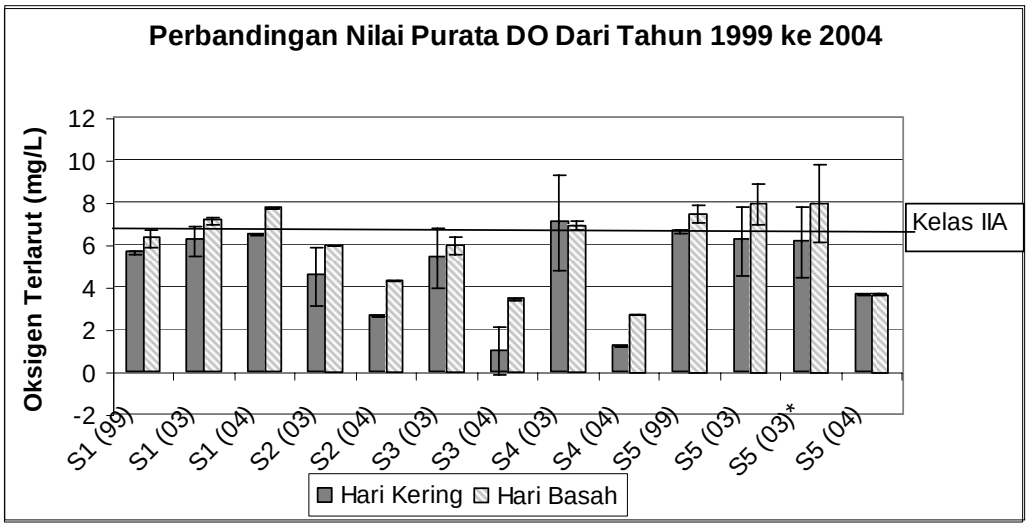

Rajah 3: Perbandingan nilai purata DO antara stesen pada tahun 1999-2004.

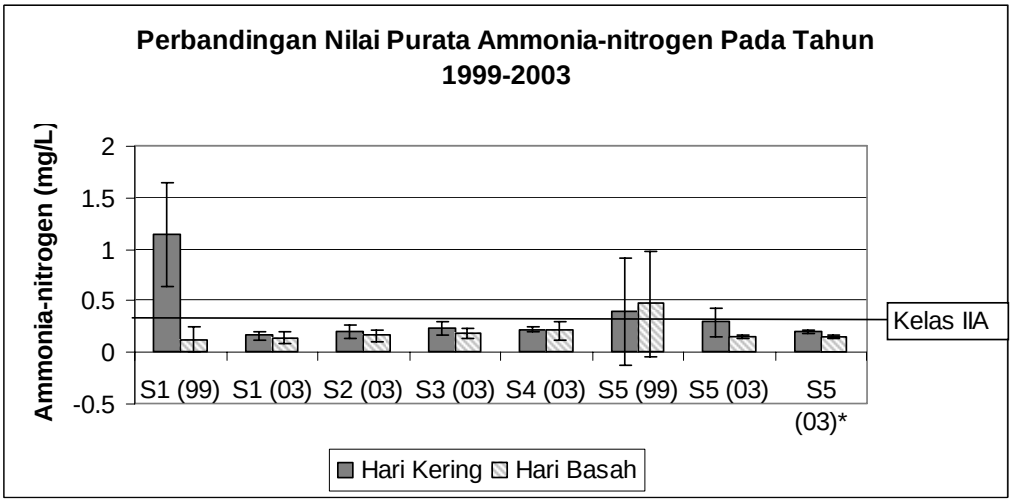

Rajah 4: Perbandingan nilai purata Ammonia-nitrogen pada tahun 1999-2003.

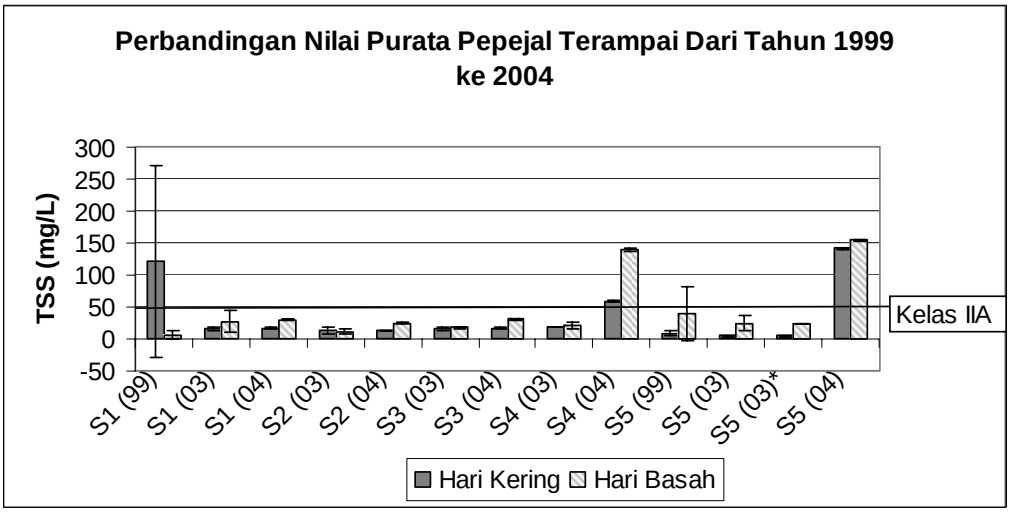

Rajah 5: Perbandingan nilai purata pepejal terampai dari tahun 1999-2004

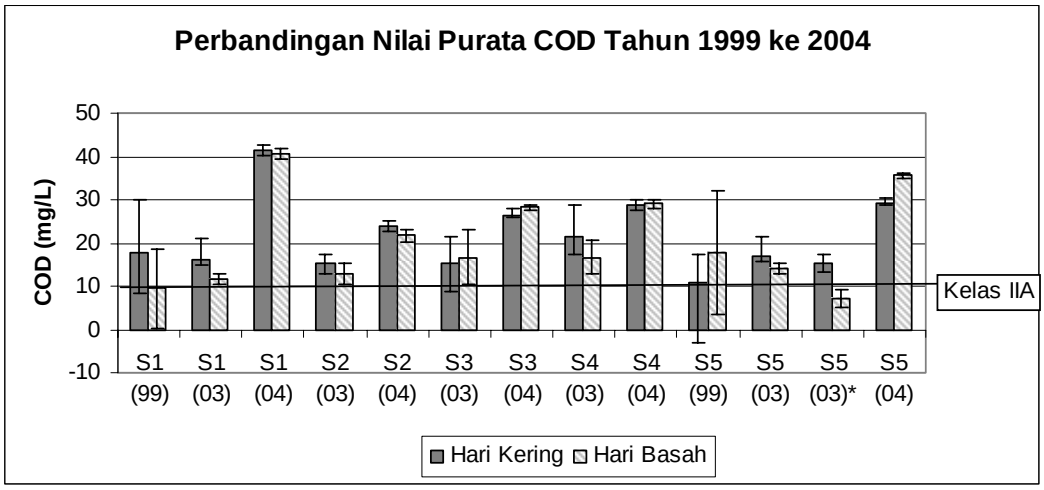

Rajah 6: Perbandingan nilai purata COD pada tahun 1999-2004

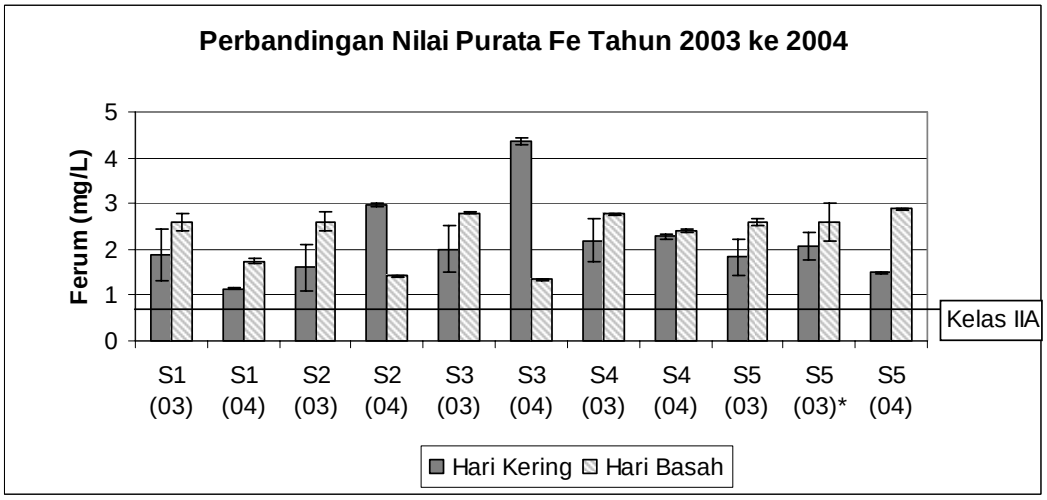

Rajah 7: Perbandingan nilai purata Fe pada tahun 2003-2004

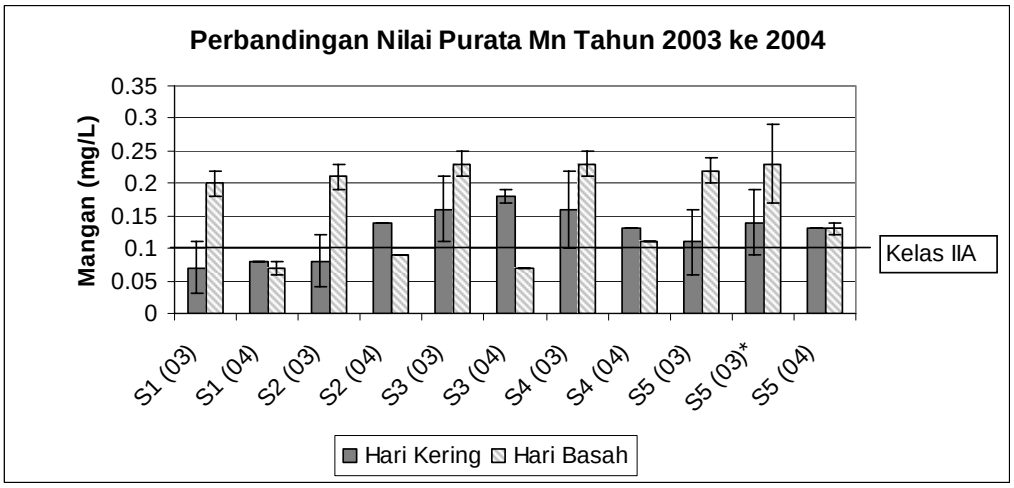

Rajah 8: Perbandingan nilai purata Mn pada tahun 2003-2004.

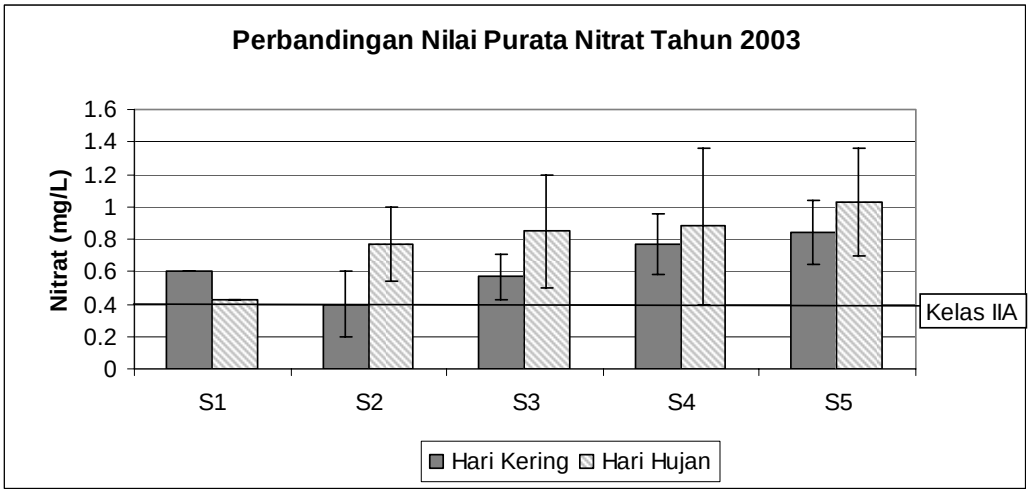

Rajah 9: Perbandingan nilai purata nitrat pada tahun 2003.

JADUAL 1: Nilai purata Koliform Jumlah dan Koliform Najis pada pada Tahun 2003

Parameter / Stesen	Koliform Jumlah (MPN/100ml)	Koliform Najis MPN/100ml)
S1	Nd	Nd
S2	40,000	10,000
S3	350,000	120,000
S4	360,000	320,000
S5	10,000	Nd

JADUAL 2: Indeks Kualiti Air bagi stesen kajian ini secara keseluruhan

Stesen / Parameter	S1	S2	S3	S4	S5
DO	85.87	50.32	40.18	46.88	60.70
SiDO	94.17	50.08	35.06	44.93	65.41
BOD	1.22	0.94	1.23	1.16	1.81
SiBOD	18.1	18.32	18.09	18.14	17.62
COD	22.79	18.46	21.67	23.91	21.5
SiCOD	11.38	5.56	11.59	11.17	11.61
AN	0.39	0.18	0.21	0.22	21.5
SiAN	10.07	12.24	11.77	11.61	10.42
SS	36.34	15.69	20.13	58.87	61.46
SiSS	11.91	14.66	13.78	10.95	10.79
pH	7.04	7.53	7.63	7.93	7.45
SipH	12.52	11.57	11.46	11.04	11.65
IKA	84.70	72.87	74.40	72.79	76.95
Kelas IKA	II	III	III	III	II

Kesimpulan

Hasil kajian menunjukkan bahawa parameter yang telah melangkau Kelas II adalah Pb, sulfat, nitrat, COD, koliform jumlah, koliform najis, Fe, dan Mn. Alur Ilmu perlu dikawal dan dipantau kualiti airnya secara berjadual oleh pihak pengurusan UKM secara bersepadu untuk mempastikan air di alur ini adalah bersih dan sesuai dijadikan sumber bernilai astetik dalam konsep 'Universiti Dalam Taman'. Ini memerlukan penglibatan pelbagai peringkat warga UKM secara bersepadu dan menyeluruh. Strategi dan langkah pelaksanaan yang sistematik perlu dilakukan secara berterusan.

Penghargaan

Penyelidik dan penulis merakamkan penghargaan kepada individu dan pihak jabatan di UKM yang telah memberikan kerjasama dan maklumat dalam menjayakan kajian ini.

Rujukan

APHA (American Public Health Association). 1992. *Standard methods for the examination of water and wastewater.* 18th Edition. American Public Health Association, AWWA, AWPCF, Washington.

Chee Fong Hoe 2004. Kajian Kualiti Air Sistem Perairan 'Alur Ilmu' dalam Kampus UKM Bangi. Kajian yang sedang dijalankan sebagai sebahagian daripada kerja tesis untuk memperolehi Izajah Sarjana Muda Sains Dengan Kepujian, Jabatan Kimia, FST, UKM.

Chong Wai Leng 1999. Kajian Efluen Kolam Pengoksidaan Kumbahan Dan Sistem Saliran Sekitar Kampus UKM. Tesis Yang Dikemukakan Untuk Memperolehi Izajah Sarjana Muda Sains Dengan Kepujian, FST, UKM.

Goodman, A. H. 1980. Potable water quality. Dlm. Lewis, W. M. (pynt.). *Development in water treatment* – 1, hlm. 1-32. GB: Applied Science Publishers and Materials.

Hammer, M.J. 1986. *Water and wastewater technology*. Second Edition. John Wiley & Sons, Inc. Canada.

Mazlin Bin Mokhtar, Ismail Bin Bahari & Ng Chee Hong 2001. Pengelasan Kualiti Air 1998: Dari Pantai Ke Kuala Linggi. *Malaysian Journal of Analitycal Sciences, Vol. 6, No. 1: 178-187.*

Ooi Yih Yong. Kajian Kualiti Efluen Air Yang Keluar Dari Sistem Saliran UKM Ke Sungai Langat. Tesis Yang Dikemukakan Untuk Memperolehi Izajah Sarjana Muda Sains Dengan Kepujian, FST, UKM.

Rump, H.H 199. *Laboratory manual for the examination of water, waste water and soil*. Third Edition, Wiley-VCH, Verlag GmbH, Weinheim.

Tan Bee Heong 2003. Kajian Kualiti Air Sistem Saliran (Alir Ilmu) Kampus UKM Bangi. Tesis Yang Dikemukakan Untuk Memperolehi Izajah Sarjana Muda Sains Dengan Kepujian, FST, UKM.

Tȍlgyessy, J. (pnyt.) 1993. *Chemistry and biology of water, air and soil environment aspects.* Elsevier Science Publishers, Amsterdam.

Malaysian Journal of Analytical Sciences, Vol. 9, No. 3 (2005): 396 - 405

KAJIAN AWAL KUALITI AIR SUNGAI KILIM, LANGKAWI: KAJIAN KES BAGI PENGURUSAN SUMBER AIR BERSEPADU DI SEBUAH PULAU, MALAYSIA

Mazlin B. Mokhtar, Ibrahim Komoo & Ooi, S. T.

Institut Alam Sekitar dan Pembangunan (LESTARI)
Universiti Kebangsaan Malaysia
43600 UKM BANGI, Selangor Darul Ehsan, Malaysia

Abstrak

Kajian ini adalah suatu kajian awal kualiti air pada sebahagian Sungai Kilim, Langkawi sebagai kajian kes bagi Pendekatan Pengurusan Sumber Air Bersepadu di sebuah pulau di Malaysia. Lembangan Sungai Kilim mempunyai kepentingan dalam pelbagai aspek seperti formasi geologi unik Macincang, hutan bakau, sumber makanan akuatik, laluan pengangkutan air, sumber air keperluan domestik dan pelancongan. Empat stesen telah dipilih untuk pensampelan kualiti air di Sungai Kilim iaitu di $06^0$24'59.2"U $099^0$51'47.6"T, $06^0$25'31.3"U $099^0$52'07.9"T, $06^0$26'17.6"U $099^0$52'35.3"T dan $06^0$24'18.1"U $099^0$51'31.1"T. Kualiti air di semua stesen secara keseluruhannya tergolong dalam Kelas II-III mengikut Piawaian Interim Air Kebangsaan Malaysia (INWQS).

Abstract

This preliminary water quality study was carried out along a certain stretch of Kilim River in Langkawi, as a case study using the Integrated Water Resources Management (IWRM) approach. Kilim River basin is special because of its unique geological Macincang limestone formation, mangrove forests, aquatic food resources, pathways for water transportation, water sources for domestic consumption and ecotourism. Four stations were selected along Kilim River in this preliminary study and they were at $06^0$24'59.2N $099^0$51'47.6"E, $06^0$25'31.3"N $099^0$52'07.9"E, $06^0$26'17.6"N $099^0$52'35.3"E and $06^0$24'18.1"N $099^0$51'31.1"E. The overall classes of river water for these stations were Class II-III based on the Interim Water Quality Standards (INWQS) of Malaysia.

Pengenalan

Pengurusan Bersepadu Sumber Air (IWRM) menekankan bahawa keseimbangan antara sumber air dan penggunaannya adalah amat penting untuk pembangunan mampan. Namun, pembangunan ekonomi dan pertambahan populasi yang pesat meningkatkan permintaan air dan menimbulkan masalah pencemaran sungai serta kemungkinan konflik kekurangan sumber air pada masa hadapan. Kajian dijalankan berdasarkan enam parameter untuk penentuan Indeks Kualiti Air (IKA), iaitu oksigen terlarut (DO), permintaan oksigen biokimia (BOD),

permintaan oksigen kimia (COD), ammonia nitrogen (NH_3-N), jumlah pepejal terampai (TSS) dan pH. Sungai Kilim dipilih sebagai lokasi kajian awal untuk pengurusan bersepadu sumber air di Langkawi kerana ia merupakan tempat strategik dari aspek geologi, biologi dan sosiologi. Ia juga penting untuk penduduk tempatan sumber makanan akuatik, rekreasi, sumber air untuk tujuan domestic.

Pengurusan air juga melibatkan integrasi antara masyarakat dan setiap individu. Sumber air perlu dijaga untuk menjamin bahawa ia adalah mencukupi dan selamat untuk digunakan oleh generasi akan datang. Objektif kajian ini dilakukan adalah untuk:

a. menentukan nilai parameter Indeks Kualiti Air (IKA) di Sungai Kilim berdasarkan enam parameter yang disarankan oleh JAS iaitu DO, BOD, COD, NH_3-N, TSS dan pH,
b. menentukan dan membandingkan kualiti dan kelas air di empat stesen di Sungai Kilim berdasarkan IKA sebagai kajian awal untuk pengurusan bersepadu sumber air di Langkawi,
c. membandingkan data kajian ini dengan nilai-nilai Piawai Interim Kualiti Air Kebangsaan Malaysia (INWQS).

Bahan dan Kaedah

Kajian ini dijalankan di Sungai Kilim dan sampel air diambil dari empat stesen yang berlainan (Rajah 1 & 2). Ciri-ciri setiap stesen ditunjukkan dalam Jadual 1.

Jadual 1: Lokasi, ciri dan perihalan ringkas stesen kajian ini

Stesen	Kedudukan	Masa Pensampelan	Ciri-ciri
Stesen 1 (S1)	$06^0$24’18.1”U $099^0$51’31.1”T	10:45 pagi	Jeti Kilim, hilir sungai dan terdapat banyak bot berlabuh, air kelihatan keruh.
Stesen 2 (S2)	$06^0$24’59.2”U $099^0$51’47.6”T	11:18 pagi	Berdekatan Restoran Sangkar Ikan, terdapat tandas dan perahu di sekitar.
Stesen 3 (S3)	$06^0$25’31.3”U $099^0$52’07.9”T	11:48 pagi	Berdekatan dengan muara Sungai Kilim.
Stesen 4 (S4)	$06^0$26’17.6”U $099^0$52’35.3”T	1:34 ptg	Berdekatan dengan Pulau Tanggok, air di stesen ini kelihatan jernih.

Kaedah pensampelan

Pensampelan telah dilakukan pada 14.05.2004. Sebanyak empat kawasan pensampelan telah dipilih pada Sungai Kilim dan kedudukan stesen pensampelan ditentukan dengan menggunakan alat “Global Positioning

System, model 12 Channel, buatan Garmin".

Botol hitam BOD, botol kaca dan botol polietilena digunakan dan dilabel dengan nombor stesen, parameter sampel dan masa. Sebelum sampel air diambil, botol dibilas dengan air sungai yang hendak dikaji terlebih dahulu. Apabila sampel air diambil, botol dimasukkan ke dalam air sungai untuk mengisi air sampel bagi mengelakkan kemasukan udara dari atmosfera ke dalam botol.

Kaedah Pengawetan

Sampel air untuk ujian nitrogen ammonia dan permintaan oksigen biokimia diproses sebaik sahaja balik dari lapangan dalam masa 24 jam. Sampel air untuk parameter lain diproses dalam masa penyimpanan yang disarankan oleh APHA (Jadual 2).

Jadual 2: Cara-cara pengawetan, jenis botol dan masa penyimpanan yang digunakan mengikut parameter

Parameter	Jenis botol	Pengawetan	Masa penyimpanan
BOD	BOD	Simpan pada 4^0C	6 jam
COD	Polietilena atau kaca	Asidkan dengan H_2SO_4 ke pH≤2, simpan pada 4^0C	7 hari
NH_3-N	Polietilena atau kaca	Asidkan dengan H_2SO_4 ke pH≤2, simpan pada 4^0C	7 hari
TSS	Polietilena atau kaca	Simpan pada 4^0C	7 hari

Pengukuran parameter *in-situ*

Parameter yang ditentukan di lapangan adalah jumlah pepejal terlarut, pH, suhu, kekonduksian dan oksigen terlarut. Suhu (^{0}C), pH, kekonduksian (μS/cm) dan oksigen terlarut (mg/l) diukur dengan menggunakan alat YSI 556 multi parameter. Alat dikalibrasi dan digunakan berdasarkan buku panduan alatan YSI.

Analisis kimia

i) BOD_5 (Kaedah APHA 5210 B, 1995)

Ujian BOD 5 hari digunakan untuk mengukur parameter BOD. Sampel air sungai diisi ke dalam dua botol berkaca hitam yang berasingan. Oksigen terlarut salah satu sampel air diukur secara *in-situ* dan bacaannya dicatatkan sebagai DO_{awal}. Sementara sampel air yang satu lagi dieramkan pada suhu 30^0C selama 5 hari. Selepas 5 hari, kandungan oksigen terlarut diukur sekali lagi dengan menggunakan meter oksigen terlarut model YSI 556 yang sama dan bacaan dicatatkan sebagai DO_{akhir}. BOD ditentukan dari perbezaan DO_{awal} dan DO_{akhir}:

BOD_5 (mg/l) = DO_{awal} - DO_{akhir}

Persamaan (1)

ii) COD (Kaedah APHA 5220 B, 1995)

Kaedah yang digunakan ialah Kaedah Refluk Terbuka. Sebanyak 50ml sampel air diambil untuk direfluk. Sampel tersebut dimasukkan ke dalam kelalang refluk dan 1g $HgSO_4$ dan 5ml reagan asid sulfurik ditambah secara perlahan-lahan. Percampuran dilakukan dalam kukus air untuk mengelakkan kemungkinan kehilangan bahan organik yang mudah meruap. 25ml larutan 0.0417M kalium dwikromat ditambah ke dalam campuran dan digoncang. Campuran tersebut direfluk selama 2 jam, batu didih ditambah untuk mengelakkan letupan. Pencairan dibuat dengan menambah air suling nyahion sehingga ke tahap 100ml. Larutan $K_2Cr_2O_7$ yang berlebihan dititrat dengan larutan ferum (II) ammonium sulfat 0.25M (FAS). Beberap titis larutan ferrion diguna sebagai penunjuk. Takat akhir titratan tercapai apabila warna larutan bertukar dari warna hijau kepada merah-keperangan. COD dalam sampel ditentukan dengan menggunakan formula berikut:

$$COD = \frac{(A - B) \times M \times 8000}{\text{Isipadu sampel}}$$

Persamaan (2)

Di mana A = Isipadu blank

B = Isipadu sampel yang dititrat

M = Kemolaran FAS

iii) NH_3-N (Kaedah APHA 4500-NH_3C, 1992)

Kaedah Nessler digunakan untuk mengukur parameter NH_3-N. 25ml sampel air nyahion dimasukkan ke dalam silinder masing-masing. Tiga titis penstabil mineral ditambahkan ke dalam silinder dan digoncang. Kemudian, 3 titis agen penyerak polivinil alkohol ditambahkan ke dalam silinder dan digoncang supaya percampuran sempurna berlaku. Selepas itu, 1ml reagen Nessler ditambah ke dalam silinder dan ditutupkan. Silinder digoncang dan dibiarkan selama 1 minit. Seterusnya, campuran dimasukkan ke dalam sel sampel dan dianalisis dengan spektrofotometer HACH DR 2010 yang telah diselaraskan kepada nombor program 380 dan jarak gelombang 425nm. Air nyahion digunakan sebagai blank.

iv) TSS (Kaedah APHA 2450 D, 1995)

Kaedah Gravimetri digunakan untuk mengukur parameter TSS. Kertas turas selulosa-nitrat jenis Whatman GF/F bersaiz 0.45µm dan berdiameter 47nm dikeringkan pada suhu 103^0C dalam ketuhar dan ditimbang supaya berat kering ditentukan. 200ml sampel air dituras dengan menggunakan kertas turas tersebut dan dikeringkan dalam piring petri kaca bertutup pada suhu 103^0C dalam ketuhar. Selepas itu, kertas turas ditimbang sekali lagi dengan menggunakan neraca elektronik. Langkah pengeringan dan penimbangan dilakukan berulang kali sehingga berat tetap diperolehi dan tiada perubahan berat yang melebihi 0.5mg. TSS dalam sampel ditentukan dengan menggunakan formula berikut:

Jumlah pepejal terampai (mg/l) =

$$\frac{A - B \times 100}{V}$$

Persamaan (3)

Di mana A = Berat kertas turas selepas penurasan (mg)

B = Berat kertas turas sebelum penurasan (mg)

V = Isipadu air sampel (ml)

Bacaan parameter *in-situ* diambil pada permukaan, 1 m, 2 m, 3 m, 4 m dan 5 m ke bawah paras air di Stesen 1 dan 2 manakala kedalaman di Stesen 3 dan 4 mencapai 3 m dan 2 m masing-masing.

Keputusan

Keputusan bacaan parameter *in-situ* adalah seperti berikut:

Stesen 1

Kedalaman	Suhu (^{0}C)	Kekonduksian (µS/cm)	TDS (mg/l)	Saliniti (ppt)	DO (ppm)	pH	DO (%)
0 m	31.33	5882	34.11	34.37	3.95	8.06	63.7
1 m	31.35	5884	34.11	34.37	4.02	8.22	64.6
2 m	31.34	5883	34.12	34.38	4.24	8.28	69.3
3 m	31.33	5883	34.12	34.38	4.28	8.33	69.8
4 m	31.32	5881	34.12	34.38	4.30	8.36	69.8
5 m	31.29	5879	34.12	34.38	4.18	8.38	67.3

Stesen 2

Kedalaman	Suhu (^{0}C)	Kekonduksian (µS/cm)	TDS (mg/l)	Saliniti (ppt)	DO (ppm)	pH	DO (%)
0 m	31.46	5905	34.17	34.43	4.61	8.39	76.0
1 m	31.47	5906	34.17	34.43	4.51	8.48	74.3
2 m	31.45	5904	34.17	34.43	4.47	8.51	72.8
3 m	31.45	5904	34.17	34.44	4.70	8.52	73.3
4 m	31.44	5903	34.17	34.43	4.38	8.52	70.1
5 m	31.44	5903	34.17	34.43	4.15	8.52	67.0

Stesen 3

Kedalaman	Suhu (^{0}C)	Kekonduksian (µS/cm)	TDS (mg/l)	Saliniti (ppt)	DO (ppm)	pH	DO (%)
0 m	31.41	5913	34.24	34.52	4.69	8.46	76.7
1 m	31.39	5905	34.22	34.49	4.47	8.49	70.8
2 m	31.33	5902	34.23	34.51	4.25	8.50	70.0
3 m	31.35	5905	34.23	34.51	4.42	8.52	72.1

Stesen 4

Kedalaman	Suhu (^{0}C)	Kekonduksian (µS/cm)	TDS (mg/l)	Saliniti (ppt)	DO (ppm)	pH	DO (%)
0 m	30.27	5602	33.09	33.25	2.54	7.84	41.0

1 m	30.26	5601	33.09	33.25	2.75	7.83	43.4
2 m	30.25	5607	33.29	33.29	2.77	7.84	44.1

Sampel air di permukaan setiap stesen diambil untuk analisis kimia di makmal dan keputusan yang diperolehi adalah seperti berikut:

BOD

Stesen	BOD_{awal} (ppm), A	BOD_{akhir} (ppm), B	A – B
Stesen 1	3.60	2.67	0.93
Stesen 2	4.48	3.52	0.96
Stesen 3	4.33	3.01	1.32
Stesen 4	2.41	1.78	0.63

COD

Stesen	Bacaan awal (ml)	Bacaan akhir (ml)	Isipadu FAS (ml)	COD (mg/l)
Blank	0.0	25.0	25.0	0
Stesen 1	0.0	24.7	24.7	24
Stesen 2	24.7	48.8	24.1	72
Stesen 3	8.3	32.2	23.9	88
Stesen 4	9.0	31.4	22.4	208

NH_3-N

Stesen	Bacaan (mg/l)	Faktor pencairan	NH_3-N (mg/l)
Stesen 1	1.45	2	2.9
Stesen 2	0.01	25	0.25
Stesen 3	0.26	5	1.3
Stesen 4	0.15	5	0.75

TSS

Stesen	Berat kertas turas kering, A (g)	Berat kertas turas + residu kering, B (g)	B – A
Stesen 1	0.091	0.109	0.018
Stesen 2	0.092	0.110	0.018
Stesen 3	0.087	0.109	0.022
Stesen 4	0.092	0.107	0.015

Perbincangan

Keputusan kajian parameter mengikut aras kedalaman air di Stesen 1, 2 dan 3 menunjukkan bahawa terdapat perubahan mendadak pada lapisan 'thermocline' atau 'metalimnion' pada aras kedalaman antara 1-2 meter atau 2-3 meter. Ini adalah suatu fenomenon yang menarik dan harus diselidiki lagi pada masa hadapan khususnya untuk melihat pengaruh musim hujan dan kering ke atas paras tersebut.

Stesen 2 dipilih sebagai contoh untuk mendapatkan profil kedalaman bagi parameter *in-situ* dan dibandingkan

dengan Piawaian Interim Kualiti Air Kebangsaan Malaysia (INWQS).

Daripada profil-profil yang diplot, didapati bahawa suhu dan konduktiviti berkurang mengikut kedalaman air. Suhu dipengaruhi oleh cahaya matahari, suhu di permukaan air lebih tinggi disebabkan pancaran cahaya yang kuat manakala semakin dalam ke bawah air, pancaran semakin berkurangan. Suhu yang tinggi merangsang komuniti fitoplankton menjalankan proses fotosintesis dalam kadar yang maksimum. Kekonduksian juga dipengaruhi oleh suhu, ia berubah mengikut perubahan suhu dan kedalaman. Konduktiviti sampel air di S2 adalah relative tinggi dan dikelaskan dalam Kelas IV mengikut INWQS.

Profil-profil TDS, saliniti, DO dan pH menunjukkan peningkatan nilai apabila kedalaman air meningkat. Nilai garis panduan bagi TDS di dalam air minuman ialah 1000 mg/L untuk menghindarkan kesan fisiologi ke atas pelbagai organ dalam tubuh manusia. Maka, kandungan TDS yang rendah di S2 menunjukkan bahawa ia adalah sesuai untuk dijadikan sebagai air minuman.

DO berkurang apabila kedalaman meningkat kerana terdapat pemeliharaan hidupan laut seperti ikan dan udang di sekitar Restoran Sangkar Ikan di S2. Hidupan-hidupan tersebut memerlukan oksigen terlarut dari permukaan air dan menyebabkan DO yang rendah pada permukaan air. Selain itu, oksigen terlarut mungkin dikurangkan oleh bahan terlarut, terampai atau termendap di permukaan air melalui reaksi pengoksidaan tak organik atau proses biologi dan kimia. Walau bagaimanapun, kualitinya masih dikelaskan dalam Kelas II mengikut INWQS dan sesuai digunakan untuk minuman dan tujuan rekreasi.

Secara umumnya, kualiti air di keempat-empat stesen di Sungai Kilim, Langkawi dikelaskan dalam Kelas IIA berdasarkan Piawaian Interim Kualiti Air Kebangsaan Malaysia (INWQS). Namun, kandungan permintaan oksigen kimianya adalah relative tinggi.

Bacaan DO untuk S2, S3, dan S4 adalah tinggi dan berada dalam julat 3-5 mg/L (Kelas III) manakala untuk S1 pula, DOnya agak rendah iaitu dalam julat 2-3 mg/L (Kelas IV). Kekurangan oksigen terlarut di S1 disebabkan kadar peresapan oksigen ke dalam jasad air yang rendah kerana kadar aliran air sungainya yang perlahan berbanding dengan stesen yang lain.

Nilai BOD untuk S1, S2 dan S3 adalah rendah (<1 mg/L) manakala S4 mencatatkan nilai 1.32 mg/L. Salah satu faktor yang menyebabkan nilai BOD yang tinggi di S4 adalah tindakan mikroorganisma dalam proses penguraian aerobik bahan organik dan kehadiran zarahan terampai yang tinggi. Walau bagaimanapun, nilai BOD untuk keempat-empat stesen dikelaskan dalam Kelas I mengikut INWQS.

S2 mencatatkan nilai COD yang rendah (Kelas II), S3 dan S4 mencatatkan nilai COD yang agak tinggi dan dikelaskan dalam Kelas IV mengikut INWQS manakala S1 mencatatkan nilai CODnya tergolong dalam Kelas V. S1 terletak di jeti Sungai Kilim dan terdapat banyak bot yang berlabuh di situ. Kesan penumpahan minyak dari bot-bot menurunkan kualiti

airnya dan menyebabkan pencemaran. Agen-agen pengoksidaan yang kuat dalam keadaan berasid mengoksidakan sebatian organik dalam air kepada karbon dioksida dan air.

Kepekatan NH_3-N pada S2 mencatatkan nilai yang relative tinggi (Kelas V), S3 dikelaskan dalam Kelas II, S4 dalam Kelas IV dan S1 dalam Kelas III. S3 mempunyai nilai NH_3-N yang paling rendah disebabkan oleh penyerapan NH_3-N oleh tumbuh-tumbuhan makrofit seperti teratai. Ammonia nitrogen dapat diguna terus oleh tumbuh-tumbuhan akuatik atau dinitrifikasikan kepada nitrat. Kehadiran bahan-bahan organik seperti protein dan urea dari sekitar Restoran Sangkar Ikan di S2 menyebabkan nilai NH_3-N yang relative tinggi di S2.

Sampel air di semua stesen kelihatan jernih dan mencatatkan nilai TSS yang sangat rendah (Kelas I) manakala untuk pH pula, sampel air di S1, S2, S3 dan S4 adalah sedikit beralkali dan dikelaskan dalam Kelas II mengikut INWQS. Kealkalian sampel air disebabkan oleh pembentukan batu kapur yang paling mudah terlarut di sekitar Sungai Kilim.

Mengikut Indeks Kualiti Air (IKA), kualiti air di Stesen 3 di Sungai Kilim, Langkawi dikelaskan dalam Kelas II manakala Stesen 1, 2 dan 4 dikelaskan dalam Kelas III. Maka, air di Stesen 3 sesuai untuk bekalan air yang memerlukan rawatan konvensional, untuk perikanan jenis yang sensitif dan tujuan aktiviti rekreasi yang melibatkan sentuhan. Air di Stesen 1, 2 dan 4 pula sesuai untuk bekalan air yang memerlukan rawatan ekstensif, sebagai air minuman untuk haiwan ternakan dan pemeliharaan ikan jenis toleransi dan bernilai komersial.

RUJUKAN

1. APHA. 1992. *Standard methods for the examination of water and wastewater.* Ed Ke-18. Washington: American Public Health Association (APHA), AWWA. WPCF.
2. APHA. 1995. *Standard methods for the examination of water and wastewater.* Ed Ke-19. Washington: American Public Health Association (APHA), AWWA. WPCF.
3. Boyd, C. E. 1990. *Mutu air kolam ikan di kawasan beriklim panas.* Terj. Mohd. Salleh Kamarudin, Siti Shapor Siraj & Noor Azhar Shazili. Kuala Lumpur: Dewan Bahasa dan Pustaka.
4. *Draf Rancangan Struktur Langkawi 1990-2005.* 1990. Majlis Daerah Langkawi, Kedah.
5. GWP, Global Water Partnership. 2001. *Integrated Water Resources Management.* Sweden: Elanders Novum AB.
6. Harper, D. 1992. *Eutrophication of freshwater, principles, problems and restroration.* London: Chapman & Hall.
7. Hashimah Talib, Shahabudin Mustapha & Mohd Asri Mohd Noor. 1996. *Garis panduan kualiti air minum.* Terj. Universiti Teknologi Malaysia.
8. Hem, J. D. 1970. *Study and Interpretation of the chemical characteristics of natural water.*

Ed Ke-2. Washington: U. S. Government printing office.
9. Hem, J. D. 1989. *Study and Interpretation of the chemical characteristics of natural water.* Washington: U. S. Geological Survey.
10. JAS, Jabatan Alam Sekitar. 1993. *Laporan kualiti alam sekitar Malaysia 1993.* Kuala Lumpur: Kementerian Sains, Teknologi dan Alam Sekitar.
11. *LANGKAWI – Senario Pembangunan.* 1987. Pejabat Daerah Langkawi.
12. Laporan Tahunan 2003. *Pulau Langkawi – Water Supply System*. Jabatan Kerja Raya Negeri Kedah Darulaman.
13. Mazlin Mokhtar, Mohd. Talib Latif & Lee, Y. H. 2003. *Kimia Air*. Kuala Lumpur: Utusan Publications & Distributors Sdn. Bhd.
14. Mazlin Bin Mokhtar, Ismail Bin Bahari & Ng, C. H. 2001. Pengelasan Kualiti Air 1998: Dari Pantai Ke Kuala Linggi. *The Malaysian Journal of Analytical Sciences*. **6**: 178-187

Langkawi

Rajah 1: Peta Pulau Langkawi dan sistem sungai utamanya (Sumber: Brosur Pelancongan Langkawi)

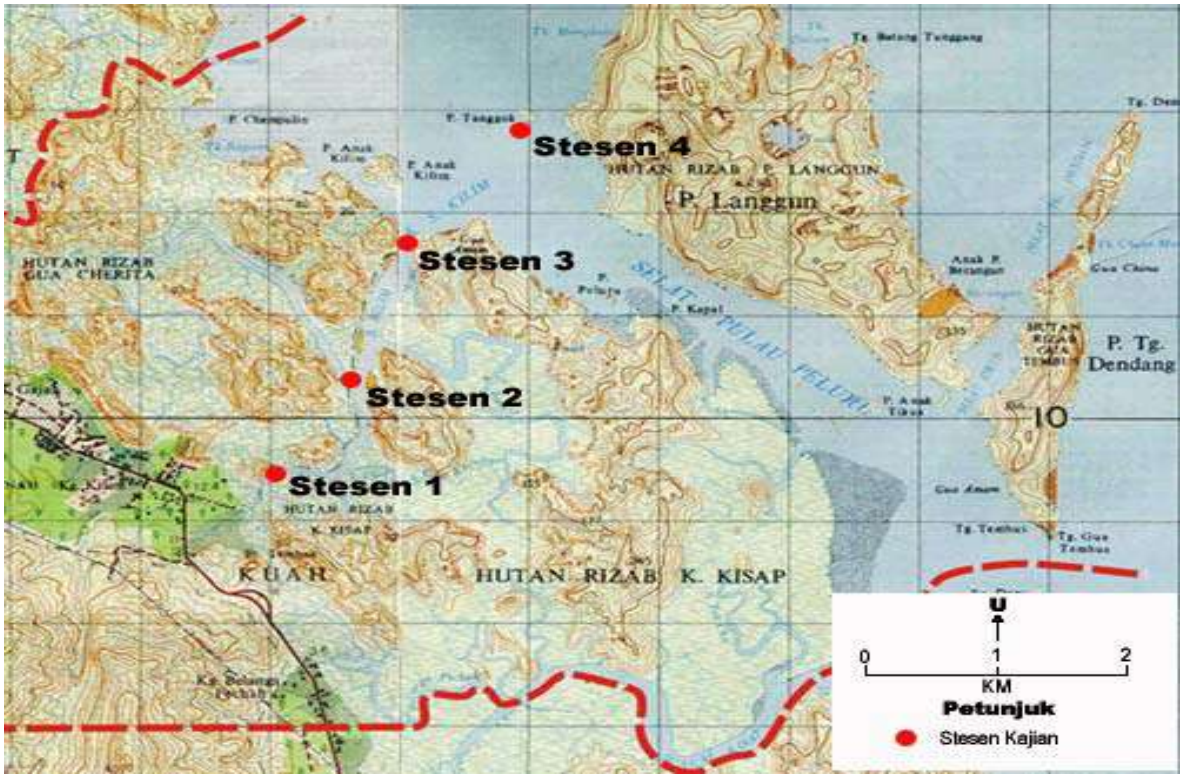

Rajah 2: Lokasi stesen pemantauan dan pensampelan kajian ini (Sumber: Jabatan Pemetaan Negara)

Malaysian Journal of Analytical Sciences, Vol.9, No. 3(2005): 406 - 417

PERFORMANCE AND PROPERTIES OF Zn/LiI-Li_2WO_4 - Li_3PO_4/METAL OXIDE ELECTROCHEMICAL CELLS

A.H. Ahmad and R.H.Y. Subban

[1]*Faculty of Applied Science, MARA University of Technology, 40500 Shah Alam, Selangor D.E, Malaysia*

Abstract. The performance of an all solid-state cell Zn/LiI-Li_2WO_4-Li_3PO_4/metal oxide is studied. The cells were assembled by successively pressing the anode, electrolyte and cathode as a single 3-layered pellet. The metal oxides used are MnO_2 and V_2O_5. The open circuit voltage (OCV) obtained is about 1.2 V. The cell was discharged at constant currents of 20μA, 50μA and 100μA. The dependence of the open circuit voltage on temperature was studied for the cell before and after discharge. From these data the Gibb's free energy and thermoneutral potential of the cell were obtained. For all the three cells, the dependence of OCV on temperature appeared linear with positive slope between 25º and 100º C. The change in Gibb's free energy of formation for all cells increases with temperature. Before discharge, the Zn/ MnO_2 and Zn/ MnO_2: V_2O_5 cells showed negative enthalphy and positive thermoneutral potential E_H indicating exorthermic reaction occured. After discharge, the cells showed positive value in the enthalphy and negative value of thermoneutral potential E_H. This indicates endothermic reaction occurred during discharge.
Key words: Solid electrolyte, Electrochemical cells, OCV, discharge characteristics, thermodynamics parameters, enthalphy

Introduction

It has been reported that many mono and divalent ions have high mobilities in lithium based electrolytes [1]. This enables elements like zinc to be used as the anode in electrochemical cells. Usually Zn//metal oxide cells make use of an alkaline electrolyte such as KOH. In this work, the solid state electrochemical cell utilizes a LiI-Li_2WO_4-Li_3PO_4 electrolyte. This material was prepared by mixing each component in the weight ratio chosen and calcining the pelletized mixture at 70ºC for 7 days. The material has been characterized by FTIR and confirmed to contain water. Results of the characterization of the electrochemical cell will be presented and discussed in this paper.

Experimental Techniques

Sample preparation

Different amounts of Li_3PO_4 was added to a fixed ratio of LiI:Li_2WO_4 binary system that exhibits the highest electrical conductivity in the LiI-Li_2WO_4 family (0.2 wt. % LiI-0.8 wt. % Li_2WO_4). The three components were mixed and ground throroughly and the finely mixed powder was pelletized, put on a glass slide and then placed in a boiling tube plugged with glass wool. The pelletized samples were calcined at 70° C for 7 days.

Sample characterization by FTIR

FTIR measurement was done using the Perkin Elmer FT-IR Spectrometer SPECTRUM 2000, and was performed using the KBr method. The spectrum was obtained in the 400 to 4000 cm^{-1} region at 1 cm^{-1} wave number resolution.

Battery fabrication

The solid state cells with LiI-Li_2WO_4-Li_3PO_4 solid electrolytes were constructed as follows: The cathode material was made up of MnO_2 (or V_2O_5 or both), electrolyte, activated carbon, and PVDF with a weight ratio of 60:20:10:10. PVDF was added as a binder. The anode was made up of Zn, electrolyte, activated carbon and PVDF with a weight ratio of 60:20:10:10. The electrolyte was sandwiched by the electrodes, and pressed to form a button cell as shown in Fig. 1. Three different types of zinc cells were prepared and the configurations are shown below;

(Cell1): Zn+electrolyte+C/0.75wt.%(LiI-Li_2WO_4)-0.25wt.%Li_3PO_4/ MnO_2+electrolyte+C
(Cell2): Zn+electrolyte+C/0.75wt.%(LiI-Li_2WO_4)-0.25wt.%Li_3PO_4/ V_2O_5+electrolyte+C
(Cell3): Zn+electrolyte+C/0.75wt.%(LiI-Li_2WO_4)-0.25 wt. % Li_3PO_4/ MnO_2:V_2O_5 (50:50)+electrolyte+C.

Open Circuit Voltage

All the cells were tested for the open circuit voltage (OCV). The OCV is the cell voltage under no load condition and is usually a close approximation of the theoretical voltage. The temperature dependence of the OCV was observed in the range from room temperature to 100º C before and after the cell was discharged.

Discharge characteristics

The discharge characteristics were evaluated using the BAS LG-50 galvanostat. The cells were discharged at currents of 20 µA, 50 µA and 100 µA, respectively. After discharge to 0.5 V, the OCV of the cell was measured at different temperatures. The thermodynamics parameters that is the change in entrophy dS, change in Gibb's free energy dG, change in enthalphy dH, and thermoneutral potential E_H can be calculated using the following equations [1]:

$$dS = nF \times (dE/dT) \quad (2)$$

$$dG = -nEF \quad (3)$$

$$dH = -nEF + nFT \times (dE/dT) \quad (4)$$

$$E_H = E - T \times (dE/dT) \quad (5)$$

Details of the derivation of these equations and study on thermodynamic properties can be found in the literature [2,3,4,5]

Results and Discussion

From IR studies OH^- bending and stretching modes [6] are observed until the Li_3PO_4 content exceeds 30 wt. %. At such concentration of Li_3PO_4 (40 and 45 wt. %) the FTIR spectrum showed the absence of OH^- bending mode between 1380 and 1580 cm^{-1} (Fig.2). Likewise the OH^- stretching mode is also absent within the 2800-3800 cm^{-1} region (Fig. 3). The existence of OH^- stretching and bending modes is evident of physiosorbed water. Hence the variation in conductivity for samples containing less than 35 wt. % of Li_3PO_4 could be due to the different amounts of free proton and lithium ions available for conduction. Since samples containing 40 and 45 wt. % of Li_3PO_4 do not show the presence of OH^- bending and stretching, it is possible that these samples are pure lithium ion conductors.

Discharge characteristic curves of cell 1 at room temperature for discharge currents of 20 µA, 50 µA and 100 µA are shown in Fig. 4. For the cell discharged at 20 µA, it takes about 30 hours for the voltage to drop to the cut-off voltage of 0.5 V from the voltage 1.17 V at time zero. For the cell discharged at 100 µA, cut-off voltage was reached in 6 hours from 1.14 V at time zero. For the cell discharged at 50 µA, it takes about 18 hours to reach 0.5 V from about 1.17 V.

The cell with the same configuration is allowed to discharge at 20 µA but at 100 C (Fig.5). When the temperature of the cell reaches 150 C, the OCV also increased to about 1.2 V. Even though the OCV has increased but the discharge profile of the cell at high temperature was poor compared to the cell discharged at room temperature for the same discharge current. At room temperature the time taken for the cell to reach the cut off voltage at 0.5 V was almost 30 hours but at 100 C the cell reached the cut off voltage in less than 10 hours.

Fig. 6 showed the discharge characteristics of Cell (2) using V_2O_5 and cell (3) using a combination of V_2O_5: MnO_2 in the ratio (50:50) as the cathode active material. Discharge curve for Cell (1) with MnO_2 as cathode is also included for comparison. All cells were discharged at 20 µA at room temperature. Cell (2) took about 70 hours to reach cut-off voltage and for Cell (3) about 75 hours. A careful look at the curves in Fig. 7 reveals the discharge occurs in steps indicating various degrees of intercalation in the cathode active material during the discharge process. According to Singh et al. [1] structural changes in the cathode occur at the transition sites, which causes subsequent intercalation to occur at other sites [1]. For cell (1) discharged at 20 µA, the measured OCV was 1.17 V. For cell (2), the measured OCV was 1.15V. For cell (3), the measured OCV was 1.19.

The variation of OCV against temperature for Cell (1) before and after discharge is shown in Fig. 7. The OCV of the cell after discharge is found to increase with temperature. Other reports [1,2,3] on thermodynamic properties of cells showed similar results of linear dependence of the OCV on the temperature. Before discharge, the OCV of the battery increased with the temperature from 1.17 V at room temperature to 1.25 V at 150°C. The OCV of the cell is lower after discharge at all temperatures compared to the OCV of the cell before

discharge. According to Singh et al. [1], this behaviour of the cell is the result of intercalation which caused stoichiometry and structural changes in the cathode.

The values of dE /dT calculated from the slope of the straight line graphs for cell 1 in Fig. 7 was used to obtain d*G,* d*H*, and E_H. The values of these parameters are shown in Fig. 8(a), (b) and (c) respectively. The increase in Gibb's free energy of formation with increase in temperature indicates that the thermodynamic stability of the system increases with temperature [5]. The variation of thermal properties with temperature is shown in Fig. 8. The change in entropy after discharge is greater than the change in entropy before discharge in the temperature range between 20ºC to 100ºC. From Fig. 8, it can be observed that the enthalphy and thermoneutral potential of the battery before discharge is negative and positive respectively implying that the chemical reaction is exothermic while for the battery which was allowed to discharge, the enthalphy is positive and the thermoneutral potential becomes negative indicating that the chemical reaction is endothermic.

For all the three cells, the increase in OCV with temperature is governed by the thermodynamics of the cell. As the cells Zn/MnO_2 and Zn/MnO_2: V_2O_5 were put to discharge, the electrochemical reaction changes from exorthermic to endothermic.

Conclusions

Based on the results on battery characterization obtained, $LiI\text{-}Li_2WO_4\text{-}Li_3PO_4$ solid electrolyte prepared at low sintering temperature is applicable to solid state Zn/metal oxide cells. This shows that a number of metals including Zn can be used as the anode in a solid state cell using lithium based electrolyte. Among the various types of cells investigated, Cell (3) showed the best performance at room temperature as Cell (3) exhibits the longest continuous discharge time and the highest OCV. The main cathode materials in Cell (3) is a mixture of V_2O_5 and MnO_2.

Results on the thermodynamics parameters of the cells confirmed the nature of the chemical reaction that takes place inside the battery during the discharge process. The change in OCV with temperature before discharge indicates that some exothermic reactions have taken place and after discharge some endothermic reactions have occurred to increase the OCV of the cell.

Reference

1. K. Singh, S.S. Bhoga, N.H. Thorat, Solid State Ionics 86-88 (1996) 931-934
2. H. F. Gibbard, J. of Electrochem. Soc. 126 (1978) 513
3. C.R. Schlaikjer and N. Marinsic, J. Electrochem. Soc. 126 (1979) 513
4. L.A. Zabdyr, J. Electrochem. Soc. 131 (1984) 2157
5. S.K. Mittal and J.F. Elliott, J. Electrochem. Soc. 131 (1984) 1194
6. W.O. George and P. S. Mc Intyre, in Infrared Spectroscopy, D. J. Mowthorpe (ed), John Wiley & Sons (1990)
7. K. Singh, P. Ambekar and S.S. Bhoga, R.U. Tiwari in Solid State Ionics: Trends in the new millennium, B.V.R. Chowdari, S.R.S. Prabaharan, M. Yahaya (eds), World Scientifics Publishing Co. (2002) 177-184
8. L. Telli, A. Hammouche, B. Brahimi, R.W. De Donker, J. Power Sources 103 (2002) 201-206
9. C.Q. Zhang and X.G. Zhang, Solid State Ionics160 (2003) 155-159
10. N. Laksmi and S. Chandra, J. Power Sources 108 (2002) 256-260
11. V. Klasons in " Handbook of batteries", D. Linden (ed), McGraw –Hill, Inc, New York (1995) 22.1-22.22
12. A. Nasar, J. of Alloys and Compounds 217 (1995) 167-175

Figure Captions:

Fig. 1: Schematic representation of fabricated cell.

Fig. 2: FTIR spectra of pure Li_3P0_4 and samples with various wt. % of Li_3P0_4 with wave number in the range 1380-1580 cm^{-1}

Fig. 3: FTIR spectra of pure Li_3P0_4 and samples with various wt. % of Li_3P0_4 with wave in the range 2800-3900

Fig. 4: Discharge characteristics curve for Zn+C / LiI-$LiWO_3$-Li_3PO_4 / MnO_2+C cell at room temperature

Fig. 5: Discharge characteristics curve for Zn+C / LiI-$LiWO_3$-Li_3PO_4 / MnO_2+C cell at room temperature and at 100 C

Fig. 6: Discharge characteristics curve for cells having the same zinc anode but different types of cathode at room temperature. V=V_2O_5, M=MnO_2

Fig. 7: Variation of OCV with temperature for Zn+C / LiI-$LiWO_3$-Li_3PO_4 / MnO_2+C cell before and after discharge

Fig. 8: (a) Change in Gibb's free energy (d*G*) versus temperature for Zn/MnO_2 cell
(b) Change in enthalphy (d*H*) versus temperature for Zn/MnO_2 cell
(c) Thermoneutral potential (E_H) versus temperature for Zn/MnO_2 cell

Fig. 1

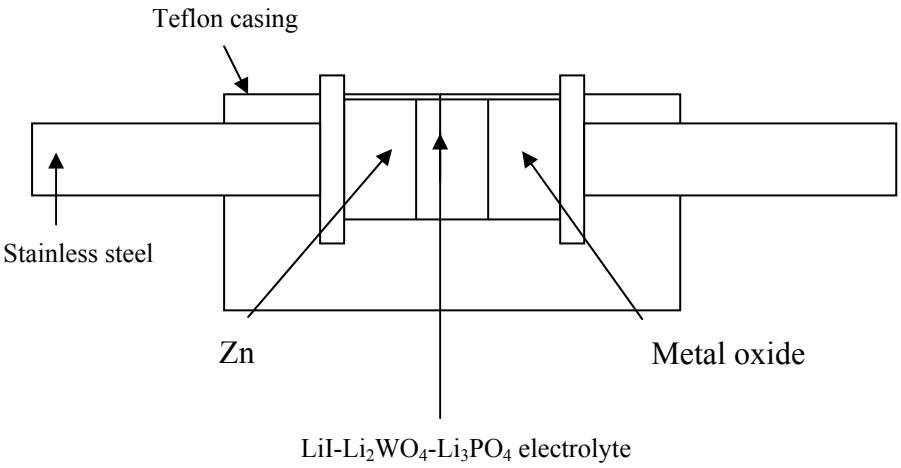

Fig. 2

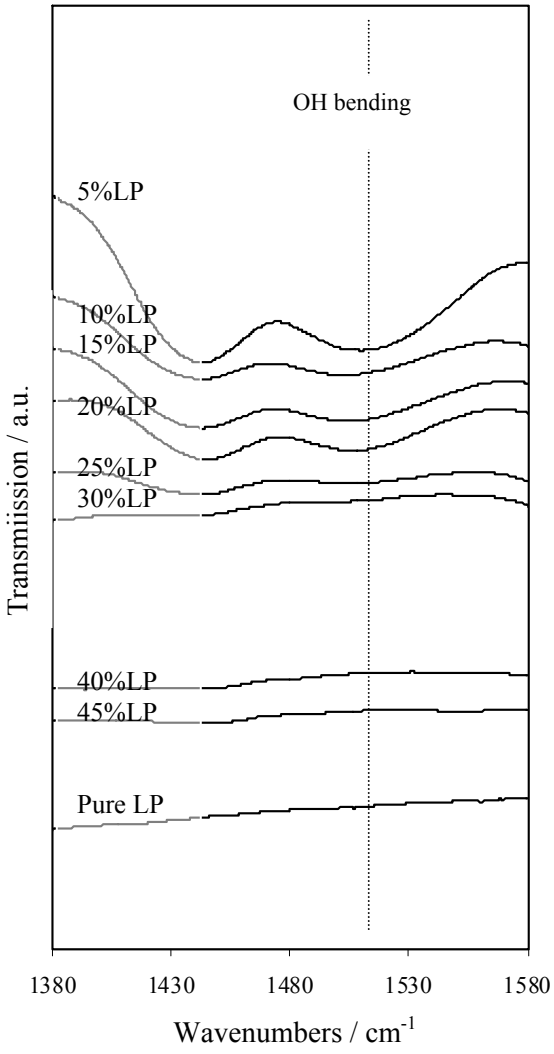
OH bending
5%LP
10%LP
15%LP
20%LP
25%LP
30%LP
40%LP
45%LP
Pure LP
Transmiission / a.u.
1380
1430
1480
1530
1580
Wavenumbers / cm-1

Fig. 3

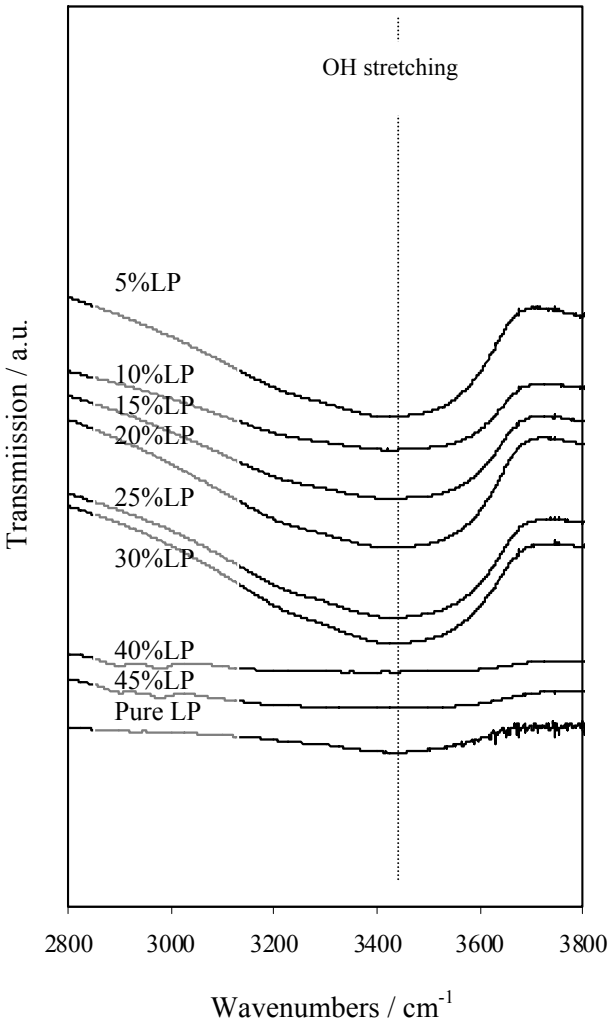
OH stretching
5%LP
10%LP
15%LP
20%LP
25%LP
30%LP
40%LP
45%LP
Pure LP
Transmiission / a.u.
2800
3000
3200
3400
3600
3800
Wavenumbers / cm-1

Fig. 4

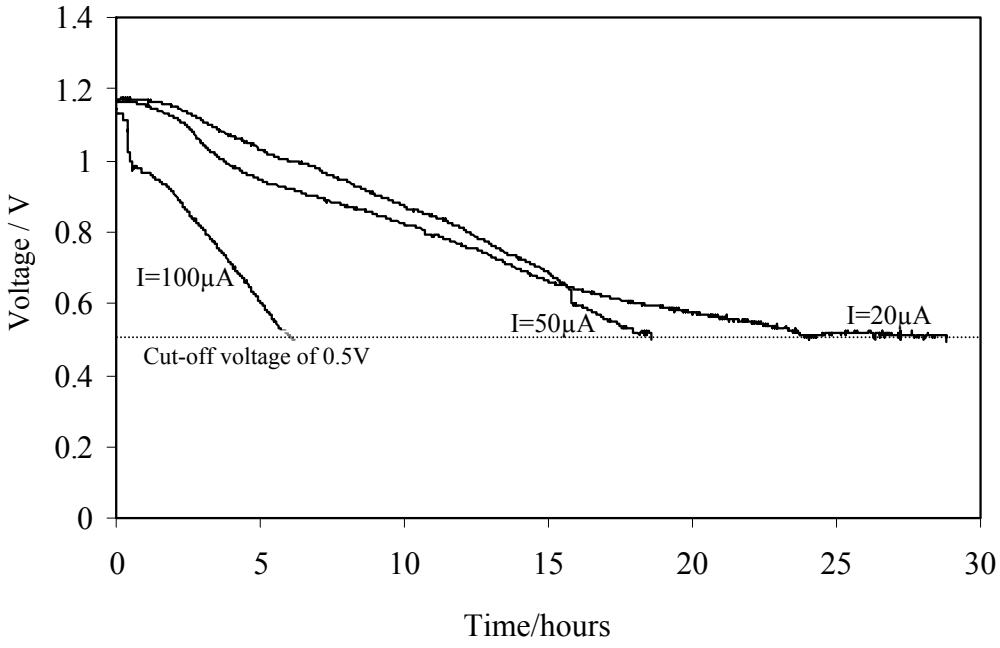
1.4
1.2
1
0.8
0.6
0.4
0.2
0
Voltage / V
I=100µA
I=50µA
I=20µA
Cut-off voltage of 0.5V
0
5
10
15
20
25
30
Time/hours

Fig.5

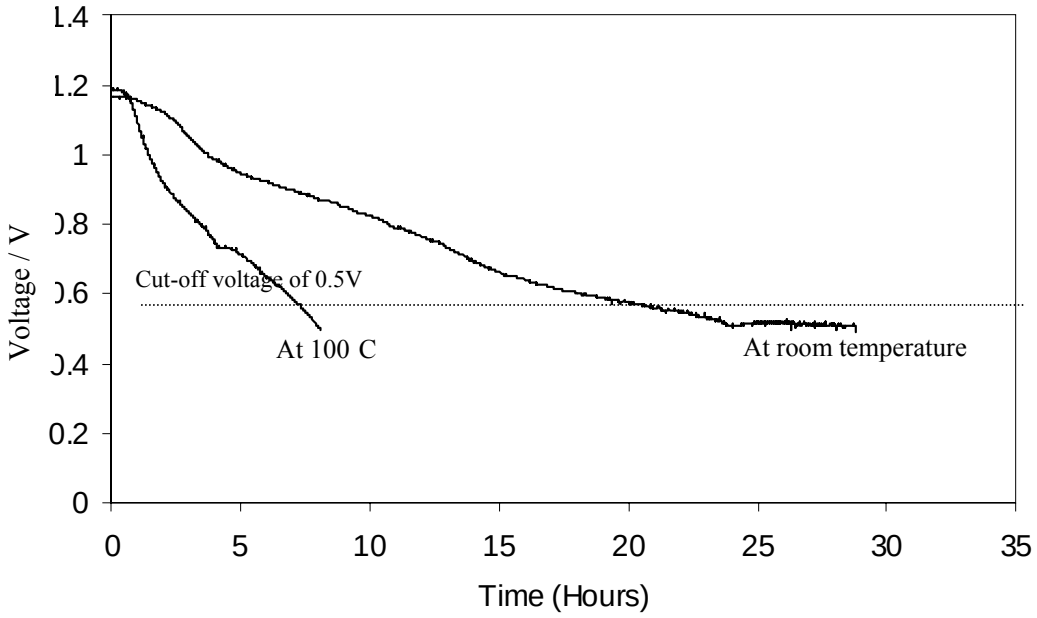
1.4
1.2
1
0.8
0.6
0.4
0.2
0
Voltage / V
Cut-off voltage of 0.5V
At 100 C
At room temperature
0
5
10
15
20
25
30
35
Time (Hours)

Fig. 6

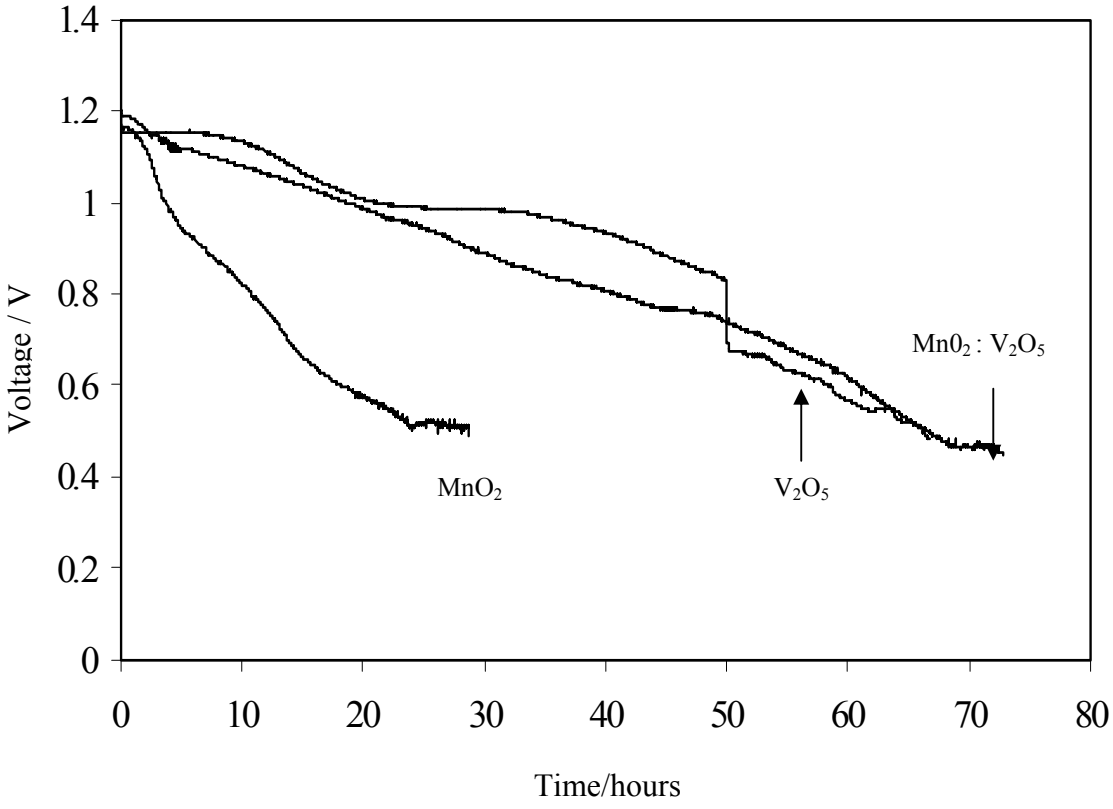
1.4
1.2
1
0.8
0.6
0.4
0.2
0
Voltage / V
0
10
20
30
40
50
60
70
80
Time/hours
MnO_2
V_2O_5
$Mn0_2 : V_2O_5$

Fig. 7

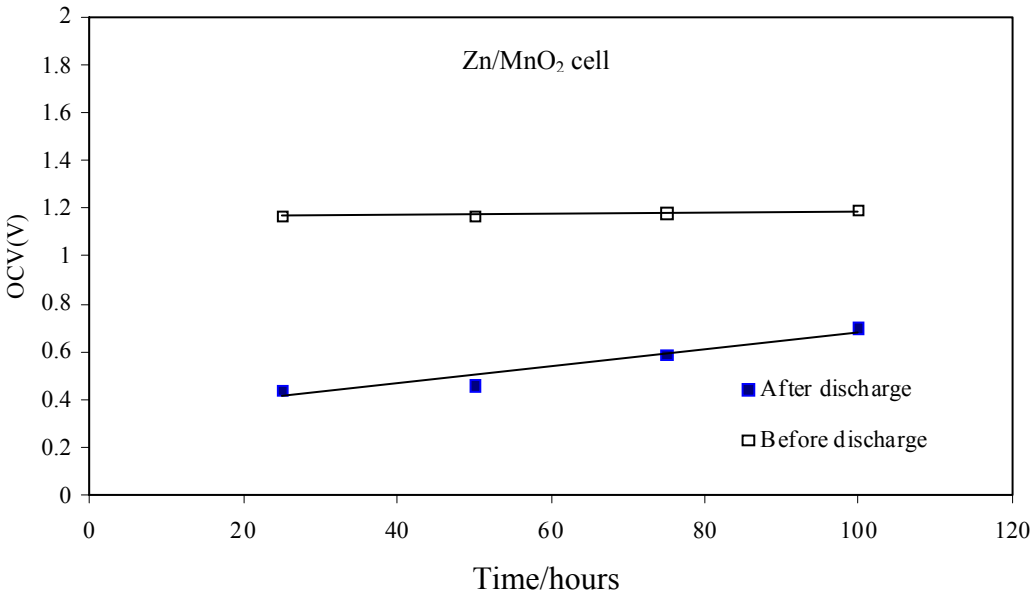
Zn/MnO2 cell
OCV(V)
Time/hours
After discharge
Before discharge
0
0.2
0.4
0.6
0.8
1
1.2
1.4
1.6
1.8
2
0
20
40
60
80
100
120

Fig. 8

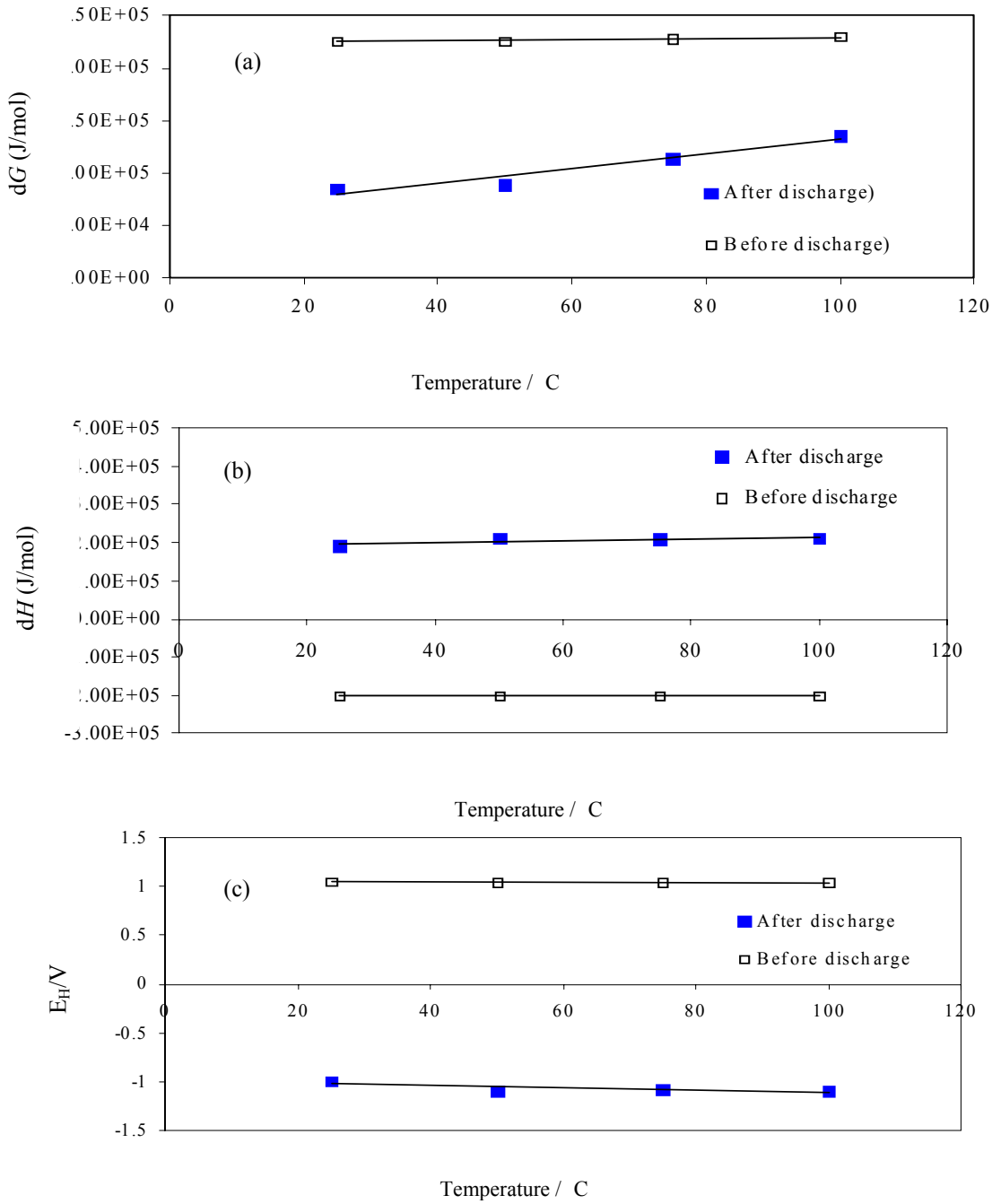
(a)
dG (J/mol)
.50E+05
.00E+05
.50E+05
.00E+05
.00E+04
.00E+00
0
20
40
60
80
100
120
After discharge)
Before discharge)
Temperature / C
(b)
dH (J/mol)
.00E+05
.00E+05
.00E+05
.00E+05
.00E+00
.00E+05
.00E+05
-5.00E+05
After discharge
Before discharge
Temperature / C
(c)
E_H/V
1.5
1
0.5
0
-0.5
-1
-1.5
After discharge
Before discharge
Temperature / C

Malaysian Journal of Analytical Sciences, Vol.9, No. 3(2005): 418 - 425

TURBULENCE MODELING IN THE RISER OF A CIRCULATING FLUIDIZED BED USING CFD SOFTWARE

Ahmad Hussain[1, *], Farid Nasir Ani[1], Amer Nordin Darus[1], Zainal Ahmad[1] and Azeman Mustafa[2]

[1]*Faculty of Mechanical Engineering, Universiti Teknologi Malaysia, Skudai, 81310, Johor, Malaysia*
[2]*Faculty of Chemical and Natural Resources Engineering, Universiti Teknologi Malaysia, Skudai, 81310, Johor, Malaysia*

*Corresponding author. Phone: +607-5534785, Fax: +607-5566159
Email: ahmad@siswa.utm.my

Abstract

For the last few decades, Circulating Fluidized Bed Combustion (CFBC) technology is being used to burn biomass waste while meeting stringent emission requirements for control of SO_2 and NO_x emission. However, complex flow patterns are encountered when heat, mass and momentum heat transfer are interlinked which in turn controls the SO_2 and NO_x emissions. 2D simulations were done using FLUENT Ver. 6.1, a CFD package by Fluent Inc. Sand particles and air were used as fluidizing materials. The results discuss the turbulent flow behaviour using k-ε turbulence model. The simulations show that velocity profiles along the riser height are influenced by the exit geometry. The riser exits clearly showed the regions of flow separation and reattachment. The increased turbulence was also reported in riser exits and connector, which in turn yields lower SO_2 and NO_x emissions.

Abstrak

Pada beberapa tahun kebelakangan, teknologi pembakaran lapisan terbendalir pengedaran (CFBC) telah digunakan untuk membakar bahan buangan biojisim dan pada masa yang sama memenuhi keperluan piawai yang ketat bagi pengawalan pelepasan SO_2 dan NO_x. Walau bagaimanapun, pengudaran udara yang kompleks bertemu apabila haba, jisim dan momentum pengaliran haba dikaitkan yang mana dapat mengawal pelepasan SO_2 dan NO_x. Simulasi 2D telah diperolehi dengan menggunakan perisian FLUENT Ver. 6.1, sebuah pekaj perisian CFD daripada Fluent Inc. Campuran butiran pasir dan udara digunakan sebagai agen terbendalir. Keputusan eksperimen membincangkan pengaliran gelora dengan menggunakan model gelora k-ε. Simulasi menunjukkan profil halaju pada ketinggian corong dipengaruhi oleh bentuk geometri pada bahagian keluaran. Bahagian keluaran corong menunjukkan dengan jelas kawasan aliran pemisahan dan pencantuman semula. Didapati bahawa terdapat peningkatan aliran gelora pada bahagian keluaran corong dan penghubung, dimana akan menghasilan pelepasan SO_2 dan NO_x yang rendah.

Keywords: CFBC, CFD, flow separation, FLUENT, turbulence, velocity profiles.

Introduction

Most flows of engineering importance in fluid mechanics and heat transfer are almost turbulent; this means the fluid motion is highly random and unsteady [1].

Turbulence is a natural phenomenon in fluids that occurs when velocity gradients are high, resulting in disturbances in the flow domain as a function of space and time [2].

Although turbulence has been the subject of intensive study for the past century, it appears that many difficulties still remain unresolved, particularly in flows with high Reynolds numbers. It is important to gain a clear understanding of the nature of the turbulent flow [3].

The k-ε model is still widely used in industry for flows in realistic geometries. The application of turbulent flows in power industry has encouraged the development of general purpose CFD codes applicable to complex geometries and efficient turbulent modeling tools. Today general purpose widely used CFD codes all use the k-ε model. The two equation model of turbulence states that Reynolds stresses are proportional to strain rate of the mean flow and

the proportionality factor which is automatically computed by solving two transport equations for turbulent kinetic energy k and dissipation rate ε. [4]

CFB used for Simulation

Figure 1 shows the schematics of the CFB used for simulation. The system consists of an air supply device (blower), a distributor of stainless steel, a fast column of Plexiglas and primary and secondary cyclones of steel and a solid feeding system. The riser and its exit are made of Plexiglas to see the flow behaviour and to perform image analysis

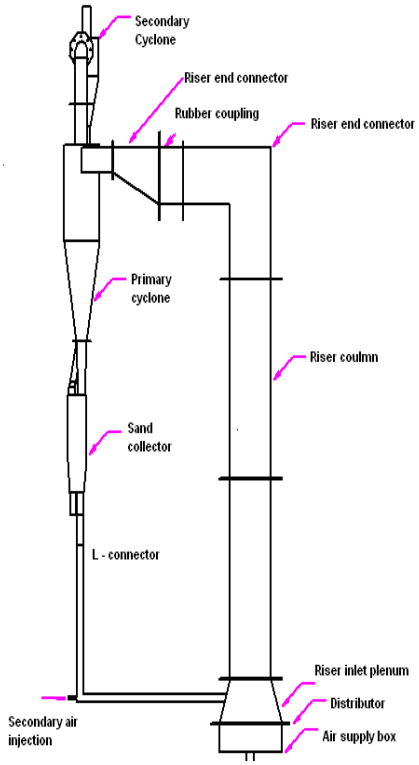

Figure 1. CFB Test Rig at UTM

The simulation work described here was done on a riser of rectangular cross-section of 265 (width) x 72 (depth) x 2649 (height) mm^3. The operating parameters were chosen to so give dynamical similarity with a large CFBCs. Simulation was done using FLUENT 6.1, a computational fluid dynamics (CFD) package by Fluent Inc. [5]. Sand particles and air were used as the solid and gas phases, respectively. The parameters used in the simulation work are summarized in the Table 1.

Table 1: Parameters used in simulation work

Parameter	Range of values
Gas velocity (ms^{-1})	5
Particle velocity (ms^{-1})	2 m/s
Properties of air	Density: 1.225 kg m^{-3} Viscosity: 1.79 x 10^{-5} kg/m.s
Properties of particle (sand)	Density: 2500 kg m^{-3} Diameter: 100X 10^{-6} m
Exit Geometries Simulated	Right angel exit, right angle exit with baffle and
Volume fraction of sand	0.03
Multiphase model	Eulerian granular multiphase model

Eulerian multiphase mixture model

The FLUENT modeling is based on the three-dimensional conversation equations for mass, momentum and energy. The differential equations are discretized by the Finite Volume Method and are solved by the SIMPLE algorithm. As a turbulence model, the k-ε was employed; this consists of two transport equations for the turbulent kinetic energy and its dissipation rate. The FLUENT code utilizes an unstructured non-uniform mesh, on which the conservation equations for mass, momentum and energy are discretized. The k-ε model describes the turbulent kinetic energy and its dissipation rate and thus compromises between resolution of turbulent quantities and computational time.

Table 2: List of FLUENT Models used in simulation

Model	Settings
Space	2D
Time	Steady
Viscous	Standard k-epsilon turbulence model
Wall Treatment	Standard Wall Functions
Multiphase Model	Eulerian
Body forces	Enabled

In the FLUENT computer program that the governing equations were discretized using the finite volume technique. The discretized equations, along with the initial and boundary conditions, were solved to obtain a numerical solution.

The model used for simulating the gas-solid flow is the Eulerian Multiphase Mixture Model (EMMM). The EMMM solves the continuity equation for the mixture, the momentum equation for the mixture, and the volume fraction equation for the secondary phase, as well as an algebraic expression for the relative velocity.
By using the mixture theory approach, the volume of phase q, V_q is defined by

$$V_q = \int_V \alpha_q \, dV$$

and

$$\sum_{q=1}^{n} \alpha_q = 1$$

The effective density of phase q is $\hat{\rho} = \alpha_q \, \rho_q$

Where ρ_q is the physical density of phase

I.Conservative Equations

The general conservation equations from which the solution is obtained by FLUENT are being presented below:

II.Conservation of mass

The continuity equation for phase q is

$$\frac{\partial}{\partial t}(\alpha_q \rho_q) + \nabla.(\alpha_q \rho_q \vec{v}_q) = \sum_{p=1}^{n} \dot{m}_{pq}$$

where $\vec{v}_q$ is the velocity of phase q and $\dot{m}_{pq}$ characterizes the mass transfer from the pth to qth phase.

From the mass conservation we can get:

$$\dot{m}_{pq} = - \dot{m}_{qp}$$

and

$$\dot{m}_{pp} = 0$$

Usually, the source term ($\sum_{p=1}^{n} \dot{m}_{pq}$) on the right hand side of equation is zero.

III.Conservation of Momentum

The momentum balance for phase q yields

$$\frac{\partial}{\partial t}(\alpha_q \rho_q \vec{v}_q) + \nabla.(\alpha_q \rho_q \vec{v}_q \vec{v}_q) = -\alpha_q \nabla p + \nabla.\bar{\tau}_q + \alpha_q \rho_q \vec{g} + \sum_{p=1}^{n} \left(\vec{R}_{pq} + \dot{m}_{pq} \vec{v}_q\right) + \alpha_q \rho_q (\vec{F}_q + \vec{F}_{lift,q} + \vec{F}_{vm,q})$$

Where $\bar{\tau}_q$ is the qth phase stress-strain tensor.

$$\bar{\tau}_q = \alpha_q \mu_q (\nabla \vec{v}_q + \nabla \vec{v}_q^{\,T}) + \alpha_q (\lambda_q - \frac{2}{3}\mu_q) \nabla.\vec{v}_q \bar{I}$$

Here μ_q and λ_q are the shear and bulk viscosity of phase q, $\vec{F}_q$ is an external body force. $\vec{F}_{lift,q}$ is a lift force, $\vec{F}_{vm,q}$ is a virtual mass force, $\vec{R}_{pq}$ is an interaction force between phases, and p is the pressure shared by all phases.

$\vec{v}_q$ is the interphase velocity and I can be defined as follows.

If $\dot{m}_{pq} > 0$ (i.e., phase p mass is being transferred to phase q), $\vec{v}_{pq} = \vec{v}_p$;

If $\dot{m}_{pq} < 0$ (i.e., phase q mass is being transferred to phase p), $\vec{v}_{pq} = \vec{v}_q$;

and $$\vec{v}_{pq} = \vec{v}_{qp}$$

The above equation must be closed with appropriate expressions for the interphase force $\vec{R}_{pq}$. This force depends on the friction, pressure, cohesion, and other effects, and is subject to the conditions that

$$\vec{R}_{pq} = -\vec{R}_{qp} \text{ and } \vec{R}_{qq} = 0$$

FLUENT uses the following form:

$$\sum_{p=1}^{n} \vec{R}_{pq} = \sum_{p=1}^{n} K_{pq} (\vec{v}_p - \vec{v}_q)$$

Where $K_{pq} = K_{qp}$ is the interphase momentum exchange coefficient.

Turbulence model

In order to account for the effects of turbulent fluctuations of velocities the number of terms to be modeled in the momentum equations in multiphase is large and this makes the modeling of turbulence in multiphase simulations extremely complex. The turbulence model used for the current simulations is based on Mixture Turbulence Model (MTM). The κ and ε equations describing this model are as follows:

$$\frac{\partial}{\partial t}(\rho_m \kappa) + \nabla . (\rho_m \vec{v}_m \kappa) = \nabla . \left(\frac{\mu_{t,m}}{\sigma_\kappa} \nabla \kappa \right) + G_{\kappa,m} - \rho_m \varepsilon$$

and

$$\frac{\partial}{\partial t}(\rho_m \varepsilon) + \nabla . (\rho_m \vec{v}_m \varepsilon) = \nabla . \left(\frac{\mu_{t,m}}{\sigma_\varepsilon} \nabla \varepsilon \right) + \frac{\varepsilon}{\kappa} (C_{1\varepsilon} G_{\kappa,m} - C_{2\varepsilon} \rho_m \varepsilon)$$

Where the mixture density and velocity, ρ_m and $\vec{v}_m$, are computed from:

$$\rho_m = \sum_{i=1}^{N} \alpha_i \rho_i$$

$$\vec{v}_m = \frac{\sum_{i=1}^{N} \alpha_i \rho_i \vec{v}_i}{\sum_{i=1}^{N} \alpha_i \rho_i}$$

The turbulent viscosity, $\mu_{t,m}$, is computed from:

$$\mu_{t,m} = \rho_m C_\mu \frac{\kappa^2}{\varepsilon}$$

and the production of turbulence kinetic energy, $G_{k,m}$, is computed from

$$G_{\kappa,m} = \mu_{t,m} (\nabla \vec{v}_m + (\nabla \vec{v}_m)^T) : \nabla \vec{v}_m$$

Boundary conditions

At the inlet, all velocities and volume fractions of both phases are specified. The pressure is not specified at the inlet because of the incompressible gas phase assumption (relatively low pressure drop system). The initial velocity of gas and solid phase is being specified as mentioned in Table 1.

The meshing was done using Gambit 1.2. Fine meshing was done for riser inlet and exit sections in order to analyze them in a better way. Under relaxation factors were tuned to achieve convergence. The convergence tolerance was set at 0.001.

The main parameters of the flow inside the system are calculated using an iteration calculation procedure performed by FLUENT. An iterative cycle starts with the introduction of the initial data and/or initial guessed values, boundary conditions, physical conditions and constants. In a second step the program calculate the velocity field from the momentum equation. Then, the mass balance equations as well as the pressure equation are solved.

The next step is to update again the values of the parameters for both phases. The final step is to check on convergence which criterion is fixed by the user. If the convergence criterion is achieved the simulation will stop and give the final results of the system. If not, certain correction values are used to adjust the calculated values and the calculation will start all over again, using as initial data these last corrected values of each parameter.

The coefficient of restitution quantifies the elasticity of particle collisions. It has a value of 1 for fully elastic collisions and 0 for fully inelastic collisions. It is utilized to account for the loss of energy due to collision of particles, which is not considered in the classical kinetic theory. **T**he restitution coefficient is close to unity. In this study, a particle-particle restitution coefficient of 0.95, and a particle-wall restitution coefficient of 0.9 were used [6].

Results and disscussions

A gross behaviour of a CFB is being presented here. Inward/outward motion, secondary flows of the first kind, tangential acceleration/deceleration, and cavity formation near riser exits is mechanisms can account for asymmetric flow in the exit region.

If more solids accumulate near the riser exit then fewer solids reside in the return leg. The lower rate of solids circulation may cause the solids volume fraction in the riser and connector to be lower. However, if the solids accumulation near the riser exit extends into these components, the solids volume fraction may be larger.

Figure 2 indicates that a right angle exit with internal baffle and a blind T riser exits show that the solids volume fraction is more or less constant in the lower half of the riser. In the upper half, a strong increase of solids volume fraction with elevation was observed for the blind T exit, whereas a decrease is found for the right angle exit with the internal baffle. The size and shape of the upstream exit region is strongly dependent on the design of the riser exit.

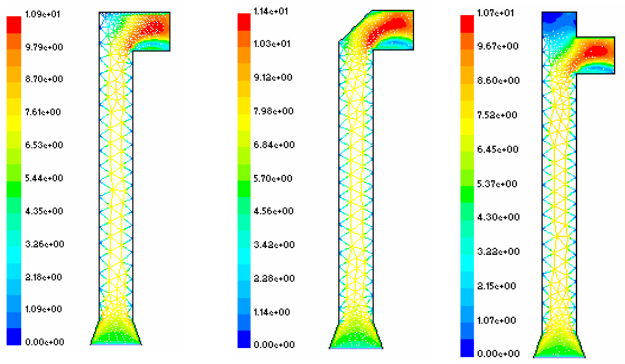

Figure 2. Contours of velocity profile in exit geometries

From Figure 3, it can be inferred that the turbulence is more pronounced in the right angled and baffled exits. The blind T exit accumulated more solids than the right angle exit, and yielded a higher solids volume fraction in the riser. The solids hold-up is greater for the exit with baffle. The blind T exit shows larger solids volume fractions along the entire riser height, and an increase of solids volume fraction with elevation in the upper half of the riser.

The solids volume fraction remains constant near the exit with internal baffle, but show an increase with elevation in the upper half of the riser for the right angle exit and blind T exit. The slip distribution in the various exits are different with right angle exit and with baffle showing greater slip than blind T exit.

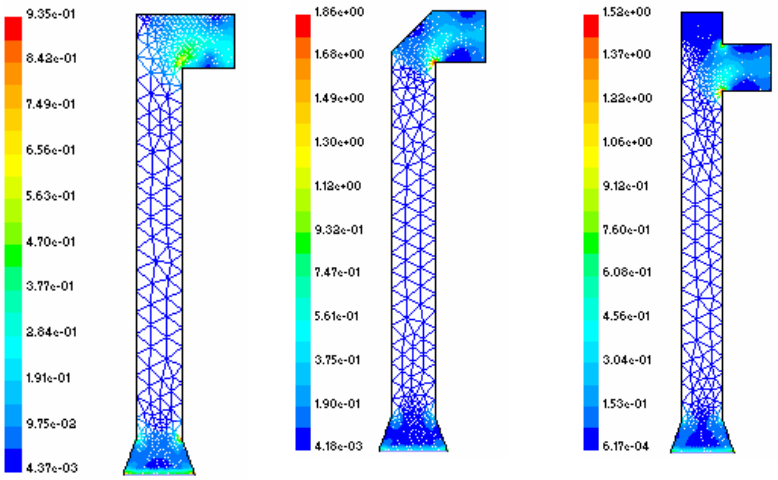

Figure 3. Contours of slip velocity

All the above investigations suggest that riser exits can reduce solids hold-up in the riser and yield a region upstream where the solids volume fraction decreases with elevation. Riser exits yield an apparently unaffected solids volume fraction profile or increased solids hold-up and invoke a region where the solids volume fraction increases with elevation.

CONCLUSIONS

All the above investigations suggest turbulence in the riser as well its exits can reduce solids hold-up in the riser. Riser exits yield an apparently unaffected solids volume fraction profile or increased solids hold-up and invoke a region where the solids volume fraction increases with elevation. This suggests an upstream exit region to be

defined as the region upstream of the riser exit where flow properties are affected by the riser exit. Similarly, a downstream exit region can be defined as the region downstream of the riser exit where flow properties are affected by the riser exit. The (overall) exit region is the region of the CFB where flow properties are affected by the riser exit, and comprises the upstream exit region, downstream exit region and the riser exit itself. The upstream exit region is generally characterized by a Core/Annulus structure, but that the solids mass flux profile may be asymmetric. Some riser exits appear to invoke regions near the riser wall where solids motion is upwards.

References

[1] Wan M. N. (1987). Numerical Prediction of Turbulent flow using k-**ε** Model. *Universiti Teknologi Malaysia.*

[2] Chung T. J. (2002). Computational Fluid Dynamics. Cambridge University Press, UK.

[3] Taghipour, F., Ellis, N. & Clayton, W. (2003). CFD Modeling of a two-dimensional Fluidized Bed Reactor, University of British Columbia.

[4] Hirch C., Periaux J. and Onate E. (1992) Computational methods in Applied Sciences. Elsevier Science Publishers, Amsterdam, The Netherlands.

[5] Fluent 6.1, (2001). User's guide. Fluent Incorporated, USA.

[6] Weinstein, H, H.J. Feindt, L. Chen, R.A. Graff (1992). The measurement of turbulence quantities in a high velocity fluidized bed. *Proceedings of 7th International Conference on Fluidization,* O.E. Potter, D.J. Nicklin (eds), Engineering Foundation, NY, 305 - 312.

Malaysian Journal of Analytical Sciences, Vol.9, No. 3(2005): 426 - 433

PENCEMARAN LOGAM BERAT DI DALAM AIR TASIK DAN SEPANJANG SUNGAI PELEPAH KANAN DI KAWASAN BEKAS LOMBONG BIJIH BESI, TIMAH DAN TEMBAGA DI KOTA TINGGI, JOHOR

Wan Mohd Razi Idris, Sahibin Abdul Rahim, Tukimat Lihan, *Baba Musta, *Adong Laming, Azman Hashim, Shahril Nizam Mohd Yusuf dan Leanor Valerie Anyi

Program Sains Sekitaran, Pusat Pengajian Sains Sekitaran dan Sumber Alam
Fakulti Sains dan Teknologi, Universiti Kebangsaan Malaysia
43600 Bangi, Selangor.

*Jabatan Geologi, Sekolah Sains dan Teknologi, Universiti Malaysia Sabah
Beg Berkunci 2073, 88999 Kota Kinabalu, Sabah

ABSTRAK

Kajian yang dijalankan ini bertujuan untuk melihat pencemaran kandungan logam berat di dalam tasik dan di sepanjang Sungai Pelepah Kanan yang terdapat di sekitar kawasan bekas lombong bijih besi, timah dan tembaga di Kota Tinggi, Johor. Sebanyak 7 stesen persampelan air di ambil di dalam tasik bekas lombong dan di sepanjang Sungai Pelepah Kanan. Parameter analisis yang ditentukan melibatkan penentuan Suhu, pH, kekonduksiaan elektrik, oksigen terlarut, peratus ketepuan bes dan kepekatan enam jenis logam berat iaitu Fe, Cd, Cu, Mn, Co dan Zn. Hasil kajian menunjukkan paras kepekatan logam berat yang dikaji adalah melebihi paras minimum bagi Piawaian Interim Kualiti Air Kebangsaan Negara Malaysia (INWQS) dan melebihi had kualiti air minuman bagi Pertubuhan Kesihatan Sedunia (WHO) bagi kandungan logam berat seperti Cd di dalam air tasik iaitu 0.08 ± 0.01-0.07 ± 0.02 mg/I serta Fe, Mn dan Cd di dalam sungai Pelepah Kanan iaitu 0.31 ± 0.05-0.65 ± 0.04 mg/I, 0.29 ± 0.02-0.30 ± 0.02 mg/I dan 0.04 ± 0.01-0.11±0.11 mg/I. Pencemaran logam berat di kawasan ini tidak bercorak setempat iaitu di kawasan dalam dan sekitar lombong sahaja tetapi juga di sepanjang Sungai Pelepah Kanan akibat daripada luahan aktiviti perlombongan yang dijalankan

Kata kunci: logam berat, air, tasik, sungai, bekas lombong, Kota Tinggi

PENGENALAN

Aktiviti perlombongan bijih besi, timah dan tembaga di kawasan ini telah bermula semasa zaman Jepun lagi. Kawasan ini telah dilombong secara lombong dedah untuk mendapatkan bijih timah (Adong 2001). Topografi sebahagian besar dari kawasan ini adalah berbukit, mempunyai kawasan air terjun dan mengandungi banyak tebing curam di sekitarnya. Di kawasan ini terdapat dua tasik bekas lombong, salah satu daripadanya mengalir melalui susuh bukit yang memasuki Sungai Pelepah Kanan. Di dalam tasik tersebut terdapat hidupan akuatik seperti ikan, lumut dan rumpair. Aktiviti perlombongan seperti pemecahan, penggalian dan penimbunan pecahan batuan atau sisa tanih mendedahkan kepada tindakan air larian permukaan secara larut lesap, luluh larut dan hakisan (Jumaat 1992). Ini menyebabkan berlakunya ketoksikan sistem sungai dan air tanih menyebabkan kepekatan logam berat yang tinggi dalam jasad air. Efluen yang dihasilkan semasa proses pengekstrakan untuk mendapatkan bijih tembaga akan dibuang ke dalam sungai dan seterusnya mengakibatkan pencemaran air berlaku (Sengupta 1993). Kehadiran logam berat yang berlebihan di sekitaran sungai boleh mendatangkan kesan ketoksikan terhadap organisman bentos dan bentik serta manusia dan haiwan yang menggunakannya. Kajian ini cuba melaporkan paras kepekatan kandungan logam berat di dalam air tasik bekas lombong dan juga di sepanjang Sungai Pelepah Kanan akibat daripada aktiviti perlombongan yang dijalankan.

BAHAN DAN KAEDAH

Persampelan air dilakukan di tujuh stesen iaitu dua stesen di dalam bekas tasik lombong dan lima stesen di sepanjang sungai Pelepah Kanan. Persampelan air dilakukan sebanyak dua kali iaitu pada bulan Julai dan September. Stesen 1 dan 2 merupakan kawasan tasik bekas lombong, Stesen 3 ialah kawasan aliran sungai yang hampir dengan tasik, Stesen 4 ialah kawasan berdekatan dengan resort, Stesen 5 ialah kawasan rekreasi manakala stesen 6 dan tujuh merupakan kawasan berhampiran dengan ladang getah dan pertanian campur Semasa persampelan air sungai dan tasik beberapa parameter kualiti air diukur secara in situ. Parameter-parameter ini ialah Ph, suhu, kekonduksiaan elektrik dan kandungan oksigen terlarut diukur secara in situ. Kandungan oksigen terlarut ditentukan dengan menggunakan Dissolved Oxygen Meter Model YSI 56. Penentuan kandungan logam berat pada sampel-sampel yang telah diawet dengan menggunakan asid nitrik pekat dan dianalisis menggunakan kaedah nyalaan spectrometer serapan atom (Perkin Elmer Model 33100)

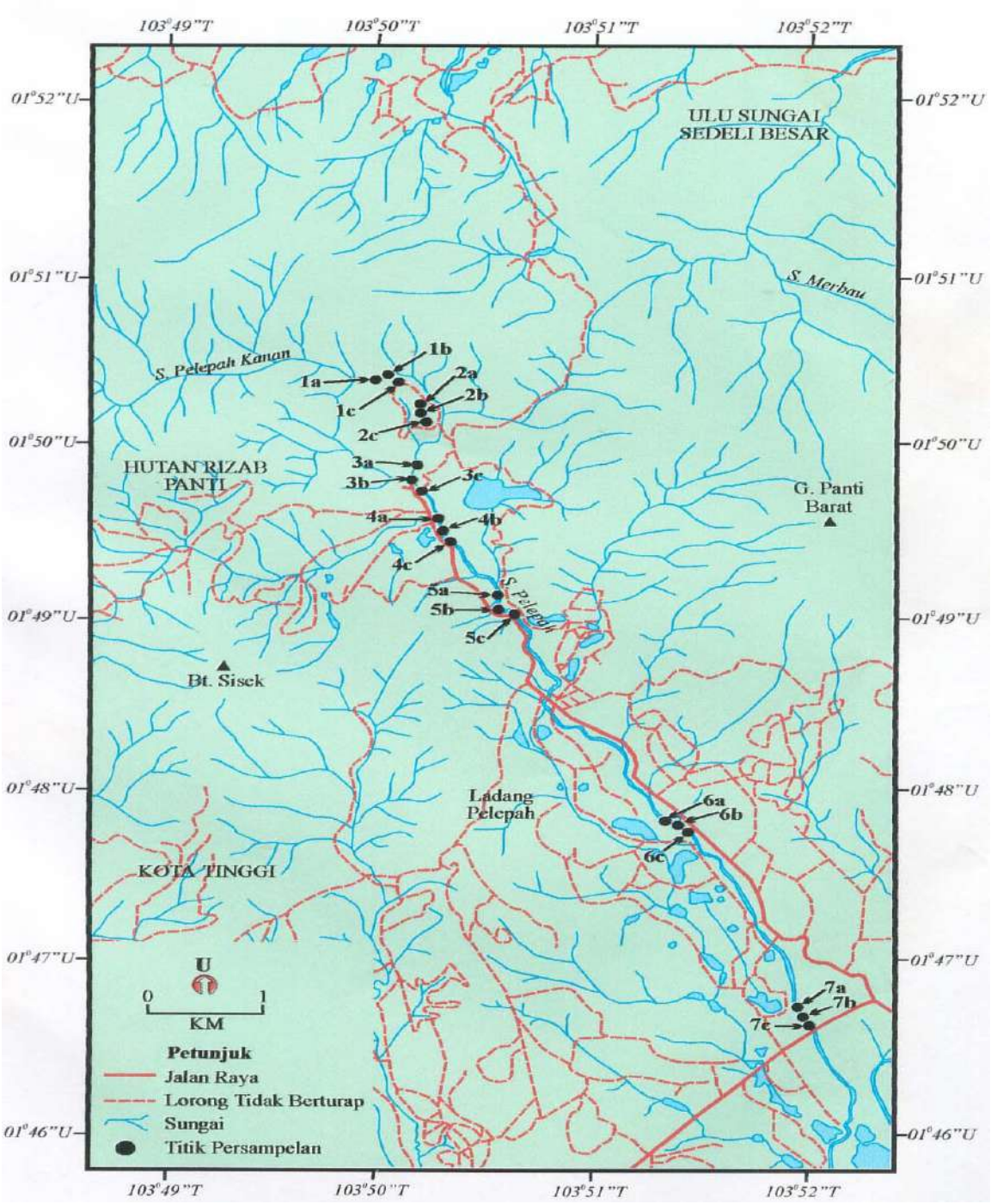

Rajah 1: Stesen persampelan air di kawasan bekas lombong di Kota Tinggi, Johor

HASIL DAN PERBINCANGAN

Parameter Suhu

Purata suhu bagi semua stesen persampelan seperti ditunjukkan di dalam Rajah 1, adalah memuaskan dan berada dalam julat 25°C-29°C. Suhu air di stesen 2 mencatatkan nilai suhu yang rendah iaitu 25°C manakala stesen 1 mencatatkan nilai suhu yang tinggi iaitu 29°C. Nilai yang tinggi pada stesen 1 adalah disebabkan oleh tasik bekas lombong yang terkepung, manakala stesen 2 merupakan air tasik yang mengalir mengikut susuh bukit ke Sungai Pelepah. Menurut Camp & Meserve (1970) suhu air akan lebih tinggi jika aliran air di dalam suatu sistem air tersebut perlahan. Suhu air di sepanjang Sungai Pelepah Kanan tidak banyak berbeza di antara satu sama lain. Suhu air sungai berubah mengikut waktu, keamatan sinar matahari dan kedalam sungai tersebut.

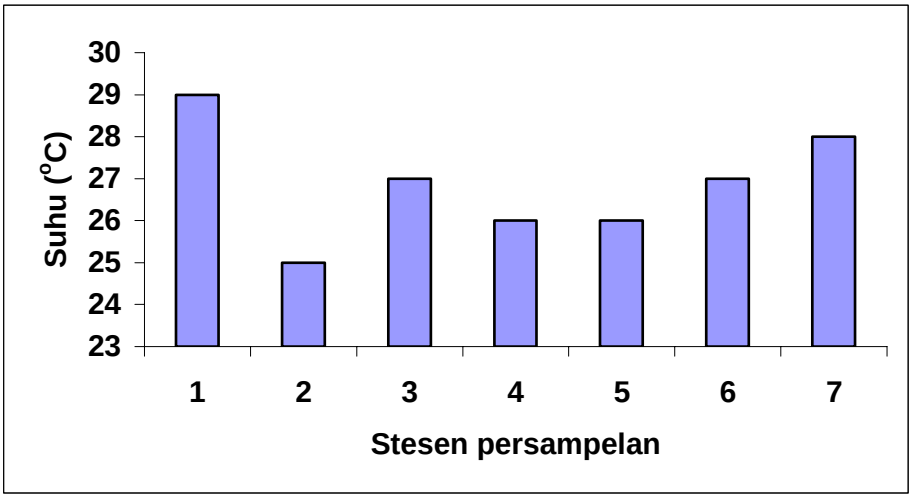

Rajah 1: Purata suhu bagi setiap stesen persampelan

Parameter pH

Purata pH bagi setiap stesen persampelan ditunjukkan dalam Rajah 2. Julat pH bagi semua stesen adalah di antara 6.8 hingga 6.13. Nilai pH tidak menunjukkan variasi yang ketara di antara air tasik bekas lombong dan Sungai Pelepah Kanan. Stesen 3 dan 6 mencatatkan purata pH yang tertinggi dan hampir neutral. Nilai ini memenuhi piawai interim yang disarankan bagi tujuan rekreasi iaitu 6.0-9.0 (Jabatan Alam Sekitar 1986). Nilai paling rendah adalah di stesen 5 iaitu merupakan kawasan rekreasi yang mungkin berpunca daripada pembuangan sampah sarap oleh

pengunjung di kawasan itu. Kawasan pertanian tidak banyak menunjukkan penurunan pH iaitu di stesen 6 dan 7.

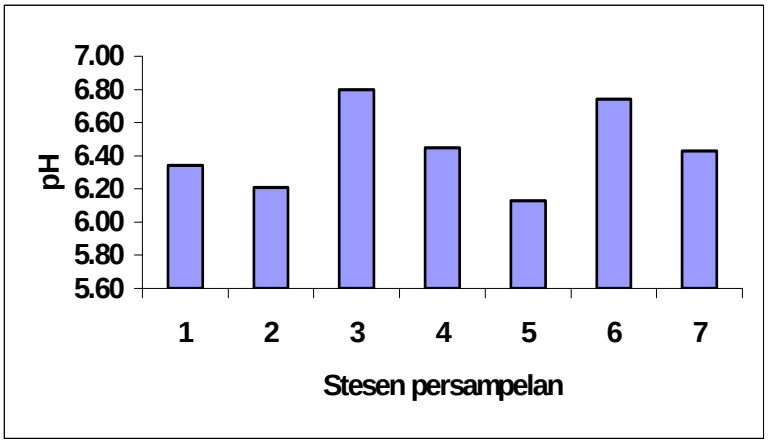

Rajah 2: Purata pH bagi setiap stesen persampelan

Parameter Oksigen Terlarut (DO)

Nilai purata oksigen terlarut (DO) di dalam air tasik bekas lombong dan Sungai Pelepah kanan ditunjukkan dalam Rajah 3. Di dapati nilai DO adalah berjulat di antara 3.95 mg/l hingga 5.75 mg/l. Nilai DO yang rendah adalah di stesen 1 iaitu 3.95 mg/l yang merupakan kawasan tasik bekas lombong. Nilai yang rendah ini mungkin dipengaruhi oleh suhu air yang tinggi di stesen tersebut. Keadaan sungai yang berjeram dan air yang deras juga dapat mempengaruhi nilai DO. Menurut Tolgyesssy (1993) sebarang pergerakan di permukaan air dapat meningkatkan DO. Stesen 3 mempunyai nilai DO yang tinggi disebabkan arusnya yang deras kerana berekatan dengan kawasan air terjun. Nilai DO bagi stesen 1 dan 2 bagi kawasan air tasik bekas lombong tergolong dalam kelas 3 bagi INWQS, manakala bagi dan stesen 3 hingga 7 bagi sepanjang Sungai Pelepah tergolong di dalam kelas 2 dan 3 bagi INWQS.

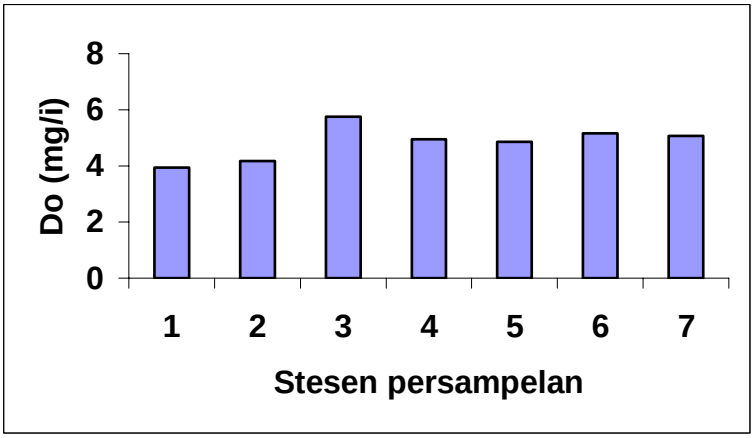

Rajah 3: Purata oksigen terlarut bagi setiap stesen persampelan

Parameter Kandungan Logam Berat

Kepekatan logam berat yang dikaji ditunjukkan dalam Rajah 4. Paras Kepekatan logam berat adalah melebihi paras minimum bagi Piawaian Interim Kualiti Air Kebangsaan Negara Malaysia (INWQS) dan dan melebihi had kualiti air minuman bagi Pertubuhan Kesihatan Sedunia (WHO) bagi kandungan logam berat seperti Cd di dalam air tasik iaitu 0.08 ± 0.01-0.07 ± 0.02 serta Fe, Mn dan Cd di dalam air sungai Pelepah Kanan iaitu 0.31 ± 0.05-0.65 ± 0.04mg/I, 0.29 ± 0.02-0.30 ± 0.02mg/I dan 0.04 ± 0.01-0.11±0.11mg/I. Pencemaran logam berat yang berlaku di kawasan ini tidak bercorak setempat iaitu di kawasan dalam dan sekitar lombong sahaja tetapi juga di sepanjang Sungai Pelepah Kanan akibat daripada luahan aktiviti perlombongan yang dijalankan. Manakala bagi stesen 6 dan 7 peningkatan Fe, Mn dan Cd mungkin berpunca daripada penggunaan baja untuk meningkatkan mutu dan kualiti tanaman sayur-sayuran.

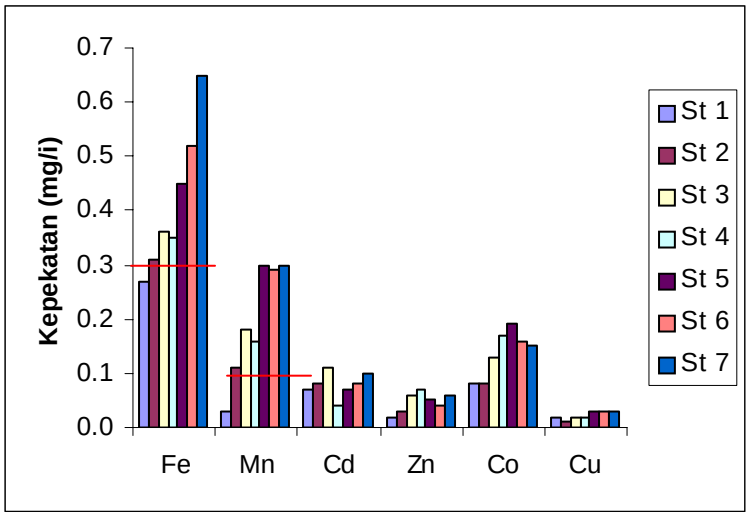

Rajah 4: Purata kandungan logam berat bagi setiap stesen persampelan

KESIMPULAN

- Pencemaran logam berat yang berlaku di kawasan ini tidak bercorak setempat iaitu di kawasan dalam dan sekitar lombong sahaja tetapi juga di sepanjang Sungai Pelepah Kanan.

- Aktiviti perlombongan yang dijalankan telah memberi kesan terhadap peningkatan kepekatan logam berat Fe, Mn dan Cd menyebabkan berlakunya pencemaran di sepanjang Sungai Pelepah Kanan manakala bagi unsur Cu, Co dan Zn di dalam air tasik dan di sepanjang Sungai Pelepah Kanan masih berada di bawah paras maksimum yang dibenarkan

.

PENGHARGAAN

Penulis ingin mengucapkan ribuan terima kasih kepada Kementerian Sains dan Teknologi di atas kurniaan peruntukan penyelidikan IRPA 09-02-02-0009-EA 064. Penghargaan juga ditujukan kepada Encik Fauzi Sayuti atas penggunaan alat AAS (Atomic Absorption Spectrophotometry) untuk penentuan kandungan logam berat di dalam air.

RUJUKAN

American Public Health Association, American Water Works Association & Water Pollution Control Federation. 1992. *Standard method for the examination of water and wastewater*. Washington: American Public Health Association

Adong Laming (2001). *Permineralan besi, timah dan tembaga di Lombong Air Terjun*, *Kota Tinggi, Johor.* Tesis Sarjana Muda Sains UKM.

Camp, T.R. & Meserve, R.L. 1974. *Water and its impurities*. Ed. Ke-2. United States of America: Dowden, Hutchinson & Ross, Inc.

Jumaat Salimon, 1992. Taburan logam berat di perairan sekitar lombong tembaga Mamut dan empangan Lohan. *Prosiding Simposium Sumber Alam Kebangsaan Pertama., Jil. 2 , 119-126*

Jabatan Alam Sekitar. 1986. *Executive Summary: water quality criteria and standards for Malaysia. Jil. 1*. Kuala Lumpur: Kementerian Sains, Teknologi dan Alam Sekitar.

Jabatan Alam Sekitar. 1998. Malaysia: *Laporan kualiti alam sekeliling*. Kuala Lumpur: Kementerian Sains, Teknologi dan Alam Sekitar.

Salomons, W & Forstner,U. 1984. Metal in the Hydrocycle. New York: Springer-Verlag.

Sengupta, M. 1993. *Environmental impact of mining*: monitoring, restorationand control. New York: Lewis Publishers

Tolgyesssy, J. 1993. *Chemistry and biology of water, air and soil*: environmental aspect. Chechoslovakia; Elsevier Science Publishers.

Malaysian Journal of Analytical Sciences, Vol.9, No. 3(2005): 434 - 443

KANDUNGAN LOGAM BERAT DALAM SEDIMEN TASIK BEKAS LOMBONG BIJIH BESI/TIMAH /TEMBAGA DAN SUNGAI PELEPAH KANAN DI KOTA TINGGI, JOHOR

Wan Mohd Razi Idris, Sahibin Abdul Rahim, Tukimat Lihan, *Baba Musta, *Adong Laming, Azman Hashim, Shahril Nizam Mohd Yusuf dan Leanor Valerie Anyi

Program Sains Sekitaran, Pusat Pengajian Sains Sekitaran dan Sumber Alam
Fakulti Sains dan Teknologi, Universiti Kebangsaan Malaysia, 43600 Bangi, Selangor.

*Jabatan Geologi, Sekolah Sains dan Teknologi, Universiti Malaysia Sabah
Beg Berkunci 2073, 88999 Kota Kinabalu, Sabah

ABSTRAK

Kajian ini dijalankan untuk menentukan kandungan logam berat yang terdapat di dalam sedimen tasik dan di sepanjang sungai Pelepah Kanan sekitar kawasan bekas lombong bijih besi, timah dan tembaga di Kota Tinggi, Johor. Sampel sedimen (0-20cm) telah diambil dari tujuh stesen persampelan. Parameter yang mempengaruhi pengayaan logam berat seperti taburan saiz partikel, pH dan peratus kandungan bahan organik (BOT) di dalam sedimen juga ditentukan. Kandungan logam berat ditentukan menggunakan teknik pendarflour sinar X (XRF). Hasil kajian menunjukkan nilai purata As, Cu, Cr, Co, Pb, Zn dan Ni di dalam sedimen tasik adalah masing-masing 162±2.52-218±25.93µg/g, 32±36.56 - 62±3.51µg/g, 11±2.51 - 216 ±11.5µg/g, 22 ± 4.04-70±43.92µg/g, 40 ± 11.5-49 ± 49.36µg/g, 56 ± 2-105 ± 50.12µg/g dan 6 ± 1.53-4 ± 1.73µg/g. Manakala purata kandungan As, Cu, Cr, Co, Pb, Zn dan Ni di dalam sedimen sungai adalah masing-masing 114±14.73-264±25.7µg/g, 64 ±5.13-238±24.68µg/g,9±2.08-22±2µg/g,16±2.89-101±38.59µg/g, 19±9.54 49±49.36µg/g, 48±4.58-105±50.12µg/g dan 4±0.71-8±1.53µg/g. Taburan saiz partikel di kawasan ini di dominasi oleh tekstur berpasir dengan kandungan melebihi 50%. Nilai purata dan sisihan piawai bagi parameter sedimen seperti pH dan peratus bahan organik adalah masing-masing 4.62±0.03-4.49±0.43 dan 2.44±0.16-5.18±2.60, manakala bagi sedimen sungai adalah masing-masing 5.54±0.11-5.79±0.06 dan 0.59±0.11-1.41±0.25. Analisis korelasi menunjukkan bahawa peratus bahan organik mempunyai korelasi positif dengan kandungan As dan Zn pada paras keertian 5% dan 0.1%, sementara pH mempunyai korelasi positif dengan kandungan Cu pada paras keertian 5%. Kandungan As, Cr, dan Pb mempunyai korelasi positif dengan kandungan Zn pada paras keertian melebihi 5%. Kandungan Co mempunyai korelasi negatif dengan Cr dan Ni pada paras keertian 5% dan 0.1%. Unsur As dan Cr masing-masing mempunyai korelasi positif pada paras keertian 5% dengan Cu dan Ni Kepekatan kandungan As melebihi paras ketoksikan bagi sedimen tasik dan sungai pada semua stesen persampelan. Kepekatan kandungan Co dalam sedimen tasik adalah melebihi paras ketoksikan pada stesen 1, manakala bagi sedimen sungai adalah pada stesen 4 dan 5. Kepekatan Cu melebihi paras ketoksikan pada stesen 3 dan berpotensi toksik pada semua stesen persampelan bagi sedimen sungai. Manakala kepekatan unsur Ni, Pb, Cr dan Zn masih berada pada bawah paras ketoksikan bagi sedimen tasik dan sungai kecuali unsur Zn bagi sedimen tasik.

Kata Kunci: logam berat, sedimen, bekas lombong, Kota Tinggi

PENGENALAN

Lombong Air Terjun atau juga dikenali sebagai Lombong Pelepah Kanan merupakan sebuah bekas lombong bijih besi, timah dan tembaga yang terkenal di daerah Kota Tinggi (Rajah 1). Aktiviti perlombongan di kawasan ini bermula pada tahun 1941 sehinggalah bijihnya kehabisan dan ditinggalkan begitu sahaja pada tahun 1990-an. Rezab bijih timah di kawasan ini dianggarkan antara 10 hingga 40 juta ton bergred 0.5% timah (Adong 2001).

Di kawasan itu masih terdapat bekas tapak rumah, bangunan pemprosesan serta alat pemprosesan bijih timah yang ditinggal begitu sahaja. Kawasan bekas lombong ini telah terbiar dalam jangka waktu yang panjang. Keadaan ini berpotensi menyumbang kepada persekitaran yang toksik dan berbahaya. Aktiviti perlombongan seperti pemecahan, penggalian dan penimbunan pecahan batu atau sisa tanah penutup telah mendedahkan kepada tindakan air larian permukaan secara larutlesap, runtuhan dan hakisan (Jumaat 1992).

Di samping itu kawasan ini juga mempunyai permukaan topografi dan landskap yang rata, berteres-teres, bentuk muka bumi yang cacat dengan lubang dan tasik terbiar dalam berbagai bentuk dan saiz serta timbunan bijih timah dan amang yang berselerak di sekitarnya. Terdapat teres yang dipotong terlalu curam kemungkinan mendedahkan kepada proses hakisan akibat ketiadaan tumbuhan penutup bumi sebagai media penyerap air hujan. Masalah ini akan menjadi lebih serius sekiranya hakisan dan runtuhan dari timbunan itu terus memasuki sungai yang berhampiran dan mengalir ke tempat yang lebih rendah kerana ianya masih mengandungi kepekatan logam-logam mineral yang tinggi menyebabkan peningkatan kandungan logam berat di dalam sedimen tasik dan sungai yang akan memberi kesan toksik kepada tanaman, manusia dan haiwan. Kajian ini cuba melaporkan paras kepekatan logam berat di dalam sedimen tasik dan di sepanjang Sungai Pelepah Kanan akibat daripada aktiviti perlombongan yang dijalankan.

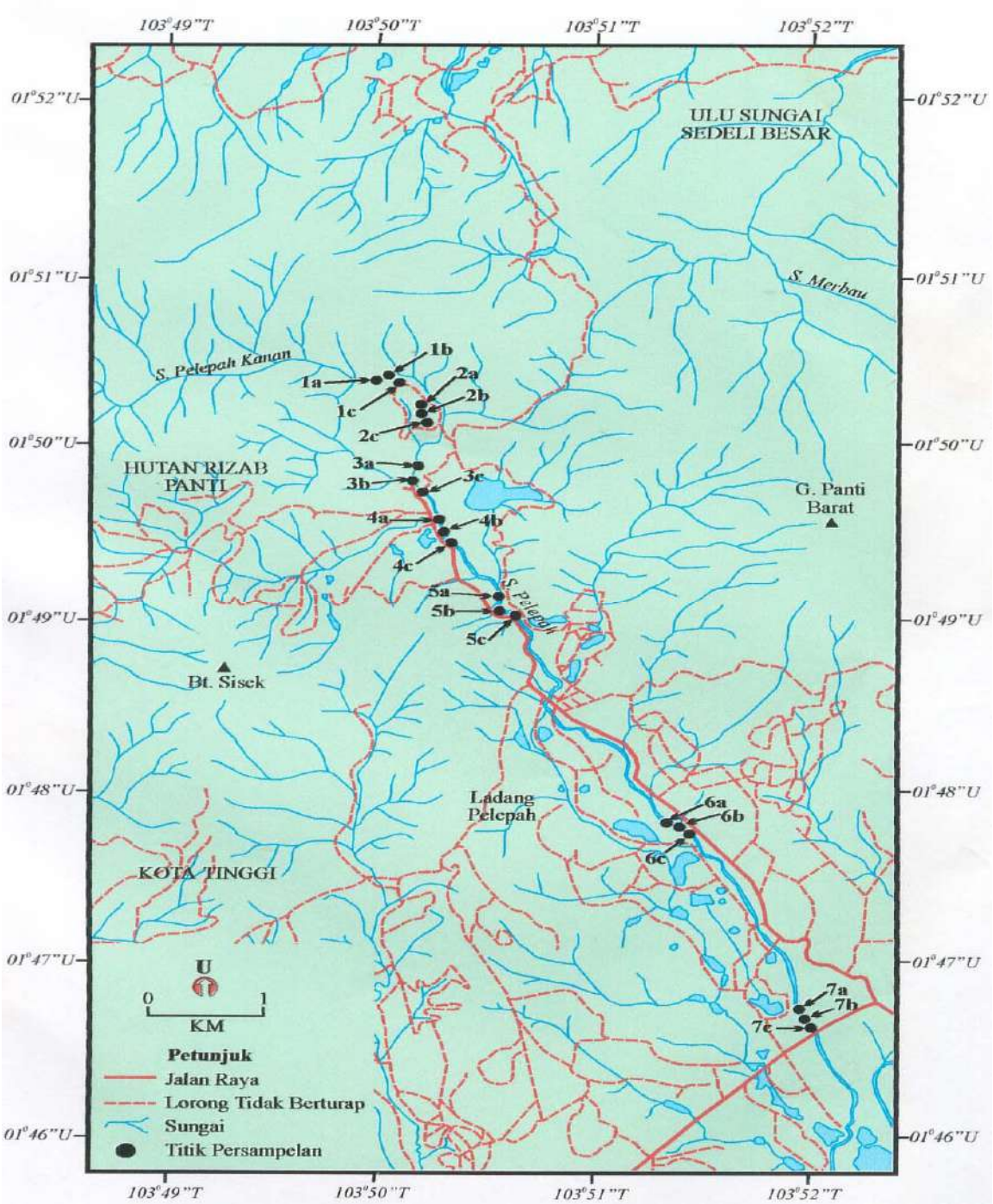

Rajah 1: Peta menunjukkan lokasi persampelan sedimen tasik dan sepanjang Sungai Pelepah Kanan, di Kota Tinggi, Johor.

BAHAN DAN KAEDAH

Sebanyak 21 sampel sedimen tasik dan sepanjang sungai Pelepah Kanan telah diambil daripada 7 stesen persampelan iaitu Stesen 1 dan 2 merupakan kawasan tasik bekas lombong, Stesen 3 ialah kawasan aliran sungai yang hampir dengan tasik, Stesen 4 ialah kawasan berdekatan dengan resort, Stesen 5 ialah kawasan rekreasi manakala stesen 6 dan tujuh merupakan kawasan ladang getah dan pertanian campur (Rajah 1). Sampel sedimen diambil (250g) menggunakan dutch auger dan di simpan di dalam beg plastik yang bersih untuk analisis makmal. Kandungan logam berat dalam sedimen ditentukan menggunakan teknik pendaflour Sinar-X (XRF) dengan kaedah pellet tekan (Norrish & Hutton, 1969). Peralatan untuk penentuan ini ialah 'Philips PW 1480 X-ray Digital' dan spectrometer dikawal menerusi perisian mikrokomputer On Line Alpha (De Jongh, 1973; 1979). Logam berat yang ditentukan daripada sampel sedimen termasuklah As, Co, Cr, Cu, Ni, Pb dan Zn. Penentuan taburan saiz partikel menggunakan kaedah pipet dan pengayakan kering (Abdulla 1996). Kandungan bahan organik ditentukan dengan kaedah pembakaran dan pH ditentukan di dalam nisbah 1:2.5 bagi tanih:air suling (Metson 1956).

HASIL DAN PERBINCANGAN

Analisis taburan saiz partikel, pH dan peratus kandungan bahan organik (BOT) ditunjukkan di dalam Jadual 1. Taburan saiz partikel menunjukkan purata kandungan pasir adalah sangat tinggi iaitu (58-98%), kandungan kelodak (1-14%) dan kandungan lempung (1-29%). Secara keseluruhanya sedimen tasik bekas lombong mempunyai peratusan lempung dan kelodak yang paling tinggi berbanding dengan stesen lain kerana ia merupakan sebuah kawasan tasik yang terkepung iaitu air tidak dapat mengalir keluar menyebabkan sedimen tersebut terkumpul dan termendak di dasar tasik dan kemungkinan juga berpunca daripada hakisan tebing tanih yang terdapat di sekitarnya yang terus masuk ke dalam tasik dan sebaliknya bagi stesen di sepanjang Sungai Pelepah Kanan kerana ia merupakan sebuah sungai yang mengalir dan berdekatan dengan kawasan air terjun yang mempunyai arus yang mengalir dengan deras menyebabkan kandungan lempung dan kelodak terserak jauh di sepanjang sungai tersebut.

Nilai purata pH sedimen mempunyai sela di antara 4.49±0.43-5.79±0.06. Nilai purata paling tinggi ditunjukkan di stesen 3 dan purata paling rendah di stesen 1 iaitu merupakan kawasan tasik bekas lombong. Nilai yang rendah ini mungkin dipengaruhi oleh peningkatan kandungan

bahan organik akibat pereputan daun-daun dan rating-rating kayu yang terdapat di dalam tasik tersebut. Menurut Metson (1956) nilai pH di kawasan kajian menunjukkan sela dari asid kuat kepada berasid.

Jadual 1: Nilai pH, peratus kandungan bahan organik (BOT) dan taburan saiz partikel sedimen tasik dan sungai Pelepah Kanan di Kota Tinggi, Johor

Stesen	Replikasi	pH	BOT (%)	Pasir (%)	Kelodak (%)	Lempung (%)
*1	a	4.06	2.2	68	4	28
	b	4.92	6.36	75	8	19
	c	4.49	6.99	57	18	25
	Purata	**4.49 ± 0.43**	**5.18 ± 2.60**	**66**	**10**	**24**
*2	a	4.59	2.62	56	14	30
	b	4.65	2.33	58	14	28
	c	4.62	2.39	59	13	28
	Purata	**4.62 ± 0.03**	**2.44 ± 0.16**	**58**	**14**	**29**
3	a	5.77	1.38	95	2	3
	b	5.86	1.11	95	2	3
	c	5.75	1.33	93	3	4
	Purata	**5.79 ± 0.06**	**1.28 ± 0.14**	**94**	**3**	**3**
4	a	5.66	0.78	98	0	2
	b	5.65	0.75	99	0	1
	c	5.84	0.9	98	1	1
	Purata	**5.72 ± 0.11**	**0.81 ± 0.08**	**98**	**1**	**1**
5	a	5.63	1.13	99	0	1
	b	5.57	1.47	98	1	1
	c	5.42	1.62	95	4	1
	Purata	**5.54 ± 0.11**	**1.41 ± 0.25**	**97**	**2**	**1**
6	a	5.79	0.76	97	1	2
	b	5.5	0.62	98	1	1
	c	5.75	0.55	97	1	2
	Purata	**5.68 ± 0.16**	**0.64 ± 0.11**	**97**	**1**	**2**
7	a	5.72	0.71	97	1	2
	b	5.66	0.51	99	0	1
	c	5.87	0.56	97	1	2
	Purata	**5.75 ± 0.11**	**0.59 ± 0.11**	**98**	**1**	**1**

* Sedimen tasik

.

Kandungan bahan organik mempunyai sela daripada 0.59% hingga 5.18%. Nilai tertinggi adalah di stesen 1 dengan purata 5.18±2.60. Nilai yang tinggi ini disebabkan stesen tersebut mempunyai peratusan lempung yang tinggi berbanding dengan stesen lain. Menurut Tam & Wong (1999) sedimen yang halus mempunyai peratusan bahan organik yang tinggi berbanding dengan yang

kasar. Manakala peratusan kandungan bahan organik terendah adalah di stesen 7 dengan purata 0.59±0.12. Nilai yang rendah ini disebabkan oleh tekstur kasar iaitu pasir lebih mendominasi di stesen ini. Purata kandungan bahan organik ini adalah sederhana ke sangat rendah berdasarkan pengkelasan oleh Acres et al. (1975)

Komposisi logam berat

Komposisi logam berat di dalam sedimen ditunjukkan pada Jadual 2. Purata komposisi logam berat mengikut turutan kepekatan menurun bagi sedimen tasik ditunjukkan oleh As, Zn, Co, Cu, Pb, Cr dan Ni manakala bagi sedimen sungai adalah As, Cu, Co, Zn, Pb, Cr dan Ni.

As dan Cu : Purata komposisi As sangat tinggi pada semua stesen pencerapan. Sela kepekatannya adalah daripada 114±14.73 hingga 264±25.7 µg/g. Nilai purata tertinggi ditunjukkan oleh stesen 3 dan paling rendah ditunjukkan oleh stesen 4. Unsur logam berat Cu mempunyai sela purata di antara 62±3.51 hingga 238±24.68 µg/g, paling tinggi ditunjukkan oleh stesen 3 dan paling rendah ditunjukkan oleh stesen 2. Stesen 3 menunjukkan bacaan paling tinggi bagi kedua-dua jenis unsur logam kerana stesen ini terletak berhampiran dengan longgokkan amang yang mungkin terhakis masuk ke dalam sungai serta larut resap daripada air larian permukaan.

Co dan Zn : Purata komposisi Co mempunyai sela di antara 70±43.92 hingga 129±10.97 µg/g, paling tinggi ditunjukkan oleh stesen 4 dan paling rendah ditunjukkan oleh stesen 1. Unsur Zn mempunyai sela di antara 94±15.87 hingga 105±50.12 µg/g. Nilai purata tertinggi ditunjukkan oleh stesen 1 manakala purata terendah ditunjukkan oleh stesen 3.

Ni, Pb dan Cr : Purata komposisi Ni mempunyai sela di antara 4±0.71 hingga 8±1.53 µg/g. Nilai paling tinggi ditunjukkan oleh stesen 6 dan paling rendah oleh stesen 5. Unsur logam berat Pb mempunyai sela di antara 19±9.54 hingga 49±49.36 µg/g, dengan kepekatan paling tinggi adalah di stesen 1 dan paling rendah di stesen 5 manakala unsur Cr mempunyai sela di antara 9±2.08 hingga 24±5.29 µg/g. Nilai paling tinggi adalah di stesen 6 dan paling rendah di stesen 4.

Jadual 2 : Kandungan logam berat (µg/g) di dalam sedimen tasik dan Sungai Pelepah Kanan

Stesen	Replikasi	Kepekatan logam berat (µg/g)						
		As	Co	Cr	Cu	Ni	Pb	Zn
*1	a	188	19	4	0	6	13	53
	b	236	97	27	72	3	105	153
	c	229	93	16	25	3	28	109
	Purata	**218±25.93**	**70±43.92**	**16±11.5**	**32±36.56**	**4±1.73**	**49±49.36**	**105±50.12**
*2	a	164	24	11	62	4	28	56
	b	162	17	14	66	6	40	58
	c	159	24	9	59	7	51	54
	Purata	**162±2.52**	**22±4.04**	**11±2.52**	**62±3.51**	**6±1.53**	**40±11.5**	**56±2**
3	a	278	44	20	259	6	49	100
	b	234	46	20	245	5	48	76
	c	279	51	24	211	5	35	106
	Purata	**264±25.7**	**47±3.61**	**21±2.31**	**238±24.68**	**5±0.58**	**44±7.81**	**94±15.87**
4	a	130	133	8	84	5	52	47
	b	111	117	11	89	5	36	53
	c	101	138	7	84	1	27	44
	Purata	**114±14.73**	**129±10.97**	**9±2.08**	**86±2.89**	**4±2.31**	**38.33±12.66**	**48±4.58**
5	a	98	141	5	64	bdl	29	46
	b	112	98	14	126	3	10	63
	c	131	64	8	127	4	18	63
	Purata	**114±16.56**	**101±38.59**	**9±4.58**	**106±36.09**	**4±0.71**	**19±9.54**	**57±9.81**
6	a	143	14	30	121	9	47	61
	b	115	19	20	75	8	21	48
	c	124	14	22	76	6	30	49
	Purata	**127±14**	**16±2.89**	**24±5.29**	**91±26**	**8±.1.53**	**33±13.2**	**53±7.23**
7	a	125	18	22	65	7	35	51
	b	143	24	20	68	9	54	51
	c	114	9	24	58	7	18	63
	Purata	**127±14.64**	**17±7.55**	**22±2**	**64±5.13**	**8±1.15**	**36±18**	**55±6.93**
****Paras kritikal**		**20-50**	**25-50**	**75-100**	**60-125**	**100**	**100-400**	**70-400**

* Sedimen tasik **Kabata Pendias dan Pendias (1992) bdl-bawah had pengesanan

Pengkelasan paras kritikal kandungan logam berat di dalam sedimen adalah berdasarkan kepada (Kabata Pendias dan Pendias 1992). Secara umumya kepekatan kandungan As melebihi paras ketoksikan bagi sedimen tasik dan sungai pada semua stesen persampelan. Kepekatan kandungan Co dalam sedimen tasik adalah melebihi paras ketoksikan pada stesen 1, manakala bagi sedimen sungai adalah pada stesen 4 dan 5. Kepekatan Cu melebihi paras ketoksikan pada stesen 3 dan berpotensi toksik pada semua stesen persampelan bagi sedimen sungai. Manakala kepekatan

unsur Ni, Pb, Cr dan Zn masih berada pada bawah paras ketoksikan bagi sedimen tasik dan sungai kecuali unsur Zn bagi sedimen tasik.

Korelasi di antara logam berat dengan parameter sedimen

Korelasi di antara logam-logam berat sesamanya dan dengan parameter sedimen ditunjukkan di dalam Jadual 3. Di dapati bahawa As, Cr dan Pb mempunyai korelasi positif signifikan dengan kandungan Zn pada paras keertian melebihi 5%, manakala unsur Cr dan Ni masing-masing mempunyai korelasi negatif signifikan pada paras keertian 5% dan 0.1% dengan Co. Unsur As dan Cr masing-masing mempunyai korelasi positif signifikan pada paras keertian 5% dengan Cu dan Ni. Logam-logam yang lain tidak menunjukkan sebarang korelasi yang signifikan.

Analisis korelasi di antara logam berat dengan parameter sedimen menunjukkan bahawa peratus bahan organik mempunyai korelasi positif yang signifikan dengan kandungan As dan Zn pada paras keertian 5% dan 0.1%, sementara pH mempunyai korelasi positif signifikan dengan kandungan Cu pada paras keertian 5%. Peratus pasir, lempung dan kelodak didapati tidak menunjukkan pengaruh yang signifikan dengan semua logam berat. Korelasi positif menunjukkan logam-logam berat dan paramater sedimen ini wujud bersama, manakala korelasi negatif menunjukkan logam-logam berat dan parameter sedimen ini saling bersaing untuk menduduki tempat yang sama di dalam sedimen.

Jadual 3: Korelasi di antara logam berat dengan parameter sedimen tasik dan Sungai Pelepah Kanan

	As	Co	Cr	Cu	Ni	Pb	Zn
As	1						
Co	-0.151	1					
Cr	0.337	**-0.456***	1				
Cu	**0.524***	0.003	0.333	1			
Ni	0.019	**-0.796*****	**0.501***	0.021	1		
Pb	0.418	0.106	0.404	0.155	0.077	1	
Zn	**0.790*****	0.109	**0.476***	0.310	-0.195	**0.585****	1
PH	-0.236	0.168	0.380	**0.550***	0.076	-0.010	-0.166
% BOT	**0.492***	0.187	0.039	-0.269	-0.355	0.386	**0.730*****
% Pasir	-0.376	0.092	0.289	0.380	0.165	-0.136	-0.287
% Lempung	0.326	-0.228	-0.275	-0.431	-0.050	0.156	0.223
% Kelodak	0.363	-0.157	-0.158	-0.297	-0.106	0.165	0.328

Paras keertian korelasi: * signifikan pada 5%, ** 1%, *** 0.1%

KESIMPULAN

- Kepekatan logam berat As, Co dan Cu melebihi paras kritikal bagi sedimen sungai, manakala bagi sedimen tasik adalah As dan Co
- Hanya peratus kandungan bahan organik tanih (BOT) dan pH mempengaruhi komposisi logam berat As, Zn dan Cu
- Pencemaran logam berat As, Co, Cu berlaku di sepanjang sungai Pelepah Kanan akibat daripada luahan aktiviti perlombongan yang jalankan

PENGHARGAAN

Penulis ingin mengucapkan ribuan terima kasih kepada Kementerian Sains dan Teknologi di atas kurniaan peruntukan penyelidikan IRPA 09-02-02-0009-EA 064. Penghargaan juga ditujukan kepada Encik Hamid Othman di Makmal Sinar X, Program Geologi, Pusat Pengajian Sains Sekitaran dan Sumber Alam, FST, di atas penggunaan alat XRF untuk penentuan kandungan logam berat.

RUJUKAN

Abdulla, H.H. 1966. A study on the development of podzol profiles in Dovey Forest. Ph. D. Thesis, University of Wales.

Adong Laming (2001). Permineralan besi, timah dan tembaga di Lombong Air Terjun, Kota Tinggi, Johor. Tesis Sarjana Muda Sains UKM.

Acres, B. D., Bower, R. P., Borrough, P. A., Folland, C. J., Kalsi, M. S., Thomas, P. and Wright, P. S. (1975). *The Soils of Sabah. Volume 1. Classification and Description*. Land Resource Study No. 20, Land Resource Division, Ministry of Overseas Development, England.

Alloway, B.J. (1995). *Heavy metals in soils*. Blackie Academic and Professional, London.

Kabata-Pendias, A. and Pendias, H. (1992). *Trace elements in soil and plants* (2nd ed.). CRC Press, Boca Raton, Fla

De Jongh, W.K. (1973). X-ray fluorescence analysis applying theoritical matrix corrections. Stainless Steel. *X-ray Spectrometry, 2(151).*

De Jongh, W.K. (1979). The atomic number Z=0: Loss and gain on Ignition in XRF analysis treated by the JN-equations. *X-ray Spectrometry, 8(52).*

Jumaat Salimon, 1992. Taburan logam berat di perairan sekitar lombong tembaga Mamut dan empangan Lohan. *Prosiding Simposium Sumber Alam Kebangsaan Pertama., Jil. 2 , 119-126*

Landon, J.R. (ed.) (1991). *Bookers Tropical Soil Manual*. Hongkong: Longman Scientific and Technical

Metson, A. J. (1956). Methods of chemical analysis for soil survey samples. *Bull. N.Z. Dept. Scient. Ind. Res. No. 12.*

Norrish, K. and Hutton, J.T., 1969. An accurate X-ray spectrographic method for the analysis of a wide range of geological samples. Geochim Et Cosmochima

Malaysian Journal of Analytical Sciences, Vol.9, No. 3(2005): 444 - 444

CHARACTERISTIC AND COMPOSITION OF *KEKABU* SEED OIL *(CEIBA PETANDRA)*

Khairul Asmak Abd. Kadir, Jumat Salimon[1]

School of Chemical Sciences and Food Technology, Faculty of Science and Technology, Universiti Kebangsaan Malaysia, 43600 Bangi, Selangor, Malaysia.

[1]Corresponding author: 03-89215424; Fax: 603-89215410; 03-8925 6086; e-mail: jumat@pkrisc.cc.ukm.my

Abstract
Crude oil was extracted from crushed *kekabu* (*Ceiba Petandra*) seed in hexane for 3 hours at 60 ^{o}C by soxhlet extractor. Its fat content, fatty acid composition and physicochemical properties were investigated. The yield of the oil was 20-25%. The most dominant fatty acids found were linoleic (42.3%), palmitic (22.5%) and oleic C18:1 (20.9%). The characteristics of the oil are discussed and compared to other edible oils.

Abstrak
Minyak kasar biji kekabu (*Ceiba Petandra*) diesktrak dengan heksana selama 3 jam pada suhu 60 ^{o}C melalui kaedah pengekstrakan soxhlet. Kandungan lemak, asid lemak dan sifat-sifat fizikokimia minyak biji kekabu dikaji. Hasil kajian menunjukkan biji kekabu mengandungi minyak sebanyak 20-25%. Asid lemak linoleik, palmitik dan oleik merupakan asid lemak yang paling dominan dalam minyak biji kekabu dengan peratusan sebanyak 42.3%, 22.5% dan 20.9% masing-masing. Ciri-ciri minyak biji kekabu dibincangkan dan dibandingkan dengan beberapa minyak yang lain.

Key words: *Kekabu* seed oil, linoleic acid, PUFA

Introduction

Malaysia has wide diversity sources of local seed oil. Unfortunately, the potentials and the benefits of these sources are less pronounced due to less research and commercialization effort has been made. For instance, *Ceiba Petandra* of the family of Bombacaceae or locally known as *kekabu*.

Originally, *kekabu* tree was a native to South America; it now has spread to the primary rainforests of West Africa and the Southeast Asian rainforests of the Peninsular Malaysia and Indonesia. The tree is a medium to large, deciduous tree with tier, horizontal branches. The fruits or seedpods are oblong, thick, and woody and contain a cotton-like fiber known as *kekabu* fibre. While still on the tree, the fruits burst open after the leaves have fallen, exposing this cotton-like fiber. *Kekabu* fiber/lint is very well known economic product; a silky floss, which varies in colour from grey to white, inside the fruit. The lint, which forms the floss, is outgrowths of the inner wall of the fruit [1]. It is used to make furniture, insulation materials, stuffing in pillows and mattresses. It is also used as buoyancy materials inside some life jackets because the fiber has lightweight and waterproof materials [2].

The *kekabu* seeds contain 25% of oil that is brownish-yellow in colour, liquid at ordinary temperatures shows the same biological constituent as a well-known cottonseed oil [6]. Unfortunately, up till now, *kekabu* seeds in Malaysia, remain abandoned and being discarded without realizing its importance.

The aim of this study is to report the chemicals composition of the *kekabu* seeds oil as well as its physical and physicochemical characteristics.

Malaysian Journal of Analytical Sciences, Vol.9, No. 3(2005): 445 - 448

FATTY ACIDS COMPOSITION OF ENZYMATICALLY TRANSESTERIFIED OMEGA-3 ENRICHED VEGETABLE OILS

H.A. Zakeri, K-N. Ku Nordin, W.S. Tham, H.Y. Mah and K.W. Ooi

Department of Biological Sciences, Faculty of Science and Technology, Kolej Universiti Sains dan Teknologi Malaysia (KUSTEM), Mengabang Telipot, 21030 K. Terengganu, Terengganu Darul Iman

Abstract

The application of enzymatic transesterification for production of vegetable oils containing omega-3 polyunsaturated fatty acids was investigated. Three vegetable oils were used as substrates and together with cod liver oil, were catalysed by immobilized *Rhizomucor miehei* lipase in water-saturated hexane. The composition of seven major fatty acids from transesterified samples was determined using gas chromatography. Gas chromatogram of cod liver oil showed that it contains about 2.6% α-linolenic acid (ALA), 18.6% eicosapantaenoic acid (EPA) and 18.0% docosahexaenoic acid (DHA). Soybean oil consisted of about 6.1% ALA with no EPA and DHA observed. EPA and DHA were also absent in chromatograms of sunflower and corn oils. On the other hand, there was less than 1% of ALA present in both oils. After transesterification, the omega-3 fatty acids composition of each vegetable oil was: soybean oil, 4.6% ALA, 6.3% EPA and 6.3% DHA; sunflower oil, 1.3% ALA, 7.2% EPA and 6.1% DHA; and corn oil, 1.3% ALA, 6.0% EPA and 3.3% DHA.

Keywords: Omega-3 fatty acids, gas chromatography, lipase-catalyzed transesterification, cod liver oil, vegetable oil

Introduction

Alpha-linolenic acid (ALA), eicosapentaenoic acid (EPA) and docosahexaenoic acid (DHA) are long chain, polyunsaturated fatty acids (PUFAs) belong to the family of omega-3 fatty acids. ALA is a 18-carbon fatty acid with 3 double bonds (18:3n-3), EPA is a 20-carbon fatty acid with 5 double bonds (20:5n-3), and DHA is a 22-carbon fatty acid with 6 double bonds (22:6n-3). Consumption of ALA, EPA and DHA in large quantities may reduce heart diseases, arthritis, diabetes and even cancer [1-2]. However, EPA and DHA cannot be synthesized *de novo* by the body and therefore are derived from the diet or dietary supplements. Excellent sources of EPA and DHA are marine fish oils including blue fin tuna, herring and cod liver oil [3]. Most of the vegetable oils, on the other hand, contain little or no of these fatty acids [4]. Vegetable oils are rich in another type of PUFA called omega-6 fatty acids which are not interconvertible with omega-3 fatty acids. However, some vegetable oils such as linseed oil, are rich in ALA that can be metabolically converted to EPA and DHA [1].

Apart from the many benefits of fish oils, they are not consumed on a regular basis as an essential part of the diet. Vegetable oils, on the other hand are more commonly consumed as cooking oils or as one of the ingredients in confectionery fats. Therefore, they may be more acceptable media for providing EPA and DHA in the diet. Incorporation of EPA and DHA into vegetable oil has the potential to improve the nutritional quality of the oil. One of the ways to do this is by transesterification. Transesterification has an ability to alter the physical characteristics of fats and oils by rearranging their chemical composition resulting in fats and oils having completely different properties than the original fats or oils [5]. Transesterification reactions using enzymes as catalysts are more favourable than chemical catalysts. Enzymes in general are very efficient catalysts, environmentally acceptable, can react under mild conditions and are not bound to their natural role [6]. Furthermore, enzymes show specificity which can be exploited to produce 'tailor-made' fats or oils [5].

In this study, analysis was done on seven major fatty acids (i.e. palmitic acid, stearic acid, oleic acid, linoleic acid, ALA, EPA and DHA) composition of three vegetable oils after transesterification with cod liver oil, which

is the source of omega-3 fatty acids. The degree of omega-3 fatty acids incorporated into the three vegetable oils were determined. Transesterification was done by using immobilized *R. miehei* lipase as catalyst.

Experimental

Materials

All the oils analyzed (cod liver oil, corn oil, sunflower oil and soybean oil) were commercially available. Immobilized *Rhizomucor miehei* lipase (Lipozyme IM-60) was purchased from Novozymes Industry, Denmark. All solvents used were of analytical grade.

Transesterification reaction

The reaction mixtures for transesterification consisted of vegetable oil and cod liver oil blend (1:1 w/w ratio) in water-saturated hexane (4:1). The reaction was started by the addition of 1% (w/v) Lipozyme IM-60. The mixture was agitated in an orbital shaker at 200 rpm at 60°C. At the end of the reaction (6 hours), acetone:ethanol (1:1) mixture was added and the enzyme was filtered out.

Prior to fatty acid analysis, free fatty acids were removed by titrating the transesterified mixture with 0.1 M sodium hydroxide (NaOH) to a phenolphthalein end-point. The hydrolytic activity of the enzyme was calculated from this according to the formula by Ghazali et al. [7].

Fatty acids analysis

For fatty acids analysis, triglycerides were methylated by adding 0.1 mL 2 N potassium hydroxide (KOH) solution in methanol to each 0.05 g sample. The mixture was left to stratify till upper layer became clear. 0.1 μL from the upper layer was then injected into a Hewlett-Packard 4890D gas chromatograph equipped with a fused silica capillary column, Supelco's Omegawax 320 (30 m x 0.32 mm i.d. x 0.25 μm film thickness) and an FID detector. The gas chromatograph was connected to a HP integrator model 3398A. The carrier gas was helium with the flow rate at 25 cm/sec. Both the detector and injector were operated at 260°C and 250°C, respectively. The column temperature was 150°C. Split ratio was 100:1. The peaks of fatty acid esters were identified using standard fatty acids (Supelco, Bellafonte, USA).

Results and Discussion

Gas chromatograms of cod liver oil, non-transesterified soybean, sunflower and corn oils are shown in Figure 1. From the chromatograms, it was observed that the peaks for EPA and DHA were only present in chromatogram of cod liver oil (Figure 1A). It was also observed that the peak for stearic acid (i.e. peak 2 on the chromatograms) was not fully separated from the rest of the peaks. The peaks formed on the chromatograms in Figure 1 correspond to the fatty acids composition of cod liver oil and non-transesterified vegetable oils listed in Table 1 and Table 2, respectively. Of the seven fatty acids analyzed in cod liver oil, 43.3% is polyunsaturated fatty acids (PUFA, consisted of linoleic acid, ALA, EPA and DHA), 35.8% is monounsaturated fatty acids (MUFA, consisted of oleic acid), and 20.9% is saturated fatty acids (SaFA, consisted of palmitic and stearic acids). Most of the non-transesterified vegetable oils studied, consisted of higher percentage of PUFA than the cod liver oil (Table 2). However, these fatty acids are made mostly of linoleic acid, an omega-6 fatty acid with no EPA and DHA detected. The only omega-3 fatty acid present in these vegetable oils is ALA. These observations are in line with the findings by Bruinsma and Taren [3] and Drummond and Brefere [4].

The chromatograms of transesterified vegetable oils (i.e. omega-3 enriched oils) are shown in Figure 2. The chromatograms plus the degree of hydrolysis calculated after transesterification for each vegetable oil has shown that transesterification did occur. According to Willis and Marangoni [5], minimum hydrolytic activity was important to ensure that appropriate amount of water was only used for removal of fatty acyl groups from the glycerol backbone, the first step in any transesterification reaction. The degree of hydrolysis was the highest in transesterified corn oil (i.e. 3.78%). This was followed by sunflower oil with 2.6% and soybean oil with 2.5%. As shown in Table 2, transesterification has altered the fatty acid composition of all the vegetable oils studied.

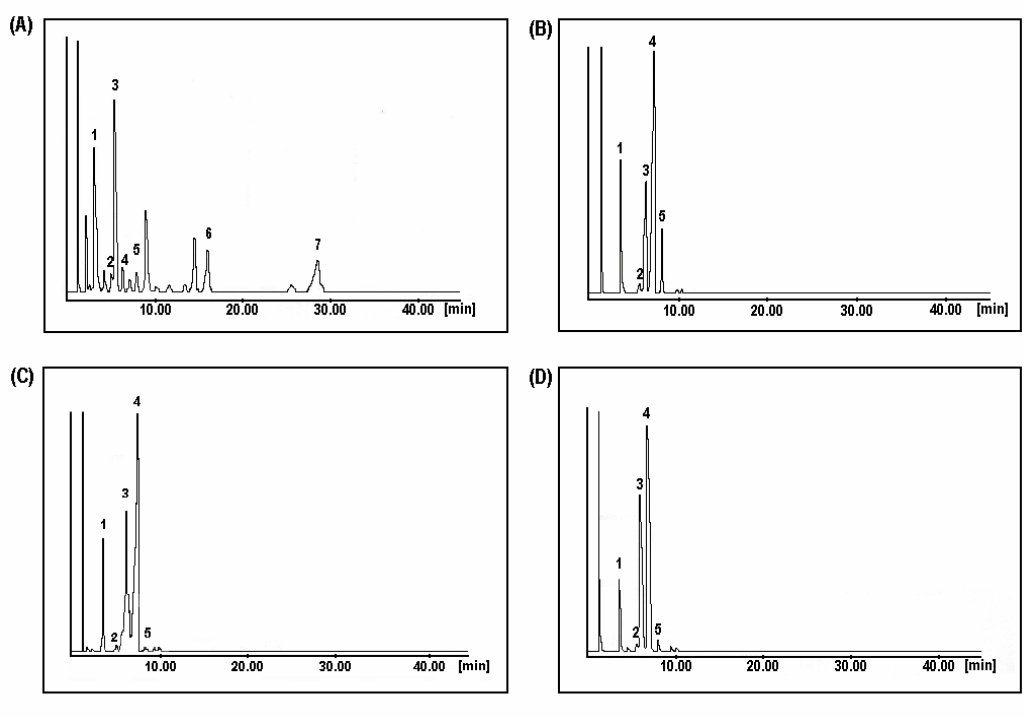

Figure 1: Gas chromatograms of cod liver oil (A), soybean oil (B), sunflower oil (C) and corn oil (D).
1 is palmitic acid, 2 is stearic acid, 3 is oleic acid, 4 is linoleic acid, 5 is linolenic acid (ALA), 6 is eicosapentaenoic acid (EPA) and 7 is docosahexaenoic acid (DHA).

Table 1: Fatty acids composition of cod liver oil

Fatty acid		Wt. (%)
Palmitic	C16:0	17.58
Stearic	C18:0	3.33
Oleic	C18:1	35.77
Linoleic	C18:2	4.12
ALA	C18:3	2.63
EPA	C20:5	18.61
DHA	C22:6	17.96

Table 2: Fatty acid composition (wt %) of triglyceride of vegetable oils and vegetable oils transesterified with cod liver oil

Fatty acid	Vegetable oils					
	Soybean oil		Sunflower oil		Corn oil	
	A	B	A	B	A	B
C16:0	10.72	13.99	6.51	11.34	12.09	15.92
C18:0	2.81	1.75	1.54	3.35	0.85	2.55
C18:1	28.98	31.85	25.40	26.75	33.8	34.27
C18:2	51.37	35.27	65.86	43.91	52.61	36.68
C18:3	6.12	4.61	0.69	1.32	0.65	1.32
C20:5	0.00	6.28	0.00	7.23	0.00	6.00
C22:6	0.00	6.25	0.00	6.10	0.00	3.26

A – vegetable oil B – transesterified vegetable oil

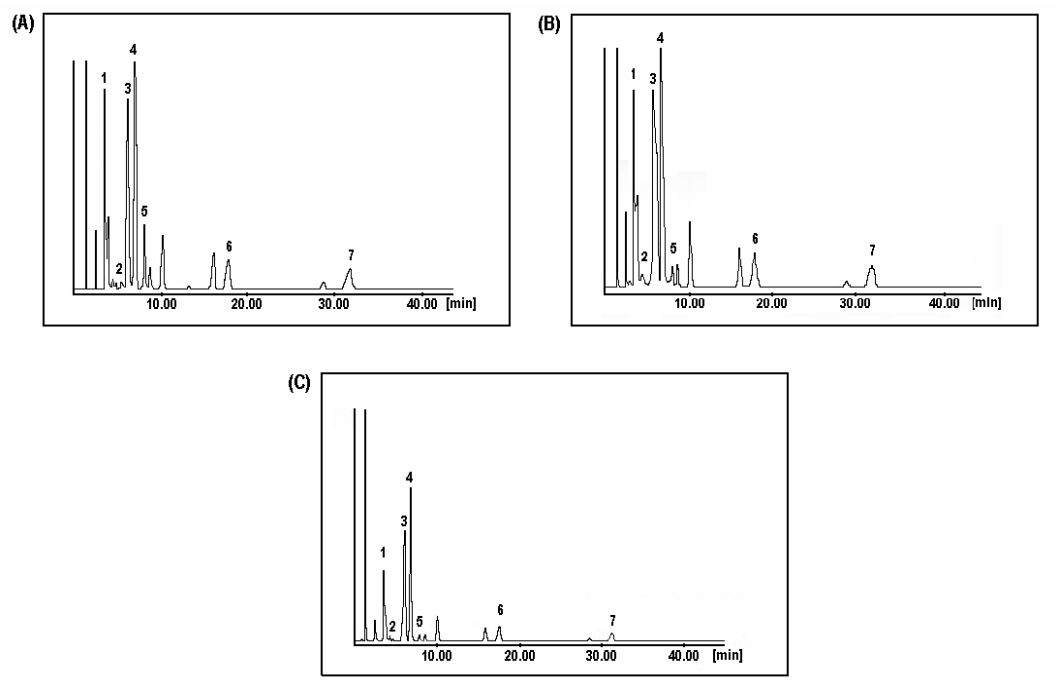

Figure 2: Gas chromatograms of omega-3 enriched soybean oil (A), sunflower oil (B) and corn oil (C). 1 is palmitic acid, 2 is stearic acid, 3 is oleic acid, 4 is linoleic acid, 5 is linolenic acid (ALA), 6 is eicosapentaenoic acid (EPA) and 7 is docosahexaenoic acid (DHA).

Transesterification lowered the composition of linoleic acid and increased the composition of ALA, EPA and DHA. However, a decrease in ALA was observed in transesterified soybean oil. The extent of ALA and EPA incorporation was the highest with sunflower oil (i.e. about 1.3% and 7.2%, respectively). In comparison, the extent of DHA incorporation was the highest with soybean oil (i.e. about 6.3%). From the results obtained, it can be concluded that enzymatic transesterification can be applied to produce a new and improved vegetable oils with enhanced nutritional value. However, more studies are to be carried out to determine if these vegetable oils are ready for human consumption.

Acknowledgement

Support for this study by KUSTEM (vot. no.: 54124) is gratefully acknowledged.

References

1. Hazra, A.; Tripathi, S.K. and Ghosh, A. 1999. Pharmacology and therapeutic potential of the n-3 polyunsaturated fatty acids, eicosapentaenoic acid (EPA) and docosahexaenoic acid (DHA) in fish oils. *Indian J. Pharmacology*. 31:247-264.

2. Uauy, R. and Valenzuela, A. 2000. Marine oils: the health benefits of n-3 fatty acids. *Nutrition*. 16(7-8):680-684.

3. Bruinsma, K.A. and Taren, D.L. 2000. Dieting, essential fatty acid intake and depression. *Nutrition Rev*. 58(4):98-108.

4. Drummond, K.E. and Brefere, L.M. 2003. *Nutrition for Foodservice and Culinary Professionals. 5th ed.* John Wiley and Sons: New York. Pp. 139-179.

5. Willis, W.M. and Marangoni, A.G. 1998. Enzymatic interesterification. Pp. 665-698 in C.C. Akoh and D.B. Min eds. *Food Lipids: Chemistry, Nutrition and Biotechnology*. Marcel Dekker Inc.: New York.

6. Faber, K. (1995) *Biotransformations in Organic Chemistry - A Textbook (2nd edn.)*, Springer-Verlag: Berlin. pp. 80-104.

7. Ghazali, H.M.; Hamidah S. and Che Man, Y.B. 1995. Enzymatic transesterification of palm olein with nonspecific and 1,3-specific lipases. *J. Am. Oil Chem. Soc*. 72(6):633-639.

Malaysian Journal of Analytical Sciences, Vol.9, No. 3(2005): 449 - 452

IDENTIFICATION AND CHEMICAL PROFILING OF MARINE SPONGES FROM TERENGGANU ISLANDS: A PRELIMINARY STUDY

Khamsah Suryati Mohd[1], Habsah Mohamad[2], Jasnizat Saidin and Faizah Shaharom[1]

Institute of Oceanography[1],Chemistry Department, Faculty of Science and Technology[2], College University Science and Technology Malaysia, 21030 Kuala Terengganu, Terengganu.

Key words: Marine sponges, chemical profiling, spicules, *Aaptos*

Abstract

The ability to rapidly identify known or undesirable compounds in natural products is a critical step in an efficiently run natural products discovery program. Due to the co-existence of multi-components, identification, authentication as well as standardization of natural products was a challenging task. An effective way in research area of natural products was to construct the chromatographic chemical profiling also called chromatographic fingerprint. Marine sponges are potential sources of many unique metabolites, including cytotoxic and anticancer compounds. Many species of marine sponge are taxonomically not established and by examining the morphological criteria alone is insufficient. 17 specimens of marine sponges of Terengganu Islands were subjected to thin layer chromatography to investigate the potential of this method in providing profiles that can be used as species-specific chemotaxonomic markers. The profiles of each specimen were compared to each other from the same and different localities. Several specimens with identical profile were in agreement with their morphological criteria suggesting that the profile can be used to distinguish them from other group of sponges.

Introduction

Marine sponges (phylum Porifera) are sessile invertebrate which can be found mainly in marine environment (only 1% of the species inhabits freshwater) (1). The potential of marine sponges as a source of novel molecules has not been extensively investigated. As compared to other marine lifeforms, bioactive compounds have been detected especially frequently in sponges. Sponges produce toxins and other compounds to repel and deter predators (2, 3). Of the investigated marine sponges, >10% has exhibit cytotoxic activity (4), suggesting production of potential medicinals.

There are many species of marine sponge which taxonomically not established. Furthermore, sponge of the same genus also not so easy to differentiate due to plasticity of their morphological features (5). Intraspecific variation in chemistry (known as chemical profiling) has been documented extensively among terrestrial plants but not so popular in marine sponge research. The characters used for species identification are mainly morphological, and it seems that morphology alone might be too limited and time consuming for the identification and authentication of species boundaries in many sponges. In order to identify and characterize chemical constituents of sponges as well as to establish the identification of species, the used of chemical profiling allows resources to be kept on tract and dereplication of undesired result due to confusion over species variation can be avoided (6). This prompted us to investigate

comparatively the chemical pattern of marine sponges collected along Terengganu waters. In this paper, we presented our preliminary finding of this study.

Experimental

Specimen Preparation

The marine sponges were collected via SCUBA at a depth of 8 to 15 meters of Bidong, Redang and Perhentian Island, Terengganu. Voucher specimens have been deposited at the Museum Biodiversity, Institute of Oceanography, College University Science and Technology, Kuala Terengganu, Terengganu. Microscopical investigation was done on spicules and spicule arrangements on each of the specimen. The organisms were immediately frozen after collection and dried in oven (50^{o}C) prior extraction. Methanol extract of 17 specimens (Table 1) were subjected to thin layer chromatography.

Table 1: Sponges collected from Terengganu Islands

No	Specimen ID	Locality
1	B02/005	Pulau Bidong
2	B02/003	Pulau Bidong
3	B01/008	Pulau Bidong
4	B01/007	Pulau Bidong
5	B02/008	Pulau Bidong
6	B02/004	Pulau Bidong
7	B02/006	Pulau Bidong
8	B02/007	Pulau Bidong
9	R01/001	Pulau Redang
10	R02/001	Pulau Redang
11	R03/001	Pulau Redang
12	P01/001	Pulau Perhentian
13	P02/001	Pulau Perhentian
14	P03/001	Pulau Perhentian
15	B01/001	Pulau Bidong
16	B02/001	Pulau Bidong
17	B03/001	Pulau Bidong

Thin Layer Chromatography

The extracts were run on normal phase TLC plates; precoated silica gel GF_{254} of 0.25 mm thickness, subjecting to ascending chromatography. Mobile phase: chloroform: methanol (8.4: 1.6). Plates visualized under UV 365 nm and UV 254 nm without treatment.

Results and Discussion

Microscopical Identification

Sponge identification involving a series of investigation including shape, size, colour (live and preserved), texture, mucus production and smell, surface ornamentation and skeletal structure. Spicules and spicule arrangement are major characteristic to indicate classes of sponge taxonomy. Microscopical analysis revealed that all spicules of 17 specimens are silicate, indicating class Demospongiae. Specimen of B02/005, B02/003, B01/008,B01/007, B02/008, B02/004, B02/006 and B02/007 showing different types of spicule in both megascleres and microscleres; indicating that they are not the same species. As for sample R01/001, R02/001,

R03/001, P01/001, P02/001, P03/001, B01/001, B02/001 and B03/001, microscopical examination revealed that they belong to genus *Aaptos*. They possessed a strongyloxeas as a primary spicules, some spicules are straight or curves styles or subtylostyles. Ectosomal spicules styles, rare of subtylostyles (Figure 1).

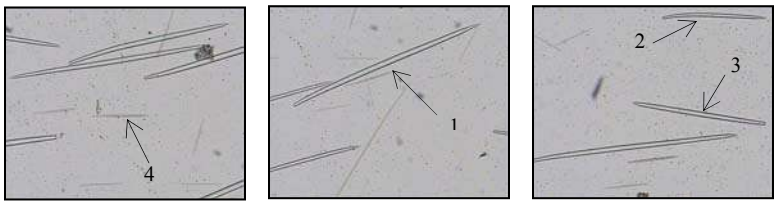

Figure 1: Spicules of B01/001
1: megascleres- strongyloxeas; 2: curve styles; 3: straight styles; 4: microsceleres- styles

Thin Layer Chromatography

TLC chromatogram of developed plates are shown in Figure 2 and 3. TLC of specimen B02/005, B02/003, B01/008, B01/007, B02/008, B02/004, B02/006 and B02/007 did not show any similarities. But for specimen R01/001, R02/001, R03/001, P01/001, P02/001, P03/001, B01/001, B02/001 and B03/001, the consistency in TLC pattern can be seen suggesting that they are belong to the same group (genus). They possess characteristically two main spot at Rf 0.25 and Rf 0.88, intense yellow and blue fluorescence, respectively. This finding also in agreement with morphology characters as well as the microscopic examination.

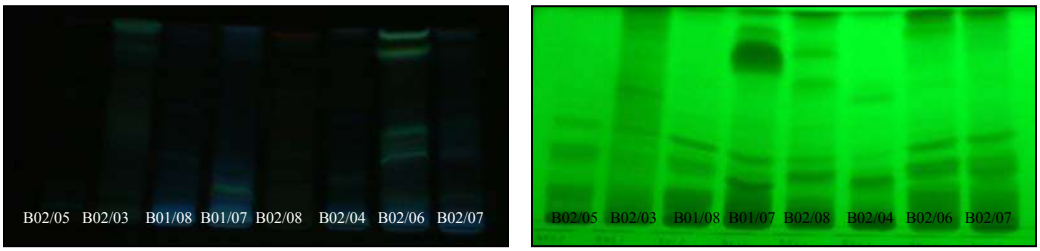

Figure 2. TLC chromatogram of B02/005, B02/003, B01/008, B01/007, B02/008, B02/004, B02/006 and B02/007 under UV 365 nm and 254 nm.

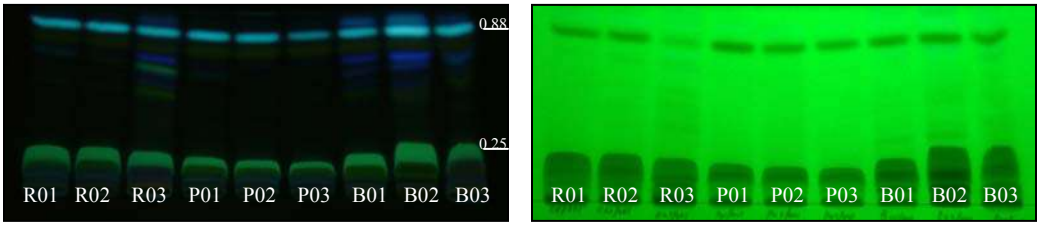

Figure 2. TLC chromatogram of R01/001, R02/001, R03/001, P01/001, P02/001, P03/001, B01/001, B02/001 and B03/001 under UV 365 nm and 254 nm..

The divergence in chemical composition between sponges collected at the same locality is demonstrated suggesting that apart from morphology examination, chemical profiling also provide useful results. As for the specimen that give same profile, which identify as *Aaptos sp.* show that chemical markers can be of great utility for the species level systematic of sponges.

The results presented here is a preliminary finding. The investigation is in progress to characterize and establish a chromatographic profiling which could provide the images of chemical components of not only the establishment of marker compounds but also other active or potential bioactive constituents.

Acknowledgement

The authors wish to thank the Ministry of Science, Technology and the Environment Malaysia for the fund provided under the Intensified Research in Priority Areas Research Grant (No. 01-02-12-0068-EA10707).

References

(1) Belarbi, E. H., Raminez, D. M., Ceron Garcia, M. C., Contreras Gomez, A., Garcia Camacho, F., Molina Grima, E. (2003). Cultivation of explants of marine sponge *Crambe crambe* in closed systems. *Biomol Eng* 20: 333-337.

(2) Uriz, M. J., Turon, X., Becerro, M. A., Galera, J. (1996). Feeding deterrence in sponge. The role of toxicity, physical defenses, energetic contents, and life-history stage. *J Exp mar Biol Ecol* 205: 187-204.

(3) Pawlik, J. R., McFall, G., Zea, S. (2002). Does the odor from sponges of genus *Ircinia* protect them from fish predators? *J Chem Ecol* 28: 1103-1115.

(4) Zhang, W., Zhang, X., Chao, X., Xu, J., Zhao, Q., Yu, X. (2003). Optimizing the formation of *in vitro* sponge primorphs from the Chinese sponge *Styletella agminata* (Ridley). *J Biotechnol* 100: 161-168.

(5) Kelly-Borges, M., Robinson, E. V., Gunasekara, S. P., Gunasekara, M., Gulavita, N. K., Pomponi, S. A. (1994)

(6) Bobzin, S. C., Yang, S., Kasten, T. P. (2000). Application of liquid chromatography-nuclear magnetic resonance spectroscopy to the identification of natural products. *J Chrom B* 748: 259-267.

Malaysian Journal of Analytical Sciences, Vol.9 No.3(2005): 453- 457

FATTY ACID COMPOSITION OF SOME MALAYSIAN LOCAL FRUITS

Suhana Samat, Jalifah Latip and Mamot Said

School of Chemical Science and Food Technology, Faculty of Science and Technology, Universiti Kebangsaan Malaysia(UKM), 43600 Bangi

Abstract. The seeds oil of seven Malaysian local fruits, i.e. three *Lansium domesticum* varieties (duku, duku langsat and langsat), durian (*Durio zibethinus*), rambutan (*Nephelium lappaceum*), rambutan gading (*Nephelium cuspidatum* Blume) and mangosteen (*Garcinia mangostana*) were analysed for their fatty acid composition. These fruits were collected from various locations around Bandar Baru Bangi, Selangor. The fatty acid composition were determined by gas chromatography after converting the oils into methyl ester of their fatty acids. Results showed that the seeds oil of *Lansium domesticum* varities (duku, duku langsat and langsat) were high in unsaturated fatty acids. For instance, oil from duku langsat seed contained 62.88% linoleic acid and duku contained 21.21% oleic acid. While the other seeds like rambutan, rambutan gading and durian contained 38.41%, 38.22% and 37.43% arachidic acids respectively, while mangosteen were very high in stearic acid (56.96%). In conclusion, the major saturated fatty acids found in the seed oil were palmitic, stearic and arachidic acids, while the major unsaturated fatty acids were oleic and linoleic acids.

Abstrak. Minyak daripada tujuh jenis buah-buahan tempatan Malaysia, iaitu tiga varieti langsat *Lansium domesticum* (duku, duku langsat dan langsat), durian (*Durio zibethinus*), rambutan (*Nephelium lappaceum*), rambutan gading (*Nephelium cuspidatum* Blume) dan manggis (*Garcinia mangostana*) telah dianalisis komposisi asid lemaknya. Buah-buahan tersebut diperolehi dari sekitar Bandar Baru Bangi, Selangor. Komposisi asid lemak ditentukan dengan menggunakan kromatografi gas setelah lemaknya ditukarkan kepada ester metal asid lemak. Hasil kajian menunjukkan minyak daripada varieti *Lansium domesticum* (duku, duku langsat dan langsat) tinggi kandungan asid lemak tak tepu. Contohnya. duku langsat mengandungi 62.88% asid linoleik, manakala duku mengandungi 21.21% asid oleik. Sedangkan minyak daripada biji lain seperti rambutan, rambutan gading dan durian mengandungi 38.41%, 38.22% dan 37.43% asid arakidik, manakala bagi biji buah manggis kaya dengan asid steraik (56.96%). Kesimpulannya, asid lemak tepu utama dalam minyak biji buah-buahan tempatan ialah palmitik, stearik dan arakidik, manakala asid lemak tak tepu utama pula ialah asid oleik dan linoleik.

Keyword: local fruit seed, fatty acid composition and seed.

Introduction

In recent years, researches on nutrition have been focused mostly on calories and energy conversion factors of foods consumed. These developments stimulate research on the fats and oils since they have the highest energy content compared to proteins and carbohydrates [1]. Today, fats and oils (collectively known as triacylglycerols) are recognized for their nutritional, functional and organoleptic properties. Fats and oils have held unique, universal appeal that is well entrenched in the history of culinary science and yet to be matched by other food component [2]. Fats and oils are obtained from both animal and plant sources, only those from plant sources are cholesterol free In evaluating the nutritional quality of oil, the data on the fatty acid composition are very important [3]. Medium chain triacylglycerols (MCT) are the basis of new group of fats known as structured lipids (SLs) which have found application in clinical nutrition and treatment of diseases [4]. Within the class of structured lipids, two subgroups of fats must be recognized – the medium chain triglycerides (MCTs) and long chain triglycerides (LCTs). SLs are triacylglycerols (TAGs) that have been modified by incorporation of new fatty acids, restructured to change the position of fatty acids. Basically SLs contain mixture of short-, medium-, and long fatty acids attached to the glycerol backbone for specific functionality [5] (Fig. 1). SL are developed for specific purposes, such as to produce a reduced calorie fats and enhance the nutritive value of the foods. SLs is panacea for all disease or metabolic conditions. To achieve

maximum effect, SLs will have to be designed on a case-by-case basis for targeting a specific disease conditions or for food use [6]. MCTs are much more readily metabolized for energy than LCTs but have low tendency to be incorporated into adipose tissues to form depot fat. Current applications of MCTs take advantage of their quick absorption and oxidation. MCTs should not to be given alone, however. They are usually given in

combination with LCTs to meet the essentially fatty acid requirements. It is necessity of an MCT/LCT combination that inspired the development of structured lipid (SLs). The medium chain fatty acids could be easily obtained from either coconut oil which contain 4.6-9.4% and 5.5-7.8%, or in palm kernel oil contains 2.4-6.2% and 2.6-5.0% of C8:0 and C10:0 respectively [7]. While the tropical fruits seeds may be the main sources of long fatty acids. Therefore, the aims of the present investigation are to identify the best sources of long chain fatty acid from local fruit seeds. In order to select the best and high level of long chain as arachidic acid sources, it is imperative to study the fatty acids composition of Malaysian local fruit seeds.

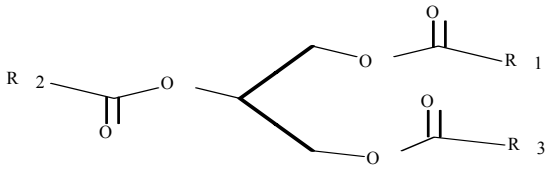

R 1 , R 2 = short/medium chain FAs
R 3 = long chain FA

Figure 1: General structure of structured lipids containing medium and long chain fatty acids.

Experimental

Raw Materials

Seven Malaysian local fruits, i.e. three *Lansium domesticum* varieties (duku, duku langsat and langsat), durian (*Durio zibethinus*), rambutan (*Nephelium lappaceum*), rambutan gading (*Nephelium cuspidatum* Blume) and mangosteen (*Garcinia mangostana*) were purchased from various locations around Bandar Baru Bangi, Selangor. The rinds and pulps of the fruits were removed manually and the seeds were collected. About 10kg of each fresh fruits were used for the studies.

Oil extraction

The seeds were then dried in laboratory oven at 60ºC for 4 days. The seeds were ground and about 45g ground seeds were extracted for 16 hour with n-hexane in a Soxhlet apparatus to obtain the fat/oil. Figure 1 shows the scheme of oil extraction applied. The n-hexane extract was filtered and the oil recovered in a rotary evaporator. Residual hexane was removed by heating the samples to 60ºC while flushing the oil with a stream of nitrogen. Fat/oil was placed in air tight vials and stored at -4°C until analyzed.

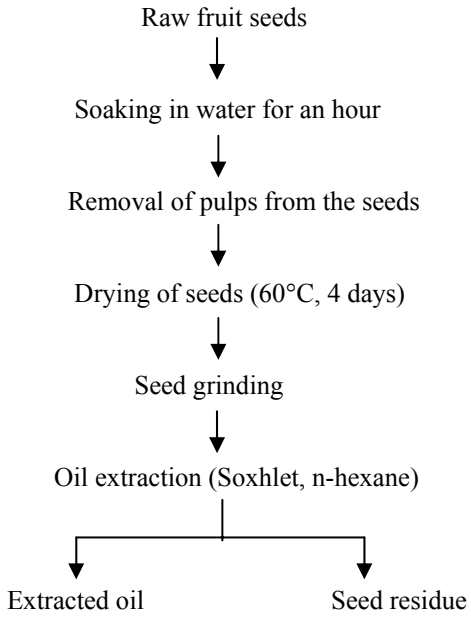

Figure 2: Fat extraction of fruit seeds

Fatty acid analysis

The fatty acid composition of the seed oils was determined based on fatty acid methyl esters (FAME) according to the method of [8]. Two ml of methylation solution (a mixture of sodium methoxide and methanol) was added into 0.1µl of samples, and the mixture was shaken for 10 seconds and waited for 30 minutes until the mixtures separated into two phases. Then 5µl of the methylated samples (upper phase) was injected into Agilent 6890 series Gas chromatography equipped with flame ionization detector (FID), column (BPX 710, 60m long, 0.32mm i.d., film thickness 0.25µm) with the following conditions: the column oven temperature was programmed from 120-180°C at 4°C /min and hold to 210°C for 4 minits and the injector and detector temperature were set at 240°C, split ratio 1:60. Analysis was carried out with nitrogen as carrier gas at 1.5ml/min. A small quantity of FAME solution (1µl) was introduced onto the column. The peaks were identified by comparing the retention times of the sample FAMEs with standard FAMEs, followed by plotting the log of retention times against equivalent carbon length (ECL). The percentage of each peak was calculated as the percentage of the total area of all the peaks [9]. The results of the present study are means of duplicate analyses from each samples collected.

Thermal properties

Thermal properties of the extracted oils were analyzed by using differential scanning calorimeter (DSC 822e Metler Toledo) equipped with a thermal analysis data station. The calorimeter was calibrated with indium (melting point, 156.6°C; ΔH_f : 28.45 J/g). Samples (2 - 4mg) were weighed in a thermo balance (TA), in an aluminium SFI capsules with a precision of ±0.01mg. An empty capsule was used as a reference. The temperature program for the calorimeter was:

a) cooling to -40°C and heating at 10°C/min to 60°C. Registration of the melting profile.
b) heating at 60°C for 10 min and cooling at 10°C/min to -40°C. Registration of the crystallization profile.

Temperatures of the melting and crystallization were determined based on the onset and end set readings in the thermograms obtained.

Result and Discussion

Fatty acid composition

The fatty acid compositions of seven Malaysian local seed fruits are presented in Table 1. Fatty acids greater than eicosaenoic acid (C20:1) were not detected in the seed oils. Similarly low molecular weight acids (lauric and miristic) were absent in all samples investigated. However, palmitic (C16:0) acid was detected in all samples with the highest content was found in langsat (43.88%). Stearic acids (C18:0) also found in all samples but the highest level was found in mangosteen (56.96%). Arachidic acid (C20:0) present in all samples investigated with rambutan is the highest (38.41%) and mangosteen the lowest (0.70%). It is evident from the results that the main saturated fatty acids found in the local seed oils were palmitic, stearic and arachidic acids.

Palmitoleic acid (C16:1) was detected in all samples and the highest (1.88%) is found in duku seed oil. The major unsaturated acids in the seed oils investigated were oleic (C18:1) and linoleic (C18:2) acids with the latter was found in the greater proportion. Linoleic acid was found the highest (62.88%) in duku langsat seeds oil but the lowest (1.53%) in rambutan fat/oil. While for the oleic acid (C18:1), the highest (38.11%) was found in rambutan gading oil and the lowest (6.11%) in langsat oil The seed oils of all seven samples investigated were richer in linoleic than oleic acids. Eicosenoic acid (C20:1) was detected in all samples except in rambuatn gading oil. The seed oils of all seven samples investigated had lowest level of polyenoic fatty acids than monoenoic fatty acids. From the average figures presented, it appears that there are not significant differences in the arachidic acid content of rambutan (38.41%) and rambutan gading (38.22%) seed oils.

Thermal behavior of seed oils

The melting profiles of the seed oils extracted were analyzed by differential scanning calorimetry (DSC) and the result is shown in Table 2. Results show that during melting, there are low melting fractions of mangosteen (19.73°C), duku (18.25°C) rambutan (6.74°C), rambutan gading (6.61°C), durian (6.24°C), and duku langsat (-1.75°C). However there was no low melting fraction for langsat. The highest melting fractions for duku, duku langsat, langsat rambutan, mangosteen, durian and rambutan gading were 51.91°C, 49.88°C, 49.62°C, 32.78°C, 26.40°C 26.24°C, and 23.54°C respectively. All the samples completed the phase changes around 30-50°C. The

melting enthalpy of mangosteen, rambutan, rambutan gading, durian, duku langsat, duku and langsat were 107.98 J/g, 69.24 J/g, 66.86J/g, 65.10 J/g, 12.32 J/g, 10.66 J/g and 1.46 J/g respectively. This showed that the fats from mangosteen was the hardest and langsat the softest. As shown in Table 2, all the fats studied showed two maxima for melting. The first one corresponds to the low melting fraction, and the second one corresponds to the higher melting fraction. While for the crystallization, most of the samples analyzed showed more than one peaks except duku, duku langsat and langsat. The first peaks of crystallization of rambutan, rambutan gading durian, mangosteen, duku and duku langsat, were 21.02°C, 20.97°C, 20.01°C, 16.81°C, 11.92°C and -4.74°C respectively. The second peaks crystallization of rambutan, rambutan gading, durian and mangosteen, were 3.43°C, 3.40°C, 2.93°C and -8.28ºC respectively. The crystallization entalphy (ΔH_c) of mangosteen, rambutan, durian, rambutan gading, duku and duku langsat were 61.95 J/g, 50.62 J/g, 50.19 J/g, 49.61J/g, 15.64 J/g and 8.02 J/g.

According to Hagemann [10], lipids (fatty acids, acylglycerides, fats and oil) from vegetable origin generally demonstrate polymorphism and more frequency, solidify in three different crystalline forms: α, β' and β, with correspondingly higher melting temperatures. Polymorph α (lowest melting point) is generally present after rapid cooling processes from melted fat. Form β' with a higher melting or melting point than the previous one, is generated through solidification of fat under certain conditions or temperatures or due to transition from form α. Polymorph β, the most stable crystalline form, is produced from the other two form by incubating at slightly higher melting temperatures than for the α form.

Table 1: Fatty acid compositions (%) of some Malaysain local seed oils

Fatty acid	Rambutan (Nephelium lappaceum) (Mean±S.E)	Rambutan gading (Nephelium cuspidatum Blume) (Mean±S.E)	Mangosteen (Garcinia mangostana) (Mean±S.E)	Durian (Durio zibethinus) (Mean±S.E)	Duku (Mean±S.E)	Duku langsat (Mean±S.E)	*Langsat (Mean±S.E)*
C16:0	4.49±0.53	2.88±0.002	3.71±0.07	5.43±0.16	7.48±0.09	18.62±0.42	*43.88±0.52*
C18:0	7.82±0.24	1.25±0.71	56.96±2.08	8.08±0.24	7.37±0.05	4.82±0.09	*12.84±0.04*
C20:0	38.41±3.03	38.22±0.53	0.70±0.12	37.43±1.13	4.86±1.25	1.42±0.34	*3.58±0.09*
C16:1	0.37±0.06	0.22±0.003	-	0.51±0.02	1.88±0.07	0.17±0.07	*1.17±0.08*
C18:1	32.10±2.98	38.11±1.43	17.46±0.03	36.75±1.11	21.21±0.42	6.72±0.08	*6.11±0.01*
C20:1	5.53±0.22	-	0.15±0.01	6.19±0.19	16.37±0.56	1.53±0.07	*1.46±0.14*
C18:2	1.53±0.36	2.61±0.06	15..98±2.12	2.33±0.34	3.00±0.14	62.88±0.48	*7.07±0.24*
TSFA TUFA	25.36±1.89 19.77±1.81	21.17±0.63 19.97±0.31	30.68±1.14 16.79±2.16	25.47±1.54 22.89±0.83	24.86±0.69 21.24±0.59	12.42±0.43 35.66±0.34	30.15±0.33 7.91±0.24

[a]Each value represent the mean of duplicate. TSFA, Total Saturated Fatty Acid; TUFA, Total Unsaturated Fatty Acid

Table 2: Melting behavior of some Malaysain local seed oils

Samples	Weight (mg)	ΔH_f (J/g) Melting	ΔH_f (J/g) Crystallization	Transition temperature				
				Melting			Crystallization	
				1	2	3	4	5
Rambutan gading	4.38	66.86	49.61	6.61	23.54	n.d	20.97	3.40
Rambutan	5.96	69.24	50.62	6.74	24.31	32.78	21.02	3.43
Durian	5.72	65.10	50.19	6.24	23.10	26.24	20.01	2.93
Duku langsat	10.27	12.32	8.02	-1.75	n.d	49.88	-4.74	n.d
Duku	7.28	10.66	15.64	18.25	n.d	51.91	11.92	n.d
Langsat	4.02	1.46	-	n.d	n.d	49.62	n.d	n.d
Mangosteen	4.47	107.98	61.95	19.73	22.33	26.40	16.81	-8.28

Acknowledgements

The research is supported by the IRPA no: 09-02-04-004 BTK/ER/008.

References

1. Kinsella, J.E. 1988. Food Lipids and Fatty acids: Importance in Food Quality, Nutrition and Health. *Food Technology*. 42 (10): 124 -145
2. Akoh, C.C. 1998. Structured Lipids in *Food Lipids*: Chemistry, Nutrition and Biotechnology. New York: Marcel Dekker, Inc
3. Ezeagu, I.E., Petzke, K.J., Lange, E. A & Metges, C.C. 1998. Fatty Acid Composition of Oils Extracted from Selected Wild Gathered Tropical Plant Seeds from Nigeria. *J. Amer. Chem. Soc*. 75(8): 1031-1035
4. Kennedy, J.P.1991. Structured Lipids: Fats of the Future. *Food Technology*. 45(11): 76-83
5. Haumann. 1997. Structured Lipids. *INFORM*. 8(10): 1004-1011
6. Akoh, C.C. 1995. Structured Lipids- enzymatic approach. *INFORM*. 6(9): 1055-1061
7. Gunstone, F.D., Harword, J.L. & Padley, F.B. 1994. *The Lipid Handbook*. 2nd edn. Chapmann & Hall Ltd.
8. Timms, R.S. 1978. Artefact peaks in the preparation & gas liquid chromatographic determination of methyl esters. *Aust. J. Dairy, Technol.* 33(1):4-6
9. AOAC.1990. *Official Methods of Analysis of the Association of Official Analytical Chemists*, 13th edn. Washington DC, USA
10. Hagemann, J.W. 1988. Thermal Behavior and Polymorphism of Acylglycerides in Garti,N & Sato,K. Crystallization and Polymorphism of Fat and Fatty Acids. 31**.** Marcel Dekker, N.Y

Malaysian Journal of Analytical Sciences, Vol.9, No. 3(2005): 458 - 462

Conversion of Industrial Wastes into Commercially Viable Products

Mohd Shahir Zakaria[1], Rose Aini Kamarudin[1] and Hairul Fariz Shamsuddin[2]

[1]*Universiti Tenaga Nasional, Kajang*
Km 7, Jalan Kajang-Puchong, 43009 Kajang, Selangor. Tel:603-8921 2020 Fax:603-8928 3506

[2]*Universiti Putra Malaysia*
43400 Serdang, Selangor

Abstrak

Bahan buangan industri dan proses pembuangannya telah menarik minat yang besar dalam tahun yang kebelakangan ini, didalam konteks 'revolusi bersih' untuk memupuk pembangunan industri yang bersih. Kertas ini membincangkan dua jenis sisa industri iaitu gypsum merah dan abu terbang. Gypsum merah adalah bahan buangan daripada industri pengeluaran pigmen putih, TiO_2, daripada bijih ilmenit. Abu terbang pula adalah sisa daripada loji tenaga yang menggunakan arang batu sebagai bahan bakar. Pencirian kedua-dua bahan buangan ini telah dijalankan menggunakan teknik-teknik seperti Mikroskopi Electron Pengimbas (SEM), serakan tenaga sinar-X (EDX) dan Pembelauan Sinar-X (XRD). Mikrograf SEM bagi gypsum merah menunjukkan sifatnya yang amorfus, padat dangan saiz partikel yang tidak seragam. Kehadiran sebatian besi memberikan warna kemerahan kepada gypsum merah. Kemudian untuk abu terbang dari loji tenaga Kapar, ia dikenalpasti bersifat amorfus, partikel berbentuk sfera dan mempunyai taburan saiz partikel yang luas bergaris pusat purata, 7.261 ± 5.770 μm. Dua sebatian utama yang boleh dijumpai didalam abu terbang ialah silikon dioksida (SiO_2) dan mullit, $Al_6Si_2O_{13}$. Hasil keputusan pencirian terdahulu bagi kedua-dua gypsum merah dan abu terbang, beberapa potensi penggunaannya telah dicadangkan antaranya sebagai bahan dalam licau (gerlis), komponen tanah liat dan sebagainya. Kajian awalan telah dijalankan untuk mencari kegunaan gypsum merah dan abu terbang. Kedua-duanya bahan tersebut menunjukkan potensi untuk digunakan sebagai licau (gerlis) untuk permukaan jubin seramik.

Abstract

Industrial waste and its disposal have attracted major interest in recent years, in the context of 'clean revolution' to promote clean industrial development. This paper discusses two industrial waste *i.*e. red gypsum and fly ash. Red gypsum is a waste product in the manufacture of the white pigment, TiO_2, from the ore ilmenite. The latter *i.e.* fly ash is a waste product from coal-fired power plants. The characterizations of both waste materials have been studied using Scanning Electron Microscopy (SEM), Energy Dispersive X-ray (EDX) and the X-Ray Diffraction techniques. The SEM micrograph for the red gypsum showed that it is amorphous, compact with non-uniform particles sizes. The presence of the iron compound gives the reddish coloration to the red gypsum. As for the fly ash from TNB plant in Kapar, it is found to be amorphous in nature from the SEM micrograph with spherical particles of broad particle size distribution having a mean diameter of 7.261 ± 5.770 μm. Two major compounds found in the fly ash are silicon dioxide (SiO_2) and mullite, $Al_6Si_2O_{13}$. As a result from the earlier characterization of both red gypsum and fly ash, several potential applications of these wastes have been proposed i.e. as glaze constituent, clay body components etc. Preliminary investigation has been done to find an application for both red gypsum and fly ash. Both red gypsum and fly ash have shown potential to be used as glaze on ceramic tiles.

Keyword: red gypsum, fly ash, waste, glaze.

Introduction

Red gypsum is an industrial waste material, which is produced in abundant from industries that synthesized the white pigment, titanium dioxide (TiO_2), using the sulfate method. Red gypsum is reddish brown in color with texture like that of semi-dried mud or clay. From a previous study, red gypsum was shown to be microcrystalline to amorphous in nature with non-uniform particles. In addition, it was also revealed that red gypsum comprised mainly of hydrated and anhydrous $CaSO_4$ and Fe_2O_3. As for the fly ash from TNB power station in Kapar, Selangor it is found to be amorphous in nature from the SEM

micrograph with spherical particles of broad particle size distribution having a mean diameter of 7.261 ± 5.770 μm. Two major compounds found in the fly ash are silicon dioxide (SiO_2) and mullite, $Al_6Si_2O_{13}$. From the chemical analysis, fly ash contains mainly vitreous material comprising SiO_2, Al_2O_3 and Fe_2O_3 and in smaller amounts CaO, MnO, TiO_2, K_2O and Na_2O. Glaze is a thin, nearly homogeneous layer composed of molten silicate mixture, which is formed by inorganic oxides and silica. Its appearances can be either lustrous or matt, and could be colored or colorless. Major constituents of glaze are silica, flux and refractory materials. In this particular study, both red gypsum and fly ash were investigated for their potentials as glaze on tiles. A standard zinc-based glaze formulation was identified in which the calcium carbonate and silica in the original formulation was substituted with red gypsum and fly ash respectively.

Experimental

Standard Zinc Oxide Glaze

Zinc oxide, calcium carbonate, potash feldspar, kaolin and silica were weighed according to the standard zinc-based glaze formulation and placed in a plastic container. The mixture was then placed in an electric mortar. 150 ml of water was added and the mixture was stirred at high speed for 60 minutes. The consistency of the mixture was like pancake batter and it was applied on the commercial tiles, which had been cut into 1" square. The tiles were dried naturally prior to firing at 1200ºC in a furnace.

Components	Zinc Oxide	Calcium Carbonate	Potash Feldspar	Kaolin	Silica
Amount (grams)	8.55	25.35	35.30	5.45	25.35

Table 1. Standard Zinc Oxide Glaze Compositions

Figure 1. Glaze Preparation Method

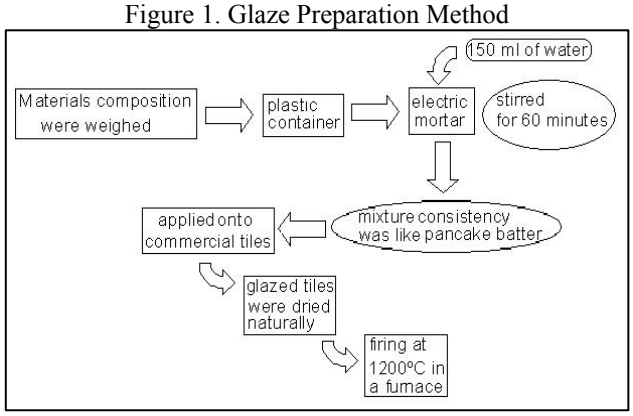

Red Gypsum Glaze

The method used is similar to that of the standard zinc-based glaze however; red gypsum was used in place of calcium carbonate (Table 2).

Table 2. Red Gypsum Glaze Compositions

Formula No.	Zinc Oxide	Red Gypsum	Potash Feldspar	Kaolin	Silica
1	8.55	25.35	35.30	5.45	25.35
2	5.75	17.05	23.74	32.99	20.46
3	4.56	13.50	18.80	14.52	48.62

Fly Ash Glaze

The method used is similar to that of the standard zinc-based glaze. However, here fly ash was added into the original composition. The percentage of fly ash added was shown in Table 3.

Table 3. Fly Ash Glaze Compositions

Formula No.	Zinc Oxide	Calcium Carbonate	Potash Feldspar	Kaolin	Silica	Fly Ash
1	5.00	25.00	35.00	10.00	0.00	25.00
2	5.00	25.00	35.00	10.00	10.00	15.00
3	5.00	25.00	25.00	10.00	10.00	25.00

Red Gypsum and Fly Ash Glaze

The method used is similar to that of the red gypsum glaze with fly ash added (15 % of total weight). Refer Table 4.

Table 4. Material Composition for Glaze combination of Red Gypsum and Fly Ash

Components	Zinc Oxide	Red Gypsum	Potash Feldspar	Kaolin	Silica	Fly Ash
Amount (gm)	5.00	25.00	35.00	10.00	10.00	15.00

Control Samples

Control sample for both wastes were made by using the red gypsum or fly ash entirely in the glaze formulation without any addition of other components except water.

Results and Discussion

Visual Examination Of Glazed-Tiles

The visual examinations were made based on the following characteristics i.e. glossiness, smoothness, color and presence and severity of defects.

Pure Red Gypsum Glaze

When the tile glazed with red gypsum only was fired, the surface was found to be slightly shiny, orange to dark brown in color and black spots present. These dark spots were presumably Fe_2O_3 that hardened upon cooling.

Figure 3. Red Gypsum Glaze before firing

Figure 4. Red Gypsum Glaze after firing

Pure Fly Ash Glaze

After firing the surface of the tile was found to be very powdery and quite rough. The original grey color of the fly ash before firing turned to light brown. Powdery surface observed in the center of the tile may have resulted from incomplete melting of the fly ash which is known to contain mainly silica with a high melting point (1700 ^oC).

Figure 5. Fly Ash Glaze before firing

Figure 6. Fly Ash Glaze after firing

Standard Zinc Oxide Glaze

A standard zinc oxide based glaze with the composition as shown in Table 1 was used. The glazed tiles were found to be glossy and homogeneous. However, some crazing (cracks) were also observed and the surface was not smooth. The occurrence of glaze crazing is identified to be due to the differences in thermal expansion between the tiles and the glaze.

Red Gypsum Incorporated in Zinc Oxide Glaze

In this particular glaze preparation, calcium carbonate in the standard zinc oxide glaze was replaced by red gypsum which is mainly calcium sulfate. This switch was done considering the similarity of both red gypsum and calcium carbonate. Three different variations of the glaze formulations were performed as shown in Table 2. The best glazed tile in terms of physical appearance is from formulation number 1 which contains 35.30 % feldspar, 5.45 % kaolin, 25.35 % silica, 8.55 % zinc oxide and 25.35 % red gypsum. The surface of the tile is glossy, intense brown in color with homogenous surface finish. The appearances of the tiles with the other formulations are described in Table 5.

Table 5. Red Gypsum Incorporated in Zinc Oxide Glaze

Formula No.	Appearance of Glaze
1	Very smooth, glossy homogeneous surface, brown color
2	Rough, matt, not homogeneous with white-gray color
3	Rough, semi-glossy and quite homogeneous, light gray color

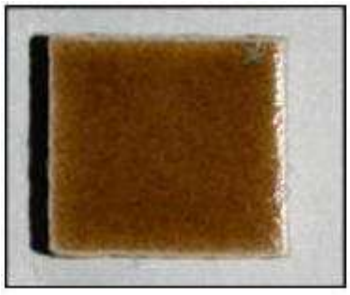

Figure 6. Formulation No. 1

Figure 7. Formulation No. 2

Figure 8. Formulation No. 3

Fly Ash Incorporated in Zinc Oxide Glaze

Three variations of the glaze formulations were performed and these are shown in Table 6. Tile number 1 with the fly ash replacing all the silica was found to be glossy, rough with intense pale yellow color surface. Tile number 2 with 10 % silica and reduced fly ash content compared to tile number 1 is also glossy but smooth and pale yellow color. Some crazing is observed on tile number 2. Tile number 3 has similar characteristics to the previous two tiles. The only difference is that tile number 3 had noticeable air bubbles underneath the glaze. However, in term of surface defect (crazing), it was observed that tiles applied with thinner layer of glaze showed less crazing. The occurrence of glaze crazing is identified to be due to the differences in thermal expansion between the tiles and the glaze.

Table 6. ***Fly Ash Incorporated in Zinc Oxide Glaze***

Formula No.	Appearance of Glaze
1	glossy, rough, intense pale yellow, some crazing
2	glossy, smooth, pale yellow, some crazing
3	glossy, rough, intense pale yellow, some crazing and air bubbles

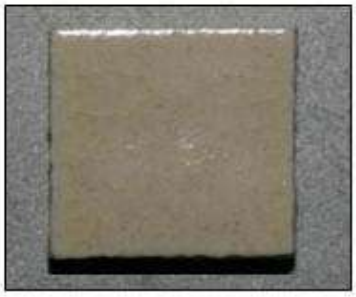

Figure 9. Formulation No. 1

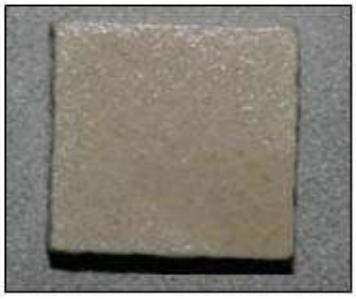

Figure 10. Formulation No. 2

Figure 11. Formulation No. 3

Combination of Red Gypsum and Fly Ash in Zinc Oxide Glaze

A glaze which combined both the red gypsum and fly ash was also tried. The glaze produced was dark brown in color, semi-glossy, smooth and quite homogenous.

Conclusion

Based on the above study, it can be concluded that red gypsum and fly ash in addition to other materials can be converted into new, useful and commercially viable products. As far as our study is concern, red gypsum and fly ash when added to other compounds (components of standard zinc oxide glaze in this case) can be used as glaze on tiles. In our study, the best-glazed formulation incorporating red gypsum was found to contain 35.30 % feldspar, 5.45 % kaolin, 25.35 % silica, 8.55 % zinc oxide and 25.35 % red gypsum. This particular glaze formulation produces glossy, smooth, colored and defect free surface. Further work will concentrate on increasing the red gypsum content without compromising on the physical appearance of the glaze. As for the glaze that uses zinc oxide formulation with fly ash added to it (refer to Table 3), the fly ash showed great potential to be utilized as glaze. However, several common glaze defects such as crazing and air bubbles were observed on the glazed tiles. The occurrence of glaze crazing is identified to be due to the differences in thermal expansion between the tiles and the glaze. This renders further investigation to eliminate the defects and thus achieving a much better quality glaze. The glaze formulation which incorporates both red gypsum and fly ash also showed potential. The glazed tiles obtained were dark brown in color, glossy, smooth and homogenous. These results showed the potential of both waste materials *i.e.* red gypsum and fly ash to be used together in one single formulation. Apart from the visual examinations discussed in this paper, there are several other tests that will be carried out on these glazed tiles i.e. scanning electron microscopy (SEM) analysis, weathering test etc. The results of these analyses will be discussed in future publications.

Acknowledgement

The authors acknowledged the support from the Ministry of Science, Technology and Environment under IRPA grant (as of Jan 2004) and Universiti Tenaga Nasional for a seeding fund to start of the project. Special thanks are directed to Dr. Ramesh of UNITEN, Dr. Teng Wang Dun and Encik Jaafar of SIRIM.

References

[1] *Chemical composition of red gypsum sample from TiO_2 landfill.*Chai Mee Kin, Rose Aini Kamarudin, Lee Fai Tsen, Proceedings of Malaysian Chemical Conference 2001, Nov 7-9, Penang.

[2] *Chemical Analysis and potential application of an industrial waste material from local paint factory.* Rose Aini Kamarudin, Chai Mee Kin, Lee Fsai Tsen, Shamsu Mohamad, Proceeding of the International Conference & Exposition on Pure and Applied Chemistry (PACCON 2002), Bangkok.

[3] *The chemical indentification of red gypsum and its potential as a glazing agent.* Chai Mee Kin, Rose Aini Kamarudin, Lee Fai Tsen, Shamsu Mohamad, Proceedings of the XIX Regional Conference on Solid State Science and Technology, 2002 Oct 31-Nov 1, Kuching.

[4] *Fly ash from Kapar Power Station – Its Characterization and Potential Application.* Rose Aini Kamarudin, Chai Mee Kin, Ramesh Singh and Lee Fai Tsen, Shamsu Mohamad, The XX Regional Conference on Solid State Science & Technology (MASS 2003), 12-14 Dec. 2003, Lumut Perak.

Malaysian Journal of Analytical Sciences, Vol.9, No. 3(2005): 463 - 474

NICOTINAMIDE HYDROLYSIS IN ACID AND ALKALINE SOLUTION: DETERMINATION OF TOTAL NIACIN IN FOODS

Fadzil Othman, Norziah Mohd.Hani and Ibrahim Che Omar[1].
*School of Industrial Technology, Food Technology Division,
[1]School of Biological Sciences
Universiti Sains Malaysia, 11800 Minden,
Penang, Malaysia.

*Corresponding author: Prof Madya Dr Norziah Mohd Hani (norziah@usm.my, Fax: 04-6573678)

Abstract

The effectiveness of autoclaving time under acid and alkaline conditions for the conversion of nicotinamide into nicotinic acid for the determination of total niacin content in various food samples were investigated. Hydrolysis of nicotinamide solution in 0.22 M $CaOH_2$ and 1 M NaOH under autoclave heating conditions (121^0C, 15 psi) for 1 hour fully converted nicotinamide into nicotinic acid. Nicotinamide did not convert into nicotinic acid after using the same heating treatment for 1 hour in hydrochloric acid solution and only 7% conversion to nicotinic acid was obtained with 2 hours heat treatment.

Determination of niacin in various food samples including vitamin drinks by Ion Pair Reversed Phase Chromatography, using Supelcosil LC-ABZ (4.6 x 150 mm) C18 column and mobile phase consisting of a mixture of 23% acetonitrile, 0.1% phosphoric acid and 0.1% sodium dodecyl phosphate is presented in this paper. Recoveries of added standard into the food samples using the HPLC method, gave results ranging from 78 – 102%. Limit of quantification for nicotinamide and nicotinic acid was 0.26mg/100g and 0.04 mg/100 g, respectively. A comparison between the HPLC method and microbiological assay for the determination of total niacin content in food samples was also made. The results obtained by microbiological assay was found to be relatively higher than HPLC except for biscuit samples.

Keywords: niacin, nicotinamide HPLC, microbiological assay.

1. Introduction

The niacin vitamers found in foodstuff includes nicotinic acid, nicotinamide, nicotinyl-esters or niacytin, and the coenzyme forms nicotinamide adenine dinucleotide (NAD) and nicotinamide adenine dinucleotide phosphate (NADP). Nicotinic acid is present in a wide variety of foods. In cereals, nicotinic acid is normally bound to the macromolecules. Free nicotinic acid, unless fortified, usually present as a minor component in most food (Eitenmiller *et al.,* 1999). Autoclaving in mineral acid solutions as well as combining autoclaving with enzymatic reactions are the common extraction procedures to liberate bound niacin in food samples. Food sources of niacin are cereals and seeds which contain primarily nicotinic acid, whereas fish and meat contain primarily nicotinamide (Rusell, 1996).

The term `total' and `free' with regards to niacin in food are defined by the extraction procedures in the analysis (Sallin *et a*l., 2001). Total niacin refers to amount of niacin extracted by autoclaving food samples in alkaline solutions, in 1 M or 0.5 M acid solution while free niacin refers to amount extracted in 0.1 M acid solution. Either acid or alkaline hydrolysis can be used to convert nicotinamide into nicotinic acid. Acid hydrolysis is usually used to estimate the biologically active form of niacin while alkaline hydrolysis releases non bio-available vitamers (Sallin *et al.,* 2001

Various researchers have been using different autoclaving time and solutions in the extraction procedures to determine niacin content in food. Roy *et al.* (1983) had extracted niacin from urea-

hydrochloric acid solutions followed by autoclaved at 120ºC for 30 minutes. Egberg (1979), Ward *et al.* (1997) and Juraja *et al.* (2003) had carried out similar extraction procedures on food samples (mainly cereal) in $CaOH_2$ and autoclaved at 121ºC for 2 hours. Tyler and Genzale (1990) treated meat, semolina and cottage cheese in $CaOH_2$ and autoclaved at 121ºC for 15 minutes.

High performance liquid chromatography (HPLC) method in determining niacin by UV detection had been performed by Skurray (1981) in meat using enzymic hydrolysates followed by treatment with NaOH and potassium bromide in sample preparation. The LC system used reversed phase C18 column and a mobile phase containing heptane sulfonate as ion pair modifier in acetate buffer. Hamano *et al.* (1988) determined nicotinic acid and nicotinamide, which have different polarities, from meat using cation exchange on Partisil SCX 25 and phosphate buffer mobile phase. Chase *et al.* (1989) used a strong anion exchange column PRP-X100 (Hamilton Co.) with 2 % acetic acid as mobile phase and UV detector at 254 nm but this method is only applicable to fortified food because of chromatographic interferences, even after the extracted food has been cleaned on florisil column. Hirayama and Maruyama (1998) used basic extraction for vinegar and jams. The extracts were subjected to an anion exchange column followed by a cation cartridge column before being injected onto Asahipak NH2P-50 column for analysis. The extracts need to be evaporated with rotary evaporator before passing through each SPE column. Hirayama (1998) then used the same basic extract to determine total niacin in vinegar.

Tyler and Genzale (1990) developed an analysis method to determine total niacin in beef, semolina and cheese. The sample was extracted in $CaOH_2$, cleaned up using C18 Sep Pak cartridge and chromatographed on C18 column with 23% Acetonitrile containing 0.1% phosphoric acid and 0.1% Sodium Dodecyl Sulphate as the mobile phase using uv detection at 254 nm. Windahl, *et al.* (1998), Ward, *et al.* (1997) and Juraja *et al.* (2003) separated nicotinic acid from cereals using C18 column and mobile phase consisting of 15% methanol, 85% water and 0.005M PIC A reagents. The extracts were cleaned using two solid phase extract (SPE) C18 followed by strong cation exchange (SCX).

The objective of the present work is to investigate the effectiveness of autoclaving time in acid and alkaline solutions for the conversion of nicotinamide into nicotinic acid. This paper also describes an HPLC method for the determination of total niacin in several types of food samples with comparison to microbiological assay method.

2. Materials and Methods

2.1 Reagents and chemicals

Nicotinic acid and nicotinamide were obtained from Sigma-Aldrich Co. USA. All other chemicals and solvents were AR grade or HPLC grade. Sodium dodecyl sulphate and oxalic acid were purchased from BDH chemicals. For sample clean-up, SPE C18 (EC) (500mg sorbent IST part number221-0050-C) and SPE Vacuum Manifold (International Solute Technology, IST) apparatus were used . HPLC-grade-water was purified in a Milli-Q system.

Standard Reference Material VMA 339 obtained from the American Association of Cereal Chemist (St Paul, MN, USA) was used for method validation.

2.2 Preparation of standards

Nicotinic acid and nicotinamide mixed stock solution of 1000 μg/ml was prepared by dissolving 100 mg nicotinic acid and 100 mg nicotinamide in 100 ml water. Nicotinamide solution (100 μg/ml) was prepared by dissolving 10 mg nicotinamide in 100 ml deionised water, kept at 5ºC and was used within one week.

A working standard solution (100 μg/ml mixed standard nicotinic acid and nicotinamide) was prepared by pipetting 10 ml of the stock solution into 100 ml of water. From this solution, further

dilutions were made to obtain working standard mixture solutions of concentration 0.05, 0.01, 0.1, 1.0 and 10 ug/ml. These solutions were prepared fresh daily.

2.3 Samples and Sample Preparation

The samples (milk powder, bread, biscuit, groundnut, banana and chicken meat) were purchased from local outlets. Bread sample was dried freeze dried; biscuit and groundnut were homogenized in a waring blender. These samples were then placed in clean and dry glass containers and kept in the dessicator. Banana and chicken meat samples were also homogenised but kept in portions of 5 g each in aluminium foil, stored frozen and were completely thawed before use.

2.4 Acid and alkaline hydrolysis for conversion of niacinimide into nicotinic acid

To two sets of 2 ml nicotinamide standard solutions (100 µg/ml), 20 ml of 0.22 M CaOH2 was added into each solutions. Triplicate solutions were made for each set. One set of solutions was heated in an autoclave for 1 hr at 121ºC (~ 15 psi) and another set for 2 hours. For NaOH and HCL hydrolysis respectively, 20 ml of 0.22 M $CaOH_2$ was replaced with 20 ml 1 N of NaOH and 1 N HCL. The cooled solutions were diluted to 50 ml with deionised water and mixed thoroughly. Twenty-five millilitres of the alkaline solution was adjusted to pH 7 with 10% oxalic acid. The solutions were centrifuged at 3000 rpm for 15 minutes and filtered through 0.45 um membrane filter before HPLC analysis.

2.5 Extraction of niacin from food sample

Alkaline extraction method described by Tyler and Genzale (1990); Ward *et al.* (1997); and Juraja *et al.*(2003) was used for the hydrolysis of niacinimide into nicotinic acid with slight modification. To apporoximately 1-2g of dry food samples and 2 – 5g of wet food samples, 0.75 g $CaOH_2$ and 20 ml of deionised water were added. For recovery test, 100 µg/ml nicotinamide solution of a suitable amount (2-5 ml) was added into food samples. The mixture was thoroughly mixed and autoclaved at 121ºC for one hour. The cooled extract was then made up to 50 ml volume with deionized water. 25 ml of extract solution was taken and adjusted to pH 7 with 10% oxalic acid which then made to 50 ml with deionised water. The resultant solutions were centrifuged at 3000 rpm for 15 minutes. 10ml of final sample extract was taken and passed through a conditioned (conditioning with methanol followed by 10 ml water) SPE cartridge C18 (end-capped). The last 3 ml solution eluted from the cartridge was collected and filtered into hplc vial for analysis. Sample drinks were diluted with water and adjusted to pH 7, filtered for HPLC analysis.

2.6 HPLC analysis

Analyses were performed with HPLC system: Waters 2690 Separation Module equipped with Waters 996 Photodiode Array Detector operating at 254nm controlled with Millennium Ver 3.2 chromatography manager data acquisition. A C18 Supelco column LC-ABZ (4.6 mm i.d. x 150 mm; 5 µm particle size) was used. HPLC separation was performed 30oC using mobile phase consisting of a mixture of 23 % acetonitrile, 0.1% sodium dodecyl sulphate and 0.1% phosphoric acid in ultra pure water Milli-Q. The pH of the solution was 2.2 and the eluent flow rate was 1 ml/min.

2.7 Microbiological Analysis

A microbiological assay was performed using *Lactobacillus plantarum* ATCC 8014 obtained from American Type Collection Centre, USA according to AOAC method 944.13 (AOAC, 1995).

3. Result and Discussion

3.1 Chromatographic separation and detection of nicotinic acid and nicotinamide

Fig. 1 shows a standard chromatogram for external calibration curve of mixed standard solutions of nicotinic acid and nicotinamide (10 µg/ml) in the LC system. The described HPLC method provides separation of nicotinic acid nicotinamide at retention time (RT) of 6.111 min and 7.699 min, respectively. Retention time shift allowed in the HPLC system was set at 5 percent (RT window). Reproducibility in RT within 10 successive runs for 10 ug/ml standard mixture solution of nicotinic acid and nicotinamide calculated as relative standard deviation (RSD) were 0.136 % and 0.137%, respectively. RSD for peak area calculation were 0.19% for nicotinic acid and 0.38% for nicotinamide.

Day-to-day variation in RT was checked and the reproducibility for 10 µg/ml mixed standard solution calculated as RSD were 1.3 % for nicotinic acid and 0.6 % nicotinamide. RSD for peak area calculation were 5 % for nicotinic acid and 2 % for nicotinamide. Linearity of standard curve obtained for mixed solutions of nicotinic acid and nicotinamide was between 0.05 µg/ml and 100 µg/ml with $r^2 = 0.9908$ and 0.9991for nicotinic acid and nicotinamide, respectively. Due to the occurrences of amide in HPLC column (Fig. 2), detection limit for nicotinamide (based on 3σ of the blank) and nicotinic acid (at 4.6σ) was 0.26 µg/ml and 0.04 µg/ml, respectively at concentration of 0.1 µg/ml solution added to the blank. Limit of quantification for nicotinamide and nicotinic acid was 0.26mg/100g and 0.04 mg/100 g, respectively.

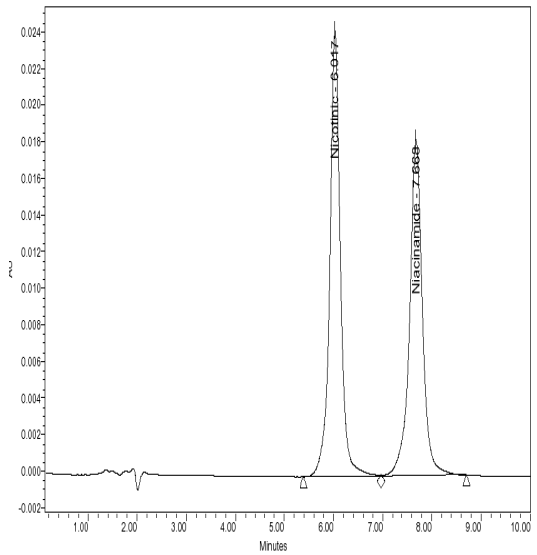

Fig 1. HPLC chromatogram of mixed standard of nicotinic acid and nicotinamide (10 µg/ml)

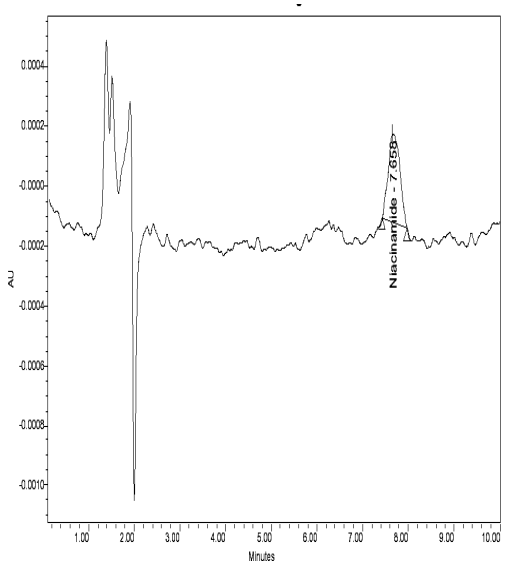

Fig 2 : HPLC chromatogram of blank run

3.2 Conversion of nicotinamide to nicotinic acid

Figure 3(a) to 3(d) show chromatograms of hydrolysis of nicotinamide(2 µg/ml solution) into nicotinic acid i.e. in 0.22 M $CaOH_2$ (Fig 3a), in 1 M NaOH (Fig 3b) and in 1 M HCL (Fig 3c & 3d) Nicotinamide was fully converted into nicotinic acid in 0.22 M CaOH2 and in 1 M NaOH after autoclaved at 121ºC for 1 hour. However nicotinamide was only converted to 7% nicotinic acid in 1 M HCL solution after autoclaved at 121ºC for 2 hours.

Table 1 shows the % conversion of nicotinimide into nicotinic acid after acid and alkaline hydrolysis of nicotinamide for 1 and 2 hrs. Windahl *et al.* (1997) also observed that nicotinamide was not converted into nicotinic acid after 8 hours steamed at 100ºC. Rees (1989) found only partial hydrolysis of nicotinamide in acid solution. Sallin *et al*. (2001) obtained the single nicotinic acid peak after performing alkaline hydrolysis on infant formula samples using 1M NaOH and autoclaved 120ºC at 1 hours. However this researcher experienced of interferences co -eluted with the nicotinic peak in the LC system used. Lahely (1999) obtained 80% of conversion nicotinamide into nicotinic acid by autoclaving 120°C for 1 hour in the presence of 0.22M $CaOH_2$. Tyler and Shrago (1980),Van Niekerk et.al.,(1984) used to hydrolyzed bound forms of niacin using 0.22M $CaOH_2$, autoclaved at 120°C for 1 hour. NaOH treatments normally release a large part of non bio-available forms of niacin in food.as well as the use of NaOH induces a gelation of the food sample. If acid is used to hydrolyze niacin, It is necessary to run both nicotinic acid and nicotinamide standard when quantifying free niacin.. One hour autoclaving at 121°C in the 0.22M $CaOH_2$ medium is sufficient to convert nicotinamide into nicotinic acid.

Table 1: Hydrolysis of nicotinamide into nicotinic acid in acid and alkaline condition autoclaved at 121°C.

	Time of hydrolysis, 1hr		Time of hydrolysis,2 hr	
	Nicotinic acid recovered µg/ml)	Conversion (%)	Nicotinic acid recovered µg/ml)	Conversion (%)
0.22 M $CaOH_2$	1.94 ± 0.15	96.7 ± 7.57	1.91 ± 0.089	95.6
1 N NaOH	2.16 ± 0.046	108.2 ± 2.26	2.2 ± 0.05	110
1 N HCL	ND*	0	0.151	7.6

ND* -- Nicotinic acid is not detected with nicotiniamide still present in amount of 2.13 µg/ml.

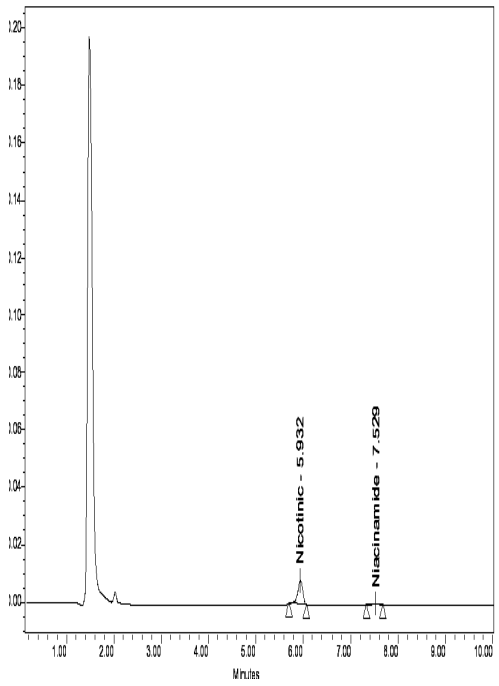

Fig 3a. HPLC chromatogram of nicotinamide in alkaline condition ($CaOH_2$, 1 hr)

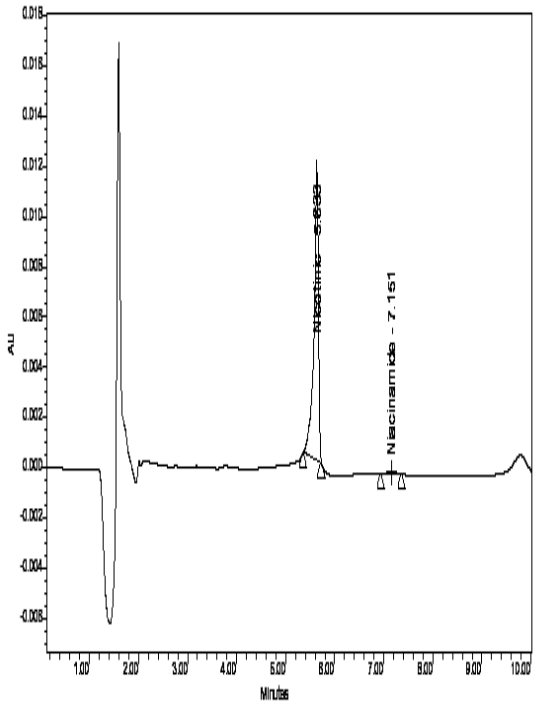

Fig 3b. HPLC chromatogram of nicotinamide in alkaline condition (NaOH, 1 hr)

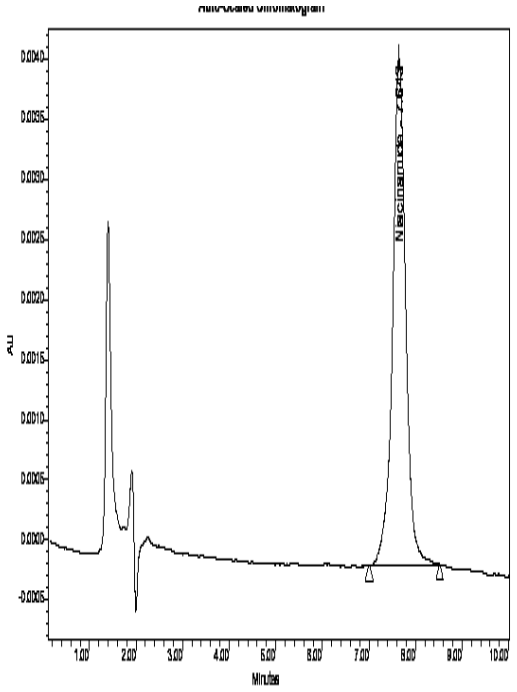

Fig 3c. HPLC chromatogram of nicotinamide in acid condition (HCL, 1 hr)

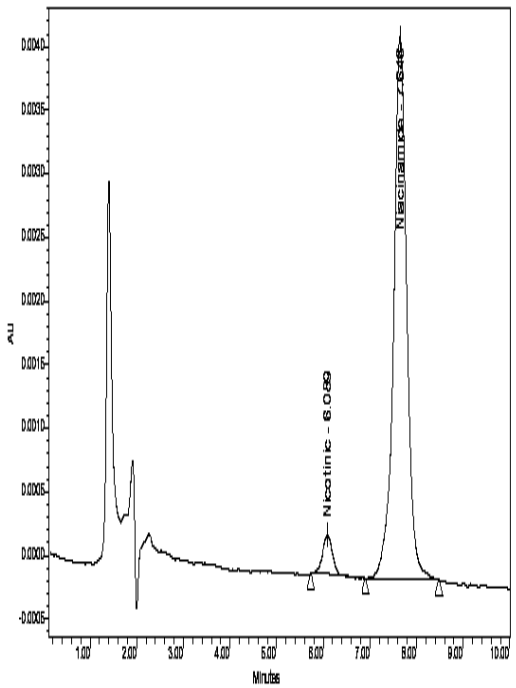

Fig 3d. HPLC chromatogram of nicotinamide in acid condition (HCL, 2 hr)

3.3 Determination of niacin in food

Samples of bread, biscuits, milk powder, ground nut, banana (pisang emas) and chicken meat (thigh) were analyzed for niacin content according to the HPLC and microbiological methods. The results are given in Table 2. *L. plantarum* ATCC 8014 used in the study was linear up to 0.05 ng/ml of nicotinic acid (or nicotinamide), as shown in graph 1. The regression analysis of 32 samples assayed by microbiological and 29 samples by HPLC is shown in graph 2. The correlation of coefficient for both methods was highly significant ($r^2 = 0.977$). Compared to the reported certified mean value of 74.94 mg/100g niacin content in reference material VMA 399, niacin content obtained by the HPLC method was 12.2% lower but was 8.3% higher by the microbiological assay. Recoveries of nicotinic acid obtained by the HPLC method and microbiological assay were in the range of 75 to 101% and 75.5 to 144%, respectively.

From the results, it was observed that niacin analyzed by microbiological assay was found to be relatively higher than those analyzed by HPLC in all samples except for biscuit. The differences in niacin content obtained between these two methods relative to microbiological assay were: bread (37%), milk powder (52%), banana (47 %), groundnut (33%), biscuit (15%) and VMA (18%). Chase *et al* (1999) reported microbiological assay results average is 11% higher than those from HPLC method. Sallin, *et al*. (2001) reported relative differences of microbiological assay of 44% – 77 % in infant cereals.

Table 2 : Comparison of niacin content in food analyzed by HPLC and Microbiological assay

	HPLC		Microbiological Assay	
Food Samples	Niacin mg/100 g	Coefficient of variance (%)	Niacin mg/100 g	Coefficient of variance (%)
Chicken meat	6.07 ± 0.62	9	6.26 ± 0.56	9
Groundnut	10.42 ± 0.44	4.2	15.76 ± 1.45	9.1
Banana	0.27 ± 0.05	18.5	0.51 ± 0.05	11.8
Bread	7.64 ± 0.78	10.0	12.3 ± 0.76	6.2
Milk powder	5.41 ± 0.06	1.0	11.3 ± 0.46	4
Biscuit	15.2 ± 0.02	0.1	13.1 ± 1.24	9.5
VMA 399	65.8 ± 3.81	5.8	81.2 ± 2.85	3.5

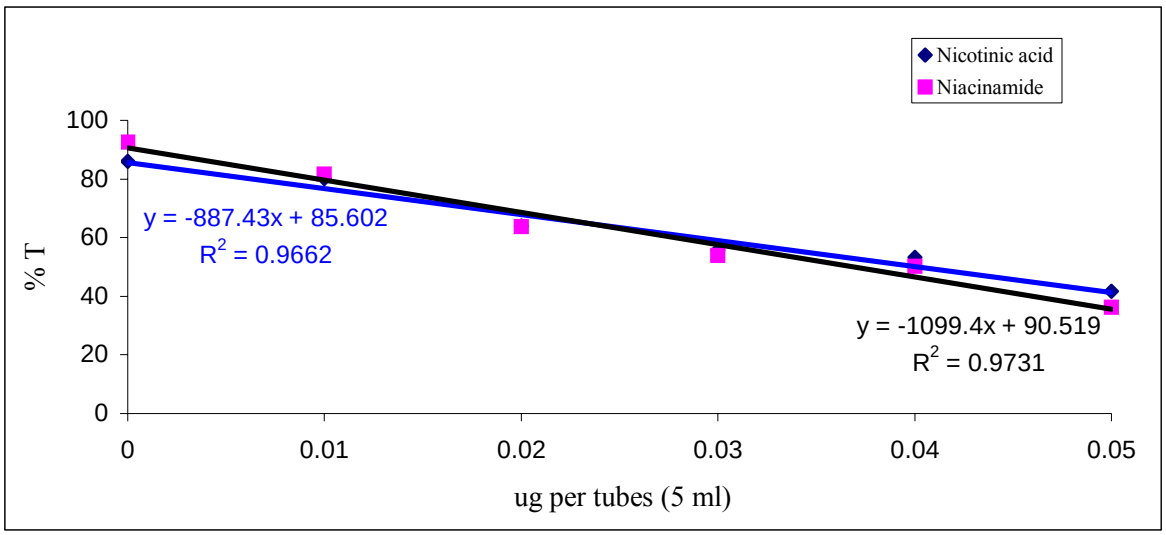

Graph 1 : *L.plantarum* ATCC 8014 respond 0 – 0.05 ug vitamin B3

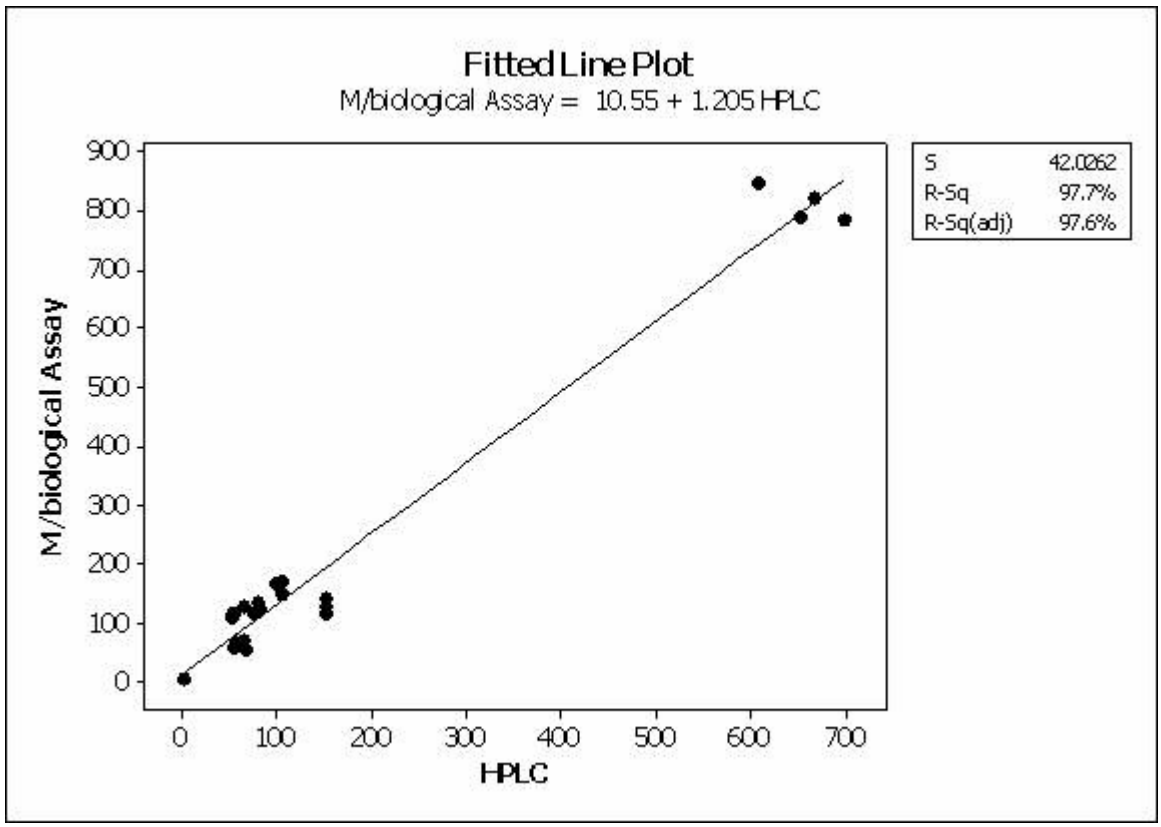

Graph 2: Linear regression for comparison of Niacin Value in Food (ug/g) by MA and HPLC

The chromatograms for the samples analyzed by HPLC are shown in Figures 4(a) to 4(g). The milk powder and banana samples contained some of the interferences which were not removed by cleaned up C18 (EC) cartridge but it did not interfere with the nicotinic acid peak. Redbull drink (fig.5(f)) injected into HPLC after dilution contained nicotinamide 16 mg/100 ml. The label claims on niacin content in some of foods analyzed were milk powder (6 mg/100 g),

bread (8.21 mg/100g), groundnut (8.45 mg/100 g) , vitamin drink (8 mg/100 ml) and redbull drink (13 mg/100 ml).

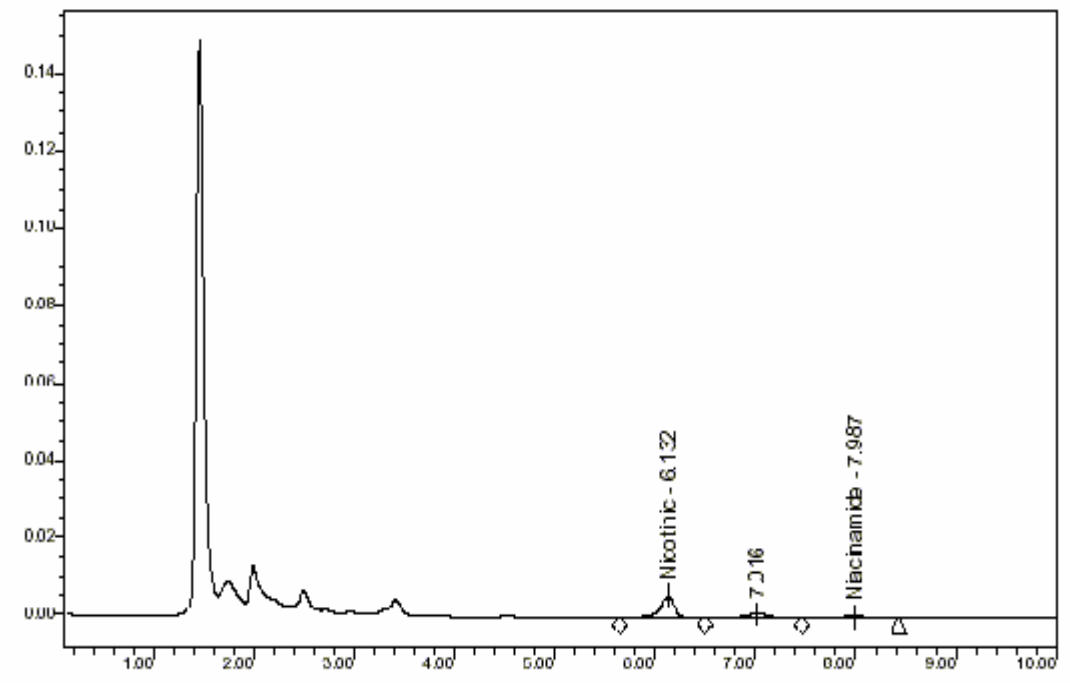

Fig 4 (a) Biscuit

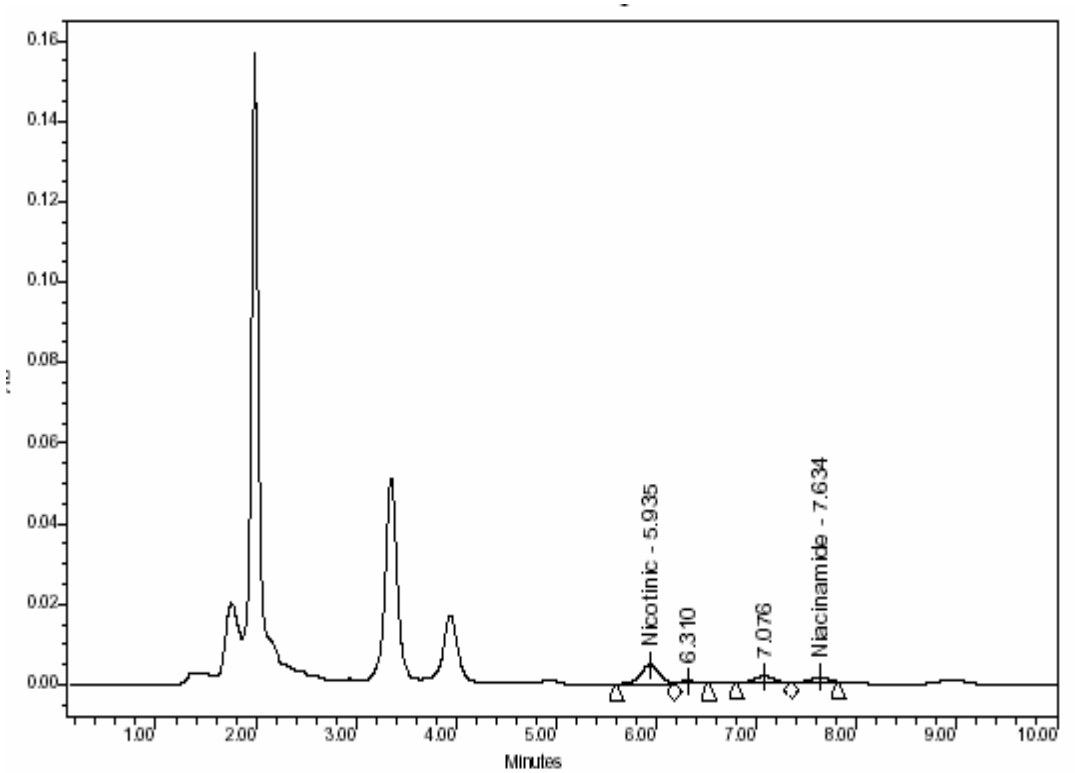

Fig 4 (b) Chicken meat

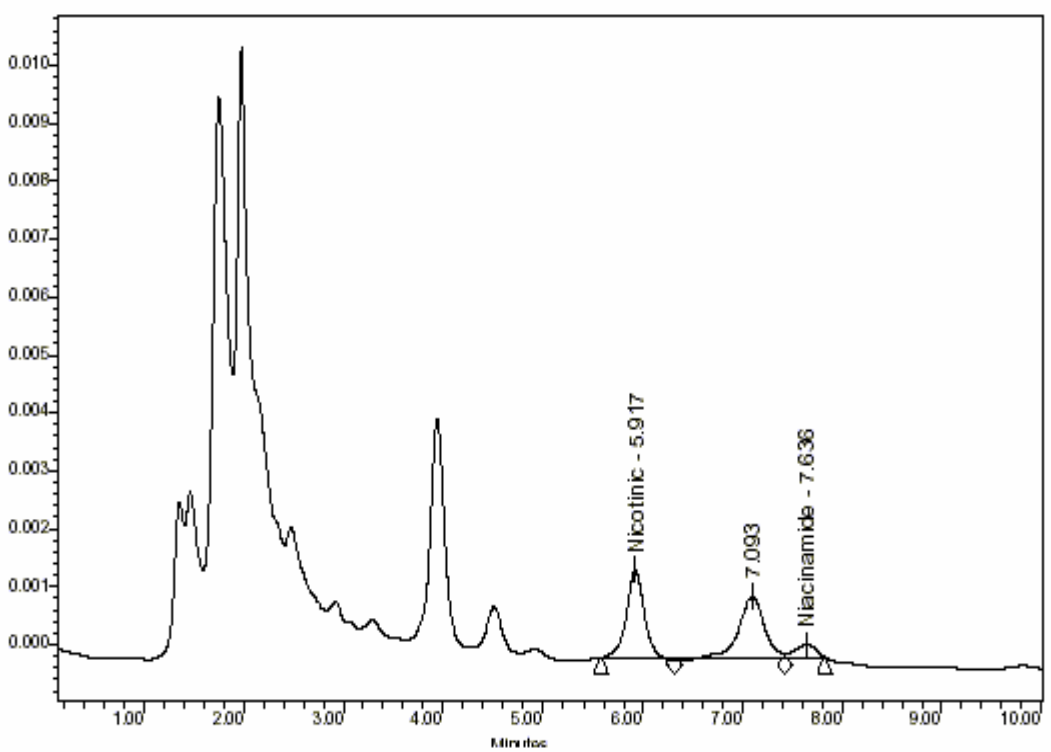

Fig 4 (c) Bread

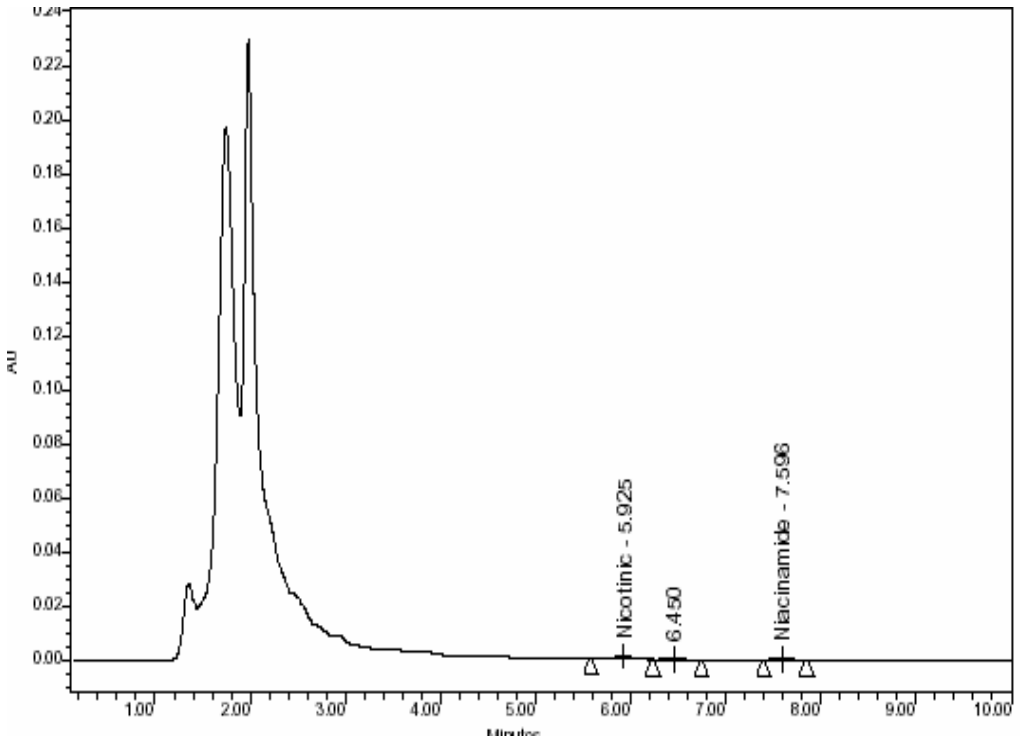

Fig 4 (d) Banana (Pisang Emas)

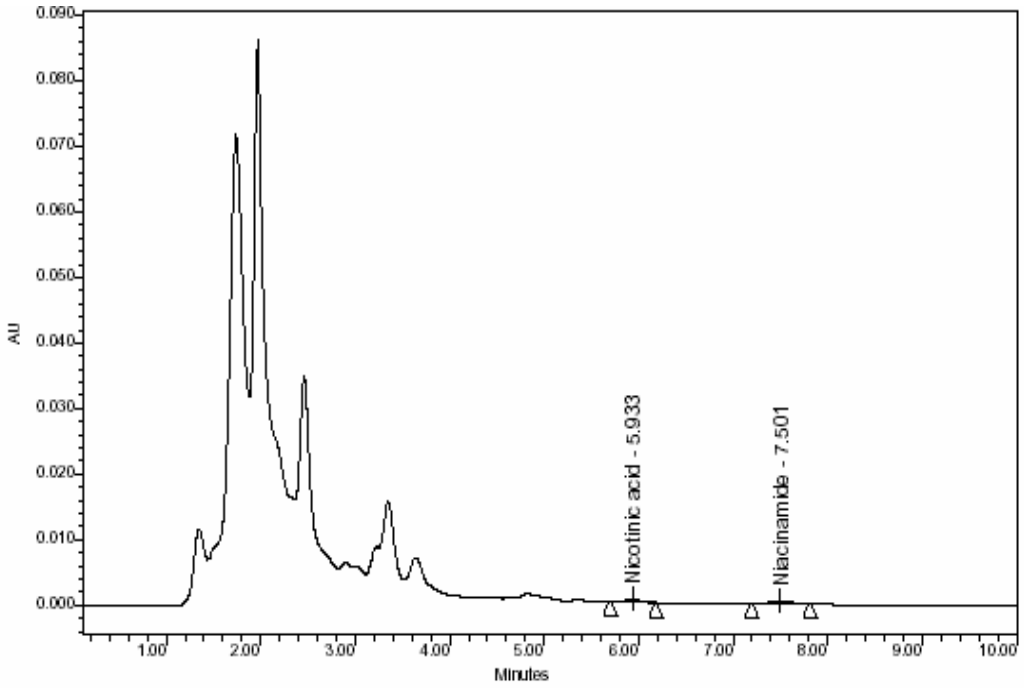

Fig 4 (e) Milk powder

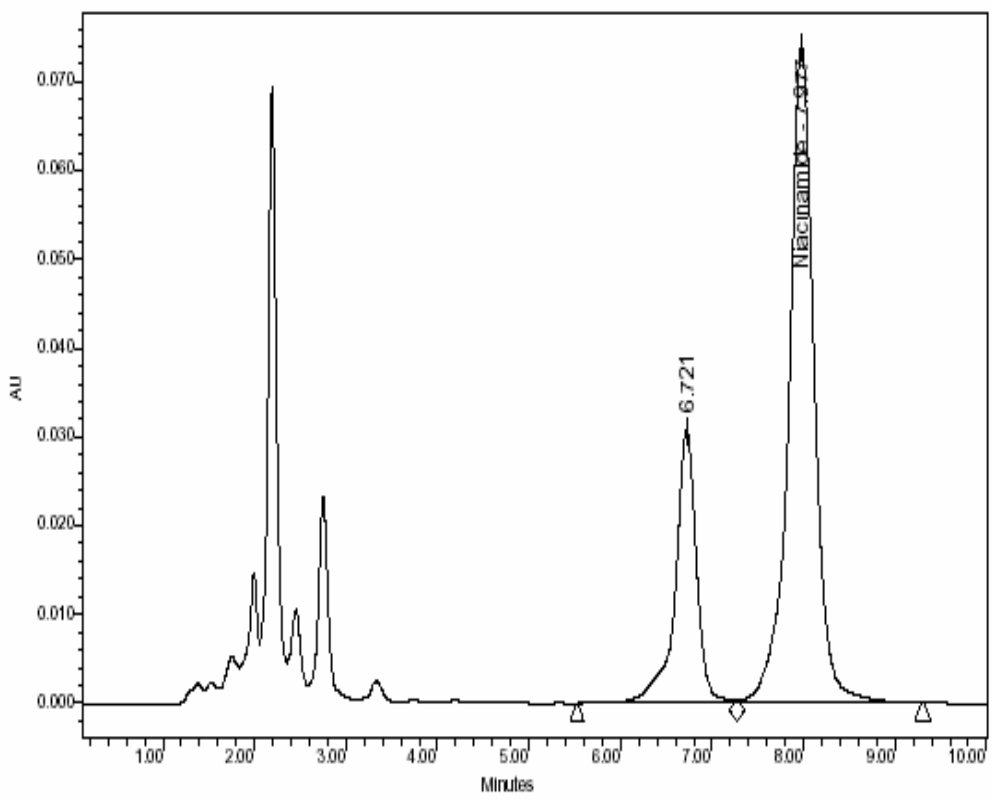

Fig 4 (f) Redbull drink (nicotinamide)

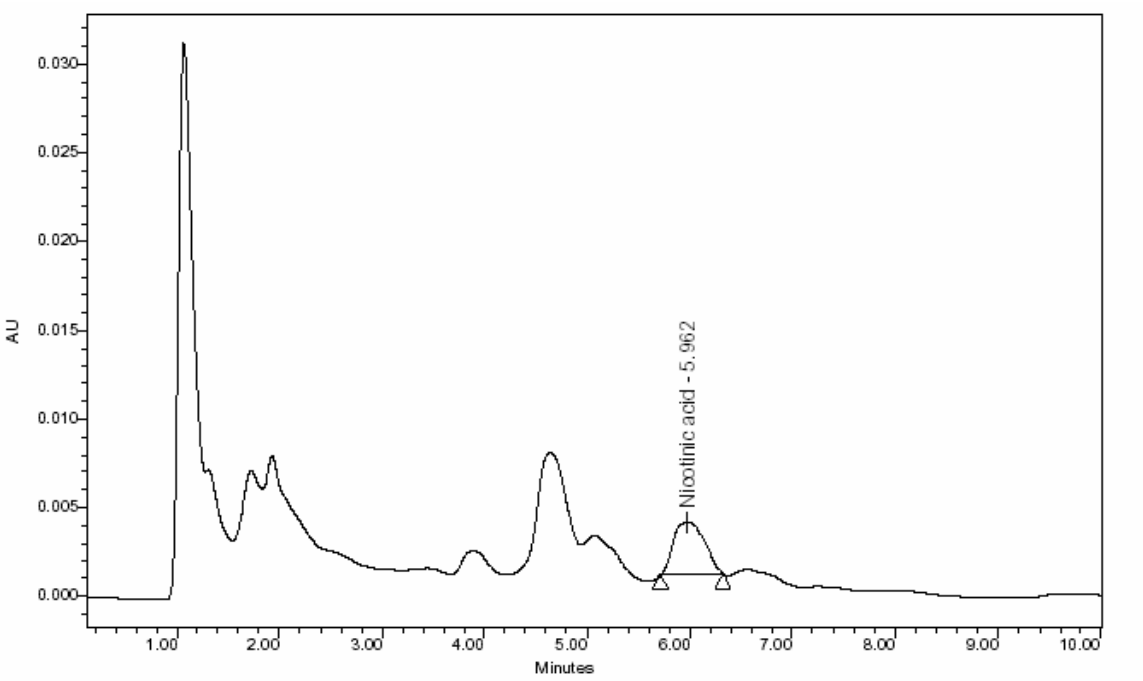

Fig 4 (g) Certified Reference Material, VMA 399

Conclusion

The study shows that autoclaving nicotinamide at 121C in $CaOH_2$ for one hour is sufficient to convert into nicotinic acid form. The method provides an alternative to the niacin HPLC method developed by Tyler and Genzale (1990), Ward *et al.* (1996) and Juraja *et al.* (2003) but modified as regards of cleaned up C 18 (EC) cartridge and the mobile phase system gave a good separation of niacin in the HPLC system prescribed. Using C18 (EC) SPE cartridge gave equivalently clean chromatogram in certain food as compared of using two SPE cartridges in Ward et al (1996) method.. Furthermore using non phosphate buffer mobile phase make it easy to maintain the LC column and Sodium Dodecyl Sulphate is less expensive as compare to other Pair Ion Chromatography reagents.

Microbiological assay and HPLC method gave results in fair agreement. Regression analysis by Minitab version 14, $p>0.05$, $R^2 = 97.7\%$ but microbiological assay more tedious and time consuming.

.

References

1. AOAC (1995).*Official Methods of Analysis*, 16th edition. *Association of Official Analytical Chemists,* Washington, D.C.:
2. Chase, G.W Jr, Landen, W.O Jr, Soliman, A,M and Eitenmiller,R.R..(1993). Liquid chromatographic analysis of niacin in fortified food products. *Journal of AOAC International*, **76**, 2, 390 – 393.
3. Egberg, D.C (1979). Automated method for niacin and nicotinamide in food products, *Journal of AOAC* , **62**, 1072.
4. Eitenmiller, R.R. and Landen, W.O. Jr (1999). Niacin In *Vitamin Analysis for the Health and Food Sciences*. CRC Press. 339-369.
5. Hamano, T., Mitsuhashi,Y., Aoki,N., Yamamoto,S and Oji,Y. (1988). Simultaneous determination of niacin and nicotinamide in meats by HPLC. *Journal Chromatography*, **457**, 403-408.
6. Hengen, N and Vries J.X. (1985). Nicotinic acid and nicotinamide. In *Modern Chromatographic Analysis of vitamins. Vol 30*. Edited by the Leehee A.P.D, Lambert, W.E and Ruyter, M.G.M. Marcel Dekker Inc.341-384.

7. Hirayama, S (1998). Determination of Small Amount of Niacin in Vinegar: Comparison of LC method and microbiological methods. *Journal of AOAC International*, **81** (6), 1273-1276.
8. Hirayama, M and Maruyama, M (1991). Determination of small amount of niacin in foodstuffs by high performance liquid chromatography. *Journal Chromatography*, 588, 171.
9. Juraja, S.M., Trenerry, V.C., Millar, G.R., Scheelings, P and Buick ,D.R. (2003). Asia Pacific Food Analysis Network (APFAN) Training exercise: Determination of niacin in cereals by alkaline extraction and HPLC. *Journal of Food Composition and Analysis*. **16**, 93-106.
10. Lahely, S., Bergaentzle, M. and Hasselmann. (1999). Fluorometric determination of niacin in foods by High-Performance Liquid Chromatography with post-column derivatization. *Food Chemistry.* **65**, 129-133.
11. Minitab Statistical Software, Minitab release 14, Minitab Inc. USA.
12. Rees, D.I. (1989). Determination of nicotinamide and pyridoxine in fortified food products by High Performance Liquid Chromatography. *Journal Micronutrient Analysis* ,**5** ,53.
13. Russell, L.F (1999). Water Soluble Vitamins. In *Handbook of Food Analysis Vol 1*. Edited by Nollet, L.M. Marcel Dekker Inc, N.York. 672-683.
14. Sallin, C.R., Blake, C.J., Genoud, D and Tagliaterri, E.G (2001). Comparison of microbiological and HPLC-fluoroscence detection methods for determination of niacin in fortified food products. *Food Chemistry*. **73**, 475-480.
15. Roy, R.B., and Conetta, A. (1976). Automated analysis of water soluble vitamins in food. *Food Technol,* **30***,* 94.
16. Skurray,G.R. (1981). A rapid method for selectivity determining small amounts of niacin, riboflavin and thiamine in Foods. Food Chemistry, **7**, 77-80**.**
17. Tyler, T.A and Genzale, J.A (1990). Liquid chromatographic determination of total niacin in beef, semolina and cottage cheese. *Journal of AOAC ,* **73** (3), 467-469.
18. Tyler,T.A and Shrago,R.R, (1980). Determination of niacin in cereal samples by
19. HPLC. *J. Liq. Chromatography***,3**,269-277
20. Van Niekerk,P.J.,Smit, S.C.C., Strydom, E.S.P., and Armbruster, G. (1984).
21. Comparison of High-Performance Liquid Chromatography and microbiological method forthe determination of niacin in foods. *Journal of Agriculture and Food Chemistry***, 32**, 304-307
22. Ward, C.M. and Trennery, V.C.(1997). Determination of niacin in cereals, meat and selected foods by capillary electrophoresis and HPLC. *Food Chemistry*, **60** (4), 667-671.
23. Windahl, K., Trennery, V.C and Ward, C.M. (1998). Determination of niacin in selected food by capillary electrophoresis and High Performance Liquid Chromatography: Acid Extractions. *Food Chemistry*, **65**, 263-270.
24. Wood, R. (1998). *Quality in The Food Analysis Laboratory*. RSC Food Analysis Monograph.UK.

Malaysian Journal of Analytical Sciences, Vol.9, No. 3(2005): 475 - 479

Penggunaan Damar Sebagai Agen Anti Kulat Dalam Pembuatan Cat Emulsi

Illyas Md Isa dan Norhayati Hashim

Fakulti Sains dan Teknologi, Universiti Pendidikan Sultan Idris 35900 Tanjong Malim Perak

Ekstrak damar meranti sarang punai, damar meranti kepong, rosin dan damar kempas dengan pelarut xilena, etil asetat, dan etanol 95% memberikan kesan positif terhadap beberapa kulat pengurai cat iaitu *Curvularia* sp. , *Aspergillus* sp. , *Penicillium* sp., *Trichoderma* sp. *Fusarium* sp. , *Rhizopus* sp. , dan *Mucor* sp. . Perencatan kulat paling berkesan terhadap ekstrak damar dengan pelarut xilena. Manakala luas perencatan *Penicillium* sp. adalah paling berkesan dengan menggunakan hasil ekstrak damar meranti sarang punai dengan pelarut xilena. Walaubagaimanapun, luas perencatan kulat adalah berbeza di antara setiap hasil ekstrak yang digunakan.

Pengenalan

Damar merupakan sejenis resin semulajadi yang boleh didapati dengan banyaknya daripada pokok-pokok yang ketinggiannya melebihi seratus kaki. Pengeluaran secara komersial dilakukan di beberapa negara seperti Indonesia, Amerika Syarikat dan China. Di Indonesia, damar merupakan salah satu komoditi eksport yang utama di mana jumlah pengeluarannya di antara 2000 – 7000 tan setahun yang bernilai U.S $ 1.6 juta [1]. Damar dikeluarkan secara traditional iaitu dengan menetak ataupun menoreh batang atau dahan pokok. Damar akan meleleh keluar daripada pokok dan mengambil masa lebih kurang sebulan untuk membeku. Biasanya damar mempunyai aroma yang tertentu dan baunya berbeza di antara satu sama lain. Pengeluaran damar secara saintifik telah dilakukan oleh beberapa penyelidik untuk menambahkan pengeluaran damar dengan menggunakan bahan kimia peransang seperti asid sulfurik [2] dan asid 2-kloroetilfosforik [3,4]. Secara tradisinya, damar digunakan oleh orang asli sebagai jamung, menampal perahu dan ramuan ubat-ubatan [5]. Di Indonesia, damar mata kucing ataupun nama saintifiknya *Shorea Javanica* digunakan di dalam industri pembuatan plastik, varnish, perusahaan batik dan digunakan sebagai ramuan ubat traditional [6]. Dalam eksperimen ini beberapa jenis damar telah digunakan iaitu damar meranti sarang punai, damar meranti kepong, damar kempas dan rosin untuk ujikaji keaktifan antikulatnya terhadap tujuh jenis kulat pengurai cat iaitu *Curvularia* sp. , *Aspergillus* sp. , *Penicillium* sp., *Trichoderma* sp. *Fusarium* sp. , *Rhizopus* sp. , dan *Mucor* sp . Pemilihan damar ini dilakukan kerana pokoknya sangat keras dan tahan terhadap serangan serangga.

Eksperimen

Pengekstrakan Damar

Damar meranti sarang punai, damar meranti kepong, dan damar kempas yang digunakan dalam penyelidikan ini diperolehi dari Hutan Simpan Ulu Slim, Perak oleh seorang bekas pegawai Institut Penyelidikan Perhutanan Malaysia (FRIM) yang berpengalaman lebih kurang 30 tahun manakala rosin diambil daripada hutan pokok pain di Universiti Putra Malaysia (UPM, Serdang, Selangor). Damar yang berbentuk ketulan keras diambil sekitar pangkal pokok dan dilakukan pembersihan dengan membuang resin yang telah teroksida. Seterusnya dibasuh dengan air dan dikeringkan. Warna ketulan damar adalah coklat kehitaman dan warna tersebut bertukar menjadi kekuningan selepas dihancurkan. Kemudian 100 g damar dibungkus dengan menggunakan kertas turas dan diekstrak dengan menggunakan soxhlet selama 24 jam. Pelarut yang digunakan adalah dipilih berdasarkan kekutuban yang berlainan iaitu xilena, etanol 95%, dan etil asetat. Pada setiap hasil pengekstrakan ini, ia dipekatkan dengan pengwap hampa gas yang berputar dan kemudiannya dikeringkan dalam oven pengering pada takat didih pelarut tersebut.

Kesan Damar Terhadap Pertumbuhan Beberapa Kulat Pengurai Cat

Kesan perencatan kulat terhadap kulat *Curvularia* sp. , *Aspergillus* sp. , *Penicillium* sp., *Trichoderma* sp. *Fusarium* sp. , *Rhizopus* sp. , dan *Mucor* sp . dengan hasil ekstrak damar meranti sarang punai, damar meranti kepong, rosin dan damar kempas dengan pelarut xilena, etil asetat, dan etanol dilakukan . Kaedah peresapan agar digunakan untuk menguji resin terhadap pertumbuhan kulat [7,8]. Terdapat 3 peringkat telah digunakan iaitu penyediaan agar Potato Dextrose (PDA), pensterilan dan pensubkulturan.

Sebanyak 39 g agar Potato Dextrose (PDA) dan 1000 ml air suling dicampurkan dan dipanaskan sambil mengacau. Selepas semua larut, ia diautoklaf pada suhu 121 ^{o}C selama 15 minit. Untuk menguji keberkesanan resin ini, 2.0 ml air suling dipipetkan ke dalam botol agar yang mengandungi kulat ujian dan kemudian larutan ini dipindahkan ke dalam botol yang mengandungi PDA lalu digoncang perlahan-lahan. Seterusnya agar PDA ini dituang ke dalam piring petri dan dibiarkan membeku lebih kurang 10 minit. Cakera kertas turas yang telah dicelup dengan pelarut yang mengandungi ekstrak dengan kepekatan 0.25 gl^{-1} kemudiannya diletak di atas permukaan agar yang telah beku tadi. Piring petri dieramkan pada suhu bilik (30 ± 2 ^{o}C) selama 24 – 48 jam.

Keputusan

Jadual 1 : Peratusan ekstrak damar dengan pelarut terpilih

Pelarut Damar	XIilena (% ekstraks)	Etil asetat (% ekstraks)	Etanol (% ekstraks)
Kempas	43.69	65.30	67.09
Meranti kepong	92.73	76.57	70.51
Meranti sarang punai	94.42	69.72	55.96
Rosin	50.32	46.78	51.97

Jadual 2 : Luas perencatan kulat terhadap pengekstrakan damar dengan menggunakan pelarut xilena

Damar Kulat	Kempas (mm^2)	Meranti kepong (mm^2)	Meranti sarang punai (mm^2)	Rosin (mm^2)
Penicillium sp.	989	880	1106	989
Trichoderma sp.	85	126	173	173
Aspergillus sp.	424	352	352	226
Curvularia sp.	503	286	503	286
Fusarium sp.	85	503	50	50
Rhizopus sp.	503	173	503	85
Mucor sp.	603	352	424	50

Jadual 3 : Luas perencatan kulat terhadap pengekstrakan damar dengan menggunakan pelarut etil asetat

Damar Kulat	Kempas (mm^2)	Meranti kepong (mm^2)	Meranti sarang punai (mm^2)	Rosin (mm^2)
Penicillium sp.	22	85	22	22
Trichoderma sp.	85	22	-	50
Aspergillus sp.	22	22	50	-
Curvularia sp.	-	-	-	-
Fusarium sp.	22	50	85	50
Rhizopus sp.	-	50	22	22
Mucor sp.	50	22	22	50

Jadual 4 : Luas perencatan kulat terhadap pengekstrakan damar dengan menggunakan pelarut etanol

Damar Kulat	Kempas (mm^2)	Meranti kepong (mm^2)	Meranti sarang punai (mm^2)	Rosin (mm^2)
Penicillium sp.	22	50	22	-
Trichoderma sp.	50	85	22	-
Aspergillus sp.	50	50	-	-
Curvularia sp.	22	50	50	22
Fusarium sp.	50	22	50	50
Rhizopus sp.	22	22	50	22
Mucor sp.	-	-	50	-

Rajah 1 : Kesan ekstrak damar dengan menggunakan pelarut xilena terhadap kulat *Penicillium* sp. 1: damar kempas 2 : rosin 3 : damar meranti kepong 4 : damar meranti sarang punai

Rajah 2 : Kesan ekstrak damar dengan menggunakan pelarut xilena terhadap kulat *Curvularia* sp. 1: damar kempas 2 : rosin 3 : damar meranti kepong 4 : damar meranti sarang punai

Perbincangan

Penyelidikan ini dilakukan untuk menguji kesan yang ditunjukkan oleh ekstrak damar meranti sarang punai, damar meranti kepong, rosin dan damar kempas dengan pelarut xilena, etil asetat, dan etanol 95% terhadap pertumbuhan beberapa kulat pengurai cat iaitu *Curvularia* sp. , *Aspergillus* sp. , *Penicillium* sp., *Trichoderma* sp. *Fusarium* sp. , *Rhizopus* sp. , dan *Mucor* sp. [9]. Daripada Jadual 1 didapati bahawa pelarut xilena menghasilkan pengekstrakan melebihi 90% bagi damar meranti sarang punai dan damar meranti kepong dan ia juga agak sesuai digunakan sebagai pelarut kerana hasil pengekstrakannya adalah lutsinar. Bagi pelarut etanol dan etil asetat, pelarut ini kurang sesuai digunakan kerana hasil pengekstrakannya adalah berkeladak dan tidak lutsinar.

Pertumbuhan kulat pada permukaan penglitup mengakibatkan kerosakan dan penguraian lapisan penglitup dan ini menyebabkan kegagalan fungsi penglitup tersebut [10]. Sedangkan serangan kulat ke atas kayu merupakan salah satu faktor utama yang menyebabkan kerosakan kayu [11]. Keputusan yang diperolehi menunjukkan bahawa zon perencatan hanya terdapat disekitar cakera yang dicelupkan dengan resin semulajadi tetapi tidak pada cakera yang dicelupkan di dalam pelarut sahaja iaitu kawalan. Ini menujukkan bahawa ekstrak damar semulajadi yang digunakan iaitu damar meranti sarang punai, damar meranti kepong, rosin dan damar kempas mempunyai kesan positif terhadap pertumbuhan kulat *Curvularia* sp. , *Aspergillus* sp. , *Penicillium* sp., *Trichoderma* sp. *Fusarium* sp. , *Rhizopus* sp. , dan *Mucor* sp.. Walaubagaimanapun keberkesanan setiap damar semulajadi ini adalah berbeza bagi setiap pelarut yang telah digunakan dan ia juga memberikan kesan yang berbeza bagi setiap kulat ini [12].

Daripada Jadual 2, 3 dan 4 di dapati bahawa perencatan kulat *Curvularia* sp (Rajah 2). , *Aspergillus* sp. , *Penicillium* sp.(Rajah 1), *Trichoderma* sp. *Fusarium* sp. , *Rhizopus* sp. , dan *Mucor* sp. adalah sangat ketara terhadap ekstrak damar meranti sarang punai, damar meranti kepong, rosin dan damar kempas dengan menggunakan pelarut xilena. Luas perencatan ekstrak damar dengan pelarut xilena memberikan perencatan terbesar bagi *Penicillium* sp. (Rajah 1) . Bagi damar kempas keluasan perencatan *Penicillium* sp. adalah 989 mm^2 iaitu sebelas kali lebih luas berbanding dengan *Trichoderma* sp. dan *Fusarium* sp. dan hampir dua kali ganda dengan *Curvularia* sp. , *Aspergillus* sp. , *Rhizopus* sp. , dan *Mucor* sp. . Ekstrak damar meranti kepong dengan pelarut xilena memberikan keluasan perencatan terluas bagi kulat *Penicillium* sp. iaitu 880 mm^2 di mana hampir dua kali ganda keluasan perencatan *Aspergillus* sp., *Curvularia* sp. , dan *Mucor* sp. serta lima kali ganda keluasan *Trichoderma* sp. dan *Rhizopus* sp. . Manakala ekstrak damar meranti sarang punai dengan pelarut xilena memberikan keluasan terbesar perencatannya terhadap kulat *Penicillium* sp. iaitu 1106 mm^2 . Keluasan perencatan kulat *Curvularia* sp. *Rhizopus* sp. dan *Mucor* sp. juga ketara iaitu masing-masing 503 mm^2 , 503 mm^2 dan 424 mm^2. Bagi pengektrakan rosin dengan xilena pula, keluasan perencatan menurun dari *Penicillium* sp., *Curvularia* sp. , *Aspergillus* sp. , *Trichoderma* sp. , *Rhizopus* sp. *Fusarium* sp. , dan *Mucor* sp.

Ekstrak damar meranti sarang punai, damar meranti kepong, rosin dan damar kempas dengan menggunakan pelarut etil asetat memberikan sedikit kesan perencatan terhadap beberapa jenis kulat dan ada yang memeberikan kesan negatif. Di antara ekstrak yang memberikan kesan perencatan negatif adalah ekstrak damar kempas terhadap *Curvularia* sp. dan *Rhizopus* sp. , ekstrak damar meranti kepong terhadap *Curvularia* sp. , ekstrak damar meranti sarang punai terhadap *Trichoderma* sp. dan *Curvularia* sp. dan ekstrak rosin terhadap *Curvularia* sp. , *Aspergillus* sp. .

Daripada Jadual 4 dapatlah di lihat bahawa hasil ekstrak damar meranti sarang punai, damar meranti kepong, rosin dan damar kempas dengan pelarut etil asetat dan etanol 95 % memberikan sedikit perencatan terhadap kulat tertentu malah ada yang tidak memberikan kesan langsung. Ini menunjukkan bahawa pelarut memainkan kesan yang utama dalam proses pengekstrakan. Etanol 95% adalah sejenis pelarut yang sangat berkutub manakala damar yang digunakan tidak larut dalam air . Walaubagaimanapun damar meranti sarang punai dan rosin hampir 50% larut di dalam etanol 95% manakala damar meranti kepong dan damar kempas hampir 70% . Walaupun peratusan pengekstrakan melebihi 50% di dapati bahawa kesan perencatan kulat yang terpilih ada terlalu kecil dan ada yang tiada perencatan langsung. Ini menunjukkan bahawa bahan aktif yang dapat merencatkan kulat tidak dapat diekstrak ataupun hanya sedikit terekstrak daripada damar-damar ini. Walaubagaimanapun terdapat beberapa penyelidik [7,13] telah menggunakan pelarut etanol 95% sebagai medium pengekstrakan dan hasil pengekstrakan tersebut memberikan kesan yang positif terhadap beberapa kulat yang dipilih. Ekstrak damar kempas dan meranti kepong dengan etanol 95% memberikan kesan negatif kepada perencatan *Mucor* sp. , damar meranti sarang punai pula memberikan kesan negatif terhadap perencatan *Aspergillus* sp. manakala rosin memberikan kesan negatif terhadap empat jenis kulat iaitu *Penicillium* sp., *Aspergillus* sp. , *Trichoderma* sp. , dan *Mucor* sp.

Di antara ekstrak damar dengan pelarut xilena, etil asetat, dan etanol 95% di dapati bahawa ekstrak damar meranti sarang punai dengan pelarut ini memberikan kesan perancatan keseluruhan yang baik terhadap semua jenis kulat iaitu *Penicillium* sp., *Curvularia* sp. , *Aspergillus* sp. , *Trichoderma* sp. , *Rhizopus* sp. *Fusarium* sp. , dan *Mucor* sp. manakala ekstrak damar meranti sarang punai dengan pelarut xilena memberikan kesan perencatan yang terbesar iaitu terhadap *Penicillium* sp. . Ini menunjukkan bahawa pelarut xilena merupakan pelarut yang terbaik yang boleh mengekstrakan bahan aktif yang boleh merencatkan kulat daripada damar tersebut.

Pokok meranti adalah merupakan di antara spesies-spesies pokok yang menghasilkan kayu yang keras dan tahan terhadap organisma penebuk atau perosak lain seperti anai-anai. Ini mungkin kerana pokok meranti mengandungi bahan kimia yang boleh menghalang serangan organisma perosak tersebut. Bultman dan rakan [14] pernah melapurkan bahawa terdapat kayu tropika yang boleh tahan terhadap serangan anai-anai dan serangan kulat sehingga 158 bulan. Bahan kimia yang membolehkan daya tahan terhadap serangan makhluk perosak ini adalah kerana damar cengal mengandungi komponen berfinolik. Ini dibuktikan oleh Hill [15] yang menyatakan bahawa komponen berfenolik adalah toksik kepada kulat dan serangga. Bultman dan rakan [16] juga pernah melaporkan bahawa bahan semulajadi yang menyebabkan perencatan kulat berkemungkinan mengandungi bahan berpolifenol. Jadi kajian seterusnya juga adalah untuk mengenal pasti bahan yang dapat merancatkan kulat tersebut dan adakah ia sejenis fenolik seperti yang dikatakan oleh beberapa penyelidik yang terdahulu.

Penghargaan

Penghargaan yang tinggi diucapkan kepada Universiti Pendidikan Sultan Idris kerana meluluskan geran penyelidikan jangka pendek iaitu 04-16-02-01. Ucapan ribuan terima kasih kepada semua pembantu makmal kerana kerjasama yang diberikan untuk menyiapkan projek penyelidikan ini.

Bibliorgrafi

1. Jusuf Jafarsidik. (1987). Jenis-jenis pohon penghasil resin damar dan penyebarannya di Indonesia. *Duta Rimba*, 81-82/1987 : 7-11.
2. Ibrahim Jantan, Abu Said Ahmad and Abdul Rashih Ahmad. (1991). Tapping of oleo-resin from *Dipterocarpus kerrii. Journal of Tropical Forest Science* **3**(4), 348.
3. Adam, C.M. (1990). Traditional and Chemical techniques for stimulation of Shorea Javanica (Dipterocarpacea) resin exudation in Sumatra. Economic Botany 44(4), 463
4. Kadir, A.B.A., Kochnummen, K.M., Meng, W.T. and Moir, G.F.T. (1986). Treatment of *Dipterocarpus kerrii* with ethrel. Malaysia Forester 49 : 108.
5. Burkill, I.H. (1935). Adictionary of economic products of the Malay Peninsula. Volumes 2. Crown agents for the colonies, London.
6. Farooqi. M.I.H., (1990). Leguminosae important source of gums and resins. Economic Botany Information Service, Lucknow.
7. Darah, I and Lakshmy, R. (1994). *Journal of Bioscience*, **15**,42.
8. Darah, I. and Halim, O. (1995). *Journal of Ethnopharmacology*, **45**,151.
9. Alexopoulos, C.J. (1979). Introduction Mycology, 3rd Ed.. John Wiley and Son, New York.
10. Jansen, M.L. (1986). *J. Oil Col. Chem. Assoc*., **68**,117.
11. Zeno, W.W., Frank, N.J. and Peter, S.P. (1994). Organic Coating : Science and Technology, Vol 2, John Wiley & Sons, New York.
12. Darah, I. and Annie-Clara, A. (1992). *Malaysia Applied Biology*, 21(1), 71.
13. Ibrahim Jantan and Abu Said Ahmad (1995). Oleoresins of Three Pinus Species from Malaysian Pine plantations. In ; *Chemical prospecting in the Malaysian Forest*, Ismail, G., Mohamed, M. and Din, L.(Eds.) , Pelanduk Publications, Kuala Lumpur.
14. Bultman, J.D. and Southwell, C.R. (1976). *Biotropica*, **8**(2), 71
15. Hill, R.R. (1973). *J. Oil Col. Chem. Assoc*., **56**, 251.
16. Bultman, J.D. and Parrish, K.K. (1979). *Int. Biodeterior. Bull*. (ISSN 0020-6164) 15(1).

Malaysian Journal of Analytical Sciences, Vol.9, No. 3(2005): 480 - 486

PHOTOOXIDATION OF CHLORINATED HYDROCARBON USING TIO_2 THIN FILM

Ng Sook Chuin[1], Mohd Yusuf Othman[2], Wan Azelee Wan Abu Bakar[3], Noor Khaida Wati Mohd Saiyudi[4]

Chemistry Department, Faculty of Science, Universiti Teknologi Malaysia, 81310 Skudai

Abstract: The gas phase photooxidation of chloroform, dichloromethane and carbon tetrachloride were investigated using doped and undoped TiO_2 thin film irradiated by UV light with maximum wavelength at 354 nm. Thin films TiO_2 coated on pyrex glass cylinders were prepared using the sol-gel dip coating technique. In this research, the dopants used were Mn^{2+}, Fe^{2+} and Fe^{3+}. The Mn^{2+} and Fe^{2+} -doped TiO_2 were prepared with 1:0.01, 1:0.005, 1:0.001, 1:0.0005 and 1:0.0003 atomic ratios. Meanwhile, Fe^{3+} -doped TiO_2 were prepared with 1:0.001, 1:0.0005 and 1:0.0003 atomic ratios. In order to determine the optimum dopant ratio, photooxidation of dichloromethane, chloroform and carbon tetrachloride were conducted using all catalyst samples. Mn^{2+}, Fe^{3+} and Fe^{2+} doped catalysts have an optimum ratio of 1:0.0005. The addition of Fe^{2+} and Fe^{3+} into TiO_2 increased the photooxidation of chloroform, carbon tetrachloride and dichloromethane. Mn^{2+} is detrimental to the photooxidation of carbon tetrachloride, dichloromethane and carbon tetrachloride. Therefore, although dopants affect the photoactivity of TiO_2, the effects due to the type and concentration of dopants and VOCs used can not be ignored.

Key words: Photocatalysis, photooxidation, TiO_2

Introduction

Chlorinated hydrocarbons are a group of important environmental pollutants and are a source of danger to the environment. Chlorinated aliphatic hydrocarbons such as dichloromethane, chloroform, trichloroethylene and tetrachloroethylene are widely distributed in the environment. They are introduced to the environment from various sources mainly from their use as solvents in paints, adhesives, degreasers, colour removers or related products (1). The improper disposal of chlorinated hydrocarbons has been considered hazardous and carcinogenic in air pollution (2). Chlorinated hydrocarbons are usually more difficult to convert, oxidation of chlorinated hydrocarbons produce HCl, and sometimes Cl_2, which can attack and deactive the catalyst (3).Nowadays, the main goal of research and development in the area is the use of the technique for air purification and waste water treatment, forming part of a group of processes known as Advanced Oxidation Technologies (AOTs). These methods offer the advantage of destroying the pollutants, in contrast to conventional techniques such as activated carbon or air stripping that only transfers the contaminants from one phase to another. In this way, organic or inorganic compounds and even microorganism, are degraded or transformed into less harmful substances (4). These processes can readily mineralize simple organic molecules into CO_2 and H_2O at ambient conditions using molecular oxygen as the primary oxidant, but complex pollutants are often more difficult to degrade with undesirable intermediates and by-products formed. In addition, the rate of decomposition is usually slow (5).

When a photon of energy higher or equal to the bandgap energy is adsorbed, an electron from valence band is promoted to the conduction band and generates a hole in valence band. The e^- and h^+ can recombine on the surface or in the bulk of the particle in a few nanoseconds or can be tapped in surface states where they can react with donor or acceptor. Holes which have sufficient energy can react with surface adsorbed organic compounds or with $OH^-$and water molecules to form the reactive •OH radical (Eq. 1-3) (4, 6).

$$h^+ + OH^- \longrightarrow \bullet OH \quad (1)$$

$$h^+ + H_2O \longrightarrow \bullet OH + h^+ \quad (2)$$

$$h^+ + R \longrightarrow R_{(OX)} \quad (3)$$

For a semiconductor photocatalyst to be efficient, the different interfacial electron processes involving e^- and h^+, must compete effectively with the major deactivation processes involving e^- and h^+ recombination (6).
Heterogeneous photocatalysis using TiO_2 has several attractions: (a) TiO_2 is relatively inexpensive, (b) it dispenses with the use of other coadjutant reagents, (c) it shows efficient destruction of toxic contaminants, (d) it operates at ambient temperature and pressure and (e) the reaction products are usually CO_2 and H_2O, or HCI, in the case of chlorinated organic compounds (7).
The future possible uses of TiO_2 as a semiconductor are based on its photocatalytical properties. In general, metal catalysts are preferred, in spite of their high cost, because of their higher activity (8). Doping of TiO_2 produces crystal defects and surface modifications, which alter the photocatalytic properties of TiO_2 (9). The deposited metal on the surface of TiO_2 can act as a sink for photoinduced charge carrier, promoting interfacial charge-transfer process. This can increase the lifetime of the holes and suppress the electron-hole recombination, beneficial to the PC oxidation of organic pollutants (10). Besides, the addition of metal ions M^{n+} can trap electron at the semiconductor surface (Eq. 4).

$$M^{n+} + e^- \longrightarrow M^{(n-1)+} \quad (4)$$

In highest concentrations the dissolved metal ions have detrimental effect on the rate of organic substrate removal, which was attributed to oxidation of reduced metals by •OH or photogenerated holes (11).
In the present work, the effects of concentration and type of dopant on the photodegradation of VOCs (dichloromethane, chloroform and carbon tetrachloride) were investigated. The dopants that were chosen in this study were Mn^{2+}, Fe^{2+} and Fe^{3+}.

Experimental

Chemicals

All chemicals used were reagent-grade. In TiO_2 sol-gel preparation, ethanol (99.7%) was purchased from Hayman Limited, polyethylene glycol (2000) and diethanolamine were purchased from Merck-Schuchandt and titanium tetraisopropoxide (97%) was purchased from Aldrich. The transition metal ions precursors used as dopants were Ferrous sulphate (Goodrich chemical), Manganese acetate (Hayashi Pure Chemical) and Iron Nitrate (Riedel-de Haen). The VOCs were dichloromethane (Fisher Scientific), chloroform (Merck) and carbon tetrachloride (J.T. Baker).

Photodegradation Experiments

All photodegradation experiments of dichloromethane, chloroform and carbon tetrachloride were conducted in a home built fix bed annulus glass reactor with a total volume of approximate 1000 mL, which was illustrated in Figure 1. The reactor is equipped with an electromagnetic pump to circulate the sample, a glass compartment to place the catalyst and UV light and a septum to inject sample into the reactor. The UV radiation (~354 nm) that was used in the photodegradation experiments was provided by a light source from a 6 W black lamp (Toshiba Litec Co.).

The amount of VOCs that had been oxidized was analyzed using gas chromatography Shimadzu GC-14A which was coupled with Shimadzu chromatopac 4A. The GC was equipped with a 2 m 15% carbowax on Csorb WNAW 80-100 Mesh packed column and a flame ionization detector. The carrier gas was helium with the pressure of 2.75 Kg/cm^2.The gases used in the flame were air and hydrogen with the pressure was 0.5 Kg/cm^2.The detection, column and injection temperatures were 200˚C, 95˚C and 150˚C respectively.

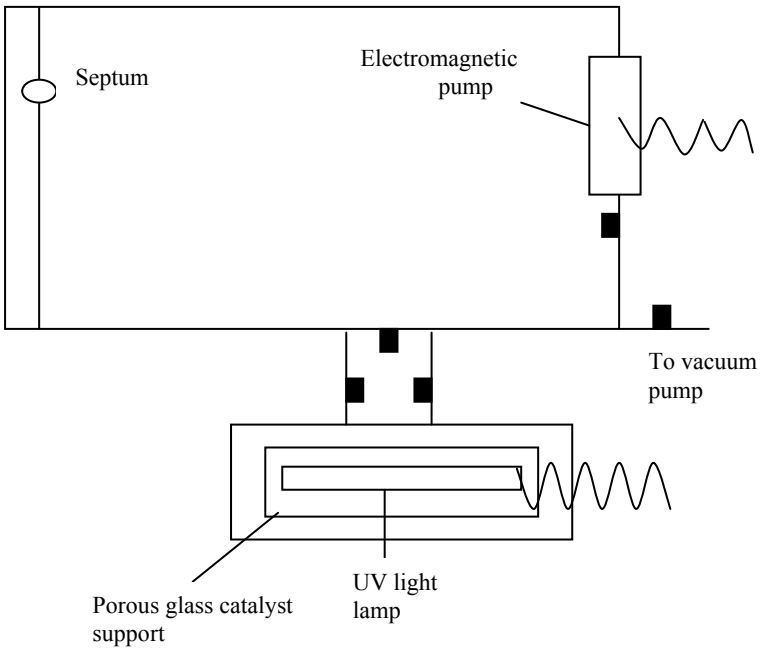

Figure 1: Schematic drawing of reactor.

Results and Discussion

Photolysis

In photolysis experiment, UV light without presence of catalyst was used in order to ensure the measured activity was contributed by photocatalytic activity and not other reactions. Table 1 showed the % photolysis of VOCs used in this study. It was found that no photolysis was detected in first 30 and 60 minutes, the photolysis in 90 minutes was rather small, in which only 0.73% and 1.13% were detected for dichloromethane and carbon tetrachloride respectively. This indicated that all gas samples in this study could not be directly decomposed by UV light of its maximum wavelength is 354 nm.

Table 1: Photolysis of VOCs for 90 minutes

Organic compounds	% Photolysis
Dichloromethane	0.73
Chloroform	0
Carbon tetrachloride	1.13

Optimum Dopant Ratios

Oxidation of dichloromethane, chloroform and carbon tetrachloride had been conducted to determine the optimum dopant ratios for Mn^{2+}, Fe^{3+} and Fe^{2+} -doped TiO_2. It can be observed that concentration of sample was decreased with the increasing of degradation time. The catalysts with optimum dopant ratios will give the highest degradation. Table 2 depicted the oxidation of dichloromethane, chloroform and carbon tetrachloride. It can be seen that optimum dopants ratio for Mn^{2+}, Fe^{3+} and Fe^{2+} -doped TiO_2 was 1:0.0005.

When different concentrations of dopant was used, optimum dopant ratio was existed. The photoactivity was decreased when the concentration of dopant was higher or lower than the optimum dopant ratio. Photocatalysis mechanism occurs through the formation of radical •OH when h^+ reacts with hydroxyl ions or electron reacts with oxygen. When the concentration of dopant is high, the reduced metals will be oxidizaed by •OH or h^+. This process will compete with the following process (Eq. 5-6).

$$h^+ + OH \longrightarrow \bullet OH \quad (5)$$

$$h^+ + H_2O \longrightarrow \bullet OH + H^+ \quad (6)$$

Additionally, some photogenerated positive holes will be attracted by negative-charged metal particles, if the accumulated negative charges are not consumed or not further transferred out of the metal particles, the negative charges will become recombination centres:

$$H^+ + e^-(metal) \longrightarrow N + energy \quad (7)$$

where N represents a neutral centre.

When the concentration of dopant is lower than optimum dopant ratio, the metal on the surface can promote interfacial charge transfer process. This migration of the generated electron to the metal particles, on the one hand, can increase the lifetime of the holes and suppress the electron-hole recombination.

Effect of VOCs

Table 2 depicted the oxidation of dichloromethane, chloroform and carbon tetrachloride for 90 minutes. It was found that different VOCs will have different degradation although same catalyst was used in the photodegradation experiment. In the degradation of chloroform, it was expected Cl• sensitized degradation had happened (Eq. 8-9). Dichloromethane only has 2 chlorine atoms in its structure, therefore Cl• sensitized degradation may lower than in chloroform. Chlorine radicals do not react with the C-Cl bond, hence carbon tetrachloride may not undergo a Cl• sensitized degradation. Therefore, the rate of degradation of the studied chlorinated hydrocarbons follows the order: $CHCl_3 > CH_2Cl_2 > CCl_4$.

$$CHCl_3 + h\nu \longrightarrow CHCl_2\bullet + Cl\bullet \quad (8)$$

$$CHCl_3 + Cl\bullet \longrightarrow CCl_3\bullet + HCl \quad (9)$$

Table 2: % degradation of VOCs for 90 minutes

Catalysts	Dopant ratios	% Degradation		
		CH_2Cl_2	$CHCl_3$	CCl_4
Mn^{2+}	1:0.0003	11.95	13.06	10.94
	1:0.0005	16.47	19.57	15.87
	1:.001	11.49	13.12	12.12
Fe^{2+}	1:0.0003	13.40	29.08	13.42
	1:0.0005	33.79	34.21	20.80
	1:.001	22.76	30.84	12.36
Fe^{3+}	1:0.0003	34.53	35.74	22.07
	1:0.0005	36.02	43.10	35.42
	1:.001	33.91	35.11	24.44
TiO_2	-	20.93	23.87	17.40

Effect of Metal ions (M^{n+})

Figure 2 showed the % degradation of dichloromethane using Mn^{2+}, Fe^{2+}, Fe^{3+}-doped TiO_2 and undoped TiO_2 as catalysts. The photodegradation of dichloromethane was significantly better with Fe^{3+}-doped TiO_2 than other doped and pure TiO_2 catalysts. Adding Fe^{3+} seems to increase the TiO_2 photoactivity. 36.02 % of CH_2Cl_2 was degraded when Fe^{3+}-doped TiO_2 was used in oxidation process. However, addition of Mn^{2+} decreased the degradation of dichloromethane. When pure TiO_2 was used during oxidation process, only 20.93% CH_2Cl_2 was degraded.

Figure 3 indicated % degradation of chloroform using Mn^{2+}, Fe^{2+}, Fe^{3+}-doped TiO_2 and undoped TiO_2 as catalysts. It showed obviously that Fe^{2+} and Fe^{3+}-doped TiO_2 gave better degradation of chloroform than pure TiO_2. Meanwhile, Mn^{2+}-doped TiO_2 showed poor degradation in the oxidation of chloroform, only 19.57 % chloroform was degraded. Fe^{3+}-doped TiO_2 showed the best degradation of chloroform among all doped TiO_2 catalysts that were used in oxidation processes. Addition of Fe^{3+}enhanced the efficiency of degradation from 23.87 % to 43.1%.

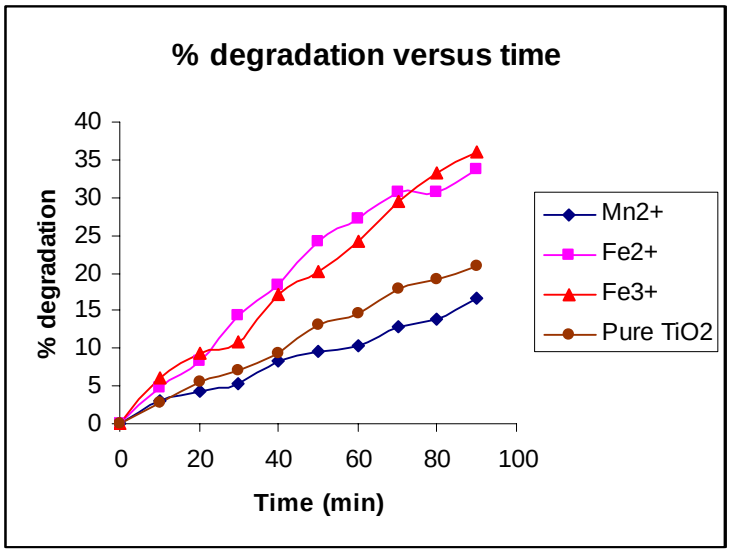

Figure 2: % of degradation of dichloromethane using Mn^{2+}, Fe^{2+}, Fe^{3+}-doped TiO_2 and undoped TiO_2 as catalysts.

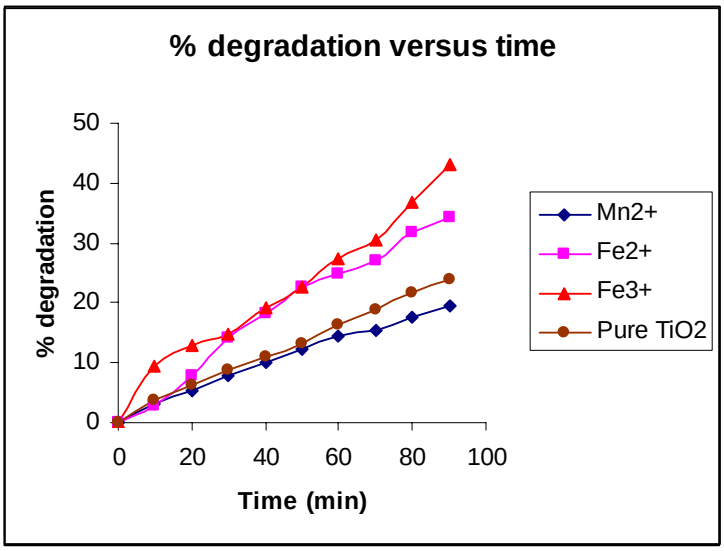

Figure 3: % of degradation of chloroform using Mn^{2+}, Fe^{2+}, Fe^{3+}-doped TiO_2 and undoped TiO_2 as catalysts.

Figure 4 depicted the % degradation of carbon tetrachloride using Mn^{2+}, Fe^{2+}, Fe^{3+}-doped TiO_2 and undoped TiO_2 as catalysts. Photooxidation of carbon tetrachloride using Mn^{2+} and Fe^{3+}-doped TiO_2 as catalysts were slightly slower than that of chloroform, which was 15.87 and 35.42% respectively. However, pure TiO_2 showed higher photodegradation of carbon tetrachloride than that of using Mn^{2+} and Fe^{2+}-doped TiO_2 as catalysts.

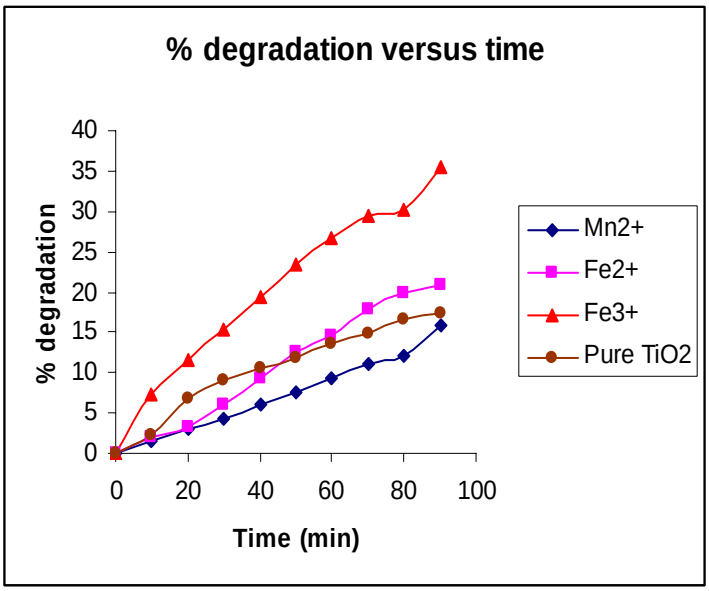

Figure 4: % of degradation of carbon tetrachloride using Mn^{2+}, Fe^{2+}, Fe^{3+}-doped TiO_2 and undoped TiO_2 as catalysts.

Fe^{2+} is relatively unstable due to the loss of exchange energy on going from d^5 (half-filled high spin) to d^6 and tends to return to Fe^{3+} (d^5). As a consequence of this proximity the e^- trapped in Fe^{2+} can be easily transferred to a neighbouring surficial Ti^{4+}.

$$Fe^{2+} + Ti^{4+} \longrightarrow Fe^{3+} + Ti^{3+} \qquad (10)$$

which can leads to interfacial electron transfer. Therefore, photocatalytic activity was increased through the migration of the generated electron to the metal particles and increased the lifetime of the holes consequently suppressed the electron-hole recombination.

For Fe^{3+}-doped TiO_2, the recombination of the photoexcited charge carriers in the nanostructure is retarded by Fe^{3+}, which can act as both an electron trap and a hole trap. The trapped hole embodied in Fe^{4+} oxidized VOCs.

The trapped hole embodied in Fe^{4+} can migrate to the catalysts surface and react with surface hydroxyl producing •OH radicals (Eq. 13). Then, the hydroxyl radical will react with VOCs and increasing the degradation.

$$Fe^{3+} + e_{cb}^{-} \longrightarrow Fe^{2+} \quad (11)$$

$$Fe^{3+} + h_{vb}^{+} \longrightarrow Fe^{4+} \quad (12)$$

$$Fe^{4+} + OH^{-} \longrightarrow Fe^{3+} + \bullet OH \quad (13)$$

It was found that degradations of under studied VOCs were low when Mn^{2+} -doped TiO_2 was used. When Mn^{2+} loses an electron to a hole, Mn^{3+} which can trap both electrons and holes will be created. This electron transfer process is not desirable due to the small energy difference between Mn^{2+} and Mn^{3+}. Therefore, the separation of the photogenerated electron and hole is not effective, consequently, the rate of recombination is expected to be high.

Conclusion

Mn^{2+}, Fe^{3+} and Fe^{2+}-doped catalysts have an optimum ratio of 1:0.0005. The addition of Fe^{2+} and Fe^{3+} into TiO_2 increased the photooxidation of chloroform, carbon tetrachloride and dichloromethane. Mn^{2+} is detrimental to the photooxidation of carbon tetrachloride, dichloromethane and carbon tetrachloride. The rate of degradation of the studied chlorinated hydrocarbons follows the order: $CHCl_3 > CH_2Cl_2 > CCl_4$.

Acknowledgement

We would like to express gratitude to MOSTE for IRPA grant (VOT 74248) and Universiti Teknologi Malaysia - PTP Schlolarship.

References

(1) Mirmohseni, A. and Oladegeragoze, A. (2004). "Determination of Chlorinated Aliphatic Hydrocarbons in Air Using a Polymer Coated Quartz Crystal Microbalance Sensor." *Sens. Actuators B*

(2) Wang, K-H. and Hsieh,Y-H. (1998). "Heterogeneous Photocatalytic Degradation of Trichloroethylene in Vapor Phase by Titanium Dioxide." *Pergamon Environ. International.* **24.** 267-274.

(3) Padilla, A.M., Corella, J. and Toledo, J.M. (1999). "Total Oxidation of Some Chlorinated Hydrocarbons with Commercial Chromia Based Catalysts." *Appl. Catal. B: Environ*. **22.** 107-121.

(4) Litter, M.I. (1999). "Review Heterogeneous Photocatalysis Transition Metal Ions in Photocatalytic Systems." *Appl. Catal. B: Environ*. **23.** 89-114.

(5) Maira, A. J., Lau, W. N., Lee, C.Y., Yue, P. L., Chan, C.K. and Yeung, K.L. (2003). "Performance of A Membrane-catalyst for Photocatalytic Oxidation of Volatile Organic Compounds." *Chem. Eng. Sci.* **58.** 959-962.

(6) Mills, A., and Le Hunte, S. (1997). "An Overview of Semiconductor Photocatalysis." *J. Photochem. Photobio. A: Chem.* **108.** 1-35.

(7) Alberici, R.M. and Jardim, W.F. (1997). "Photocatalytic Destruction of VOCs in The Gas-phase Using Titanium Dioxide." *Appl. Catal. B: Environ.* **14.** 55-68.

(8) Papaefthimiou, P., Ioannides, T. and Verykios, X.E. (1998). "Performance of Doped Pt/TiO_2 (W^{6+}) Catalyst for Combustion of Volatile Organic Compounds (VOCs)." *Appl. Catal. B: Environ* **15.** 75-92.

(9) Karvinen, S. (2003). "The Effects of Trace Elements on The Crystal Properties of TiO_2." *Solid State Sci*. **5.** 811-819.

(10) He, C., Xiong, Y., Chen, J. Zha, C. and Zhu, X. (2003). "Photoelectrochemical performance of $Ag\text{-}TiO_2$ / ITO Film and Photoelectrocatalytic Activity Towards the Oxidation of Organic Pollutants." *J. Photochem. Photobio. A: Chem.* **157.** 71-79.

(11) Butler, E.C. and Davis, A.P. (1993). "Photocatalytic Oxidation in Aqueous Titanium Dioxide Suspensions: The influence of Dissolved Transition Metals." *J. Photochem. Photobiol. A: Chem.* **70.** 273-283.

Malaysian Journal of Analytical Sciences, Vol.9, No. 3(2005): 487 - 491

Esterification of Sago Starch by Using Palm Oil Based Oleochemicals

See, Y. K. [1], Dzulkefly, K. [1], Annuar, K. [1] and Abdul Halim, A. [1]

[1] Department of Chemistry, University Putra Malaysia 43400 UPM, Serdang, Selangor, Malaysia
Email address: seeyawkoon@yahoo.com

Abstract
Starch in its natural form is limited in its scope of usage. It is due to the inherent physical-chemical properties of the starch. Chemical derivatization has been studied as a way to solve this problem by append new chemical group to the hydroxyl group. Esterification of sago starch by using palm oil based chemicals like octanoyl chloride can be done in the absence of an organic solvent. The reaction was initiated by gelatinization of sago starch with excess formic acid at room temperature followed by treatment with octanoyl chloride. A stream of nitrogen gas had been used to eliminate the hydrochloric acid produced by the reaction. The optimum concentration of formic acid appeared to be around 4.3 eq/glucose with the highest yield. The octanoyl chloride concentration of 3.8 eq/glucose had given an optimum condition for esterification. Higher octanoyl chloride concentrations led to a reduction in yield due to acid hydrolysis of starch ester by HCl liberated during reaction. A maximum yield of 86 % with degree of substitution (DS) of 1.2 was obtained after 40 min at 105 ^{o}C. Higher temperatures and longer reaction times increased the substitution of the long acyl chain into starch but reduction in yield. Esterification was evidenced by the presence of ester carbonyl group in FT-IR spectra. The intensities of carbonyl and methyl peaks were increased with the increasing of degree of substitution. Whereas, the higher the degree substitution is, the greater is the decrease in the band intensity of O-H stretching.

Key words: Sago starch; esterification; starch ester; characterization; degree of substitution (DS)

Introduction

Starch is an abundant, inexpensive, renewable, and fully biodegradable natural raw material. Regardless of its origin, starch consists of amylase and amylopectin. Starch is the main source of carbohydrate which is the most important portion of our daily diet. However, studies on chemical modifications of starches to produce starch-based material are limited. Esterification of glucoside's hydroxyl groups of starch may change its chemical and physical properties, thus new compounds may be obtained. Esterification with organic acids is known to result in thermoplastic and hydrophobic materials when the degree of substitution (DS) is high enough [1].

A number of reports exist in literature pertaining to the preparation of starch esters with the ultimate aim of significantly modifying the physical-chemical properties of starches. The starch esters are generally prepared by reacting starch with fatty acid chlorides in organic solvents such as pyridine [2, 3], toluene [4], dimethyforamide [5], or mixtures of Lithium Chloride and N, N-Dimethylacetamide [6]. This method allows a larger scale of synthesis, with almost complete derivatization (DS ≈ 3) [2]. However, many organic solvents are expensive, toxic and difficult to remove from starch and are prohibited for industrial applications, especially in the food sector so an alternative method would be desirable.

Aburto and co-workers [1] developed a method for esterifying starch with fatty chlorides in the absence of organic solvent. The esterification was initiated by the formylation of hydroxyl groups to form formate esters, which is more active. Then, the fatty acid chloride was added to the mixture to complete the reaction. In each steps, the reagents, formic acid and fatty chlorides were employed in excess. After optimization of main parameters, both a high DS (> 1.5) and recuperation yield (> 80 %) were obtained.

Methodology

Materials
Sago starches were purchased from locally refinery. Formic acid 98 %, ethanol 95 % and absolute ethanol were provided by BDH Company. Octanoyl chloride 99 % was supplied by Acros Organics.
Esterification

The esterification was carried out by the method of Aburto et al. [1]. A sample of 2.5 g sago starch was dried for 2 hours at 105 ^{o}C. The formylation reaction was carried out by impregnating the sago starch with formic acid at 25 ^{o}C for 4 min at a stirring rate of 250 min^{-1}. The reaction mixture was then heated to the require temperature. The octanoyl chloride was then added drop wise over 7 min. The temperature and stirring rate (500 min^{-1}) were maintained for time ranging from 20 to 80 min. A stream of N_2 was flowed during the reaction to eliminate the HCl formed. At the end of the reaction, 100 mL of ethanol (95 % v/v) was added and the mixture distilled at 25 ^{o}C with rotary evaporator. 150 mL of absolute ethanol was then added to precipitate the starch ester and the mixture was centrifuged at 3000 min^{-1} for 10 min. The solid phase was washed in ethanol (2 X 100 mL) and oven dried at 50 ^{o}C under vacuum for 12 hours. The recuperation yield of starch esters will be calculated from the amount solid obtained taking account of the degree of substitution (DS) [7].

$$RY(\%) = \frac{m_{ester}.162}{m_i[DS(M_n - 1) + 162]}.100\%$$

Where m_{ester} and m_i are the mass of the solid phase recuperated at the end of the reaction and the initial mass of native starch respectively. *DS* and M_n correspond to the degree of substitution and molecular mass of the corresponding fatty chain grafted onto starch. The molecular mass of the anhydroglucose unit is 162.

Analysis of the starch ester by FT-IR spectroscopy

The IR spectra were recorded on a FT-IR BX Perkin Elmer spectrometer. The starch ester was dissolved in chloroform and the solution was deposited on the surface of the NaCl cell by evaporating the solution of the sample to dryness.

Determination of the degree of substitution (DS)

Elemental analysis was carried out on a CHNS-932 Leco apparatus after drying the samples at 100 ^{o}C for 24 hours. The DS was determined by elemental analysis. From the percentage of C, H and O determined by elemental analysis, the DS was calculated by comparing experimental values with theoretical values calculated for DS ranging from 0 to 3. The DS was taken as the value which produced the closest match.

Results and Discussion

The appearance of the product, starch octanoate, after purification, was changed from that of a non-sticky and rigid powder to the non-rigid and sticky powder. The color of starch ester was changed from white (native starch) to the color that highly depends upon DS. Those with high DS have the form of a brown yellowish mass, whereas those with low DS have the appearance of a pink whitish powder. The degree of substitution for a starch derivative is defined as moles of substituents of hydroxyl groups per D-glucopyranosyl structural unit of the starch polymer; with three hydroxyl groups per unit, the theoretical maximum degree of substitution is three.

Analysis of the starch ester by FT-IR spectroscopy

The FT-IR spectra of unmodified sago starch and starch octanoate are shown in Figure 1. In the fingerprint region of the spectrum of unmodified sago starch and starch octanoate, two characteristic peaks appear between 1020 cm^{-1} and 1168 cm^{-1}, which are attributed to the anhydroglucose ring C-O stretch.

The spectrum of unmodified sago starch shows an extremely broad band due to hydroxyl groups, O-H stretching, at its most intense at 3440 cm^{-1}. The sharp band at 2926 cm^{-1} is characteristic of C-H stretches. Another characteristic peak occurs at 1644 cm^{-1}, which believe to be a feature of tightly bound water present in the starch [8].

The esterification is evidences by the presence of the ester carbonyl group stretching at 1744 cm^{-1} which shifted from that of the carbonyl of carboxylic acid groups at 1727 cm^{-1}. The intensity of the band is depending upon the DS. The occurrence of two peaks of strong intensities between 2850 cm^{-1} and 2930 cm^{-1} of esterified starch are attributed to the methyl and metylene C-H stretching associated with the octanoyl substituents, which the intensity will increase with the increasing of carbon chains have been substituted in the D-glucopyranosyl structural. The strong band at 3440 cm $^{-1}$ is attributed to the hydroxyl groups. This peak intensity is highly depending upon the DS. The higher the DS is, the greater is the decrease in the band intensity, as it can be observed for the octanoated starches with DS 0.6 and 1.2 respectively.

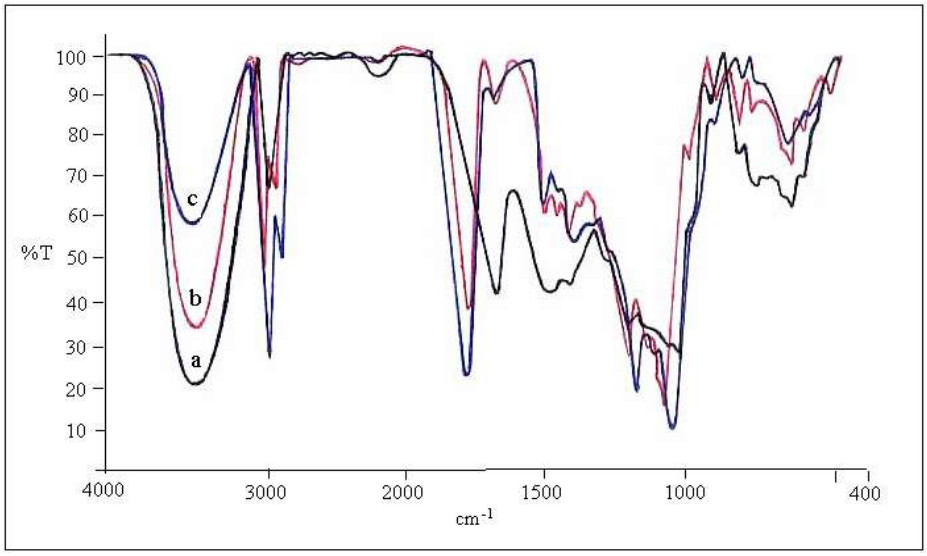

Figure 1. FT-IR spectra of (a) sago starch, (b) and (c) are esterified sago starch with DS 0.6 and 1.2 respectively.

Influence of the concentration of formic acid

Table 1. Influence of concentration of formic acid on the yield and degree of substitution of starch octanoate (3 eq/glucose of octanoyl chloride, 40 min of reaction time, 90 ^{o}C of reaction temperature).

Formic acid (eq/glucose)	***DS***	***Yield (%)***	***Appearance of reaction medium at start of reaction***
0	0	-	slightly dispersed starch
2.0	0.3	39	slightly dispersed starch formate
3.5	0.5	56	moderately dispersed starch formate
4.3	**1.0**	**72**	**highly dispersed starch formate**
5.0	0.6	66	highly dispersed starch formate
8.0	0.2	67	highly dispersed starch formate

The results in Table 1 indicate that formic acid is required for esterification. Starch that was reacted with formic acid was prior to treatment with the fatty acid chlorides in the absence of the organic solvent. Formic acid reacts with some of the alcohol functions in starch, producing their more reactive formate starch. In the absence of formic acid, the esterification reaction did not take place due to the depolymerization of starch ester by acid medium from fatty acid chloride. Whereas in the presence of formic acid, the highly reactive formate starch had stimulated the reaction between starch and fatty acid chloride. Formic acid should be applied in excess (> 3 eq/glucose) for effective reaction because one mole of formic acid may reacts with three moles of hydroxyl groups that existing in a D-Glucopyranosyl unit. Further more, 3.5 eq/glucose of formic acid was not sufficient to adequately disperse the starch formate in the reaction medium and a low yield (56 %) with a low value of DS (0.5) was obtained. At 4.3 eq/glucose of formic acid, a comparable value of DS (1.0) was obtained as well as the highest yield (72 %) of starch ester. This is due to the highly dispersion and well gelatinization of starch formate in formic acid. For an increase in formic acid concentration from 4.3 eq/glucose to 8.0 eq/glucose, the value of DS was fall from 1.0 to 0.2 with a moderate yield (66 % and 67 %). At higher concentration of formic acid, the reaction prior to deformylation, this diminishes the subsequent esterification with octanoyl chloride. The optimum concentration of formic acid appeared to be around 4.3 eq/glucose as other parameters were maintained.

Influence of the concentration of octanoyl chloride

From the results listed in Table 2, it can be seen that since the octanoyl chloride acts both as solvent and reactant it must be employed in excess (> 3 eq/glucose). Results indicate that an octanoyl chloride concentration of 3.8 eq/glucose has given an optimum condition for esterification with the highest yield of the starch ester (80 %). At lower concentrations, the volume of octanoyl chloride was not enough to disperse the starch formate. With larger amounts of octanoyl chloride, the DS was gradually rose but reduction in yield. Under this condition, the

recuperation yield will decrease due to the depolymerization of starch esters by acidic characteristic of octanoyl chloride itself and the HCl liberated during the reaction. The optimum concentration of octanoyl chloride was around 3.8 eq/glucose.

Table 2. Influence of the concentration of octanoyl chloride on the yield and degree of substitution of starch octanoate (4.3 eq/glucose of formic acid, 40 min of reaction time, 90 ^{o}C of reaction temperature).

Octanoyl chloride (eq/glucose)	***DS***	***Yield (%)***	***Appearance of reaction medium at start of reaction***
2.3	0.5	53	slightly dispersed starch formate
3.0	1.0	72	slightly dispersed starch formate
3.8	**1.2**	**80**	**well dispersed starch formate**
5.0	1.3	77	highly dispersed starch formate
6.0	1.4	67	highly dispersed starch formate

Influence of the duration of the reaction

From the results listed in Table 3, it can be seen that the reaction took a long duration of time (>20 min) in order to get the best yield. Results indicate that a timing duration of 40 min had given an optimum condition for esterification with the highest yield of the starch ester (80 %). With longer reaction times, the starch formate had enough time to react with octanoyl chloride and the DS rose slightly but it was contributed to the decreasing of recuperation yield. This condition is due to the hydrolysis of starch octanoate by the octanoyl chloride medium and HCl liberated in the reaction. Beside that, the starch octanoate also had longer time to expose to the HCl.

Table 3. Influence of the duration of the reaction on the yield and degree of substitution of starch octanoate (4.3 eq/glucose of formic acid, 3.8 eq/glucose of octanoyl chloride, 90 ^{o}C of reaction temperature)

Time (min)	***D.S.***	***Yield (%)***	***Appearance of reaction medium at start of reaction***
20	1.3	77	highly dispersed starch formate
40	**1.2**	**80**	**highly dispersed starch formate**
60	1.2	77	highly dispersed starch formate
80	1.3	75	highly dispersed starch formate

Influence of temperature

Table 4. Influence of the temperature on the yield and degree of substitution of starch octanoate (4.3 eq/glucose of formic acid, 3.8 eq/glucose of octanoyl chloride and 40 min of duration time).

Temperature (^{o}C)	***D.S.***	***Yield (%)***	***Appearance of reaction medium at start of reaction***
25	0.2	65	starch formate in suspension
45	0.2	70	starch formate in suspension
60	0.6	74	moderately dispersed starch formate
90	1.2	80	well dispersed starch formate
105	**1.2**	**86**	**highly dispersed starch formate**
120	1.3	76	highly dispersed starch formate
135	1.3	69	highly dispersed starch formate

The results indicate that the temperature highly influenced the yield and DS. The results listed in Table 4 show that for temperature between 25 ^{o}C and 45 ^{o}C, a low yield of starch ester was obtained as well as low DS. This was attributed to the suspension of starch formate. At the temperature between 60 ^{o}C and 105 ^{o}C, there was a good dispersion of starch formate in the octanoyl chloride which contributed to a higher reactivity. This led to an increase in DS and recuperation yield. For the temperature above 105 ^{o}C, the reaction rate will be shorten and make the

reaction more reactive. Under this condition, the amount of HCl liberated will be increase rapidly. Here again, the starch ester was hydrolyzed by the HCl liberated during the reaction and contributed to the decreasing of yield. The optimum condition of temperature appeared to be around 105 ^{o}C as other parameters were optimized.

Conclusion

The results presented show that the method developed by Aburto and co-workers [1] can be used to esterify sago starch with octanoyl chloride in the absence of an organic solvent. The nitrogen flow is effectively eliminating the HCl produced during the reaction by giving an 86 % yield of starch octanoate with a degree of substitution of 1.2 under the optimized factors: Concentrations of formic acid (4.3 eq/glucose) and octanoyl chloride (3.8 eq/glucose), duration of the reaction (40 min) and temperature (105 ^{o}C).

Acknowledgement

We wish to thank the government of Malaysia for financial support under IRPA program and UPM for providing research facilities.

References

1. Aburto, J., I. Alric and E. Borredon (1999(a)). Preparation of Long-chain Esters of Starch Using Fatty Acid Chlorides in the Absence of an Organic Solvent. *Starch/Stärke.* 51: 132-135.

2. Sagar, A. D. and Merrill, E. W. (1995). Properties of Fatty-Acid Esters of Starch. *Journal of Applied Polymer Science.* 58: 1647-1656.

3. Thiebaud, S., J. Aburto, I. Alric, E. Borredon, D. Bikiaris, J. Prinos and C. Panayiotou. (1997(a)). Properties of Fatty-Acid Esters of Starch and Their Blends with LDPE. *Journal of Applied Polymer Science.* 65: 705-720.

4. Thiebaud, S., M. E. Borredon, G. Baziard and F. Senocq. (1997(b)). Properties of Wood Esterified by Fatty-Acid Chlorides. *Bioresource Technology*. 59: 103-107.

5. Funakoshi, H., N. Shiraishi, M. Norimoto, T. Aoki, H. Hayashi and T. Yokota. (1979). Studies on the Thermoplasticization of Wood. *Holzforschung.* 33: 159-166.

6. Vaca-Garcia, C., S. Thiebaud, M. E. Borredon and G. Gozzelino. (1998). Cellulose esterification with Fatty Acids and Acetic Anhydride in Lithium Chloride / N, N-Dimethylacetamide Medium. *JAOCS*. 75: no. 2: 315-319.

7. Aburto, J., H. Hamaili, G. Mouysset-Baziard, F. Senocq, I. Alric, and E. Borredon. (1999(b)). Free-Solvent Synthesis and Properties of Higher Fatty Esters of Starch-Part 2. *Starch/Stärke.* 51: 302-307.

8. Fang, J. M., P. A. Fowler, J. Tomkinson and C. A. S. Hill. (2002). The Preparation and Characterisation of Series of Chemically Modified Potato Starches. *Carbohydrate Polymers.* 47: 245-252.

Malaysian Journal of Analytical Sciences, Vol.9, No. 3(2005): 492 - 496

CO_2/H_2 METHANATION ON NICKEL OXIDE BASED CATALYSTS DOPED WITH LANTHANIDE SERIES

Mohd Hasmizam Razali, Wan Azelee Wan Abu Bakar, Nor Aziah Buang and Faridah Mohd Marsin

Department of Chemistry, Faculty of Science, University Teknologi Malaysia,
81310 UTM Skudai, Johor, Malaysia. E-mail: wazelee@kimiafs.utm.my aziah@ kimiafs.utm.my

Abstract- The catalytic activity of prepared catalyst by sol gel method of 60Ni-40Ln (Ln= La^{3+}, Ce^{3+}, Pr^{3+}, Nd^{3+}, Sm^{3+}, Gd^{3+}) has been investigated for methanation of $CO_2/.H_2$ to form CH_4. The results obtained concluded that the NiO/Pr_2O_3 (60:40) catalyst shows the highest activity, with 100% methanation at 300°C. The result corresponds to the presence of higher specific surface area of NiO/Pr_2O_3 catalyst. The XRD analysis showed that this catalyst has some degree of amorphous properties and the existence of individual phases of cubic NiO and cubic Pr_2O_3 in the catalyst system, which most probably act as active site for CO_2/H_2 methanation The complimentary results obtained from SEM showed the presents of homogeneous smaller particle size, which support the good performance of NiO/Pr_2O_3 catalyst towards CO_2/H_2 methanation.

Keywords: Nickel, Methanation, Lanthanide

Abstrak-Aktiviti pemangkinan bagi mangkin 60Ni-40Ln (Ln = La^{3+}, Ce^{3+}, Pr^{3+}, Nd^{3+}, Sm^{3+}, Gd^{3+}) yang disediakan melalui kedah sol-gel di kaji untuk proses metanasi CO_2/H_2 bagi menghasilkan CH_4. Keputusan yang diperolehi menunjukkan bahawa mangkin NiO/Pr_2O_3 (60:40) memberikan aktiviti terbaik dengan 100 % metanasi CO_2/H_2 berlaku pada suhu 300 °C. Keputusan ini disebabkan oleh mangkin NiO/Pr_2O_3 memepunyai luas permukaan yang tinggi. Analisis XRD menunjukkan mangkin ini mempunyai sifat amorfos dan kehadiran fasa kubik NiO and kubik Pr_2O_3 secara individu yang berkemungkinan bertindak sebagai tapak aktif untuk proses metanasi CO_2/H_2. Keputusan yang diperolehi daripada SEM menunjukkan kehadiran partikel yang bersaiz kecil dan homogen memberikan prestasi yang baik bagi mangkin NiO/Pr_2O_3terhadap preses metanasi CO_2/H_2.

Katakunci: Nikel, Metanasi, Lantanida

Introduction

Global warming caused by enormous evolution of carbon dioxide by combustion fossil fuels has become serious problems in industrial circles. In Malaysia, a total of 5.13 tones CO_2 are emitted from fuels combustion [1]. In order to solve this problem, various types of method fro recovering and chemical fixation of carbon dioxide have been proposed. Methanation of carbon dioxide is the most advantageous reaction with respect to thermodynamics for chemical fixation of carbon dioxide, since this reaction is considerably faster than reactions to form other hydrocarbons or alcohols [3]. This reaction needs a desert area for generation of electricity with solar energy. One possible use of electricity is for production of hydrogen (H_2) by seawater electrolysis at desert coast. The hydrogen produced is used for reaction with CO_2 to form methane (CH_4) through methanation reaction using the catalyst (Refer to equation 1.1)

$$CO_2 + 4H_2 \xrightarrow[\text{catalyst}]{} CH_4 + 2H_2O \qquad (1.1)$$

The development of catalysts for methanation of carbon dioxide was the key factor [2]. The use of nickel oxide based catalyst for methanation is well established. However, studies have shown that nickel is more susceptible to coking and deactivates rapidly [4]. In this paper, the influence the addition of the lanthanide series elements on the activity and stability of Ni based catalysts were investigated with respect to the CO_2/H_2 methanation aiming to produce catalyst system with high susceptibility towards chemical and physical change. In general, lanthanide series elements are used in form of oxide in catalyst formations (although they can be introduced in the catalyst in several form) and they do not act alone but always in combination with other elements. Their role is, therefore, that being catalyst promoters (structural and electronic or stabilizers and to improve the activity or increase the thermal stability of true catalyst.

Experimental

Catalyst Preparation

Catalyst was prepared by dissolving nickel (II) nitrate hexahydrate with distilled water. Then the solution was stirred for 15 minutes. At the same time, dopant salts were weighed and transferred into second round-bottom flask. Distilled water was added until all the salt dissolved. The solution was stirred for 15 minutes. Then, both solutions were mixed and stirred continuously further 15 more minutes. The mixture was then transferred into an evaporating disc and aged in an oven at 70^{o}C for 72 hours. A greenish solid gel was formed and calcined at 400^{o}C for 17 hours.

Catalytic Testing

The catalytic activities were performed in a home-built fixed bed micro reactor of 10mm inner diameter under the atmospheric pressure. The reaction gas mixture of CO_2 and H_2 (1:4 volume ratio) was pass continuously over the catalyst. Before the catalytic measurement, the catalyst was preheated at 300^{o}C for 1 hour and silica powder was used as dilution agent. The catalytic testing was carried out at operation temperature up to 500^{o}C.

Catalyst Characterization

Structured investigation of catalyst was determined by X-ray diffraction with Cu-Kα (λ=1.54Å) radiation. Scans were performed in step mode of 0.2^{o}/second and 0.4 seconds/step. The data was collected over the range of 2θ from 10 up to 70^{o}. The particle size of the catalysts were determined according to the Scherrer equation. Nitrogen gas adsorption was carried out at 77K via Micrometrics ASAP 2010 to determine the specific surface area and morphology of the catalyst was observed by scanning electron microscopy (SEM). SEM was conducted using model Philips XL 40 with the energy of 15.0 kV.

Results and Discussion

Catalytic activities

Figure 3.1 shows the methanation of CO_2 in the presence of H_2 by prepared catalyst for undoped and doped nickel oxide based catalyst with lanthanide series elements (60:40). The additions of lanthanide series elements are effective to enhancing the catalytic activities. As a whole the prepared catalysts illustrated the complete conversion of CO_2 to methane at and below 500 ^{o}C except undoped nickel based catalyst. The low performances of the undoped NiO catalyst is probably due to the carbon deposition during the reaction at higher temperature**.** It is well known that the CO_2/H_2 methanation reaction leading to the carbon deposit on the catalyst is related to the deactivation of NiO catalyst [5]. Otherwise, the performance of doped catalyst in increases even at higher temperature indicate that the present of dopants can minimize the coking process, thus show a good catalytic activity even at higher temperature [6]. The strong interaction of NiO bond in doped NiO results in the formation of smallest particle size on the catalyst surface which are relatively stable towards carbon deposition. But among the doped catalyst, the NiO/Pr_2O_3 revealed the highest catalytic activities with 100 % conversion of CO_2 to CH_4 at 300 ^{o}C, this show that the addition of praseodymium in the Ni based catalyst is superior than the rest of the lanthanide series elements. Redox reaction occurs in the interfacial region between Ni and Pr and the electrons are transferred from Pr to Ni to maintain Ni at a lower valence, which promoted the activation of CO_2 and H_2 at lower temperature.

Catalyst Characterization

To highlight the role of dopant, X-ray diffraction analysis was carried out for the prepared catalyst. For the undoped nickel oxide based catalyst, three peaks due to NiO cubic phase detected are shaper and narrower, with high intensity which revealed higher degree of crytallinity. However, for doped NiO based catalyst, the diffractogram comprises three broad peaks, assigned to cubic phase NiO which is more amorphous. In addition peaks due to the presence of dopants is also detected [Figure 3.2]. The broadening of peaks was contributed by some degree of amorphous property in the catalyst. The diffractogram also revealed that the phase structure of NiO and dopants exist in their individual phases, whereby solid-state reaction was not occur [4]. The particle size of catalyst decrease relatively small with respect to the size of dopants used except for NiO/Pr_2O_3 catalyst. It is believed that the present of praseodymium probably can act as an anti-crystalline medium that can prevent the particle from undergoing an agglomeration process.

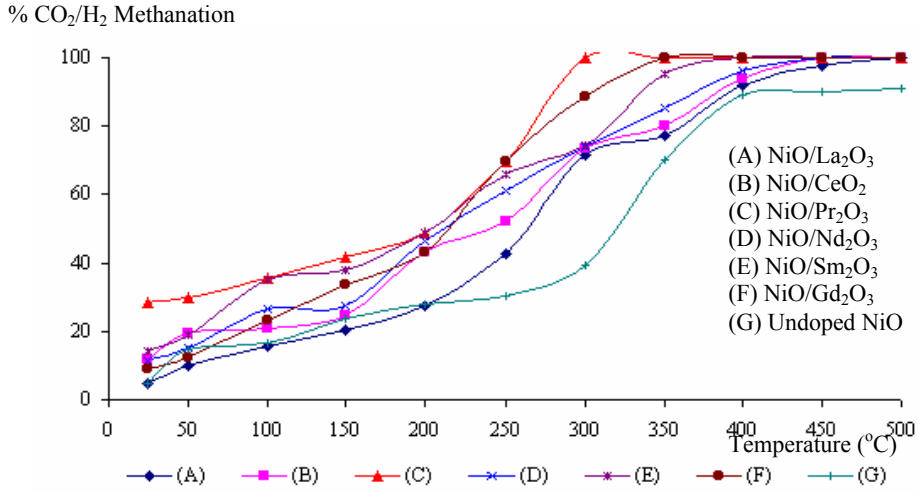

Figure 3.1 : The CO_2/H2 methanation on undoped nickel oxide and doped nickel oxide (60:40) calcined at 400 °C for 17 hours.

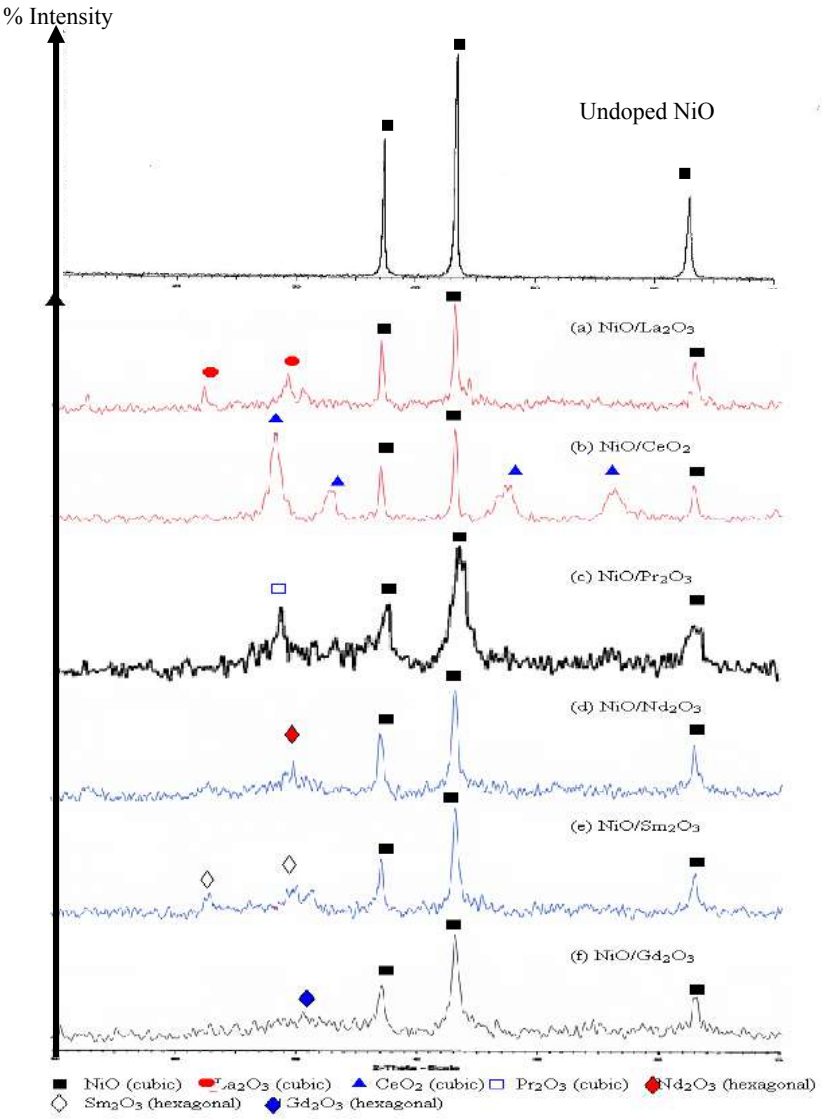

Figure 3.2: X-Ray diffractogram pattern of undoped NiO and doped NiO (60:40) catalysts calcined at 400 ^{o}C for 17 hours.

Table 3.1 shows the BET surface area of prepared catalyst. The undoped nickel oxide catalysts gave 5.60 m^2g^{-1} of BET specific surface area and the BET surface area increases with addition of dopant into nickel oxide based catalyst and the addition of praseodymium increases roughness until 74.68 m^2g^{-1}indicating this catalyst has smaller particle size compare to other samples. This result agreed well with the particle size of NiO/Pr_2O_3 derived from XRD, which give the lowest, value of 13.80 nm. The higher BET surface area for NiO/Pr_2O_3 catalyst contributed to the higher concentration of active sites, whereby possess the good performance of NiO/Pr_2O_3 catalyst [7,8].

Table 3.1: Average particle size and BET surface area of prepared catalyst.

Catalysts	Sizes of dopants cation (nm)	[a]Particle size (nm)	[b]BET surface area (m^2/g)
Undoped NiO	-	54.73	5.60
NiO/La_2O_3	0.1016	24.70	11.31
NiO/CeO_2	0.1034	21.25	20.39
NiO/Pr_2O_3	0.1013	13.80	75.58
NiO/Nd_2O_3	0.0995	20.62	23.68
NiO/Sm_2O_3	0.0964	18.60	26.42
NiO/Gd_2O_3	0.0938	16.62	27.56

a = derived from XRD using Scherrer equation
b = obtain from nitrogen adsorption

The SEM analysis in Figure 3.3 (a) undoped NiO and (b) NiO/Pr_2O_3 revealed that the morphology of the catalyst material. SEM micrograph of undoped NiO showed the formation of bulk NiO, which is less disperse and distributed non-homogeneously on the surface of the catalyst. It does can be clearly seen in Figure 3.3 (a). The formation of bulk NiO, resulted the large particle of undoped NiO based catalyst. This result shows good agreement with the XRD pattern for undoped NiO which is, sharp and narrow peaks are observed indicate high degree of crytallinity of the catalyst materials with larger particle. This phenomenon is not good for catalytic activity, thus resulted low performances of the undoped NiO catalyst.

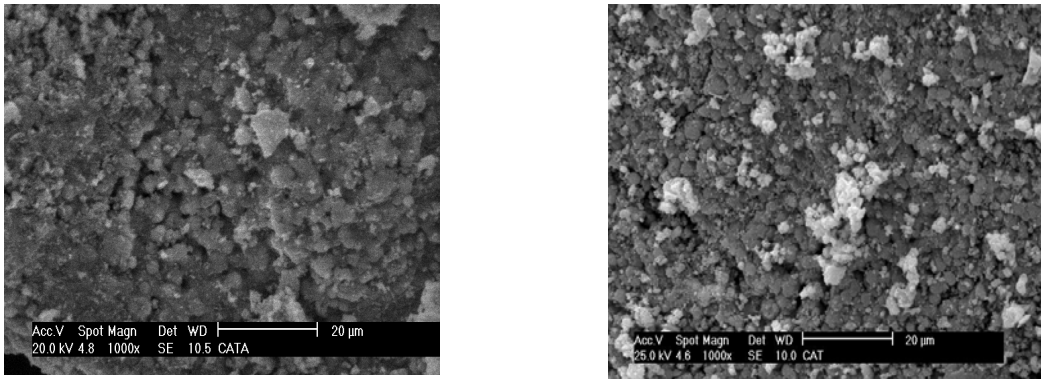

(a) (b)

Figure 3.3: SEM micrograph of (a) undoped NiO (b) NiO/Pr_2O_3 after calcinations 400 ^{o}C with magnification of 1000X and scale bar 1.7 cm: 10 µm

Meanwhile, SEM micrograph of NiO/Pr_2O_3 catalyst showed obvious different with smaller particle size uniformly distributed on the surface of the catalyst materials. The particles are spherical and well dispersed homogenously indicating this catalyst had more amorphous character [Figure 3.3 (b)].

Conclusion

Among the prepared catalyst, the NiO/Pr_2O_3 catalyst revealed highest catalytic activity with 100% methanation at 300°C. The XRD analysis of NiO/Pr_2O_3 catalyst shows the existence of individual phases of NiO cubic phase and Pr_2O_3 cubic phase, which serve as active sites for CO_2/H_2 methanation. The higher BET surface area of NiO/Pr_2O_3 catalyst contributes better performance. SEM analysis shows that the NiO/Pr_2O_3 formed homogeneous smaller size particle which support the good performance of the NiO/Pr_2O_3 towards CO_2/H_2 methanation.

Acknowledgements

The authors are grateful to the Ministry of Science, Technology and Innovation of Malaysia (MOSTI) for sponsoring this work under project IRPA (Vot 74124). We also like to thanks to the Department of Chemistry, Faculty of Science, UTM Skudai for instrument support.

References

1. Jabatan Alam Sekitar Malaysia; Laporan 'Environmental Quality Report 2000' ; Kementerian Sains, Teknologi dan Alam Sekitar ; Kuala Lumpur ; 2000
2. D.L. Trimm, Design of Industrial Catalyst, Elsevier, Amsterdam, 1980.
3. Hashimoto, K., Yamasaki, M., Meguro, S., Sasaki, T., Katagari, H. Izumiya, K., Kumagai, N., Hazabaki, H., Hakiyama, E. And Asami, K. (2002) " Material for global carbon dioxide recycling." *Corrosion Science.* **44**. 371-386.
4. Slagtern, A., Schuurman, Y., Leclerg, C., Verykios, X. and Miradotas C. (2001)." Specific Features Concerning the Mechanism of Methane Reforming by Carbon Dioxide over Ni/La_2O_3 Catalyst." *Journal of Catalyst.* **172**. 118-126.
5. Chang F, W,. Kuo M, S,. Tsay M, S. and Hsieh M, C. (2003). "Hydrogenation Of CO_2 over Nickel Catalysts on Rice Husk Ash-Alumina Prepared by Incipient Wetness Impregnation." *Applied Catalyst A: General.* **247**. 309-320.
6. Chen, Y. and Ren, S. (1997). " Effect of Addition on Ni/Al_2O_3 Catalysts Over CO_2 Methanation." *Applied Catalysis A: General.* **164.** 127-140
7. Yamasaki, M., Komori, M., Akiyama, E., Habazaki, H., Kawashima A., Asami K. and Hashimoto K. (1999). " CO_2 Methanation Catalyst prepared from Amorphous Ni-Zr-Sm and Ni-Zr-misch metal alloy precursors." *Materials Science and Engineering.* **267**. 220-226.
8. Bartholomew, C. H., Weatherbee, G. D., Rao, K. A. (2000). " On the Mechanism of CO and CO_2 methanation over Ni/SiO_2." *Applied Catalysis A: General.* **77.** 46- 58.

Malaysian Journal of Analytical Sciences, Vol.9, No. 3(2005): 497 - 503

PENCIRIAN BAHAN MESOPOROS MCM-41 YANG DIMODIFIKASIKAN DENGAN TITANIUM

F. W.Harun[1], S.R. Omar[1], H. Harun[1], A. Rinaldi[1], M. A. Yarmo[1], A. Ramli[2]

[1]Makmal Pemangkinan, Tingkat 3, Pusat Pengajian Sains Kimia dan Teknologi Makanan, Fakulti Sains dan Teknologi, Universiti Kebangsaan Malaysia, 43600 Bangi, Selangor
[2]Advanced Materials Centre SIRIM Berhad, Kulim Hi-Tech Park, 09000 Kulim, Kedah
E-mail: ambar@pkrisc.cc.ukm.my, Fax: 03-89254550

Abstrak

Bahan mesoporos Ti-MCM-41 dengan nisbah mol Si/Ti 16, 40, 60, 80 dan 100 telah berjaya disintesis secara terus melalui teknik perawatan hidroterma. Semua sampel dicirikan menggunakan teknik XRD, ICP, SEM, penjerapan N_2 dan spektroskopi DRUV-vis. Penambahan Ti ke dalam kerangka MCM-41 didapati meningkatkan nilai d_{100} dari 1.66 nm ke 2.02 nm. Keadaan ini menunjukkan pembentukan Ti dalam kerangka MCM-41 yang tersusun secara heksagonal. Penentuan unsur Ti menggunakan teknik ICP menunjukkan nilai nisbah Si/Ti adalah sepadan dengan nisbah semasa proses sintesis Ti-MCM-41. Luas permukaan BET mangkin meningkat sehingga 1119 m^2/g dengan bentuk isoterm jenis IV dikesan bagi semua sampel dan ini mencirikan Ti-MCM-41 sebagai bahan mesoporos. Tapak aktif Ti-MCM-41 yang sesuai untuk tindak balas pengepoksidaan alkena juga dikenalpasti dengan wujudnya kation Ti(IV) yang terisolasi secara tetrahedral dalam kerangka MCM-41 yang dikesan dalam spektrum DRUV-vis pada nilai serapan 215 nm.

Kata kunci: Mesoporos, Ti-MCM-41, Heksagonal, Ti Tetrahedral

Abstract

Mesoporous material Ti-MCM-41 with Si/Ti mole ratio of 16, 40, 60, 80 and 100 have been successfully synthesized by direct hydrothermal method. All samples have been characterized using XRD, ICP, SEM, N_2 adsorption and DRUV-vis spectroscopy. The incorporation of Ti in the silica matrices MCM-41 framework seems to increase the d_{100} value from 1.66 nm to 2.02 nm. This is shows the formation of Ti in the MCM-41 framework which is ordered hexagonally. Determination of Ti elements using ICP technique shows Si/Ti mole ratios are parallel with the ratio value while synthesis process of Ti-MCM-41. The BET surface area is increase to 1119 m^2/g with isotherm types IV is observed for all samples and this is characterized the Ti-MCM-41 as mesoporous materials. Active sites of Ti-MCM-41 which is suitable for epoxidation of alkenes are determined with the existing of tetrahedrally isolated Ti(IV) cation in the MCM-41 framework. The observations of these active site is done using DRUV-vis spectrum with the absorption value is 215 nm.

Keywords: Mesoporous, Ti-MCM-41, Hexagonal, Tetrahedral Ti

Pendahuluan

Mangkin poros mendapat perhatian yang luas kerana luas permukaan dan tapak aktif yang tinggi menyumbang kepada aktiviti, selektiviti dan penukaran kepada produk yang lebih tinggi. Kemasukan logam peralihan ke dalam kerangka zeolit telah membuka ruang baru dalam bidang mangkin heterogen. Mangkin VS-1 dan TS-1 masing-masing vanadium dan titanium silikat-1 menunjukkan ciri-ciri mangkin yang unik untuk tindak balas pengoksidaan substrat organik menggunakan larutan hidrogen peroksida. Tindak balas dilakukan pada suhu rendah dan sangat selektif terhadap produk [1-2]. Walau bagaimanapun, aplikasi mangkin zeolit mikroporos ini adalah sangat terhad kerana ia hanya sesuai untuk substrat yang berdiameter kecil (<6 Å).

Sekumpulan penyelidik Mobil Oil pada tahun 1992 [3] telah menemui satu bahan berpenapis berjulat mesoporos yang dihasilkan secara langsung. MCM-41 iaitu salah satu ahli kumpulan M41S mempunyai struktur liang heksagonal yang tersusun secara seragam, luas permukaan BET yang besar, sifat keporosan yang tinggi dan taburan saiz liang yang sempit serta boleh diubah daripada 15-100 Å. Kerangka

silikatnya juga boleh dimodifikasikan melalui penukargantian isomorfus separa dengan unsur seperti Al, Ti, V, Sb, Fe atau Pd [4-6]. Penukargantian dengan Ti telah menarik perhatian para penyelidik kerana kebolehan Ti-zeolit dalam mengoksidakan banyak substrat organik [2].

Bahan mesoporos dengan unsur yang sesuai untuk tindak balas redoks biasanya dihasilkan dengan memasukkan prekursor titanium semasa proses sintesis hidroterma dilakukan. Prekursor ini akan melalui satu mekanisma templat surfaktan iaitu sama ada $S^+I^-/S^+X^-I^+$, atau S^oI^o [7]. Walau bagaimanapun, bahan ini juga boleh dihasilkan melalui teknik post-sintesis seperti menggunakan titanocene [8].

Dalam kajian ini, kami akan melaporkan tentang teknik penyediaan mangkin Ti-MCM-41 dengan pelbagai kandungan titanium. Struktur bahan ini dicirikan menggunakan XRD, ICP, penjerapan N_2 dan DRUV-vis.

Bahan dan Kaedah

Sintesis

Kerangka MCM-41 dengan kandungan titanium yang berbeza-beza telah dihasilkan secara hidroterma daripada titanium (IV) ethoksida (TEOTi, Aldrich) dan SiO_2 cabosil (Aldrich). Setiltrimetilammonium bromida (CTMABr, Aldrich) dan tetrametilammonium hydroksida (TMAOH 25 wt %, Aldrich) digunakan sebagai templat surfaktan untuk menghasilkan Ti-MCM-41. Komposisi molar bagi gel yang terbentuk adalah was SiO_2 : *x* TEOTi : 0.15 CTMABr : 0.26 TMAOH : 24.3 H_2O (*x* dipelbagaikan antara Si/Ti 16-100). Prosedur penyediaan adalah seperti berikut: CTMABr dan TMAOH ditambah ke dalam air ternyahion dan dikacau sehingga larutan jernih kelihatan. Jumlah prekursor titanium ditambah secara perlahan-lahan ke dalam campuran surfaktan dan dikacau selama 2 jam. 12.5 g SiO_2 ditambah dan dikacau selama 1 jam. Gel yang terbentuk kemudian dimasukkan ke dalam oven autoklaf selama 48 jam pada suhu 373 K. Hasil yang terbentuk ditapis, dibasuh dengan air suling dan dikeringkan pada suhu 333 K. Penyingkiran surfaktan templat dilakukan menggunakan teknik pengkalsinan pada 813 K dengan pembakaran di bawah aliran N_2 selama 1 jam dengan kadar alir 150 ml min^{-1} dan 6 jam di bawah aliran O_2 dengan kadar alir yang sama.

Pencirian

Pencirian pembelauan sinar-X (XRD) dilakukan menggunakan Bruker AXS D8 Advance dengan radiasi Cu Kα (panjang gelombang, λ = 0.154 nm). Difraktometer beroperasi pada sudut rendah antara 1.5 hingga 10^o dengan kadar imbasan 0.04^o/10 saat. Analisis unsur kimia (Ti) dilakukan ke atas sampel serbuk yang dilarutkan dengan HF dan dirakamkan dengan peralatan Perkin Elmer model Optima 4300DV. Isoterm penjerapan-penyahjerapan N_2 diperolehi pada suhu 77 K menggunakan peralatan Micromeritics ASAP 2010. Sebelum dianalisis, sampel perlu dikeringkan pada suhu 523 K selama 12 jam. Luas permukaan BET dikira berdasarkan persamaan BET. Manakala taburan saiz liang diperolehi daripada lengkung nyahjerapan isoterm dan persamaan Barrett-Joyner-Halenda (BJH) seperti yang dicadangkan oleh Tanev dan Vlaev [9]. Analisis kedudukan titanium bahan bahan Ti-MCM-41 dilakukan menggunakan spektroskopi DRUV-vis model Perkin Elmer Lambda 900. Sampel serbuk dipadat dan dihomogenkan dalam sel kuartz dan spektrum dirakamkan dalam julat panjang gelombang 190-500 nm.

Perbincangan

Difraktogram pembelauan sinar-X bagi sampel Ti-MCM-41(X) di mana X adalah nisbah Si/Ti 16 hingga 100 dan sampel silika MCM-41 ditunjukkan dalam Rajah 1. Tiga puncak dikesan dengan satu puncak pantulan utama yang dilabelkan sebagai pantulan 100 pada sudut rendah iaitu kurang daripada 3^o dan dua pantulan lemah yang dilabelkan sebagai pantulan 110 dan 200. Corak pembelauan ini menunjukkan bahawa struktur bahan MCM-41 tersusun secara heksagonal [10]. Dapat dilihat anjakan puncak utama (100) dari sudut rendah ke sudut yang lebih tinggi apabila sumber titanium ditambah. Menurut Ahn et al. [11], keadaan ini mencirikan penyusutan susunan dalam julat panjang bahan Ti-MCM-41 selepas kemasukan titanium. Anjakan ini juga disebabkan oleh kemasukan titanium ke dalam kerangka MCM-41 secara tetrahedral dan nilai panjang ikatan Ti-O yang lebih tinggi berbanding Si-O. Puncak utama dalam bahan dengan kandungan titanium paling tinggi iaitu Si/Ti 16 menunjukkan intensiti yang rendah. Ini mencadangkan kemasukan titanium yang banyak sukar dilakukan kerana ia mencacatkan struktur hablur bahan MCM-41 yang disebabkan oleh diameter kation titanium yang lebih besar berbanding Si^{4+} [12]. Selain daripada itu, kemasukan Ti^{4+} juga mempengaruhi padatan surfaktan dan lapisan berkembar elektrikal (electrical double layer) dalam susunan surfaktan. Keadaan ini dilihat daripada anjakan sudut pantulan utama ke nilai yang lebih tinggi (Jadual 1) dan peningkatan nilai parameter kekisi, a_o (Rajah 2). Ini sesuai dengan Beck et al. [3] yang juga telah melaporkan nilai a_o yang lebih tinggi bagi bahan Al-MCM-41 berbanding silika MCM-41.

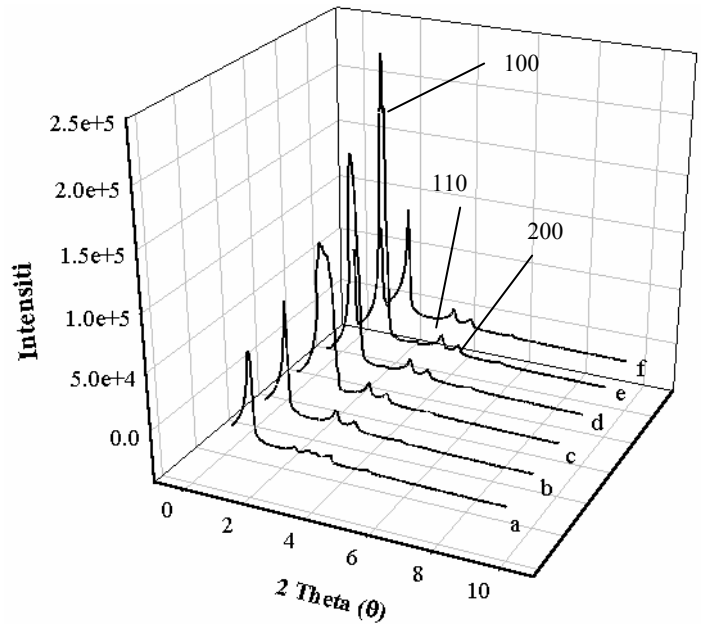

Rajah 1: Pembelauan sinar-X bagi bahan Ti-MCM-41 di mana a) Si/Ti 16, b) Si/Ti 40, c) Si/Ti 60, d) Si/Ti 80, e) Si/Ti 100, f) MCM-41

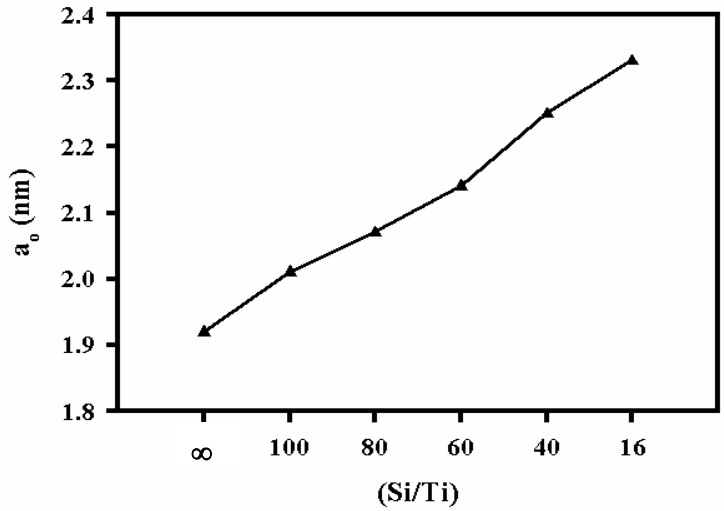

Rajah 2: Perbandingan nilai parameter kekisi, a_o terhadap perubahan kandungan Ti dalam MCM-41

Kajian morfologi permukaan menggunakan teknik mikrograf imbasan elektron (SEM) telah dijalankan ke atas bahan mesoporos silika MCM-41 dan Ti-MCM-41. Daripada kajian ini saiz, morfologi permukaan dan tahap kehomogenan bahan mesoporos yang telah dikalsin dapat diketahui seperti yang dilihat dalam Rajah 3 di bawah. Bagi silika MCM-41, dapat dilihat bahawa partikel bahan ini berbentuk sfera dengan saiz antara purata 2 – 4 μm. Bentuk dan saiz yang hampir sama juga diperolehi bagi bahan dengan kandungan Ti paling rendah iaitu Ti-MCM-41 (100). Dengan meningkatnya jumlah kandungan Ti dalam kerangka MCM-41 (Si/Ti 60), saiz partikel menjadi semakin kecil berbanding silika MCM-41 iaitu menjadi antara 0.5 – 1.0 μm. Manakala bagi bahan Ti-MCM-41(16) yang mempunyai kandungan Ti paling tinggi tidak mempunyai bentuk serta saiz yang tetap dengan darjah serakan yang tinggi.

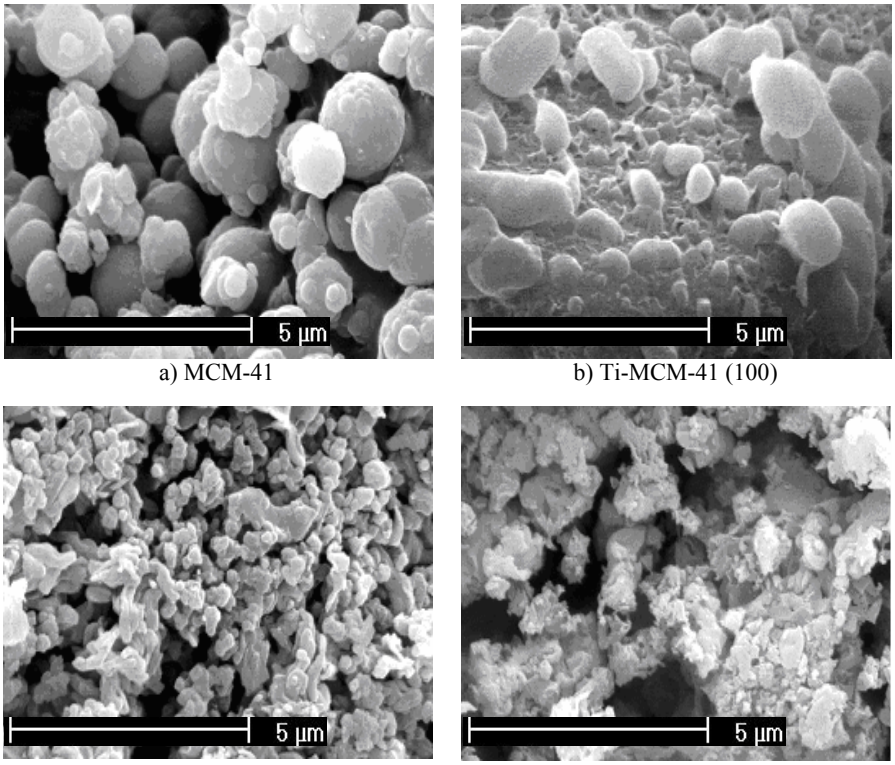

a) MCM-41 b) Ti-MCM-41 (100)

c) Ti-MCM-41 (60) d) Ti-MCM-41 (16)

Rajah 3: Mikrograf SEM bagi bahan MCM-41 dan Ti-MCM-41 selepas pengkalsinan

Analisis unsur kimia yang telah dijalankan ditunjukkan dalam Jadual 1. Semua bahan yang disintesis mempunyai jumlah Si/Ti yang sama dengan komposisi gel semasa sintesis. Ini membuktikan bahawa kesemua sumber Ti yang dimasukkan semasa sintesis gel berada di dalam pepejal bahan mesoporos yang dihasilkan.

Jadual 1: Ciri-ciri tekstur bahan mesoporos MCM-41 dengan pelbagai kandungan Ti bagi bahan Ti-MCM-41

Ti-MCM-41	ICP	Analisis XRD		Analisis Penjerapan N_2		
	Si/Ti	d_{100} (nm)	a_o (nm)	S_{BET} (m^2/g)	PSD (nm)	PWT (nm)
16	15.8	2.02	2.33	1030.94	3.61	1.28
40	39.5	1.95	2.25	1063.44	3.6	1.35
60	52.4	1.85	2.14	1069.51	3.56	1.42
80	76.2	1.79	2.07	1077.18	3.52	1.45
100	91.0	1.74	2.01	1105.05	3.5	1.49
MCM-41	-	1.66	1.92	1119.47	2.88	0.96

a_o = parameter kekisi $a_o = 2d_{100} / \sqrt{3}$, S_{BET} = luas permukaan BET, PSD = taburan saiz liang, PWT = ketebalan dinding liang (PSD – a_o)

Isoterm penjerapan-penyahjerapan N_2 menunjukkan kesemua bahan mempunyai isoterm jerapan jenis IV dalam julat tekanan relatif (p/p_o) antara 0.25 – 0.3 yang mencirikan kondensasi kapilari antara liang (Rajah 4). Luas permukaan BET dan taburan saiz liang ditunjukkan dalam Jadual 1. Luas permukaan BET bahan mesoporos ini menurun dengan kadar yang rendah apabila kandungan Ti meningkat. Seperti yang dapat dilihat, setiap sampel mempunyai luas permukaan BET yang besar seperti yang dilaporkan oleh Tanev et al. [13]. Purata saiz liang dikira berdasarkan data kaedah penjerapan Barrett, Joyner dan Halenda (BJH). Merujuk kepada Jadual 1, semakin tinggi kandungan Ti nilai saiz liang semakin meningkat. Franke et al. [14] telah menjelaskan keadaan ini berlaku kerana tiada spesis logam oksida yang terbentuk di luar kerangka bahan mesoporos silikat.

Peningkatan nilai saiz liang bagi bahan Ti-MCM-41 berbanding MCM-41 adalah disebabkan oleh penukargantian ikatan Si-O yang pendek (1.62 Å) dengan ikatan Ti-O yang lebih panjang (1.87 Å) [3].

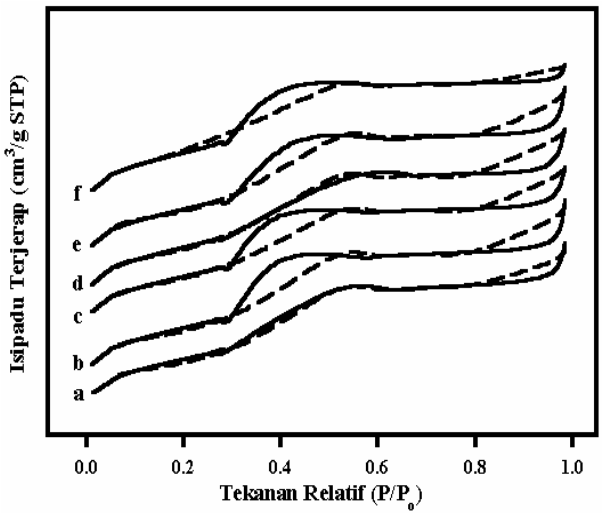

Rajah 4: Isoterma plot mesoporos Ti-MCM-41 di mana a) Si/Ti 16; b) Si/Ti 40; c) Si/Ti 60; d) Si/Ti 80; e) Si/Ti 100; f) MCM-41

Maklumat nilai ketebalan dinding menjadi semakin penting dalam menentukan sifat pemangkinan bahan Ti-MCM-41. Menurut Chen et al. [15], jika purata jarak ikatan atom $T - T$ (T = Si atau Ti) dianggap bernilai lebih kurang 3.0 Å, maka rangkaian-rangkaian dinding perlu dibina daripada tidak lebih dari tiga unit tetrahedral TO_4, di mana ia boleh dipunyai oleh tetrahedral gelang berahli 3-, 4- atau 5-. Dua daripada unit tetrahedral ini mesti boleh melalui rangkaian manakala satu lagi terselindung dalam dinding silikon. Unit tetrahedral yang terlindung ini tidak boleh melalui rangkaian yang dibina dan jika ada titanium dalam kawasan ini, ia adalah tidak aktif [16]. Nilai ketebalan dinding liang boleh dikira daripada saiz liang yang diperolehi daripada kaedah BJH ditolak nilai parameter kekisi, a_o yang dikira daripada data d_{100} XRD. Peningkatan nilai ketebalan dinding bagi bahan Ti-MCM-41 berbanding MCM-41 adalah disebabkan oleh penukargantian ikatan Si-O yang pendek dengan ikatan Ti-O yang lebih panjang [3].

Untuk bahan MCM-41 yang dimodifikasikan dengan Ti, maklumat tentang persekitaran spesis Ti diperolehi melalui teknik spektroskopi UV-vis. Kedudukan jalur serapan UV-vis boleh dikolerasikan kepada persekitaran dan koordinasi spesis titanium dalam silikat. Sebanyak tiga dekonvulasi puncak spektrum serapan iaitu 215 nm, 264 nm dan 312 nm digunakan untuk menghubungkan setiap puncak dengan spesis Ti yang berbeza dalam matriks silika MCM-41. Rajah 5 menunjukkan spektrum DRUV-vis bagi bahan Ti-MCM-41 selepas pengkalsinan pada pelbagai kandungan Ti. Seperti yang dilaporkan oleh Zhang et al. [7], sampel Ti-MCM-41 biasanya dicirikan berdasarkan jalur serapan lebar antara 215 – 220 nm dan 260 – 270 nm.

Bagi TS-1 [17] dan Ti-Beta [18], jalur puncak pada 220 nm adalah merupakan peralihan cas ligan ke logam yang melibatkan atom Ti(IV) terisolasi dalam koordinasi tetrahedral. Berdasarkan kepada pernyataan ini, jalur puncak pada 215 nm dalam bahan Ti-MCM-41 boleh dicirikan sebagai Ti(IV) yang tersiolasi secara isomorfus dalam kerangka silikat seperti yang berlaku pada TS-1 dan Ti-Beta. Dekonvulasi puncak kedua menunjukkan anjakan merah dan peningkatan puncak serapan pada 264 nm untuk bahan Ti-mesoporos MCM-41 boleh dicirikan sebagai kehadiran spesis Ti dalam koordinasi oktahedral atau dikenali juga sebagai spesis Ti heksa-koordinat yang membentuk kompleks dengan dua molekul air [19]. Selain daripada itu, puncak lemah ini juga boleh terdiri daripada sedikit kluster semipoler Ti–O–Ti yang terbentuk dalam jaringan kerangka silika MCM-41. Serapan lemah ini lebih jelas dilihat pada bahan mesoporos dengan kandungan Ti paling banyak (Si/Ti 16).

Dekonvulasi puncak ketiga dilakukan pada nilai serapan 312 nm yang mencirikan keadaan Ti terpolimer di luar kerangka MCM-41 sebagai TiO_2 [20]. Walau bagaimanapun, dalam bahan mesoporos Ti-MCM-41 yang telah dihasilkan tiada sebarang serapan pada panjang gelombang 312 nm. Ini menunjukkan bahawa dalam penghasilan bahan mesoporos Ti-MCM-41 yang bersifat amorfus, Ti mudah tersebar dalam matrik silika walaupun pada kepekatan Ti paling tinggi. Peratus nilai puncak serapan yang telah dilakukan dekonvulasi mengikut spesis Ti ditunjukkan dalam Jadual 2.

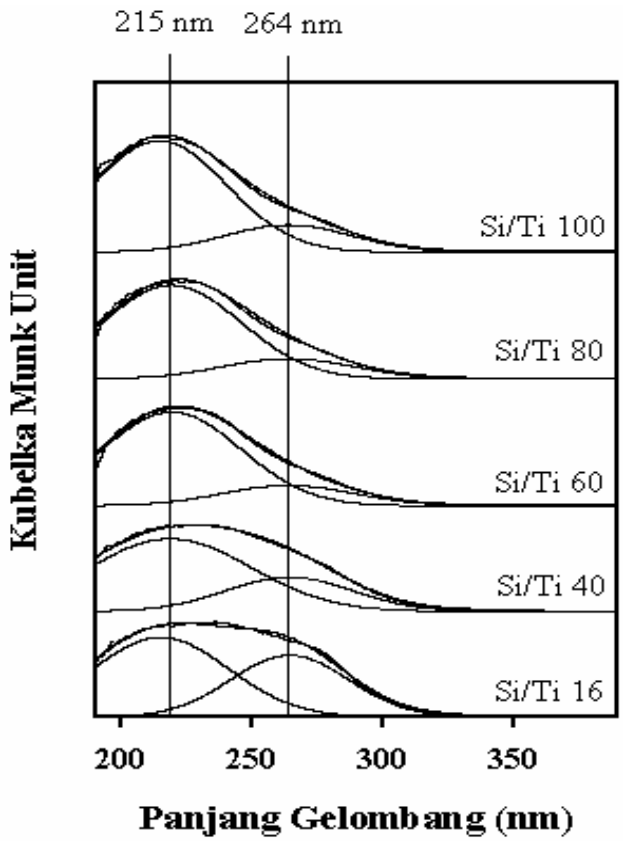

Rajah 5: Spektrum DRUV-vis bahan Ti-MCM-41 dengan pelbagai kandungan Ti

Jadual 2: Dekonvulasi puncak serapan bagi spektrum UV-vis bahan Ti-MCM-41

Ti-MCM-41	215nm Gaussian (%)	264 nm Gaussian (%)
Si/Ti 16	59.83	40.17
Si/Ti 40	73.03	26.97
Si/Ti 60	71.39	28.61
Si/Ti 80	79.8	20.2
Si/Ti 100	81.19	18.81

Daripada Jadual 2 di atas, dapat dilihat jumlah spesis Ti terisolasi secara tetrahedral iaitu pada puncak serapan 215 nm semakin meningkat dengan pengurangan jumlah kepekatan Ti dalam kerangka silikat MCM-41. Ini menunjukkkan bahawa semakin kecil kandungan Ti semakin tinggi kebolehan Ti untuk tersebar dalam kerangka MCM-41 membentuk Ti tetrahedral dan semakin kurang kebarangkalian membentuk Ti oktahedral atau semipolimer Ti-O-Ti.

Penghargaan

Setinggi penghargaan untuk Kementerian Sains, Teknologi dan Inovasi atas bantuan kewangan IRPA 09-02-02-0033 SR0004/05-03 dan National Science Fellowship (NSF).

Rujukan

[1] Taramaso, M., Perego, G. & Notari, B. 1983. Preparation of porous crystalline synthetic material comprised of silicon and titanium oxides. *US Patent* No. 4,410,501.

[2] Notari, B. 1988. Synthesis and Catalytic Properties of Titanium Containing Zeolites. *Studies in Surface Science and Catalysis* **37**: 413-425.

[3] Beck, J.S., Vartuli, J.C., Roth, W.J., Leonowick, M.E., Kresge, C.T., Schmitt, K.D., Chu, C.T.W., Olson, D.H., Sheppard, E.W., McCullen, S.B., Higgins, J.B. & Schlenker, J.L. 1992. A New Family of

Mesoporous Molecular Sieves Prepared with Liquid Crystal Templates. *Journal of American Chemical Society* **114**: 10834-10843.

[4] Huo, Q., Margolese, D.I., Ciesla, U., Demuth, D.G., Feng, P., Gier, T.E., Sieger, P., Leon, R., Firouzi, A., Chmelka, B.F., Schutz, F. & Stucky, G.D. 1994. Organization of organic molecules with inorganic molecules species into nanocomposite biphase arrays. *Chemical Material* **6**: 1176-1191.

[5] Tanev, P.T., Chibwe, M. & Pinnavaia, T.J. 1994. Titanium containing mesoporous molecular sieves for catalytic oxidation of aromatic compounds. *Nature* **368**: 321.

[6] Corma, A., Camblor. M.A., Esteve, P., Martinez, A. & Pariente, J.P. 1994. Activity of Ti-Beta catalyst for the selective oxidation of alkenes and alkanes. *Journal of Catalysis* **145**(1): 151-158.

[7] Zhang, W.Z., Wang, J.L., Tanez, P.T. & Pannavaia, T.J. 1996. Catalytic hydroxylation of benzene over transition-metal substituted hexagonal mesoporous silicas. *Chemical Communications* **8**: 979-980

[8] Maschmeyer, T., Rey, F., Sankar, G. & Thomas, J.M. 1995. Heterogeneous catalysts obtained by grafting metallocene. *Nature* **378**: 159.

[9] Tanev, P.T., Vlaev, L.T. & Lyubomir, T. 1993. An Attempt at a More Precise Evaluation of the Approach to Mesopore Size Distribution Calculations Depending on the Degree of Pore Blocking. *Journal Colloid and Interf. Science* **160**: 110-116.

[10] Beck, J.S., Calabro, D.C., McCullen, S.B., Pelrine, B.P., Schmitt, K.D. & Vartuli, J.C. 1993. Sorption eparation over modified synthetic mesoporous crystalline material. *US Patent* 5,220,101.

[11] Ahn, W.S., Lee, D.H., Kim, T.J., Seo, G. & Ryoo, R., 1999. Post-synthetic preparations of titanium-containing mesopore molecular sieves. *Applied Catalysis A: General* **181**: 39-49.

[12]Gontier, S. & Tuel, A. 1995b. Synthesis and characterization of transition metal containing mesoporous silicas, Zeolites: A Refined Tool for Designing Catalytic Sites. Dlm. Bonneviot, L. & Kaliaguine, S. (pnyt.). *Studies in Surface Science and Catalysis* **97,** hlm. 157-164. Amsterdam: Elsevier Science B.V.

[13] Tanev, P.T., Chibwe, M. & Pinnavaia, T.J. 1994. Titanium containing mesoporous molecular sieves for catalytic oxidation of aromatic compounds. *Nature* **368**: 321.

[14] Franke, O., Rathousky, J., Schulz-Ekloff, G., Starek, J. & Zukal. A. 1993. Unusual type of adsorption isotherm describing capillary condensation without hysteresis. *Chemical Communications* **9**: 724-726.

[15]Chen, C.Y., Li, H-X. & Davis, M.E. 1993b. Studies on mesoporous materials. I. Synthesis and characterization of MCM-41. *Microporous Materials* **2:** 17-26.

[16] Blasco, T., Corma, A., Navarro, M.T. & Pariente, J.P. 1995. Synthesis, characterization and catalytic activity of Ti-MCM-41 structures. *Journal of Catalysis* **156**(1): 65-74

[17] Petrini, G., Cesana, A., De Alberti, G., Genoni, F., Leofanti, G., Padovan, M., Paparatto, G. & Roffia, P. 1991. Catalyst Deactivation. Dlm. Bartholomew, C. H. & Butt, J. (pnyt.). *Studies in Surface Science and Catalysis* **68** hlm. 761. Amterdam: Elsvier.

[18]Blasco, T., Camblor, M.A., Corma, A. & Perez-Pariente, J. 1993. The state of Ti in titanoaluminosilicates isomorphous with zeolite beta. *J. Am. Chem. Soc.* **115**: 11806-11813

[19] Rajakovic, V.N., Mintova, S., Senker, J. & Bein, T. 2003. Synthesis and characterization of V- and Ti-substituted mesoporous materials. *Materials Science and Engineering:* C **23**(6-8): 817-821.

[20] Luan, Z., Maes, E. M., van der Heide, P.A., Zhao, D., Czernuszewicz, R.S. & Kevan, L. 1999. Incorporation of Titanium into Mesoporous Silica Molecular Sieve SBA-15. *Chem. Mater.* **11**: 3680-3686.

Malaysian Journal of Analytical Sciences, Vol.9, No. 3(2005): 504 - 507

STUDY ON THE MOVEMENT OF WAVENUMBER IN FTIR SPECTRUM OF C-O BOND IN NICKEL(II) BENZOATE

Zuraida Khusaimi & Azlin sanusi

International Education Centre (Intec), UiTM Seksyen 17, Shah Alam, Selangor

Abstract

Nickel(II) benzoate, a metallomesogen, is a potential low-dimensional electronic material. Metallomesogens are metal-containing liquid crystals. Liquid crystals have been known for the last hundred years [1]. Metallomesogens show electro-optical properties i.e. a ferroelectric behaviour [2,3]. It was prepared by refluxing nickel(II) acetate with benzoic acid. The structure and strength of C-O bond of the ligand of the sample was investigated by Fourier Transform Infrared Spectroscopy (FTIR). The FTIR spectrum of nickel(II) benzoate is different from its starting materials. The spectrum also shows that the wavenumber due to C-O bond stretch is **lower** in nickel(II) benzoate (1462 cm^{-1}) compared to nickel(II) acetate (1551 cm^{-1}), inferring stronger bridging bond between the ligand and the central nickel(II) ion. It may be deduced that nickel(II) benzoate is formed in the reaction above, and the driving force for the reaction is due to decrease in enthalpy (thermodynamically stable) due to formation of stronger bridging bond between the ligand and the central nickel(II) ion. There is also an increase in entropy as a result of the formation of liquid acetic acid.Thus the strength of the bridging bond is suggested to be influence mainly by an increase bond multiplicity and electron delocalisation in nickel(II) benzoate as a result of pπ-dπ orbital overlaps due to back donation from the electron-rich nickel(II) ion, producing stronger bridging bonds between the ligands and the central nickel(II) ions.

Keyword: Nickel(II) benzoate, low-dimensional electronic material, C-O bond, FTIR.

Introduction

For the last 10 years or so scientists like Tour and Reed [4] has been enthusiastically studying, synthesizing and isolating molecules exhibiting conductive, semi-conductive and super-conductive ability. One of the major advantage in the manufacturing of molecular electronics is that they are self-assembled, unlike time consuming microchip-producing technique. Computing speed can also be revolutionized to millions of times faster than of silicon material [4].

The objectives of this research are:

1. To synthesize nickel(II) benzoate.
2. To analyse the C-O bond in nickel(II) benzoate usinf FTIR.

The sample was prepared by reflux method and the product was analysed using Spectrum 2000 Fourier Transform Infrared Spectrometer.

Copper(II) benzoate, a coordination compound has been studied [5], and shown to have electronic properties and thermal stablity. It was thought that nickel(II) benzoate, another coordination compound might contain similar properties and is a potential molecular electronics.

Methodology

Experimental Objectives

It is important to ensure that the reaction between nickel(II) acetate and benzoic acid are feasible under the experimental conditions applied. The main objective is to analyse the wavenumber of C-O bond in nickel(II) benzoate, which is inversely related to the strength of the bridging bond between the ligand and the central nickel(II) ion. A change in the C-O band may suggest movement of electrons across the neighbouring bonds.

Preparation of Material

Nickel(II) acetate monohydrate and benzoic acid in a molar ratio of 1:2 were refluxed for 8 hours in acetonitrile in a round-bottom flask connected to a reflux condenser. The mixture was constantly stirred using a magnetic stirring bar. The reaction mixture was left to cool to room temperature and the paste obtained was filtered, rinsed with ethanol and dried in an oven at 60ºC for 30 minutes. The powder was purified by heating with ethanol. The solid residue was filtered, washed with ethanol and dried in the oven at 60ºC for 30 minutes.

Analysis

IR spectra were recorded on a Perkin Elmer model Spectrum 2000 FTIR spectrometer as mull in nujol or potassium bromide (KBr) pellet. The spectra for either medium is similar [5] except for the Nujol peak that appear at ~ 2900 cm^{-1}.

Result & Discussion

Nickel(II)benzoate, Synthesis and Structure

The equation for the reaction is

$$(CH_3COO)_2Ni_{(S)} + 2C_6H_5COOH_{(S)} \rightarrow (C_6H_5COO)_2Ni_{(S)} + 2CH_3COOH_{(l)}$$

The Fourier Transform Infrared (FTIR) spectra of NA and NB are shown in figure 1 and figure 2, respectively.

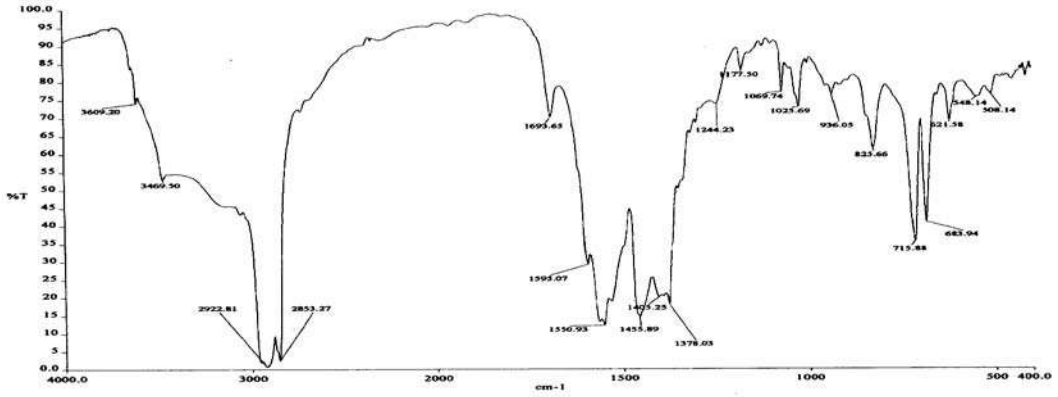

Figure 1 – nickel(II) acetate in Nujol

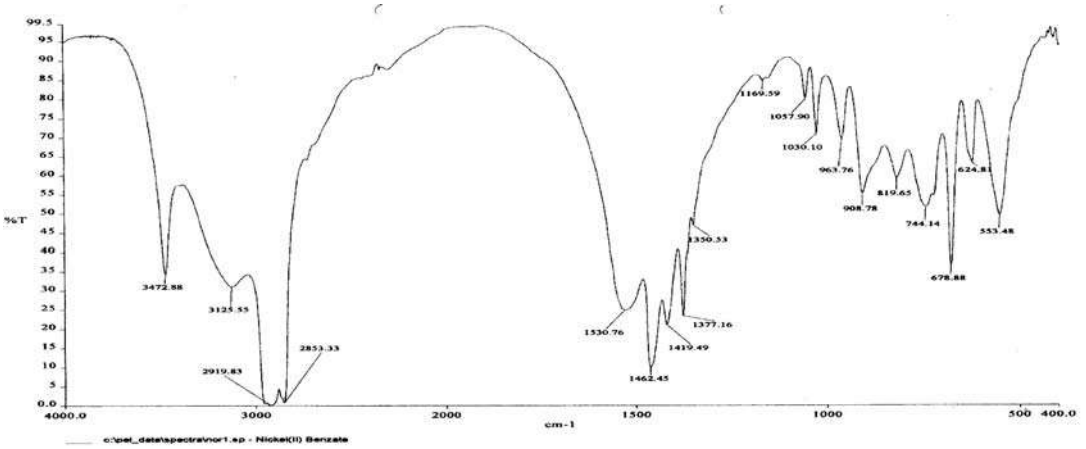

Figure 2 - Nickel(II) benzoate in Nujol

The FTIR data for benzoic acid [6], NB and NA is shown in Table 1.

Table 1 FTIR data for benzoic acid, nickel(II) acetate and nickel(II) fluorobenzoate

Bonds and Functional Group	Benzoic acid	Nickel(II) Acetate	Nickel(II) Benzoate
C-C aromatic	1600	-	1531
C-H aromatic	3600-2500	-	Covered by Nujol
C-H aliphatic	-	3469	-
-COO asymmetric	1691	1550	1462

It is observed that the spectrum of NB is different from that its starting material. The data indicates that almost all the functional groups and bonds expected for NB are present, namely aromatic C-C at 1531cm^{-1} and -COO (asymmetric structure) at 1462 cm^{-1}.
C-H aromatic band is assumed to be covered by Nujol peak which has a broad band at 2900 cm^{-1}. The data showed that the wavenumber due to C-O in NB is 1462 cm^{-1} which is lower than in NA at 1550 cm^{-1}, inferring stronger bridging bond in NB. It can be concluded that NA reacted with benzoic acid under the experimental condition employed to produce NB. The driving force for the reaction may be due to decrease in enthalpy (thermodynamically stable) due to formation of stronger bridging bond between the ligand and the central nickel(II) ion. Liquid acetic was formed as the other product.

Conclusion

The wavenumber of C-O bond in nickel(II) benzoate is 1462 cm^{-1} and the wavenumber of C-O band in nickel(II) acetate is 1550cm^{-1}.The C-O band in Nickel(II) Benzoate is lower than in nickel(II) acetate indicating stronger bridging bidentate bond between the ligand and the nickel(II) ion. This indicate that nickel(II) benzoate is a potential low dimensional electronic material.

Acknowledgement

We would like to thank Puan Ruzela Tapsir, deputy director of Intec for her support and encouragement and Dr. Norbani Abdullah and Mr. Richard Ritikos from University Malaya for FTIR analysis.

REFERENCES

1. J.Rourke, *Metallomesogens*, Warwick University Chemistry Department Publication, http://www.warwick.ac.uk/fac/sci/Chemistry/jpr/metallo.htm
2. A.M. Giroud-Godquin, *My 20 Years of Research in the Chemistry of Metal Containing Liquid Crystals*, Coordination Chemistry Reviews, 178-180 (1998), 1485-1499.
3. M. Rusjan, B. Donnio, D. Guillon and F.D. Cukiernik, *Liquid-Crystalline Materials Based on Rhodium Carboxylate Coordination Polymers: Synthesis, Characterisation and Mesomorphic Properties of Tetra(alkoxybenzoato)dirhodium(II) Complexes and Their Pyrazine Aducts,* American Chemical Soceity, Published on Web 00/00/0000, Page Est. 12, 2002.
4. R. Overton, *Molecular Electronics will Change Everything*, http://www.wired.com/wired/archives/8.07/moletronics_pr.html.
5. Zuraida Khusaimi, *Fourier Transform Infrared Spectroscopic Studies of Copper(II) Benzoate and Its Derivatives with Electron-attracting Groups*, A Dissertation submitted in partial fulfillment for the Degree of Master in Science (Analytical Chemistry and Analytical Instrumentation), Chemistry Department, Universiti of Malaya, September 2001.
6. Silverstein and Webster, *Spectrometric Identification of Organic Compounds*, 6th. Edition, John Wiley & Sons.

Malaysian Journal of Analytical Sciences, Vol.9, No. 3(2005): 508 - 513

Carbon Dioxide Sensor Based on Fluorescent α-naphthoflavone-metal Complex

Mustaffa Nawawi*, Tee Shiau Foon dan Shemalah a/p Ramasundram

Jabatan Kimia
Fakulti Sains
Universiti Teknologi Malaysia
81310 UTM Skudai
Johor

Email: musna@kimia.fs.utm.my

Abstract

α-naphthoflavone (7,8-benzoflavone) is a natural product normally used in biological studies exhibits fluorescence with excitation peak at 343 nm and emission at 426 nm. In this study, the optimum condition for the fluorescence of α-naphthoflavone was carried out by varying pH, concentration, and temperature. Results showed that the optimum pH was at 10.06 giving the highest intensity while the temperature was at 10°C - 25 °C. Linear calibration curve was obtained with an equation of y = 65.773 - 23.647 and R^2 = 0.9819. Studied on the formation of complex of α-naphthoflavone with various metals such as lanthanum, magnesium, cadmium and manganese (II) were also carried out. Results showed that lanthanum-α-naphthoflavone complex exhibit highest fluorescence intensity. The observed luminescence intensity of α-naphthoflavone and complex α-naphthoflavone-lanthanum increased with the increase in carbon dioxide concentration.

Keywords: Fluorescence; α-naphthoflavone; lanthanum; carbon dioxide; sol gel

Introduction

Carbon dioxide a by-product of many industrial processes and it is believed to aggravate the greenhouse effect of our environment. Carbon dioxide sensing techniques are applied to various fields, such as chemical, clinical analysis and environmental monitoring. The method for the detection of carbon dioxide is the atmosphere has attracted many workers. Recently, the optical carbon dioxide sensors based on the absorbance or fluorescence change of pH indicator dye have been developed [1-4]. 7,8 benzoflavone (α-naphthoflavone: ANF) is a prototype flavonoid which has been used to examine the mechanism of action on P450 enzymes [5]. ANF has been used to prevent protein inactivation since its first successful application as an aid to solubilization during purification [6] and some workers performed cells transformation tests using α-naphthoflavone as a specific monooxygenase inhibitor [7]. It was also an organic fluorescent material, which used in analytical chemistry. Porous glasses, prepared using the sol-gel method, allow incorporation of reagent for sensors into their pores [8]. In the sol-gel process a silica gel is made by hydrolysis of an alkoxide precursor followed by condensation of silanol. Evaporation of the solvent and the alcohol that is liberated during hydrolysis forms a dried gel or xerogel [9]. The sol gel process is attractive for making porous membranes for optical sensors because of the relative simple chemistry and because of the low polymerisation temperature, which allows encapsulated or attachment of organic probe molecules that are unstable at higher temperature [8-12]. In this study, we described a carbon dioxide sensor based on the fluorescence of the complex α-naphthoflavone-metal.

Experimental

Sample Preparation

α-naphthoflavone (7,8 benzoflavone) was purchased from Sigma Chemical Reagents and prepared by adding the powder (0.027 g) in 100 mL ethanol 95%. Stock solution was prepared freshly for experimental due to oxidation and degradation. Dilution was conducted for concentration effect, temperature effect, pH effect and solvent effect.

The doped silica gel matrices were prepared by hydrolysis and polycondensation of tetraethyorthosilicate (TEOS) in water and ethanol solution under acidic condition and stirring for 17 hours until the solution became

homogeneous. After the solution was cooled at room temperature for 30 minutes. Nitric acid was used as a catalyst. The organic dyes were previously dissolved in ethanol and added to gel, which coated on the glass slides. The glass slides were washed with nitric acid for 1 day and rinsed with deionised water and later with ethanol.

Characterization

Excitation and emission spectra were measured using a Perkin-Elmer Models LS-50B Luminescence Spectrometer. All measurements were performed at room temperature using 1 cm x 1 cm quartz cell.

CO_2 Detection

The CO2 detection expants carried out using a conventional gas flow apparatus. Different concentrations of carbon dioxide will bubble in the solution. The flow rate of gas always kept at constant level of 2 liters per minutes (LPM).

Results and Discussions

Luminescence emission

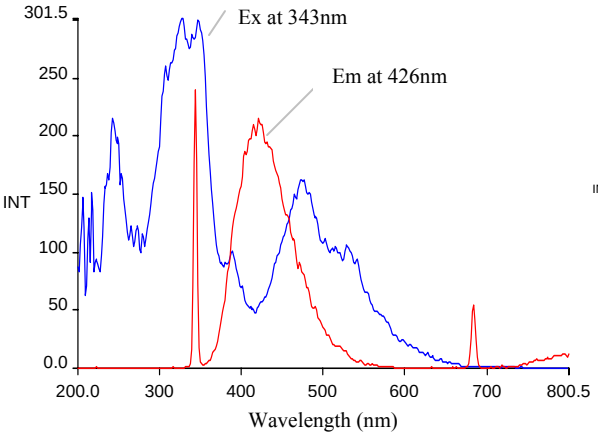

Fig 1. Emission spectrum excitation and emission of α–naphthoflavone.

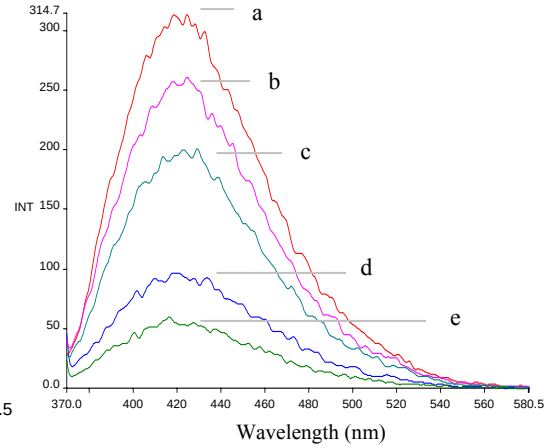

Fig 2. Standard calibration for concentration α–naphthoflavone in ethanol which a= $1x10^{-3}$, b= $5x10^{-3}$, c= $1x10^{-4}$, d= $5x10^{-4}$, e=$1x10^{-5}$

Fluorescence studies showed the excitation peak obtained at 343 nm and the emission peak was at 426 nm as in Fig 1. The stardard calibration at different concentration was carried out in the range of 1 x 10^{-3} to 1 x 10^{-5} mol /L giving a straight line with y = 65.773 - 23.647 and R^2 = 0.9819. Fig 2 shows the emission spectra of α-naphthoflavone recorded in the visible region. It was found that the emission intensity of the α-naphthoflavone increases with the increase in the concentration from 1 x 10^{-3} to 1 x 10^{-5} mol /L. No concentration quenching effect was observed in the studied α–naphthoflavone concentration range. Additionally a red shift for the emission band can be observed from low α–naphthoflavone concentration to high concentration. This may be caused by 2 factors: Firstly it may be due to the changes in the molecules polarity or polarizability. Secondly: a self-absorption process could also be responsible for the observed small red shift in the emission band.
Fig 3 shows that pH does not affect the position of emission spectrum but affects the fluorescence intensity. pH was found to enhance the peak intensity. Optimum pH for α-naphthoflavone occurred at pH 10.06. This could be due to different ionizable chemical species formed by α-naphthoflavone in solution. The effect of temperature on the emission spectra was also studied (Fig 4). From Fig 4, the intensity was found to decreases gradually with the increasing heat treatment temperature from 5^{o}C to 70^{o}C. However, the shape of the emission spectra observed for α-naphthoflavone remains unchanged.

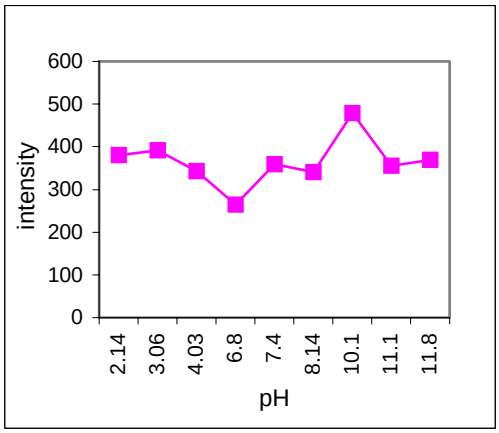

Fig 3. α-nphthoflavone at different pH.

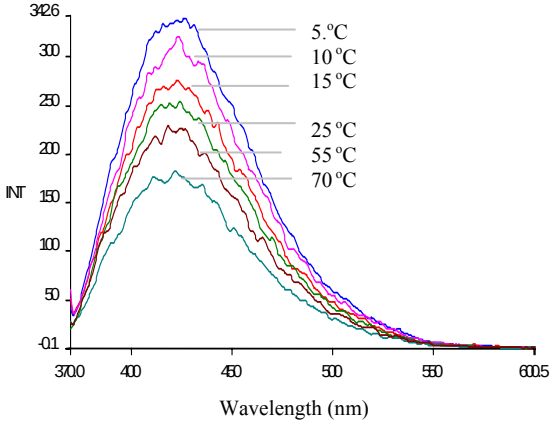

Fig 4. Effect of the temperature of α-naphthoflavone on emission spectra.

Meanwhile, the decrease in the solution temperature from 25°C to 5°C, intensity was found to be increasing 15 percent per degree Celsius.

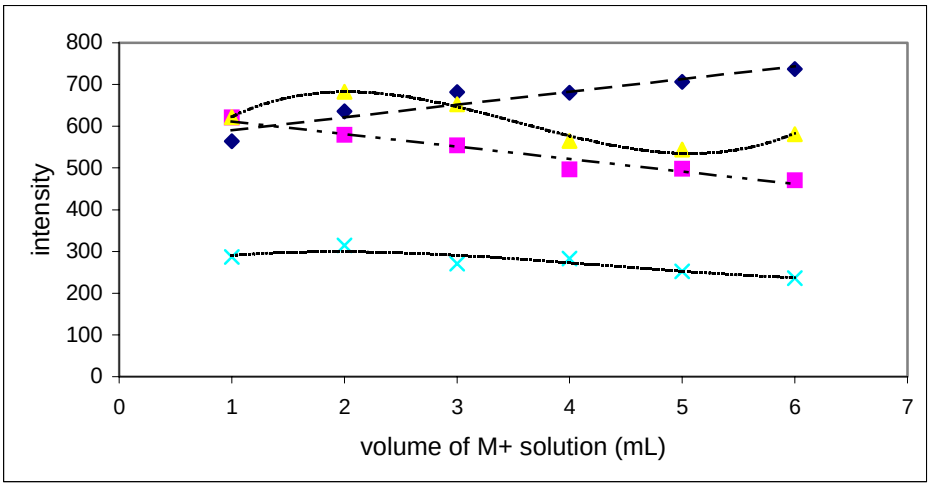

Fig 5. Calibration graph of α-naphthoflavone with various metal La ---- Mg—·— Mn -·-·- ·····Cd

As can be seen in Fig 5, results show that lanthanum exhibit as enhancing effect on the emission intensity of α-naphthoflavone-lanthanum complex. A red shift for the emission band can be observed. The linearity of the calibration graph for this complex is y = 30.727x + 559.83 and the R^2 = 0.8971. While the intensity of α-naphthoflavone-manganese complex decrease with the increases in the volume of manganese with equation y = -30.157x + 642.1 and R^2 = 0.9484. In addition, it was found that the intensity of cadmium and magnesium complexes shows a non-linear change. It was noticed that some white spots occur when left for 1 day in α-naphthoflavone-cadmium. This suggests that α-naphthoflavone aggregation occur to a significant extent in the solution. The effect of non aqueous solvent N,N-dimethyformamide on the emission spectra of α-naphthoflavone is as shown in Fig 6 and Fig 7. The fluorescence studies show that the excitation peak was observed at 385.5 nm while the emission peak is at 430.8 nm. It can be seen that the intensity is lower compare to the ethanolis . Tsed as solvent. The first assumes the presence of two simultaneous quenching process, dynamic and static in nature with or without a heterogeneous environment for the α-naphthoflavone.

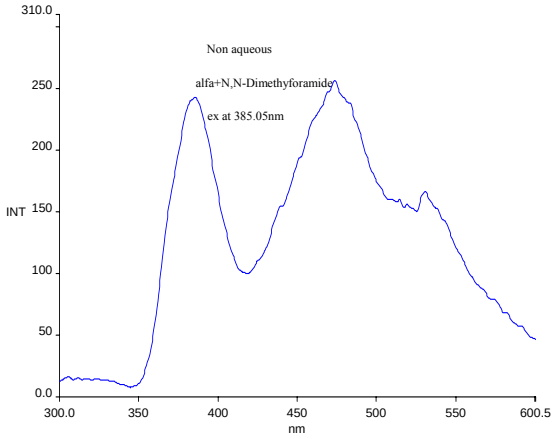

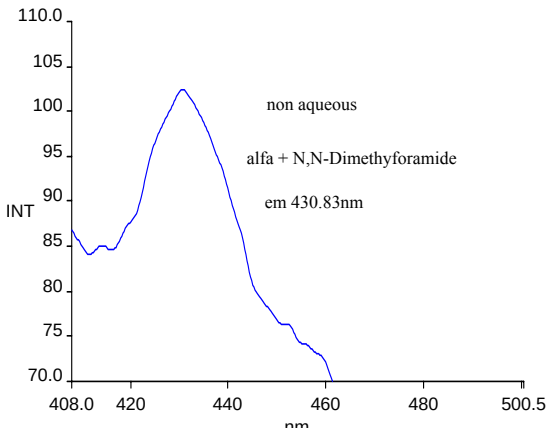

Fig 6: The excitati ne in N,N-dimethyformamide (DMF).

Fig 7: The emissi Wavele N,N-dimethyformamide (D

The effect of CO_2 on α-naphthoflavone-lanthanum complex

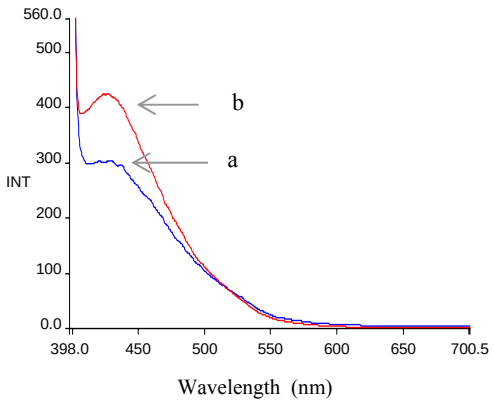

Fig 8. Emission spectra of α-naphthoflavone -lanthanum complex before (b) and after (a) exposure to CO_2 in ethanol.

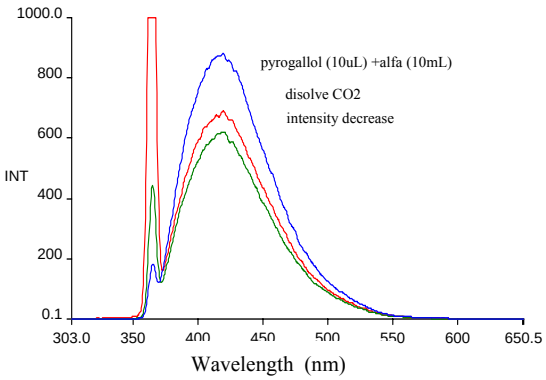

Fig 9. Emission spectra of α-naphthoflavone added with pyrogallol and exposure to CO_2 in ethanol.

There is a decrease in the emission intensity as the CO_2 concentration increases in the α-naphthoflavone-lanthanum solvent (Fig 8). It was also observed that some pH-sensitive dyes change colour upon exposure to gaseous CO_2. The presence of water is crucial for response to CO_2 is based on the hydrolysis of the dyes as shown in the following equations [2]:

$$CO_2 + H_2O \rightleftharpoons H_2CO_3 \quad (1)$$

$$H_2CO_3 + H_2O \rightleftharpoons HCO_3^- + H_3O^+ \quad (2)$$

$$HCO_3^- + H_2O \rightleftharpoons CO_3^{2-} + H_3O^+ \quad (3)$$

$$DH + H_2O \rightleftharpoons D^- + H_3O^+ \quad (4)$$

(colour A) (colour B)

Where DH and D^- are the protonated and deprotonated forms of the dye, respectively. The change of the colour in dye is sensitive to pH change of its environment.

The behaviour of emission spectra of α-naphthoflavone with different CO_2 concentration is shown in Fig 9. It was noticed that there is a decrease in emission as the CO_2 concentration increase in the ethanol-pyrogallol. In alkaline solution pyrogallol is an active reducing agent. Meanwhile in acidic condition, the emission intensity decreases because of the pH value in solution and pyrogallol change to gallic acid form.
A solution of $5x10^{-3}$ M α-naphthoflavone and 200uL NH_4OH in DMF was tested for its response to CO_2. Fig 10 shows that the emission spectra before and after exposure to gas carbon dioxide. As can be seen in the Fig 10, one emission bands is observed before exposure to CO_2 and become two emission band observed in DMF after react with CO_2. The change of emission arises from the conversion of the colourless to the yellow species. These changes were brought about from the change of the pH of the solution with dissolution of CO_2 in DMF and can be envisaged in the following reaction:

$$CO_2 + OH^- \rightleftharpoons HCO_3^- \quad (5)$$

$$H^+ + OH^- \rightleftharpoons H_2O \quad (6)$$

The emission of α-naphthoflavone in sol gel was observed and shown in Fig 11. It was noticed that the emission intensity of α-naphthoflavone coated on the surfaces of sol gel increases after an exposure to CO_2 gas. In the sol gel glass, the α-naphthoflavone is entrapped inside the pores of the matrices where it may move freely inside the pores or it may have some interactions with silanol groups on the inner surfaces of pores [13].

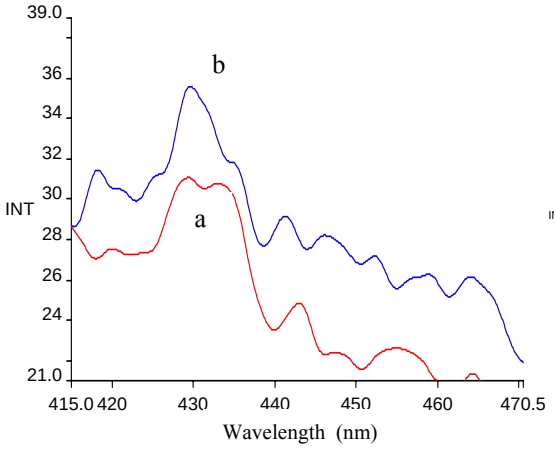

Fig 10: Emission spectra α-naphthoflavone ($5x10^{-3}$ M) and 200uL NH_4OH in DMF a) after and b) before response to CO_2

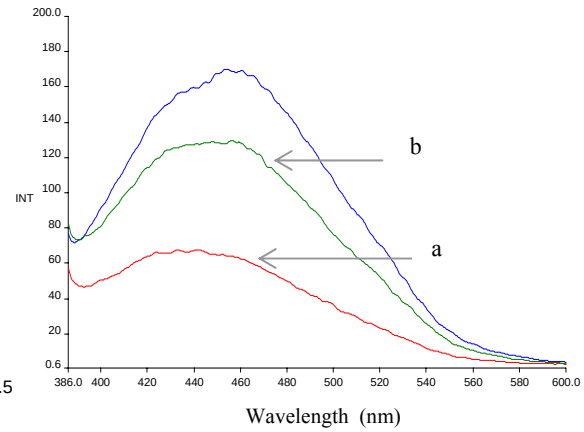

Fig 11: Emision spectra α-naphthoflavone-lanthanum in sol gel (a) and exposure to gas CO_2 (b).

Conclusion

In conclution, our study has shown that α-naphthoflavone-lanthanum and manganese have shown great potential to be used as sensing materials for CO_2 gas sensor. Different behaviour of α-naphthoflavone was observed depending on temperature, pH value and solution. The effect of CO_2 gas on α-naphthoflavone-lanthanum complex was studied. It was found that the emission intensity decreases linearly after exposure to CO_2 gas in ethanol-pyrogallol. In addition, α-naphthoflavone on sol gel has also has also shows ability as a gas sensing material.

Acknowledgements

The financial support of PTP-UTM is acknowledged.

References

1. O. S. Wolfbeis, L.J. Weis, M.J.P. Leiner, W.E. Ziegler, "Fiber-optic Fluorescence for Oxygen and Carbon Dioxide", Anal. Chem. 60 (1988) 2028-2030.
2. Ming Fat Choi and Peter Hawkins."A Novel Oxygen And / Or Carbon Dioxide Sensitive Optical Transducer", Talanta Vol. 42 No 3 (1995) 483-492.
3. A. Marsal, G. Dezanneau, A. Cornet, J.R. Morante. "A New CO_2 Gas Sensing Material". Sens. and Actuators B 95 (2003) 266-270.
4. A. Mills, A. Lepre, L. Wild, "Breath-by-breath Measurement of Carbon Dioxide Using a Plastic Film Optical Sensor, Sens. Actuators B 38/39 (1997) 419-425.
5. Uhn Soo Cho, Eun Young Park and Mi Sook Dong. "Tight-binding Inhibition by α-naphthoflavone of human Cytochrome P450 1A2". Biochim et Biophysica Acta 1648 (2003) 195-202
6. Uhn S. Cho, Hyung J. Ahn, Eun Y. Park."Influence of Ligand Binding to Human Cytochorme p450 1A2: Conformational Activation an Stabilization by α-naphthoflavone" Biochim et Biophysica Acta 1546 (2001) 412-421
7. P. Perocco , M. Mazzullo, M.Broccoli and P.l Rocchi."Inhibitory Activity of Vitamin E and α-naphthoflavone on B-carotene-Enhanced Transformation of BALB / c 3T3 Cells by Benzo(a)pyrene and Cigarette Smoke Condensate"Mutation Research 465 (2000) 151-158
8. Aryeh M. Weiss, Tsiala Saraidarov and Renata Reisfeld. Confocal. "Microscopy for Characterization of Porous Sol-gel Glasses Incorporating Luminescent Dyes". *Optical Materials.* (2001) 16: 15-20.
9. R.T. Bailey, F.R. Cruickshank, G. Deans, R.N. Gillanders and M.C. Tedford. "Characterization of a Fluorescent Sol-Gel Encapsulated Erthrosin B Dissolved Oxygen Sensor". *Anal. Chim. Acta.* (2003) 487: 101-108.
10. B. D. MacCraith, C. M. McDonagh, G. O Keeffe and A. K. Mc Evoy. "Sol-gel Coatings for Optical Chemical Sensors and Biosensors. *Sens. and Actuators B: Chem. 29* (1995): 51-57.
11. R. N. Gillanders, M.C. Tedford, P.J. Crilly and R.T. Bailey. "A Composite sol-gel / Fluoropolymer Matrix for Dissolved O_2 Optical Sensing". J. Photochem. Photobiol A: Chem. (2004)
12. Jie Lin, and Chris W. Brown. "Sol gel Glass as a Matrix for Chemical and Biochemical Sensing." *TrAc. Vol 16 No 4,* (1997), 200-209.

Malaysian Journal of Analytical Sciences, Vol.9, No. 3(2005): 514 - 520

SYNTHESIS AND CHARACTERIZATION OF CdS AS FLUORESCENCE PROBE FOR DETERMINATION OF PROTEIN

Mustaffa Nawawi *, Shemalah a/p Ramasundram and Tee Shiau Foon

Jabatan Kimia, Fakulti Sains, Universiti Teknologi Malaysia, 81310 UTM Skudai, Johor.

E-mail address: musna@kimia.fs.utm.my.

Abstract

The quantitative analysis of protein is considerably essential in biochemistry and clinical medicine. The most sensitive quantitation of protein at this present is generally based on their fluorescence. We report a new kind of luminescent particles has been employed for the quantitative analysis of protein. CdS have been prepared and modified with mercaptoacetic acid which renders the particles water soluble and biocompatible. Fluorescence studies shows when λ_{ex} = 233nm, maximum CdS peak occurred at 355nm at pH 6. Under the optimum condition, the response is linear proportional to the concentration of BSA and the calibration graph shows (y=4.7285x + 458.82 with r^2 =0.988).This method is simple, inexpensive, rapid and sensitive.

Key words: Fluorescence, CdS, protein

INTRODUCTION

The development of novel assays for proteins is a basic requisite in both clinical and laboratory tests. The most frequently used approaches for the determination of protein is the ultraviolet and visible absorption spectroscopy, Lowry method [1], dye binding method like Bradford [2], Bromocresol green procedures [3], Bromophenol blue [4],. However, they all have some limitation in terms of sensitivity, selectivity, stability and simplicity. Disadvantage of the Lowry method include low sensitivity, poor selectivity and complexity. The Bradford method is also inconvenient in operation and application due to the requirement for calibration and to the nonlinearity between the absorbance of the Coomassie brilliant blue G-250 (CBB G-250) dye-protien complex and the concentration of protein[1,2].The bromocresol green method is insensitive and susceptible to interference by turbidity[3] and the Bromophenol blue method can be used only for protein concentrations greater than than 10 mg L^{-1} [4]. Therefore, a number of assays have been continuously reported in recent years such as those based on spectrophotometric [5], electrochemical [6].

CdS is an important semiconductor owing to its unique electronic and optical properties, and its potential application in solar energy conversion, non linear optical, photo electrochemical cells and heterogeneous photo catalysis [6]. The synthesis of CdS nanoparticles has been tried by various methods such as the direct reaction of metals with sulfur powder under high temperature [7,8], the thermal decomposition of molecular precursors containing M-S bonds [9] and chemical precipitation method involving the precipitation of metal ion with Na_2S as the source of S^{2-} ions [10,11].

In recent years, colloidal semiconductor nanoparticles have the potential to overcome problems encountered by organic small molecules in certain fluorescent tagging applications by combining the advantages of high photobleaching threshold, good chemical stability and readily tunable spectral properties. This colloidal nanoparticles are very resistance to photobleaching, have a high quantum yield in aqueous solution make them attractive for labeling functionalized biomolecules for fluorescent tagging applications.

The goal of this paper is to describe the synthesis of luminescent particles for the quantitative determination of protein. Next , this paper is about exploring the new direction for the synthesis of CdS and modification of CdS semiconductor caping with thiols group such as mercapto acetic acid. This functionalized CdS will covalently linked to proteins for further studies.

EXPERIMENTAL

Apparatus

Perkin-Elmer Models LS-50B Luminescence Spectrometer was used for all fluorescence determination. The LS-50B employs a pulsed xenon source that produce a high output using a low voltage, 9.9 watts resulting in longer lamp life with minimal ozone and heat production. Photomultiplier tubes are employed as detection devices and LS-50B was connected to a computer for data processing. A pH meter Cyber-scan model equipped with a glass electrode combined was employed for the pH measurements.

Reagents

All the glassware used in this experimental work was acid washed. All the reagents were of analytical reagent grade without further purification. Doubly distilled water was used for the preparation of all solution and for all determinations. A stock Bovine Serum Albumin(BSA) purchased from Amersham Pharmacia Biotechnological solution was directly dissolved in 0.5% of NaCl solution to prepare stock solution at a final concentration of 100µg ml^{-1} and stored at 0-5^{o}C.

Procedure

The procedure employed for preparing CdS nanoparticles is as follow. The synthesis of colloidal solution was carried out in a 1000 ml three-necked round bottom flask. Then, 800ml of deionized water, 4.0 ml of 0.1 ml L -1 $(CH_3COO)_2.Cd.2H_2O$ and 4.0 ml of 0.1 mol l-1 sodium hexametaphosphate as the stabilizing agent were added to the flask. Then, the pH was adjusted to 7.0 using 0.1mol l-1 NaOH. Under vigorous stirring, 4.0 ml of 0.1 mol l -1 $Na_2S.9H_2O$, was dropped into flask slowly. Next, the CdS colloidal was concentrated to 40 ml with rotary evaporation. Then, 1.0 ml of 1 mol l-1 mercaptoacetic acid was added. The CdS particle were reacted with mercaptoacetic acid for 4 hours under the vigorous stirring. The modified CdS were diluted 50 fold and stored at room temperature. The modified CdS were used to detect the BSA(protein) .The following procedure was adopted. To a dry 1 cm quartz cell, 1 ml of CdS and 1 ml of protein standard solution was added for the determination of protein in fluorescence measurements.

RESULTS AND DISCUSSIONS

Formation of CdS nanoparticles

The CdS particles form the following solid-state reaction:

$$\mathbf{(CH_3COO)_2.Cd.2H_2O + Na_2S \xrightarrow[\text{temperature}]{\text{Room}} CdS + 2Na(CH_3COO)_2 + 2H_2O} \quad [8]$$

During the synthesis of CdS particles, we observed that one deep yellow product were formed once upon mixing the two reactant. This indicates that the chemical reaction rate of the reactive system is very fast and the nucleation rate is far excess the growth rate of small particles. Therefore, this reactive mechanism favors the formation of nano-sized CdS particles.[8] The use of capping agent mercaptoacetic acid is to limit particle growth or "Oswald" ripening[13]. Further mercapto group binds to a Cd atom and the polar carboxyl group is also available for covalent coupling to various biomolecules such protein and nucleic by cross-linking to active amine group.[14]

UV and fluorescence spectra

The UV spectra of CdS were obtained using the Ultraviolet-Visible Spectrophotometer (UV-Vis), UV-1601PC(Shimadzu, Japan). According to Figure 1, CdS capped with mercaptoacetic acid had the strong maximum absorption at 210 nm. Figure 2 shows the typical fluorescence spectra of emission peak for CdS capped mercaptoacetic acid. The emission spectra of functionalized CdS is located at 355 nm (λ_{ex} = 233nm). Maximum emission spectra was obtained by dilution of concentrated CdS to a sample 50 fold.

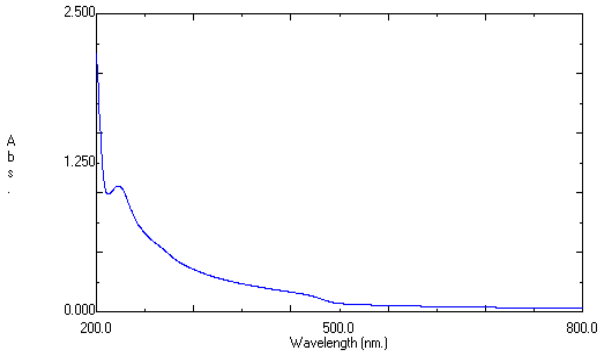

Figure 1 . UV spectra obtained for the CdS capped with mercaptoacetic acid in range of 200 nm -800 nm.

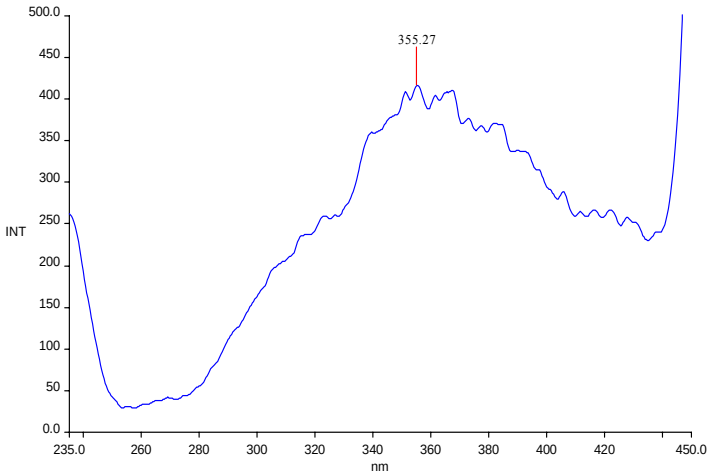

Figure 2: The fluorescence emission spectra of CdS capped with mercaptoacetic acid, λ_{ex} = 233 nm in range from 300 nm-420 nm at pH 3.

Optimization of general procedure.

Effect of pH value

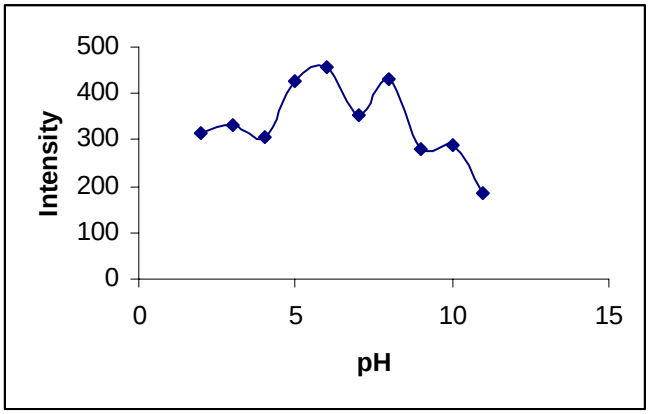

Figure 3: pH effect of CdS on fluorescence intensity

The effect of pH on the fluorescence enhancement of the system was studies (Figure 3). Result shows that pH does not affect the wavelength of emission spectrum but affect the fluorescence intensity. The fluorescence emission intensity reached a maximum over pH 6 and decreased outside of this pH. The pH was only observed in low pH region for CdS capped mercaptoacetic acid colloidal solution. These result seem to indicated that OH^- ion is difficult to approach to the CdS core of the surface modified CdS nanoparticles because of the presence of the capping agent (mercaptoacetic acid) which cover the surface of the particles.[15]. On the other hand, pH dependence also caused by proton dissociation equilibrium of the carboxyl group in mercaptoacetic acid.[15] This causes at low pH region pH 2 to 6, the intensity increases because mercaptoacetic acid combines with the CdS surface.[15]

Interaction of CdS capped mercaptoacetic acid particles with BSA

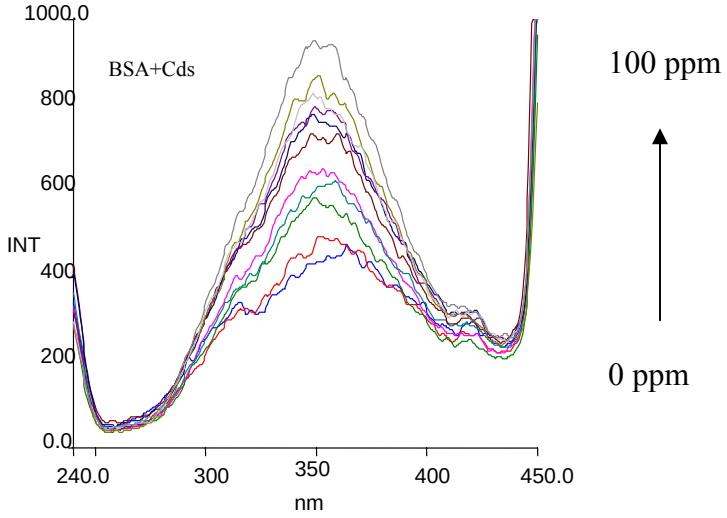

Figure 4: Emission spectra of CdS capped mercaptoacetic acid with increasing concentration of BSA: (1) 0 ppm until (11) 100 ppm

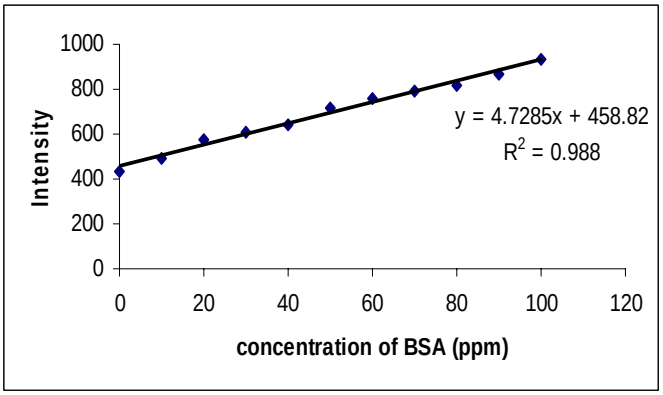

Figure 5. Calibration curves for BSA.

In our studies, quantitative determination of protein, it was found that the emission maxima of the fluorescence emission spectra of CdS capped mercaptoacetic acid and BSA is similar but the intensities are significantly enhanced (Figure 4).These result indicated that this functionalized CdS could be used as a new fluorescence probe for the sensitive determination of protein. The calibration graphs for BSA were constructed from the result obtained under the optimal condition. In Figure 5 shows the plot of intensity versus concentration (ppm) which is linear graph as shown in Figure 7($R^2 = 0.988$, n = 11).

Salt –dependent studies

Electrostatics are important for BSA binding to the nanoparticles. The change of ionic strength is an efficient method for distinguishing the binding modes between molecules and BSA. We have perform the interaction of CdS capped mercapto acetic acid and BSA by influence of salt on the emission intensity. Figure 6 shows that in the absence of BSA, the addition of NaCl to colloidal had a insignificant effect on the fluorescence intensity. However the fluorescence emission intensity of the presence of BSA(curve 2) are quenched by increasing NaCl salt concentration. Here we can conclude that the binding mechanism of functionalized CdS and BSA(protein) is non-electrostatic binding.

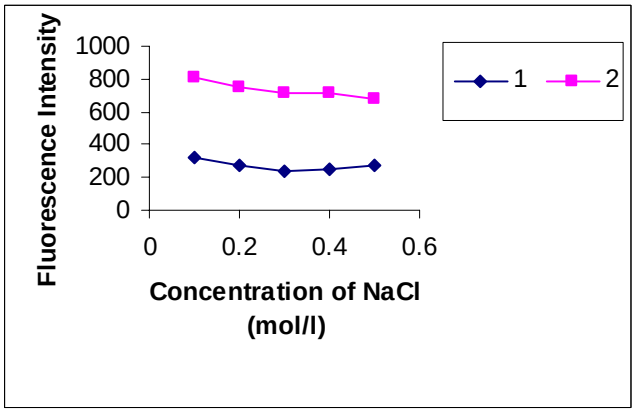

Figure 6: Effect of the concentration of NaCl solution on the fluorescence intensity in the absence (curve 1) and presence (curve 2) of BSA pH 6, colloidal CdS and BSA 50ppm

Method validation

Linearity, Precision, Limit of Detection

The method exhibited linearity over the 10- 100ppm. For determination of accuracy of the method, the reproducibility was calculated from 10 replicates of 50 ppm BSA on the same day. Relative standard deviation (RSD) of BSA is1.5%. For the inter-days accuracy determination, the RSD for day 1,day 2 and day 3 obtained for measurement of 50 ppm BSA are 1.68%,0.94%,1.27%. The result indicated that the method was reliable, reproducible and accurate. Limit of detection for BSA 50 ppm is 3.8 ppm.

Tolerance of foreign substances

In order to test the selectivity of the method for the determination of BSA, the effect of the several amino acids, salt are performed. The solution of a fixed concentration of BSA (50ppm) and each foreign substances with various concentration are mixed prior to the detection. Based on Table 1, we can see that interference of ions such as Ca^{2+},Ni^{2+},NH_4^+,Mg^{2+},Zn^{2+},Cu^{2+} only can be allowed at very low concentrations. However , the concentration of these interference ions are very lower in real biological samples. Interferences of Cysteine, Alanine Sucrose can be allowed at higher concentration but glucose, starch, urea and EDTA can be allowed only at relatively low concentration.

Table 1
Effect of the foreign substances on the determination of 50 ppm BSA

Substances	Concentration (ppm)	Enhancement/ Quenching (%)
Cys	50	-1.7
Gly	30	+2.6
Ala	70	+0.4
Fe(II)	50	-4.2
Fe(III)	40	+4.1
Ca^{2+}	30	-4.8
Cu^{2+}	10	-16.7
NH_4^+	10	-3.9
Mg^{2+}	10	-8.1
Ni^{2+}	30	-8.1
Zn^{2+}	30	-14.9
Glucose	10	-5.2
Sucrose	50	-17.5
Starch	30	-8.4
Urea	20	-14.7
EDTA	10	-15.2

CONCLUSION

Results shows that CdS form yellow color colloidal was successfully prepared. Fluorescence studies shows emission peak was obtain at 355 nm (λ_{ex} = 233nm). The maximum pH occurred at pH 6. Under the optimum condition, the response is linear proportional to the concentration of BSA and the calibration graph shows ($y = 4.7285x + 458.82$ with r^2 =0.988). Limit of detection for the BSA interaction was 3.8 ppm. Based on the result obtained from reproducibility the propose method was reliable, reproducible and accurate.

ACKNOWLEDGEMENTS

This work was supported by the Chemistry Department Faculty of Science and PTP (School of Postgraduate) for the financial support University Teknologi Malaysia, Skudai Johor Bahru.

REFERENCES

1. Lowry,O.H., N.J.Rosebrough, A.L. farr and R.J.Randall.(1951), "Protien Mesurement with Folin Phenol Reagent", J.BioChem,**193**.265-275.
2. Braford, M.M.(1976), "A Rapid and Sensitive Method for the Quantitation of Microgram Quantities of Protein Utilizing the Principle of Protein Binding", Anal Biochem.**72**.248-254.
3. Basil T.Doumas, W. Ardwatson and Homer G. Biggs(1971) "Application Standard and Measurement of Serum Albumin With Bromocresol Green" Clin.Chim. Acta **31**,87.
4. Klaus Jung, Erika Nickel, Monika Dergande (1990) "A Microalbumiria Assay using Bromophenol Blue" Clin. Chim. Acta **187**,163-172.
5. Bruchez,Marcel, .Jr.Moronne, Mario, Gin, Peter, Weiss Shimon Alivisatos,A.Paul (1998), "Semiconductor Nanocrystal as Fluorescent Biological Labels", Science, **281.**2013-2016.
6. Zhan Li, Yumin Du (2003) " Biomimic Synthesis of CdS Nanoparticles with enhanced Luminescence", Mater. Lett, **57**,2480 -248.
7. Sander F.Wuister, Andries Meijerink (2003), "Synthesis and Luminescence of (3-Mercaptopropyl)-trimethoxysilane Capped CdS Quantum Dots", J.Lumin,**102**. 338-343.
8. Wenzhong Wang, Zhihui Liu, Changlin Zheng, Congkang Xu, Yingkai Liu, Guanghou Wang (2003), "Synthesis of CdS Nanoparticles by a Novel and Simple One-Step, Solid State Reaction in the Presence of a Nonionic Surfactant.", Mater .Lett, **57**. 2755-2760.
9. G.S. Wu, X.Y. Yuan T. Xie, G.C. Xu (2003). " A Simple Synthesis Route to Cds Nanomaterials with Different Morphologies by Sonochemical Reduction", Mater. Lett.
10. Yuanfang Liu, Jinghua Zhan, Ming Ren, Karbin Tang, Weichoa Yu, Yitai Qian (2000) " Hydrothermal Synthesis of Thin Film CdS by using Surfactant and Thiocarbohyrate", Mater.Lett. **36**, 1231-1236.
11. Herron, Norman, Wang, Ying, Eckert, Hellmut (1990) "Synthesis and Characterization of Surface-Capped, Size-Quantized CdS Clusters, Chemical Control of Cluster Size", J. Am Chem. Soc. **112**, 1322-1326.
12. Alivisatos A.P.Johnson K.P.Peng X, Wilson T.E, Lowetch C.J "Organization of Nanocrystal Molecules Using DNA", Nature **382**,609-611.
13. Richard Kho, Claudia L. Torres-Martinez, Rajesh K.Mehra (2000), " A Simple Colloidal Synthesis for gram-Quantity Production of water-solube ZnS nanocrystal Powder", J.Colloid. Inter.Sci, **227**. 561-566.
14. Chan.W.C.W., Shuming Nie (1998), "Quantum Dot Bioconjuagates for Ultrasensitive nonisotopic Detection", Science, **281**.2016-2018
15. Toshio Uchihara, Satoshi Maedomari, Takeshi Komesu, Kai Tanaka.(2204)"Influence of Proton –Dissociation Equilibrium of Capping Agents on the Photo-Chemical Events of the Colloidal Solutions Containing the Thiol-Capped Cadmium Sulfide Particles",J.Photochem.Photobiol. A:Chem,161.227-232.

Malaysian Journal of Analytical Sciences, Vol9, No. 3(2005): 521 - 524

STUDY OF AURAMINE O DYE-SENSITIZED PHOTOELECTROCHEMICAL SOLAR CELL

Masnizaayu Abd. Manaf, Anuar Kassim, Mohd Zaizi Desa, Yusnita Ali

Department of Chemistry, Faculty of Science and Environmental Studies,
Universiti Putra Malaysia ,43400 UPM Serdang, Selangor, Malaysia.
e-mail : anuar@fsas.upm.edu.my

Abstrak

Dari perkembangan awal sehingga perkembangan terkini berkaitan sel solar, pelbagai kajian telah dilakukan dan dibincangkan mengenai kesan kepelbagaian parameter terhadap sel solar ini. Terdahulu, *titanium dioxide* (TiO_2) merupakan bahan semikonduktor yang sering digunakan kerana keberkesanan jurang tenaga iaitu 3.2eV dan sifatnya yang sensitif terhadap kesan cahaya. Dalam kajian ini, PEC sel solar dengan *dye* Auramine O telah dikaji memandangkan *dye* ini merupakan sejenis *dye* organik dan turut memberi hasil dalam analisis PEC sel solar. Kajian ini telah dilakukan untuk menentukan interaksi fizikal dan kimia *dye* Auramine O ke atas kaca indium titanium oxide (ITO) yang diselaputi TiO_2. Parameter yang dikaji pada kali ini adalah perbezaan lapisan TiO_2 pada filem nipis sebelum diselaputi dengan *dye* Auramine O. Penambahan '*dye sensitized'* boleh menambahkan output secara menyeluruh di dalam analisis photoelectrochemical (PEC) sel solar. Filem-filem yang telah disediakan dianalisis menggunakan *X-ray diffratometry* (XRD) dan *Fouried Transform Infrared* (FTIR). Hasil atau tindakbalas terhadap cahaya telah dinilai menggunakan *Linear Sweep Voltammetry* (LSV) dalam sistem redoks $[Fe(CN)_6]^{3-}/Fe(CN)_6]^{4-}$.

Abstract

From early development to recently development stages of solar cells, studies have been done and discussed related to the effect of different parameters. Previously, TiO_2 is the preferred semiconductor material used due to its effective band gap energy of 3.2 eV and also its sensitiveness to visible light.. In this paper, photoelectrochemical solar cell (PEC) with Auramine O dye was studied since this dye was an organic dye-sensitized beside it gives output in photoelectrochemical solar cell. A study was carried out to determine the physical and chemical interaction of Auramine O dye on TiO_2 coated on the indium titanium oxide (ITO) glass for the fabrication and testing of nanostructure dye-sensitized colloidal TiO_2 PEC thin film solar cell. The parameter studied related to the output of the PEC were different layers of TiO_2 (sol gel) coated on ITO glass before being lastly coated with the dye. The addition of dye-sensitized could enhance the overall output in the PEC. The films prepared were analyzed using X-ray diffractometry (XRD), and Fourier Transform Infrared (FTIR). The light response or output was evaluated in $[Fe(CN)_6]^{3-}/Fe(CN)_6]^{4-}$ redox system by running linear sweep voltammetry (LSV).

Key words: dye, photoelectrochemical solar cell, Auramine O

Introduction

The research of renewable sources of energy has led to an increasing interest in photoelectrochemical cell because of their possible role as transducers of solar to electrical energy [1]. The photoeffects in electrochemical systems were first observed by Becquerel [2] in his investigation on the solar illumination on
metal electrode in 1839. Later it was observed by Moser [3] and Rigollot [4] that the sensitivity of silver/silver halide and copper/copper oxide electrode could be increased by coating them with dye stuff [5, 6, 7]. Thomson [8] and Stora [9] reported that pure metal electrodes were also sensitive to light when coated with dye or immersed in a dye solution. The result of the first 100 years had been reviewed by Copeland and co-workers [10]. A summary of the properties of photoelctrochemical (PEC) cells described in the literature up to 1965 was compiled by Kuwana [11] and later work has been reviewed by Archer [12].

In this paper we report on the characterization of sol-gel TiO_2 thin films dip coated on ITO glass. This thin film then was later coated with organic dye (Auramine O) solution. The sol gel and dye coatings output were investigated by both Fourier Transform Infrared Spectroscopy (FTIR) and optical techniques.

Experimental

a- *Preparation of titanium dioxide (TiO_2) by sol gel method.*

Polyethylene glycol (PEG 2000 Wako pure chemical) of 6g was dissolved in ethanol (200ml) in a volumetric flask (600ml). The solution stirred continuously until PEG fully dissolved. Tetraisopropyl orthotitanate (TTPO Merck pure chemical) of 85.2g, diethanolamine (DEA) of 31.8g and deionized water (5.4ml) were added and the solution was made up to 600ml. using ethanol. The calculated concentration of the alkoxide in the mixture was $0.5mol^{-1}$. The molar ratio of PEG, DEA and water to the alkoxide in the mixture were 0.01:1:1 respectively. The resulting homogenous, transparent and stable sol was sealed and stirred continuously for 3 hours at ambient temperature. The sol gel was used to prepare TiO_2 thin films.

b. Preparation of Auramine O solution

The solution of Auramine O dye was prepared by pipetting a dichloromethane stock solution into 20ml flask. A 20mg of Auramine O dye and 2.0g polymethyl methacrylate (PMMA) was added. The yellow mixture was stirred for 3 hours and ready to coat on electrode.

c. Preparation of thin films and PEC solar cell.

A clean ITO glass was dipped into the sol gel and left to dry at room temperature. The thin film was then annealed for 1 hour at 500°C. The film was then cooled to room temperature before being subsequently dipped into dye solution. Again, the coated dye thin film, yellow in colour, was left dried at room temperature before send for analysis. Prior to the dye coating, the thin film was characterized using XRD. The procedure was repeated for different layers of TiO_2 prepared. The PEC solar cell was prepared using platinum as the counter electrode, Ag/AgCl as the reference electrode and the prepared thin films as the working electrode. The electrolyte used was $[Fe(CN)_6]^{3-}/Fe(CN)_6]^{4-}$ redox system.

Characterizations

The infrared spectra of the samples were taken on Perkin Elmer FTIR spectrophotometer and potassium bromide, KBr as the matrix. XRD analysis was performed using Philip PW-1390 model. An EG&G Princeton applied Research potentiostat driven by software model 270 Electrochemical analysis system was used to control the LSV process and to monitor the output of current and voltage profiles of the PEC solar cell.

Results and discussion

Figure 1 shows comparison of the photosensitivity for the electrode that was coated with different layers of TiO_2 (sol gel) and dye solution. The effect of the number of layers of TiO_2 that was coated on ITO glass prior coating with dye was clearly observed as an important parameter for optimizing the cell efficiencies as shown in figure 1. As indicated in *Table 1*, the thick layer (four layers of TiO_2 - L4) shows high output current about 4.34 mA, but have also higher recombination losses compare to thin layers (three layers -L3) that produce 5.33 mA current output, due to larger distances to the current collecting electrodes. It was shown in figure 4. Thus, in this experiment we were found that a good relation between high light absorption and low recombination losses is again reached at electrode that was dipped for a three layer of TiO_2 sol gel.

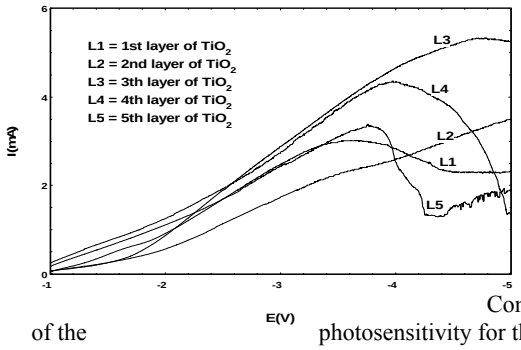

Figure 1: Comparison of the photosensitivity for the sample with different layer TiO_2 and one layer of Auramine O dye solution on ITO glass.

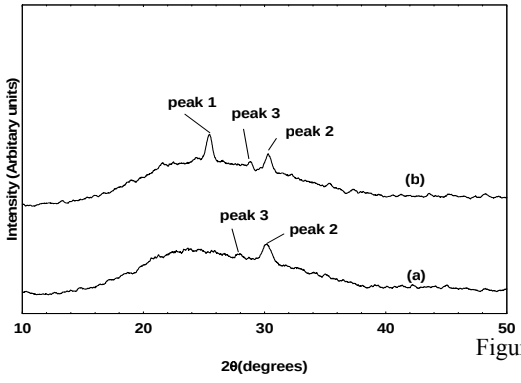

Figure 2:

XRD analysis for three layers of TiO_2 thin film (a)without heat treatment and (b)with heat-treated (T=500°C for one hour).

Table 1 : Comparison of potential (E), current (I), and resistance (R) of a different layers of TiO_2 and dye solution that was coated on ITO glass.

Thin films	E_{max} (V)	I_{max} (mA)	E/I=R ($x10^2$)
L1	3.56	3.00	11.88
L2	3.47	2.27	15.32
L3	4.72	5.33	8.86
L4	3.98	4.34	9.16
L5	3.77	3.37	11.20

Figure 2 shows XRD patterns of three layers of TiO_2 thin film with and without heat-treatment. The third layer of TiO_2 on ITO glass was chosen because it produced a highest current from photosensitivity analysis. The XRD patterns of TiO_2 with heat-treatment show well-define peaks for anatase form. Comparisons of d(Å) values (albeit 2θ degree for peak 1= 25.5, peak 2=28.89 , and peak 3=30.3) for the entire peak exists in TiO_2 with heat treatment and without heat-treated are shown in *Table 2*. The TiO_2 signals appeared very significant when the TiO_2 was heated at 500°C. This shows that heating has a significant effect on the TiO_2 crystallinity compared to the without heating. Higher intensity of TiO_2 signal indicates the higher content and better crystallinity of the resulting materials.

Table 2 : Comparison of d(Å) values for the entire peaks exists in TiO_2 thin film with and without heat- treated.

Peak	d(Å)			Compound phase
	Without heated	With heat-treated (500°C)	Standard JCPDA (anatase)	
1	-	3.52	3.52	TiO_2 anatase
2	2.36	2.36	2.38	TiO_2 anatase
3	1.71	1.71	1.70	TiO_2 anatase

Figure 3 shows the FTIR spectra of TiO_2 (sol gel) only before being coated on the ITO glass. The figure shows spectra of TiO_2 before and after heated at 500°C for 1 hour. The bands around 3402 cm^{-1} are characteristic for water molecules and appeared in both spectra. The band at 2920cm^{-1} is owing to the stretching
vibration of the C-H bond of organic compounds. The absorbances of the bands are attributed to the carbonated and bicarbonate groups. The peak at 1345 cm^{-1} is due to the vibration of ($-CH_2-CH_3$). The presence of titanium oxide is shown as a broad peak at 511.9 cm^{-1} and the Ti-O bond corresponding to the crystalline anatase phase.

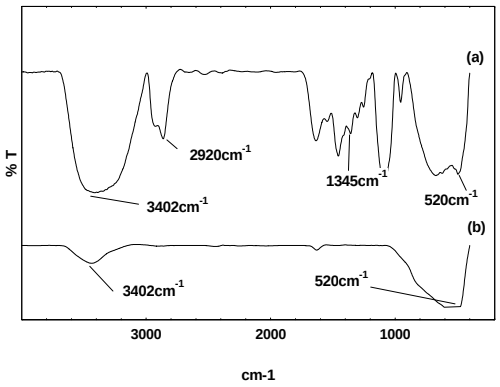

Figure 3 : FTIR spectra of TiO_2 (sol gel) only (a)before and (b)after heat-treated as described in the text.

Conclusion

From the preparation of TiO_2 (sol gel) results, its showed that this preparation method that was used in this study was a suitable tool for preparation of TiO_2 (sol gel). TiO_2 (sol gel) was characterized using FTIR spectroscopic analysis and XRD analysis. Thin films that coated with a number of layers of TiO_2 and Auramine O dye solution were also analyzed using XRD and PEC. From the results, the third layer of TiO_2 and Auramine O dye solution gave the highest current (5.33mA) in the PEC result. It concluded that the third layer of TiO_2 sol gel was the photoelectrochemical potential in this study.

Acknowledgements

The authors want to thanks to the Department of Chemistry, Faculty of Sciences and Environmental studies, Universiti Putra Malaysia and Malaysia government for giving the grant (IRPA No: 09-02-04-0324-EA001).

References

[1] Y. Yonghong, Zh. Jiayu, G. Peifi, L. Xu, T. Jinfa (1997) *Thin Solid Films*, Vol 298, 197

[2] C. Becquerel, C.R. Acad. (1839) *Sci. Paris*, Vol 9, 14.

[3] J. Moser. Mh., (1887) *Chem*., Vol 8, 373.

[4] H. Rigollot. C.R. Acad. (1893) Sci. Paris, Vol 116,878.

[5] N. Ozer, S. Sabuncu, J. Cronin (1999) *Thin Solid Films*, Vol 338, 201

[6] S. Hashimoto, H. Matsuoka, J. (1991) *Electrochem. Soc*. Vol 138, 2403.

[7] F.E. Ghodsi, F.Z. Tepehan, G.G. Tepehan, (1999) *Electrochem. Acta*, Vol 44, 3127.

[8] G.E. Thompson. (1915) *Phys. Rev*., Vol 5 536.

[9] C. Stora. J. Chim. (1937) *Phys.* Vol 34, 536.

[10] A.W. Copeland. O.D. Black. A.B. Garett. (1942) *Chem. Rev*. Vol 31, 177.

[11] T. Kuwana. (1966) *Electroanal. Chem*.Vol 1, 197.

[12] M.D. Archer. J. (1975) *Appl. Electrochem*. Vol 5 17.

PHOTODEGRADATION AND ADSORPTION OF FAST GREEN FCF IN TiO_2-CHITIN SUSPENSION

Zulkarnain Zainal*, Fatimah Julia Romeli, Mohd Zobir Hussein, Asmah Hj Yahaya and Mohamed Zaki Abd Rahman

Department Of Chemistry, Faculty Science and Environmental Studies, 43400 Universiti Putra Malaysia

*Author for correspondence
E-mail: zulkar@fsas.upm.edu.my

ABSTRACT

The photocatalytic degradation and adsorption of Fast Green FCF (FG) from aqueous solution has been investigated in suspension containing commercial TiO_2 (Degussa P-25), chitin and mixture of TiO_2-chitin. The removal of FG using a mixture of TiO_2-chitin with a mass ratio of 30/70 were found to follow first order kinetic. The presence of chitin in TiO_2 suspension enhanced the removal by 72%. The removal by using chitin and a mixture of TiO_2-chitin were rapid for the first 30 minute and reached equilibrium after 1 hour, compared to using TiO_2 alone which needed more than 4 hours. A synergy effect was observed with an increase in the apparent rate constant by 16.8 times. This was ascribed to an extended adsorption of FG on chitin followed by a transfer to TiO_2 where it is photocatalytically degraded. pH has significant effects on the adsorption and photodegradation properties at the chitin and TiO_2 surface. The pH range for optimum FG removal was between 3 to 5. Temperature has no significant effect on the equilibrium removal on photodegradation of FG by TiO_2, chitin and the mixture of TiO_2-chitin. This combined photocatalytic-adsorption system appears promising, an efficient accelerated removal of organic pollutants from water.

Keywords: titanium dioxide; chitin; photodegradation; adsorption; Fast Green FCF

INTRODUCTION

Various treatment strategies are applied for the removal of toxic organic pollutants from water. The traditional physical-chemical treatment such as nanofiltration, ozonation, combustion, among others, is efficient but has inherent limitations in applicability, effectiveness and cost. Heterogeneous photocatalysis using TiO_2 as photocatalyst recently emerged as an efficient purifying method. Several attempts have been made to increase its photoefficiency either by noble metal deposition [1], or by ion doping [1, 2], but such modification did not enhanced the photocatalytic activity and rather detrimental.

A third way to possibly increase the photocatalytic efficiency of titanium consists of adding a co-adsorbent such as silica, alumina, zeolites, clays, or activated carbon [3, 4, 5]. However, due to their high price and considering the great amount of contaminated water, research has recently directed towards alternative co adsorbents, namely low cost adsorbent, including the utilization of waste materials.

Chitin has been utilized as an adsorbent for a variety of substrates. It is a white, natural biopolymer, also a nitrogen-containing polysaccharide, related chemically to cellulose that forms a semitransparent substance and is a principal constituent of the exoskeleton or outer covering of insects, crustaceans and arachnids. Chitin can be extracted in large quantities from crab and shrimp shells, saving the cost involved in land filling the tons of crab and shrimp shells piling up along coastlines or from the broth of industrial fungal processes [6].

Various studies have been undertaken to investigate the efficiency of chitin as an adsorbent such as adsorption of various metallic ions [7], ionic species of sulfonated azo dyes, inorganic and organic acids [8] and also adsorption of blue acid dye 25, blue acid 158, mordant yellow 5 and direct red 24 [9].

The aim of the present study was to investigate the applicability of a combination of two environmentally friendly processes, adsorption on a chitin and TiO_2 based heterogeneous photocatalysis as potential water treatment technology on a laboratory scale.

MATERIAL AND METHOD

The Fast Green FCF 90.0% (FG) dyestuff is an odorless green powder obtained from *Fisher Biotech* and was used as received. A 1000 ppm stock solution of fast green was prepared using 1.0 g of fast green powder in 1000 cm^3 distilled water. Solutions required for the adsorption and photodegradation were prepared by diluting the stock. The range of concentration of prepared FG varied between 10 mg/L and 150 mg/L. The required pH value for FG solution was adjusted by adding 1.0 mol L^{-1} of HCl for acidic condition and 1.0 mol L^{-1} of NaOH for basic condition.

In this work, chitin prepared from prawn shells was used as received. Before utilization of the sorbent, the flaky chitin was ground and sieved into less than 100 μm. The photocatalyst was TiO_2 Degussa P-25, mainly anatase with a surface area of 50 m^2g^{-1}.

Adsorption and photodegradation was carried out using 0.56 g of chitin and 0.24 g of TiO_2 powder in 1000 cm^3 FG solutions at different temperature and pH, under irradiation of UV light. The mixture was slowly stirred during the adsorption and photodegradation for about four hours. Exactly 1 cm^3 of dye solutions was withdrawn every 30 minutes, filtered to separate the adsorbent and catalyst using 0.45 μm membrane filter and diluted to 5 cm^3. The concentration was determined by employing a UV-Vis spectrophotometer, Perkin Elmer Lambda 20 at a wavelength of 624.00 nm.

RESULTS AND DISCUSSION

Adsorption of Fast Green FCF

The study of FG adsorption has been performed at 25^0C on TiO_2 Degussa P25 (0.24 g) on chitin (0.56 g) and on a suspended mixture of them with the same respective masses. The results obtained and presented in Fig.1 indicated that most of adsorption occurred within 30 minute. It can be observed that FG adsorbed substantially more on TiO_2-chitin and on chitin than on TiO_2 alone (Table 1). Similar findings have been reported for the adsorption of anionic dyes onto chitin [10].

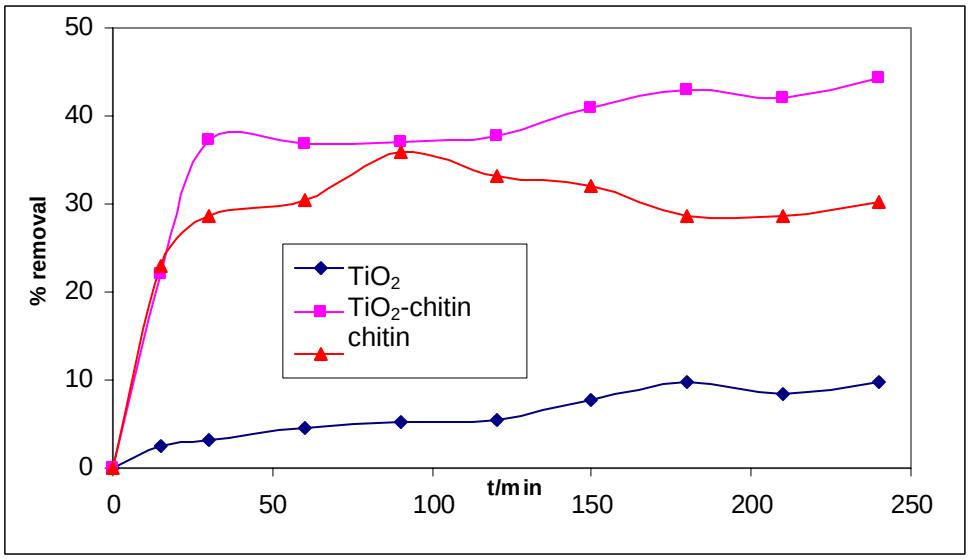

Figure 1: Adsorption of FG in dark for C_o= 100ppm, TiO_2= 0.24g, TiO_2-chitin = 0.8g, chitin= 0.56g

Table 1: % removal of FG removed in the dark

Adsorbent	% removal
TiO_2	9.73
TiO_2-chitin	44.31
Chitin	30.29

Photodegradation of Fast Green FCF

The kinetic removal for FG irradiation under UV light in Fig. 2 suggest that the equilibrium removal by using mixture of TiO_2-chitin is much higher than on TiO_2 and on chitin. The origin of this difference can be ascribed to a strong interaction between TiO_2 particles and chitin. The functional groups in chitin can act as active sites for the adsorption of FG by forming a hydrogen bond, van der Waals interactions and also by ion exchange with other group [10] and then it is degraded by TiO_2. The presence of chitin in TiO_2 suspension enhanced the removal of FG by 72% (Table 2). Photodegradation using mixture of TiO_2-chitin also was found to follow apparent first order rate, so it is reasonable to evaluate the efficiency of degradation based on the apparent first order rate constant of the process. The extent of the effect was quantified in term of a synergy factor, R (R= k_{app}(TiO_2-chitin)/ k_{app}(chitin) [11]. A synergy effect was observed with an increase in the apparent first order rate constant by a factor 16.8. The synergy effect was ascribed to an extended adsorption of FG on chitin followed by a transfer to TiO_2 where it is photocatalytically degraded.

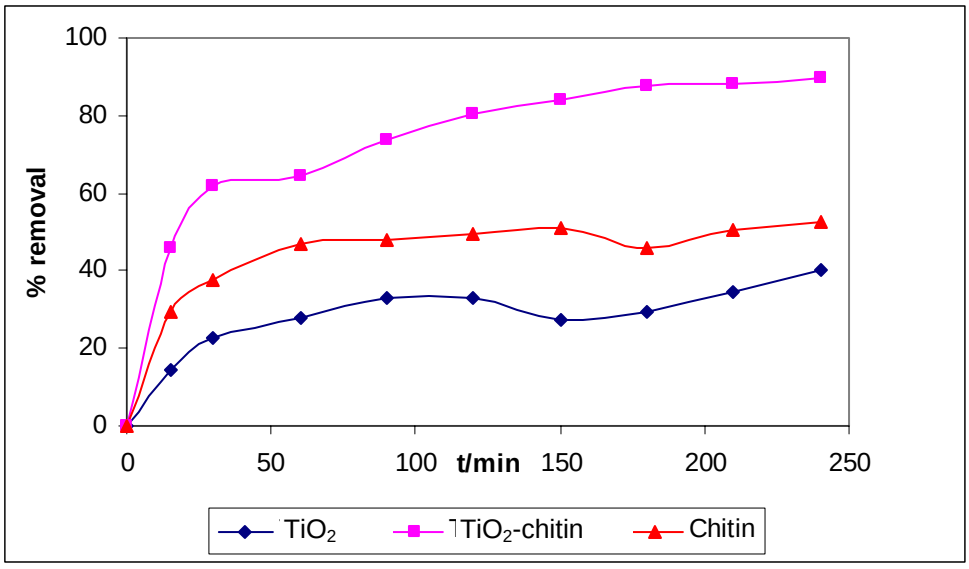

Figure 2 : Photodegradation of FG for C_o= 100ppm, TiO_2= 0.24g, TiO_2-chitin = 0.8g, chitin= 0.56g

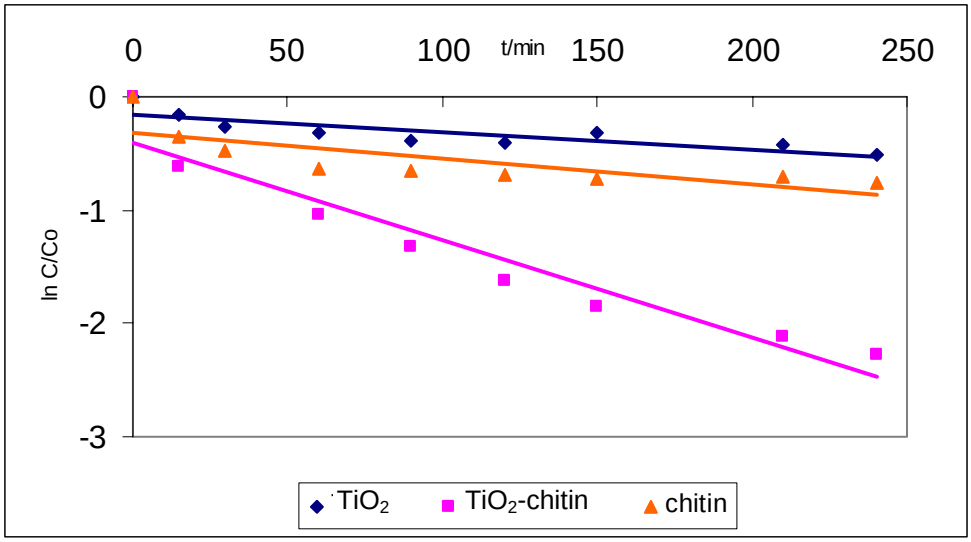

Figure 3 : First order kinetic of FG photodegradation

Table 2: First order parameters: apparent rate constant k_{app} (min^{-1}) and half life $t_{1/2}$(min)

Adsorbent/ catalyst	% removal	Apparent rate constant k_{app} (min^{-1})	Half life $t_{1/2}$ (min)
TiO_2	17.34	0.0015	2.16×10^{-3}
TiO_2-chitin	89.72	0.0084	1.20×10^{-2}
Chitin	52.77	0.0021	3.03×10^{-3}

Effect of pH

The pH value is an important parameter in photodegradation that takes place on the surface of photocatalyst. At more acidic pH values, the TiO_2 surface is positively charged, while at pH above 5.6, it is negatively charged. Therefore pH value will have significant effect on the adsorption-desorption properties at the TiO_2 surface [12].

While chitin was found to be good sorbent due to its high content of acetylamino and amino group, which act as chelating agent. The pH influences the compound in solution or the protonation or deprotonation of the chitin. A lower pH will cause the functional groups of chitin to be protonated to a higher extent and results in a stronger attraction for a negatively

charged ion in the solution [13]. However at pH below 3 the anions in the solution compete with the anionic dye, thereby decreasing adsorption. Beyond pH 7, an amino group of chitin was deprotonated and FG removal was drastically reduced [13]. For that reason from the results, FG is best adsorbed onto chitin at pH in the range 3-5.

The effect of pH on the degradation of FG is shown in Fig 3. The results indicates that photodegradation of FG using TiO_2-chitin was efficiently removed in an acidic medium of pH 3-5. This result is due to TiO_2 and chitin properties.

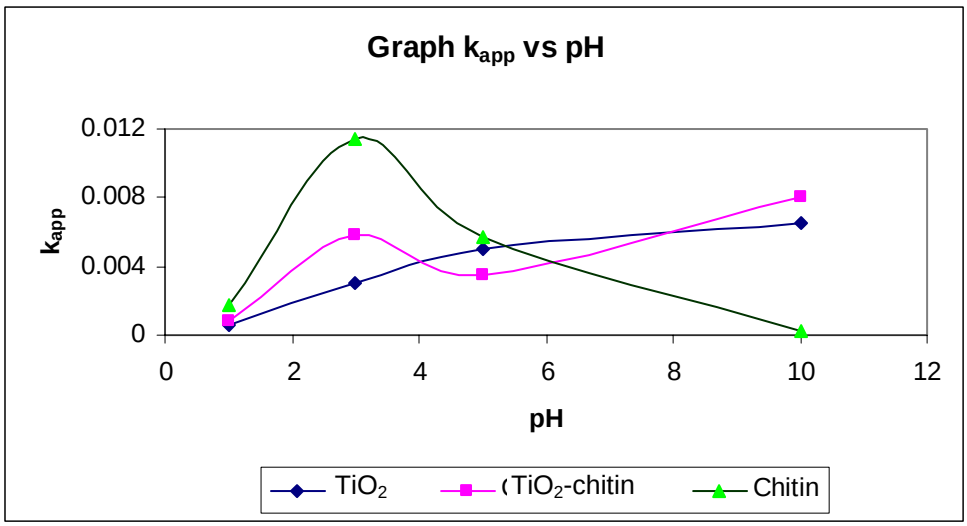

Figure 4 : Effect of pH on photodegradation

Effect of temperature

The overall process of semiconductor photocatalysis is usually not very temperature sensitive. For TiO_2 photocatalysis, irradiation is the primary source of electron-hole pair generation at ambient temperature as the band gap energy is too high to be overcome by thermal activation [12].

In case for photodegradation of FG by chitin, an increase in temperature in the range 40-50^{0}C, will be followed by decrease in sorption capacity by chitin, the same results was

obtained when the temperature was decreased to 4^0C. This due to the sorption process by chitin is exothermic [14].

As for photodegradation using mixture of TiO_2-chitin, it seems that the results obtained in Fig 5, shows the same pattern of photodegradation by chitin but with higher equilibrium removal.

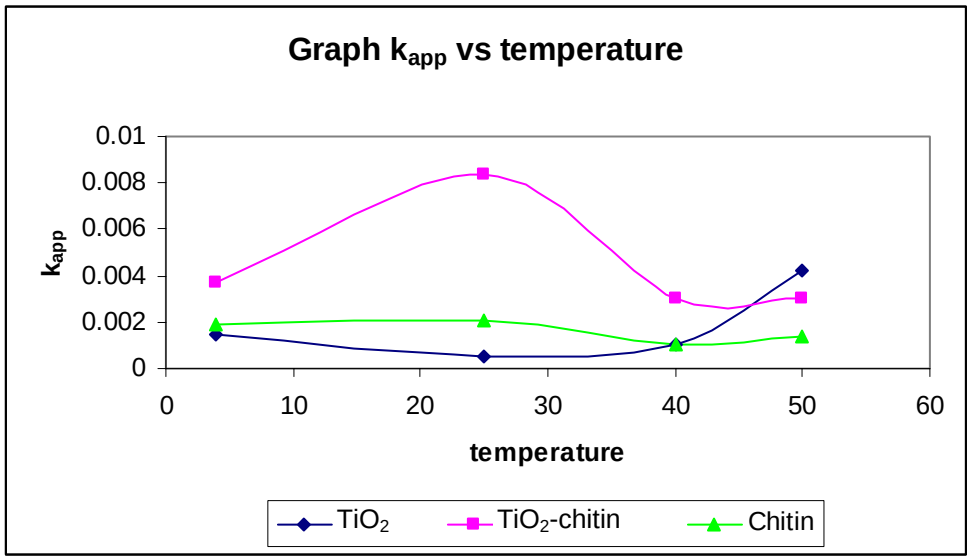

Figure 5 : Effect of temperature on photodegradation

CONCLUSION

From a practical point view, it is possible to obtained clean water in much shorter time than with TiO_2 alone. The addition of chitin to TiO_2 under UV irradiation induces a beneficial effect on the photocatalytic degradation of FG. The functional group in chitin act as active sites for the adsorption of FG solution and then it is degraded by TiO_2. The influence of pH suggests that photodegradation was not suitable at both low and high pH value. Temperature also has no significant effect on the equilibrium removal on photodegradation of FG by TiO_2, chitin and mixture of TiO_2-chitin.

ACKNOWLEDMENTS

This project was financially funded by the Government of Malaysia under an IRPA Grant No. 09-02-04-0255-EA001

REFERENCES

1. Mu, W., Herrmann, J.-M., Didier, J., and Pichat, P., *Catal. Letter*. 3, 73 (1989)
2. Herrmann, J.-M., Didier, J., and Pichat, P., *Chem. Phys. Letter*. 108, 618 (1984)
3. Tanguay, J. F., Suib, S. L., and Coughlin, R W., *J. Catal*. 117, 335 (1989)
4. Minero, C., Catozzo, F., and Pelizzetti, E., *Langmuir* 8, 489 (1992)
5. Takeda, N., Torimoto, T., Sampath, S., Kuwabata, S., and Yoneyama, H., *J. Phys. Chem.* 99, 9986 (1995)
6. Zhou, JL., *Appl. Microbiol. Biotechnol*. 51, 686 (1999)
7. Yang, T.C., Zall, R.R., Eng. *Chem. Res. Div*. 23, 168 (1984)
8. Giles, C.H., Hassan A.S.A., *J. Soc. Dyers Col*. 74, 846 (1958)
9. McKay, G. Blair, H.S., Gardner, J. R., *J. Appl. Polym. Sci*. 27, 304 (1982)
10. Longhinotti, E., Pozza, F., Furlan, L., Sanchez, N.M.N., Klug, M., Laranjeria, M.C.M., and Fávere, V.T., *J. Braz. Chem. Soc*., 9, 435 (1998)
11. Matos, J., Laine, B., Herrmann, J.-M., *App. Catal. B.*18, 281 (1998)
12. Chen, D. W. and Ray, A. K., *Water Research.* 35, 3223. (1998)
13. Z; Yeşim, S., Yücel, A., *Process Biochemistry*. 36, 157 (2000)
14. Benguella, B., Benaissa, H., *Water Research.*36, 2463 (2002)

Malaysian Journal of Analytical Sciences, Vol.9, No. 3(2005): 534 - 541

COMPARATIVE STUDY ON CLEANUP PROCEDURES FOR THE DETERMINATION OF ORGANOCHLORINE PESTICDES IN VEGETABLES

(Alvin Chai Lian Kuet[1] and Lau Seng[2])

[1]*Agriculture Research Centre, Semongok, P.O.Box 977, 93720 Kuching, Sarawak*
[2]*Universiti Malaysia Sarawak, 94300 Kota Samarahan, Sarawak*

Key words: Solid-phase extraction, silica gel cleanup, organochlorine pesticides, gas chromatography.

Abstract

A study was carried out to compare the cleanup procedures for the determination of organochlorine pesticides in vegetables. Five organochlorine pesticides and their metabolites were extracted with acetone and methylene chloride. Extracts were cleanup up by solid-phase extraction (SPE) mixed-mode column using quaternary amine and aminopropyl (SAX/NH_2) or octadecyl (C_{18}) sorbents. These cleanup procedures were compared with the routine cleanup procedure using the silica gel column chromatography. The pesticides were determined by gas chromatography with electron capture detector. The recovery results obtained from the SPE SAX/NH_2 and C_{18} cleanups in carrot, cucumber and green mustard were in the range of 58 % to 106 % as compared to 63 % to 113 % for silica gel cleanup. The benefits of the SPE cleanup compared to the silica gel cleanup were the use of solvents and chemicals are reduced, possibility of concentration of the samples, no cross-contamination as the tube is discarded after use and shorter analysis time.

Abstrak

Satu kajian telah dijalankan untuk membandingkan kaedah-kaedah pembersihan untuk menentukan racun perosak organoklorin dalam sayur-sayuran. Lima racun perosak organoklorin and metabolitnya diekstrak dengan aseton dan dwiklorometana. Ekstrak dibersihkan dengan turus ekstraksi fasa pepejal (SPE) amina kuaterner dan aminopropil atau oktadesil. Kaedah-kaedah ini dibandingkan dengan kaedah pembersihan kromatografi turus gel silica yang digunakan oleh makmal pada masa ini. Racun perosak ditentukan dengan kromatografi gas yang dilengkapkan dengan pengesan penangkapan electron. Keputusan pengembalian yang diperolehi dari SPE ialah di antara 58 % dan 106 % untuk lobak merah, timun dan sawi hijau. Untuk pembersihan gel silica pula, keputusan pengembalian yang diperolehi ialah di antara 63 % dan 113 %. Faedah menggunakan pembersihan SPE berbanding dengan silica gel ialah penggunaan larutan dan bahan kimia dapat dikurangkan, sampel dapat dipekatkan, tidak ada pencemaran sampel dan masa analisis dapat dikurangkan.

Introduction

Organochlorine (OC) pesticides have been used extensively worldwide in the early 1950s. The highly lipophilic properties of these pesticides have led to contamination of the environment and the food chain. Numerous methods have been developed for the analysis of OC pesticides using SPE cleanup. A method using C_{18} and florisil SPE as replacement for Attagel cleanup procedures for halogened organic pesticides in broccoli, carrot, celery and orange was reported (1). The recoveries obtained were comparable to or better than the later method. In this study, acetronitrile was used for extraction, while n-hexane and 5 % acetone/hexane were used as eluant for the C_{18}. 7 chlorinated hydrocarbons were evaluated using reverse phase SPE cleanup for potato, tomato, orange, carrot, broccoli and melon (2). The sample was extracted with

acetronitrile. The C_{18} SPE cartridge was used as cleanup to eliminate non-polar plant co-extractives by passing the extract through the cartridge. A multi-residue method capable of detecting 17 OC pesticides in plant and animal tissue samples was investigated (3). The pesticides were extracted with 5 % ethanol in ethyl acetate. Samples with high lipid content were cleanup by automated gel permeation chromatography (GPC) and silica gel mini-columns. Highly pigmented samples were cleaned up with SPE columns. The OC pesticides were eluted from the florisil SPE column with 15 ml 10 % ethyl acetate in hexane. A method for the determination of 251 pesticides and its metabolites in fruit and vegetable samples was reported (4). Co-extractives are removed by passing the acetronitrile extract through octadecyl (C_{18}), carbon and amino propyl SPE cleanup. Extraction of the sample with acetronitrile was followed by a salting-out step. Non-polar co-extractives were removed by passing a portion of the acetronitrile extract through an octadecyl cartridge. An aliquot of extract was further cleanup on carbon SPE tube coupled to an amino propyl cartridge with acetronitrile-toluene (3 : 1) as the elution solvent. SPE cleanup methods using SAX/NH_2 and C_{18} for the determination of pyrethroid pesticides in vegetables were investigated (5). This paper reports the findings of SPE cleanup methods using SAX/NH_2 and C_{18} for the determination of OC pesticides in vegetables.

Experimental

Nine OC pesticides, namely γ-HCH, heptachlor, α-endosulphan, dieldrin, β-endosulphan, pp'-DDD, op'-DDT, endosulfan sulphate and pp'-DDT were selected for this study. These pesticides were fortified in carrot, cucumber, and green mustard at 0.5 and 0.1 ppm levels. Three replicate fortifications for each matrix type were prepared. Extraction was carried out based on procedures described by Steinwandter (6). 10 g of sample was homogenised in a blender containing 100 ml acetone, 75 ml dichloromethane and 15 g sodium chloride for three minutes. The homogenised mixture was allowed to separate into its organic and aqueous layers. The organic phase was transferred to a beaker and 3 g of sodium sulphate was added to remove the remaining water. For the silica gel method, 2 ml of extract was transferred to a chromatographic column containing 10 g of silica gel. The pesticides were eluted with 60 ml of hexane-methylene chloride mixture (4 : 1 v/v). For SPE SAX/NH_2 method, the tube was conditioned with 10 ml of acetone : petroleum ether (1 : 2). 2 ml of extract was transferred to the SPE tube, followed by eluting with 10 ml of conditioning solvent at the flow rate of 1 ml/min. For SPE C_{18}, the tube was conditioned with 10 ml hexane : petroleum ether (1 : 1 v/v). 2 ml of extract was transferred to the tube, followed by 10 ml hexane : petroleum ether (1 : 1 v/v) for elution. The eluates collected were analysed on gas chromatograph (GC) equipped with electron capture detector (ECD). An Agilent 6890 GC equipped with ECD was used for the determination of the OC pesticides. The GC conditions were: Injector temperature, 260°C; detector 300°C; carrier flow (nitrogen) 1.2 ml/min; oven temperature, 100°C (0.2 min), rate 20°C/min to 180°C, rate 2°C/min to 250°C, rate 50°C/min to 300°C (5 min). The OC pesticides were analysed on an Ultra 1, 25 m x 0.32 mm x 0.5 μm column.

Results and Discussion

The recoveries obtained from the 9 OC pesticides in the carrot samples using the SAX/NH_2, C_{18} and silica gel cleanup methods are given in Table 1. At 0.5 ppm fortification level, the recoveries obtained using the SAX/NH_2 cleanup were found within the acceptable range of 70 –120 % (7)

except for pp'-DDT. For the C_{18} cleanup, the recoveries obtained were lower as compared to the SAX/NH_2 and silica gel methods. The recoveries obtained for all the OC pesticides except γ-HCH, heptachlor and op'-DDT were found within the acceptable range. Higher recoveries of 73.0 % to 106.0 % were obtained for the silica gel method. At 0.1 ppm fortification level, the recoveries obtained for the SAX/NH_2 cleanup were lower as compared to the C_{18} and silica gel methods. The recoveries obtained for four OC pesticides, namely γ-HCH, α-endosulphan, dieldrin and pp'-DDT were below 70%. For the C_{18} cleanup, the recoveries obtained for all the OC pesticides except heptachlor were found within the acceptable range. Except for γ-HCH and heptachlor, the recoveries obtained using the silica gel method was within the acceptable range.

Table 1. Recovery of OC pesticides from carrot samples using different cleanup methods

	0.5 ppm			0.1ppm		
Pesticide	SAX/NH_2	C_{18}	Silica gel	SAX/NH_2	C_{18}	Silica gel
	% Rec.[(a)] ± CV	% Rec.[(a)] ± CV	% Rec.[(a)] ± CV	% Rec.[(a)] ± CV	% Rec.[(a)] ± CV	% Rec.[(a)] ± CV
γ-HCH	70.0 ± 4.4	65.7 ± 2.3	81.7 ± 5.8	69.3 ± 6.1	75.7 ± 6.7	63.0 ± 5.3
Heptachlor	72.7 ± 5.9	66.3 ± 5.7	73.0 ± 2.7	83.0 ± 7.0	67.0 ± 7.9	67.7 ± 8.6
α-endosulphan	78.0 ± 4.4	75.3 ± 5.1	102.0 ± 3.6	68.7 ± 6.5	81.7 ± 1.5	71.7 ± 4.7
Dieldrin	87.3 ± 3.1	82.0 ± 4.6	103.3 ± 4.0	69.3 ± 5.9	92.3 ± 4.7	82.0 ± 3.0
β-endosulphan	83.7 ± 5.7	79.7 ± 4.5	104.0 ± 3.0	90.3 ± 3.5	93.7 ± 2.1	89.0 ± 6.1
pp'-DDD	88.3 ± 3.1	77.7 ± 3.2	106.0 ± 1.7	67.7 ± 5.7	102.7 ± 3.1	112.7± 2.9
op'-DDT	76.0 ± 8.0	65.7 ± 7.2	106.0 ± 1.0	70.0 ± 5.6	98.3 ± 3.5	113 ± 4.4
Endosulphan-sulphate	85.3 ± 4.7	80.3 ± 3.5	105.7 ± 4.2	96.0 ± 3.0	105.0 ± 2.0	94.7 ± 7.4
pp'-DDT	66.7 ± 6.7	71.7 ± 5.0	103.3 ± 1.5	89.3± 10.1	72.7 ± 2.1	73.3 ± 1.2
AV	78.6	73.8	98.3	78.2	89.2	85.2
SD	7.8	6.6	12.1	11.4	14.0	18.6

AV = average mean CV = coefficient of variation SD = standard deviation (a) n = 3

The chromatograms for the carrot samples using the SAX/NH_2, C_{18} and silica gel cleanups are shown in Figure 1. The chromatograms obtained from all the three methods showed there were no interference peaks which co-eluted with the OC pesticides between 9 min to 21 min regions. This showed that these methods were able to retain the co-extractives. The limit of detection (LOD) obtained from these methods was 0.01 ppm.

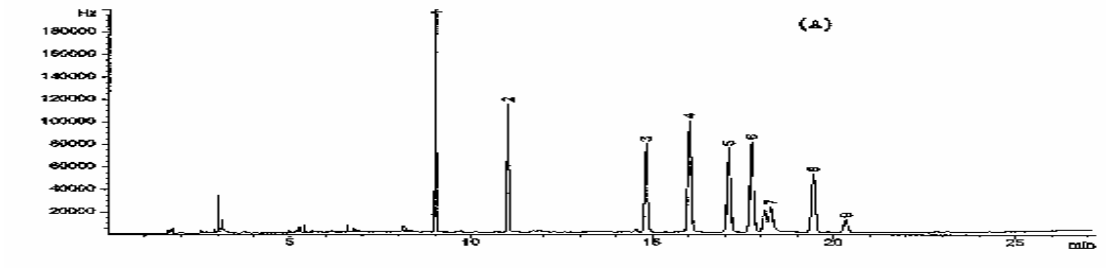

TIME (min)

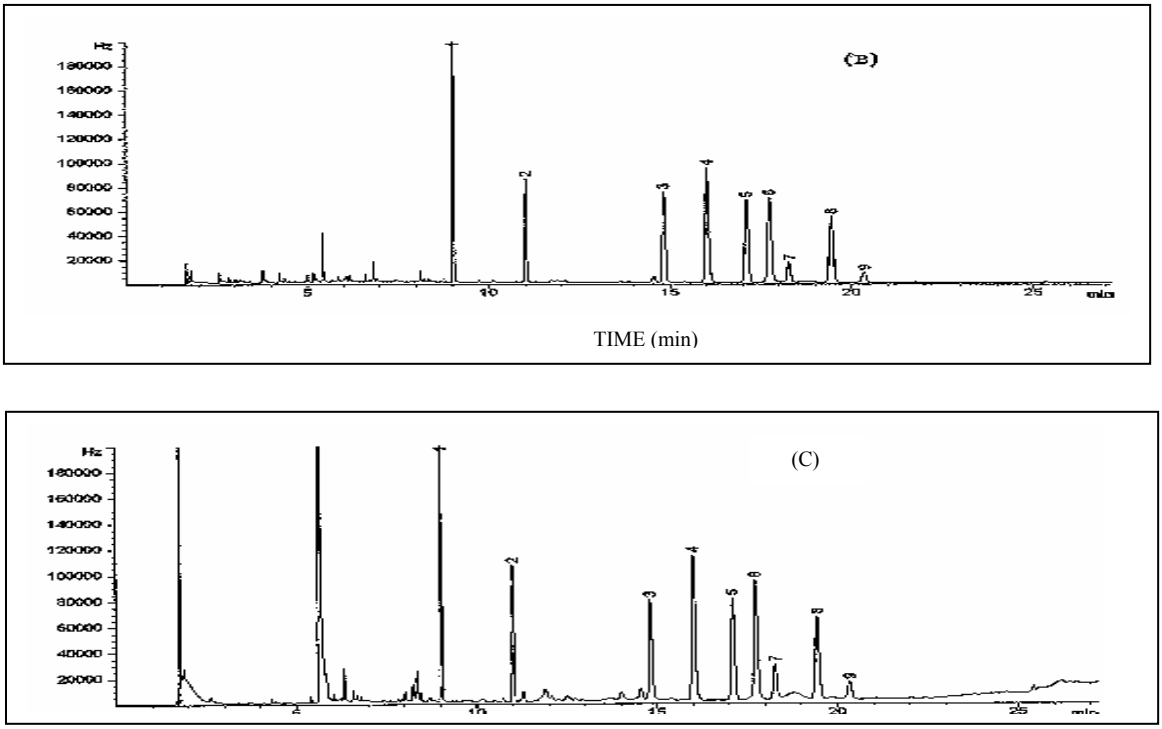

Figure 1. GC chromatograms of carrot extract after SAX/NH_2 (A), C_{18} (B) and silica gel (C) cleanup. Peaks: 1, γ-HCH; 2, heptachlor; 3, α-endosulfan; 4, dieldrin; 5, β-endosulfan; 6, pp'-DDD; 8,endosulfan sulphate; 9, pp'-DDT

The recoveries for the 9 OC pesticides fortified in the cucumber samples using the SAX/NH_2, C_{18} and silica gel cleanup methods are given in Table 2. At 0.5 ppm fortification level, the recoveries for 9 OC pesticides using the SAX/NH_2 cleanup were found within the acceptable range except γ-HCH. For the C_{18} method, the recoveries obtained for all the OC pesticides were found within the acceptable range. However, the average mean recoveries were lower as compared to the SAX/NH_2 and silica gel methods. Higher recoveries of 71 % to 109 % were obtained using the silica gel method. At 0.1 ppm fortification level, the recoveries obtained for all the OC pesticides using the SAX/NH_2 method were found within the acceptable range. For the C_{18} method, the recoveries for all the OC pesticides except pp'-DDT and heptachlor were found within the acceptable range. The recoveries obtained using the silica gel cleanup for three pesticides namely; γ-HCH, heptachlor and α-endosulfan were slightly below the acceptable range of 70 %.

Table 2. Recovery of OC pesticides from cucumber samples using different cleanup methods

	0.5 ppm			0.1 ppm		
Pesticide	SAX/NH_2	C_{18}	Silica gel	SAX/NH_2	C_{18}	Silica gel
	% Rec.[(a)] ± CV	% Rec.[(a)] ± CV	% Rec.[(a)] ± CV	% Rec.[(a)] ± CV	% Rec.[(a)] ± CV	% Rec.[(a)] ± CV
γ-HCH	69.7 ± 4.2	78.3 ± 0.6	71.0 ± 7.0	76.7 ± 1.5	74.0 ± 8.7	61.7 ± 5.0
Heptachlor	74.3 ± 4.5	71.0 ± 6.8	92.7 ± 9.2	96.0 ± 4.0	65.7 ± 5.1	63.0 ± 5.0

α-endosulphan	87.7 ± 2.1	80.7 ± 2.3	88.7 ± 2.5	81.7 ± 2.5	96.3 ± 4.0	69.7 ± 10.0
Dieldrin	93.0 ± 4.4	82.3 ± 1.2	95.0 ± 3.0	75.0 ± 1.0	79.7 ± 6.8	76.0 ± 5.0
β-endosulphan	89.3 ± 2.3	82.7 ± 2.1	101.3 ± 5.1	76.7 ± 0.9	91.7 ± 4.0	79.3 ± 8.1
pp'-DDD	95.7 ± 2.5	74.0 ± 2.7	109.0 ± 2.7	83.7 ± 2.1	100.3 ± 8.5	105.7 ± 3.2
op'-DDT	89.0 ± 7.6	77.3 ± 5.1	104.7 ± 3.8	72.7 ± 7.0	73.0 ± 4.0	110 ± 4.6
Endosulphan-sulphate	89.7 ± 4.6	81.0 ± 2.0	107.3 ± 6.0	92.7 ± 8.1	95.7 ± 1.5	87.3 ± 4.2
pp'-DDT	98.0 ± 10.4	77.0 ± 2.0	106.3 ± 1.5	106 ± 10.5	65.7 ± 2.3	75.3 ± 5.0
AV	87.4	78.3	97.3	84.6	82.5	80.9
SD	9.4	3.9	12.1	11.3	13.7	17.2

AV = average mean CV = coefficient of variation SD = standard deviation (a) n = 3

The chromatograms for the cucumber samples using the SAX/NH_2, C_{18} and silica gel methods are shown in Figure 2. All the three chromatograms showed no interference peaks between 9 min to 21 min regions where the OC pesticides were eluted. No major peaks were observed at other regions. This showed that these methods were able to retain the co-extractives. The LOD obtained using these methods were 0.01 ppm.

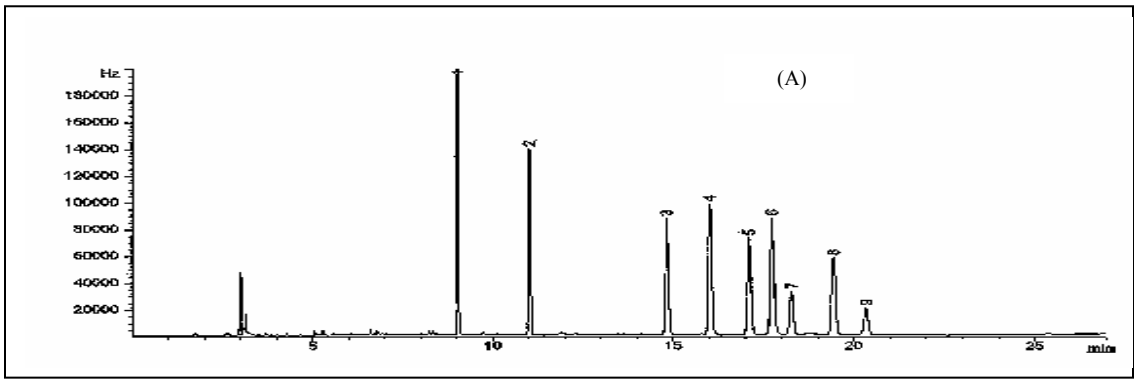

TIME (min)

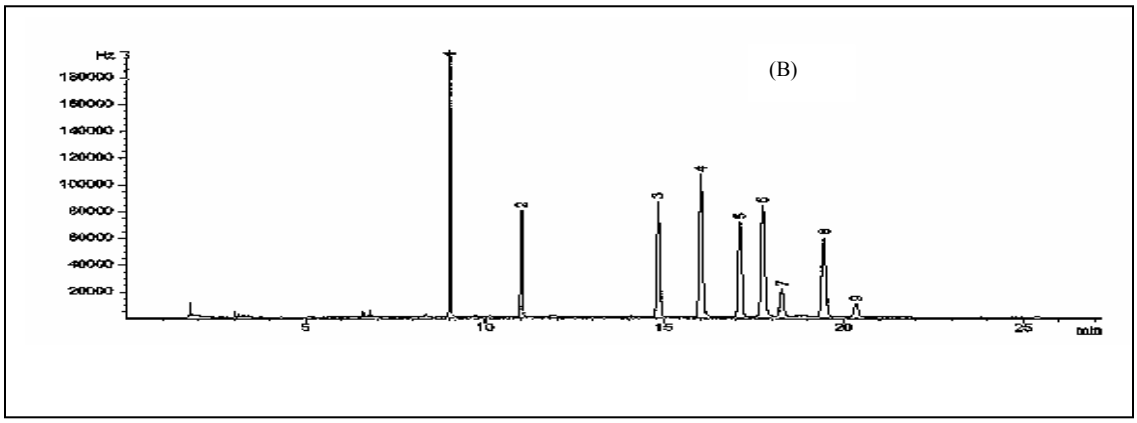

TIME (min)

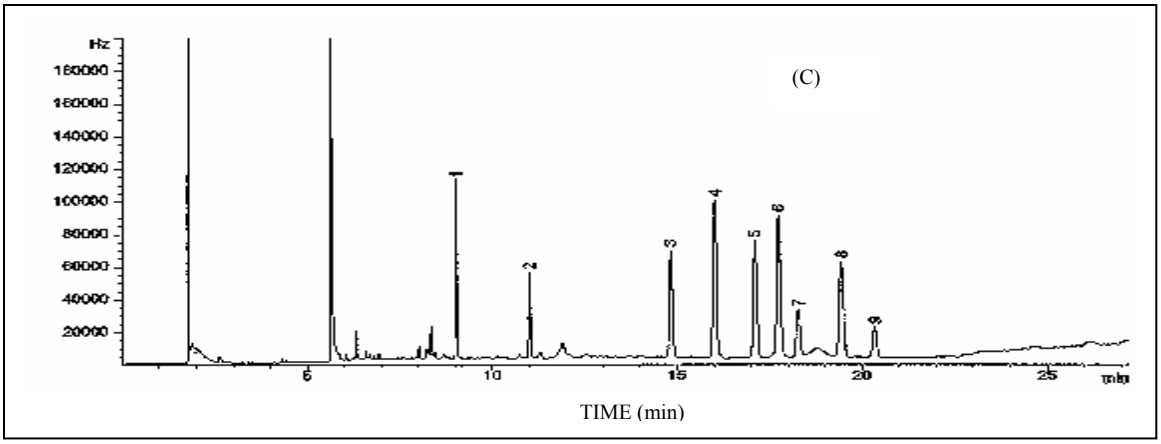

Figure 2. GC chromatograms of cucumber extract after SAX/NH_2 (A), C_{18} (B) and silica gel (C) cleanup. Peaks: 1, γ-HCH; 2, heptachlor; 3, α-endosulfan; 4, dieldrin; 5, β-endosulfan; 6, pp'-DDD; 8,endosulfan sulphate; 9, pp'-DDT

The recoveries obtained for 9 OC pesticides fortified in the green mustard samples using the SAX/NH_2, C_{18} and silica gel cleanups are given in Table 3. At 0.5 ppm fortification level, the recoveries obtained for all the OC pesticides using the SAX/NH_2 cleanup were found within the acceptable range. For the C_{18} cleanup, the recoveries obtained were lower as compared to the SAX/NH_2 and silica gel methods. The recoveries obtained for all the OC pesticides were found within the acceptable range except for heptachlor and op'-DDT. Good recoveries of 72.0 % to 103.3 % were obtained for the OC pesticides using the silica gel method. At 0.1 ppm fortification level, the recoveries for the OC pesticides using the SAX/NH_2 cleanup were within the acceptable range except op'-DDT. For the C_{18} method, the recoveries obtained for all the OC pesticides except heptachlor were found within the acceptable range. Good recoveries of 71.7 % to 100.3 % were obtained using the silica gel method.

Table 3. Recovery of OC pesticides from green mustard samples using different cleanup methods

	0.5 ppm			0.1 ppm		
Pesticide	SAX/NH_2	C_{18}	Silica gel	SAX/NH_2	C_{18}	Silica gel
	% Rec.[(a)] ± CV	% Rec.[(a)] ± CV	% Rec.[(a)] ± CV	% Rec.[(a)] ± CV	% Rec.[(a)] ± CV	% Rec.[(a)] ± CV
γ-HCH	81.0 ± 6.1	77.3 ± 6.7	72.3 ± 5.0	81.3 ± 6.5	70.7 ± 5.1	71.7 ± 3.2
Heptachlor	85.3 ± 8.3	66.7 ± 4.6	72.0 ± 5.6	94.7 ± 1.5	62.0 ± 4.0	73.7 ± 4.2
α-endosulphan	90.0 ± 7.0	78.7 ± 5.5	100.0 ± 6.1	81.3 ± 4.1	76.3 ± 6.7	94.7 ± 5.0
Dieldrin	95.7 ± 7.1	85.0 ± 2.7	103.3 ± 4.7	75.7 ± 4.1	86.7 ± 4.0	98.7 ± 3.1
β-endosulphan	96.3 ± 8.1	73.7 ± 1.5	95.0 ± 1.7	91.7 ± 2.5	86.0 ± 5.3	100.3 ± 6.1
pp'-DDD	93.7 ± 7.6	76.0 ± 4.6	101.0 ± 4.6	78.7 ± 4.7	82.0 ± 1.0	97.0 ± 4.4
op'-DDT	102.0 ± 9.5	62.7 ± 8.0	100.0 ± 1.0	58.0 ± 7.0	82.0 ± 2.0	81.3 ± 3.1
Endosulphan-sulphate	92.0 ± 7.8	73.3 ± 2.5	97.7 ± 4.7	87.0 ± 4.4	86.3 ± 4.9	98.0 ± 7.2
pp'-DDT	115.0 ± 9.5	70.3 ± 8.1	102.7 ± 8.4	86.7 ± 6.0	72.3 ± 7.6	72.0 ± 7.0
AV	94.6	73.7	93.8	81.7	78.3	87.5
SD	9.8	6.6	12.5	10.8	8.5	12.6

AV = average mean SD = standard deviation CV = coefficient of variation (a) n = 3

The chromatograms obtained for the green mustard using the SAX/NH_2, C_{18} and silica gel cleanups are shown in Figure 3. The chromatograms showed no interference peaks between 9 min and 21 min regions, where the OC pesticides were eluted. A large peak was found at 8.2 min in the SAX/NH_2 chromatogram. The LOD obtained using these cleanup methods was 0.01 ppm.

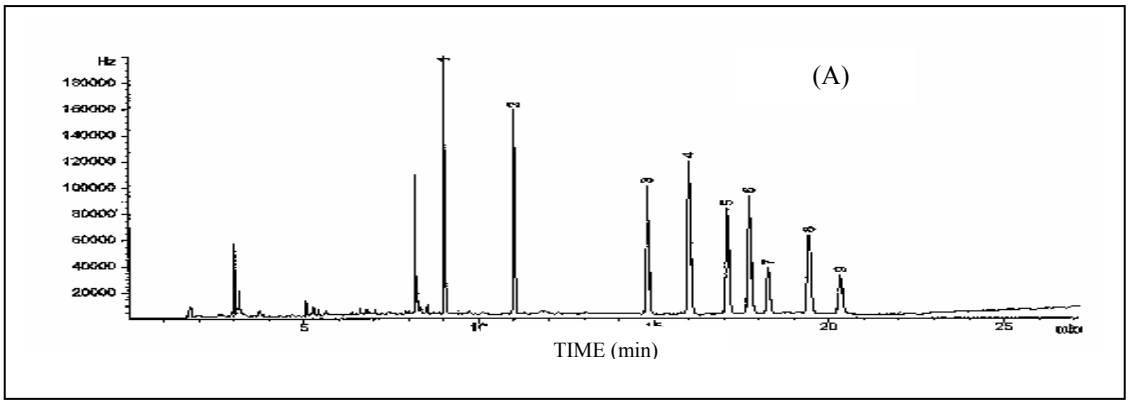

Figure 3. GC chromatogram of green mustard extract after SAX/NH_2 (A), C_{18} (B) and silica gel (C) cleanup. Peaks : 1, γ-HCH; 2, heptachlor; 3, α-endosulfan; 4, dieldrin; 5, β-endosulfan; 6, pp'-DDD; 8,endosulfan sulphate; 9, pp'-DDT

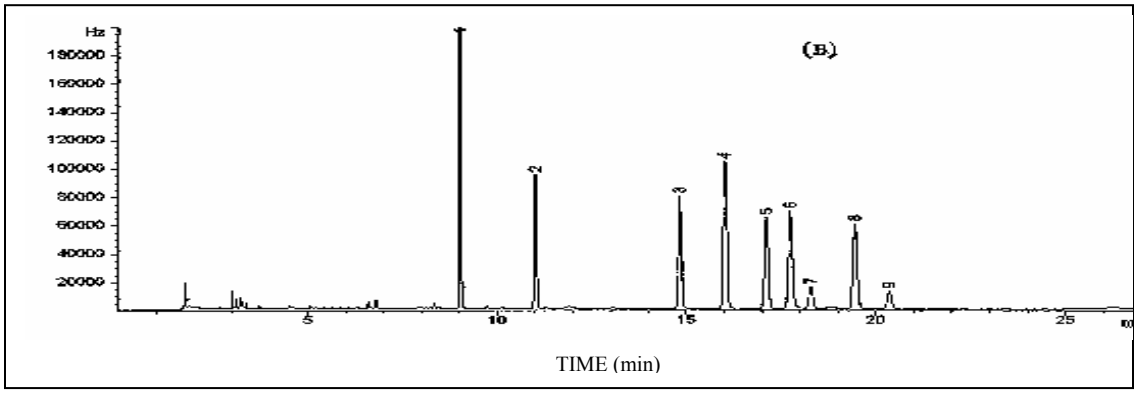

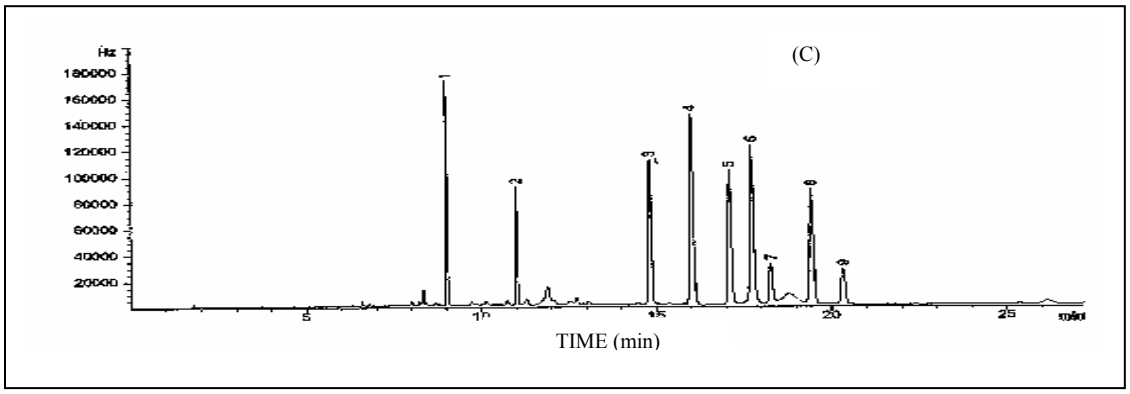

Conclusion

The studies on the SPE cleanup methods showed that SAX/NH_2 and C_{18} have the potentials to be used as an alternative method to the silica gel method currently used for OC pesticides cleanup in the laboratory. Comparable recoveries were obtained for both cleanup methods and no interfering peaks were encountered in the chromatograms. In spite of the limited range of this study, it can be predicted that the SPE cleanup can be successfully extrapolated to other pesticides and vegetables. The benefits of the SPE method compared to the silica gel method were the use of organic solvents is reduced, possibility of concentration the samples, less sorbent used, no cross-contamination and shorter analysis time.

Acknowledgement

The authors wish to thank the Universiti Malaysia Sarawak and Director of Agriculture Sarawak and Senior Assistant Director (Research) for their support of this project and permission to publish this paper. The technical assistance rendered by staff of the Pesticide Residue Laboratory especially Mr. Phillip Gudom is greatly acknowledged.

References

1. Hsu, R. C., Biggs, I. & Saini, N.K. (1991). Solid-phase extraction cleanup of halogenated organic pesticides. *J. Agric. Food Chem*. **39**, 1658-1666.

2. Lee, S.M., Papathakis, M.L., Feng, H.M., Hunter, G.F. & Carr. J.E. (1991). Multipesticide residue method for fruits and vegetables. *Fresenius J. Anal. Chem*. **339**, 376 - 383.

3. Holstege, D.M., Scharberg, D.L., Richardson, E.R. & Moller, G. (1991). Multiresidue screen for organophosphorus insecticides using gel permeation chromatography-silica gel cleanup. *J. Assoc. Off. Anal. Chem*. **72,** 394 - 399.

4. Fillion, J., Sauve, F. & Selwyn, J. (2000). Multiresidue methods for the determination of residues of 251 pesticides in fruits and vegetables by gas chromatography with florescence detection. *J. AOAC Int.* **83,** 698 - 713.

5. Chai L.K. & Lau, S. (2003) Comparative studies on the cleanup procedures for the determination of pyrethroid pesticides in vegetables. 16th Malaysian Symposium of Chemical Analysis, Kuching, Sarawak

6. Steinwandter, H. (1985). Universal 5-min on-line method for extracting and isolating pesticide residues and industrial chemicals. *Fresenius Z. Anal. Chem*. **322,** 752 - 754.

7. Parker, G.A. (1991). Validation of methods used in the Florida Department of Agriculture and Consumer Services Chemical Residue Laboratory. *J. Assoc. Off. Anal. Chem*. **74,** 868 - 871.

Malaysian Journal of Analytical Sciences, Vol.9 No. 3(2005): 542 - 551

SURFACE COVERAGE AND ACIDITY STUDIES OF BIFUNCTIONAL OXIDATIVE ACIDIC CATALYST BY INFRARED SPECTROSCOPY, ZIRCONIUM SULFATE LOADED TS-1

Zainab Ramli[1], Didik Prasetyoko[1], Hadi Nur[2] and Salasiah Endud[1]

[1]*Department of Chemistry, Faculty of Sciences, Universiti Teknologi Malaysia,81310, Skudai-Johor, Malaysia.*
[2] *Institute Ibnu Sina Fundemental Science Studies, Universiti Teknologi Malaysia, 81310, Skudai Johor, Malaysia*

Abstract*:* Bifunctional oxidative and acidic catalysts were prepared by dispersion of zirconium sulfate at various loading (2–20 wt%) on the titanium silicalite (TS-1) using wet impregnation method. The solids were calcined at 500°C before characterizing the acidity by infrared spectroscopy technique using pyridine as a probe base molecule. Results showed that both Lewis and Bronsted acidities present in the sample. However the Bronsted acid sites are only present in samples with high zirconia sulfate loading, i.e. 15 and 20 wt%, which equal to 1.76 and 2.28 Zr^{4+}/nm^2 TS-1, respectively. The formation of Bronsted acid sites is due to the presence of disulfate species on the surface of TS-1, in which based on XRD data, sample contains double layer of zirconium.

Abstrak: Mangkin dwifungsi oksida dan asid disediakan dengan penyebaran zirkonium sulfat pada berbagai muatan (2-20 wt%) pada titanium silikalit menggunakan kaedah pengisitepuan basah. Hasil pepejal dikalsin pada 500°C sebelum pencirian sifat keasidan dilakukan menggunakan teknik spektroskopi inframerah dengan piridina sebagai molekul prob bes. Keputusan menunjukkan kedua-dua keasidan Lewis and Bronsted wujud pada sampel tetapi asid Bronsted hanya terdapat pada sampel dengan muatan zirkonia sulfat yang tinggi i.e. 15 dan 20 wt% yang setara dengan 1.76 dan 2.28 Zr^{4+}/nm^2 TS-1. Pembentukan asid Bronsted disebabkan oleh kehadiran spesies disulfat pada permukaan TS-1 yang menurut data XRD, sampel tersebut mengandungi dua lapisan zirkonium.

Keywords: bifunctional catalyst, zirconium sulfate, TS-1, acidity, monolayer coverage

Introduction

Development of an efficient catalyst is important in the area of catalysis. Bifunctional oxidative and acid catalyst is one of the types and interesting catalysts that have potential uses in organic synthesis involving both oxidative and acidic sites. These catalysts have been prepared by incorporation of trivalent metal ions (Al^{3+}, B^{3+}, Fe^{3+}, Ga^{3+}) and titanium ion (Ti^{4+}) together in the framework of zeolites. Our group has developed the bifunctional catalysts using titanium silicalite (TS-1) with Ti^{4+} as the oxidative site, and metal oxides as acidic sites.

Sulfated zirconia has been paid much attention due to its significant catalytic activity in many hydrocarbon conversions [1-4]. The activity is mainly related to its acidic properties of the catalysts. Some authors are convinced that the catalysts contain both Bronsted and Lewis acid sites, which are responsible for the activity. Several studies have been done on the structure and activity of zirconia-loaded silica or alumina [5-8]. This work concentrates on the influence of the zirconium content to the acidity of the zirconium sulfate loaded titanium silicalite. In this study, Fourier transformed infrared spectroscopy (FTIR) technique was used to characterize the acidity of the catalyst using pyridine as probe base molecule as well as the metal layer coverage on the TS-1 sample.

Experiment

Preparation of Sample

Titanium silicalite, TS-1 (1% of titanium, %mol) was prepared according to the procedure described earlier by Taramasso *et a.l*[9]. The acidic precursor, white powder of zirconium sulfate anhydrous was prepared by drying of the zirconium sulfate hydrate [$Zr(SO_4)_2$ $4H_2O$] at 110°C for 72 hrs. The solid obtained was ground, followed by calcination at 500°C for 7 hrs. The calcined materials were denoted as ZS500.

Zirconium sulfate containing TS-1 was prepared by wet impregnation method. The TS-1 was added into a solution of zirconium sulfate hydrate. The mixture was stirred at room temperature for 3 hrs, followed by evaporation of the solvent at 60^{o}C. The solid was dried at 100^{o}C for 24 hrs. and calcined at 500^{o}C for 7 hrs. The resulting sample was denoted as *X*SZ/TS-1, in which *X* is the percentage of zirconium added in the sample. Table 1 summarizes the zirconium containing the samples and the preparation conditions.

Table 1. Zirconium content and preparation conditions of the samples

Sample	ZrO_2, wt%	Temp. (^{o}C); time (hrs.)
ZS500	100	500; 7
TS-1	0	550; 5
2ZS/TS-1	1.8	500; 7
5ZS/TS-1	5.1	500; 7
10ZS/TS-1	9.9	500; 7
15ZS/TS-1	15.5	500; 7
20ZS/TS-1	20.3	500; 7

.

Characterization

All samples were characterized by powder X-ray diffraction (XRD) for crystallinity and phase content of the solid materials, using Bruker Advance D8 Difractometer with the Cu Kα (λ=1.5405 Å) radiation as the diffracted monochromatic beam at 40 kV and 40 mA. Typically, powder samples were ground and spread into a sample holder before XRD scan. The pattern was scanned in the 2θ ranges between 20^{o} to 40^{o} at a step 0.020^{o} and step time 1 second. Infrared (IR) spectra of the samples were collected on a Shimadzu Fourier Transform Infrared (FTIR), with a spectral resolution of 2 cm^{-1}, scans 10 second, at temperature 20^{o}C. For acidity study, the wafer of the sample (10-12 mg) was prepared and locked in the cell equipped with CaF_2 windows, and evacuated at 400^{o}C under vacuum condition for 4 hrs. Infrared spectra of the sample were recorded at room temperature in the hydroxyl region of 4000 – 3000 cm^{-1} and pyridine vibration region at 1700 – 1300 cm^{-1}.

Results and Discussions

X-ray Diffraction

Zirconium sulfate (ZS) at various contents were dispersed on TS-1. Samples were characterized by XRD and FTIR techniques. Figure 1 shows the XRD patterns of the ZS500 and ZS/TS-1 samples. The XRD pattern of all ZS/TS-1 samples show only the diffractogram pattern of the TS-1 crystal with the absence of the diffraction line for tetrahedral or monoclinic phases of zirconia. This indicates that the ZS is highly dispersed on the surface of TS-1. It is found that the MFI structure of TS-1 is still maintained after the ZS loading. However, the XRD peaks intensities of TS-1 decrease as the loading amount of the ZS increased. It might be due to the percentage amount of the TS-1 in the samples decreased as the loading amount of the ZS increased.

The monolayer coverage of ZrO_2 can be determined from the graph of the diffraction line intensity of TS-1 at 2θ=23^{o} vs loading amount of zirconium on the samples as shown in Figure 2. It is observed that the diffraction lines of samples 2ZS/TS-1 and 5ZS/TS-1 have similar intensities to that of the parent TS-1, while for samples 10ZS/TS-1, 15ZS/TS-1 and 20ZS/TS-1 have shown lower intensities. Hence, a horizontal line can be drawn for low ZS loading and another straight line with tangent for higher ZS loading. The interception of the two lines occurs at the value 6

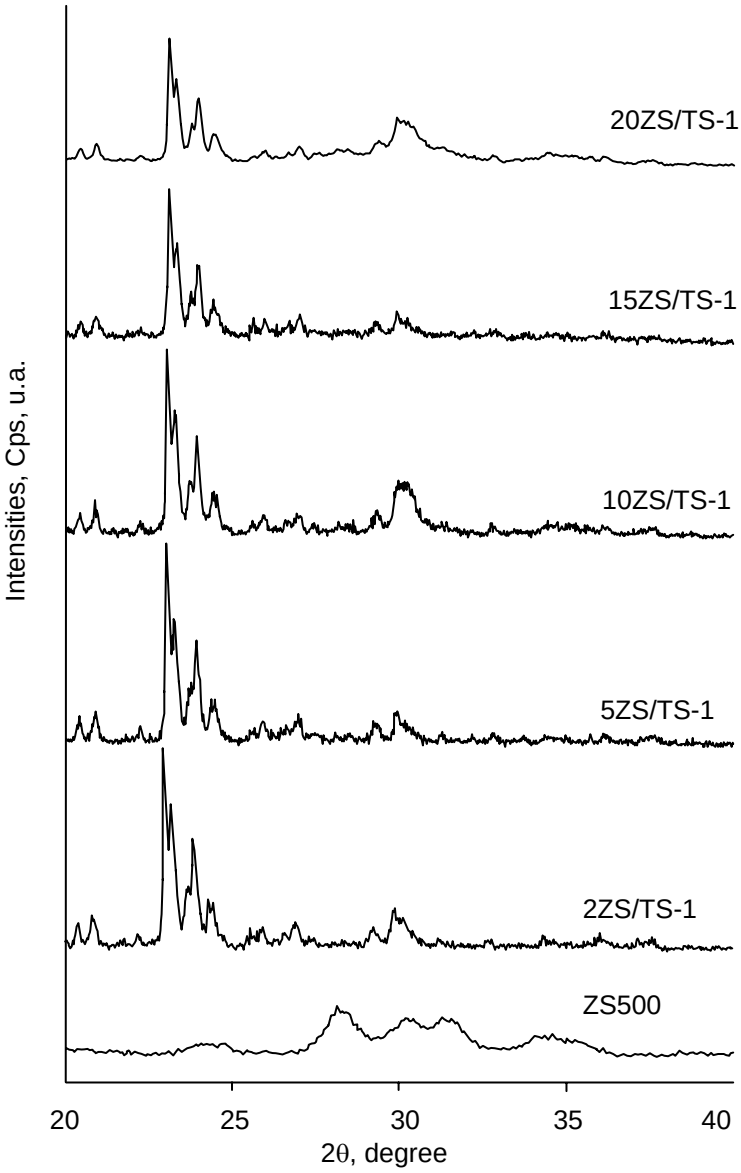

Figure 1. XRD pattern of the ZS500 and ZS/TS-1 samples

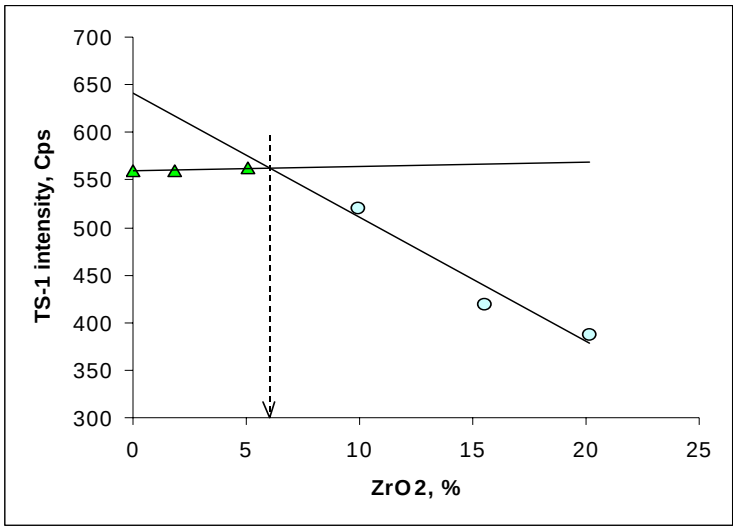

Figure 2. The graph of peak intensity of TS-1 at $2\theta = 23^{o}$ vs. loading amount of zirconium on the samples

wt%. By using the Equation 1 for calculating the surface concentration of metal dispersed in the support [10], this interception value is equal to 0.65 Zr^{4+}/nm^2 TS-1 which corresponds to the value for monolayer dispersion capacity of zirconium on the TS-1

$$C_M = \left(\frac{L_{MOx}/100}{M_{MOx}}\right)\left(\frac{N_0}{S_{BET} \times 10^{18}}\right) \quad \ldots\ldots\ldots\ldots \quad \text{Equation 1}$$

with, C_M = the surface concentration of metal dispersed (M^{n+} cations nm^{-2});
L_{MOx}, = the loading amount of metal oxides (wt.%);
M_{Mox} = the formula weight of metal oxides used;
N_0 = Avogadro constant (6.023×10^{23}), and
S_{BET} = the specific surface area ($m^2\ g^{-1}$) = 300 $m^2\ g^{-1}$ (for TS-1).

Infrared Spectroscopy

Figures 3 and 4 show the FTIR spectra of the ZS/TS-1 samples after evacuation at 400°C for 4 hrs in vacuum. In the region of hydroxyl groups (Figure 3), the peak of silanol groups at 3745 cm^{-1} of TS-1 support can still be observed for samples with low loading amount of the ZS (2ZS/TS-1 and 5ZS/TS-1). However, the peak disappeared in samples with higher ZS loading (10-20ZS/TS-1). This finding suggests that the monolayer coverage of the ZS on the TS-1 is in the ranges of 5 to 10 wt% of zirconium (0.57 to 1.12 Zr^{4+}/nm^2 TS-1), in which all silanol groups or surface of TS-1 have been covered with ZS with the maximum amount of 1.12 Zr^{4+}/nm^2 TS-1. This results supports the XRD finding for the determination of monolayer dispersion, with the value 0.65 Zr^{4+}/nm^2 TS-1.

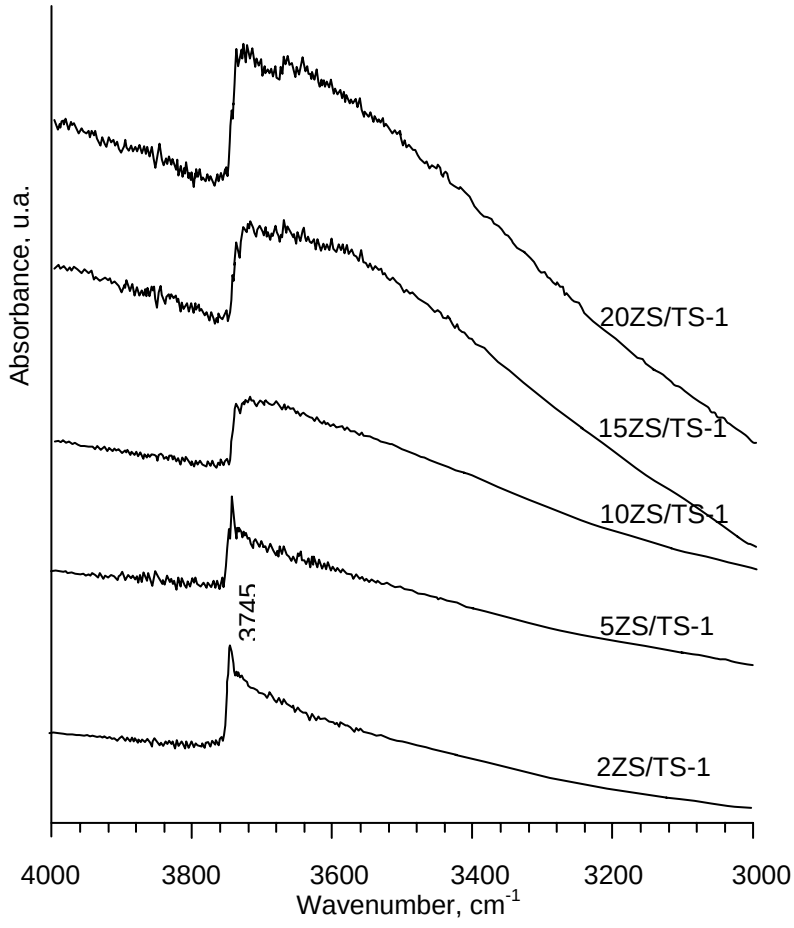

Figure 3. FTIR spectra of the ZS/TS-1 samples after evacuation at 400°C for 4 hrs in vacuum condition.

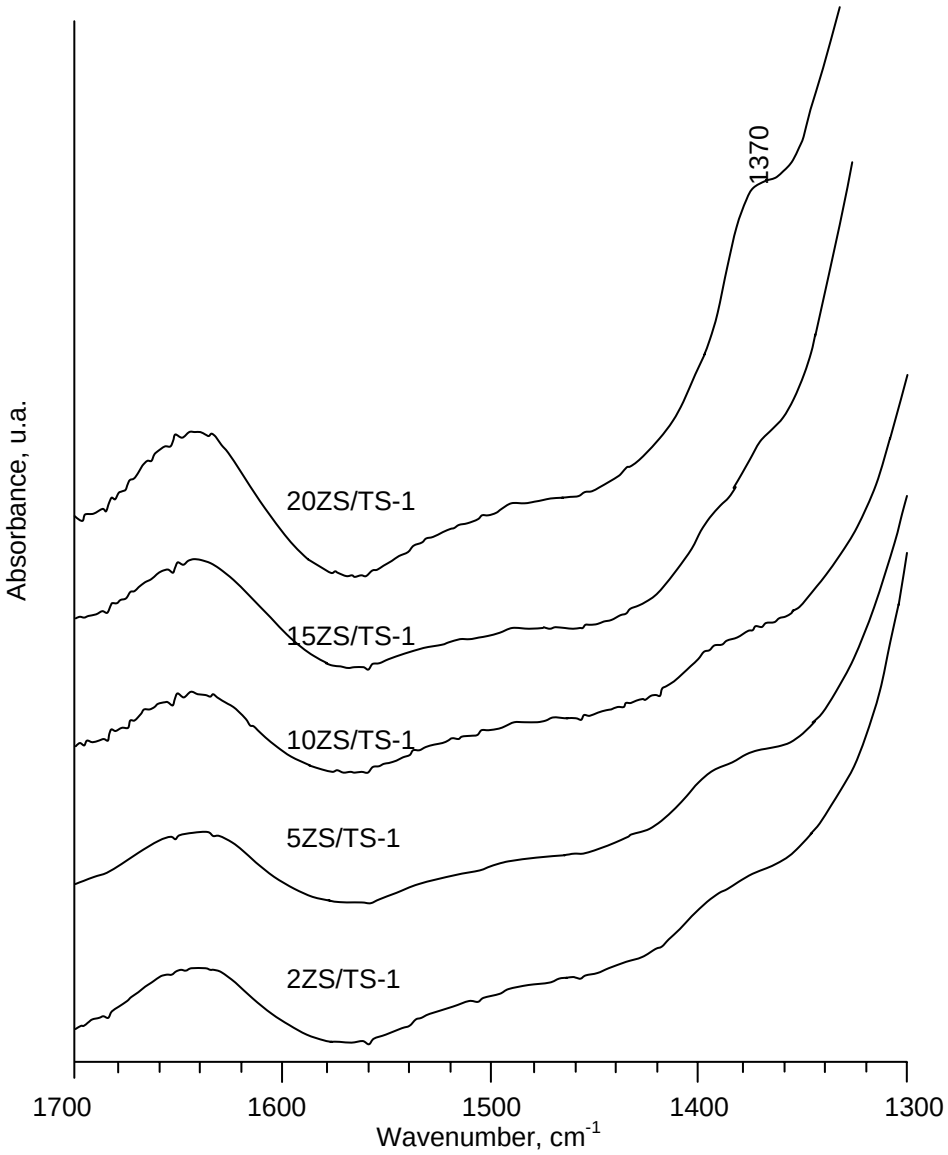

Figure 4. FTIR spectra of the ZS/TS-1 samples in the pyridine and sulfate region

The FTIR spectra of the ZS/TS-1 samples in the pyridine and sulfate region are shown in Figure 4. It is found that no peak vibration of pyridine is observed in all samples. Meanwhile, in the sulfate region in the ranges of 1400 – 1300 cm^{-1}, samples with 2-10wt% of ZS loading (samples 2ZS/TS-1, 5ZS/TS-1, and 10ZS/TS-1) show similar pattern, without peak assign for sulfate vibration. While samples with 15 and 20wt% of ZS loading (samples 15ZS/TS-1 and 20ZS/TS-1) started to show additional peak at 1370 cm^{-1}. This peak is assigned for asymmetric $\nu_{S=O}$ [11]. In addition, the intensity of the peak is significantly high in sample 20ZS/TS-1, as expected as the amount of ZS loading increased.

It is interesting to relate the surface coverage from the infrared finding with that of the XRD. The XRD data found that the monolayer dispersion is 0.65 Zr^{4+}/nm^2 TS-1, while FTIR data has shown that the asymmetric $\nu_{S=O}$ appeared on sample 15ZS/TS-1 (1.76 Zr^{4+}/nm^2 TS-1), but not for sample 10ZS/TS-1 (1.12 Zr^{4+}/nm^2 TS-1). At the value of 1.12 Zr^{4+}/nm^2 TS-1, the $\nu_{S=O}$ asymmetric is not appeared although this sample has zirconium content almost double compared to the amount of zirconium monolayer dispersion capacity from the XRD data i.e. 0.65 Zr^{4+}/nm^2 TS-1). The $\nu_{S=O}$ asymmetric is only started to appear in sample at the value 1.76 Zr^{4+}/nm^2 TS-1 which contains zirconium higher than that of the double monolayer capacity. It can be suggested that the second layer coverage will be formed after the formation of monolayer on the solid support. Therefore, it can be proposed that the asymmetric $\nu_{S=O}$ can only be observed on the sample ZS/TS-1 that contains double layer of ZS which is equal to 1.3 Zr^{4+}/nm^2 TS-1.

Pyridine Adsorption

The acidity of the samples ZS/TS-1 was monitored by FTIR spectroscopy. The types of acid sites were measured by FTIR using pyridine as probe molecule. The pyridine is adsorbed into the sample at room temperature after evacuation at 400^{o}C under vacuum. The spectra were taken at room temperature after evacuation at 150^{o}C for 1 hr. The spectra of the sample after pyridine adsorption in the region of hydroxyl groups are shown in Figure 5. It is found that, there are no significant changes of the spectra as compared to before pyridine adsorption (Figure 3). The silanol peak is still present after pyridine adsorption, indicates that the silanol groups is not reacting with pyridine. It is concluded that the silanol groups is not acidic sites. In the regions of pyridine and sulfate as displayed in Figure 6, samples 2ZS/TS-1, 5ZS/TS-1 and 10ZS/TS-1 show similar peaks at 1608 and 1444 cm^{-1}. These bands appeared when adsorbed pyridine coordinatively bound with Lewis acid sites. Meanwhile, samples 15ZS/TS-1 and 20ZS/TS-1 show additional absorption bands at 1640 and 1545 cm^{-1} correspond to pyridine interacting with the Brønsted acid sites. In addition, the peak for asymmetric $\nu_{S=O}$ disappeared after the adsorption of pyridine, indicating that the S=O is bound to pyridine. This finding suggests that the S=O acts as an active acid sites. Since the source of S=O is the ZS it indicates that ZS at high loading is responsible to the formation of Brønsted acid site in the sample. In this case, the ZR at high loading exists as the disulfate zirconium [12]. It further proves that Brønsted acid sites only present in samples containing the disulphate species, whereas samples with monolayer of zirconium having monosulfate without Brønsted acid property.

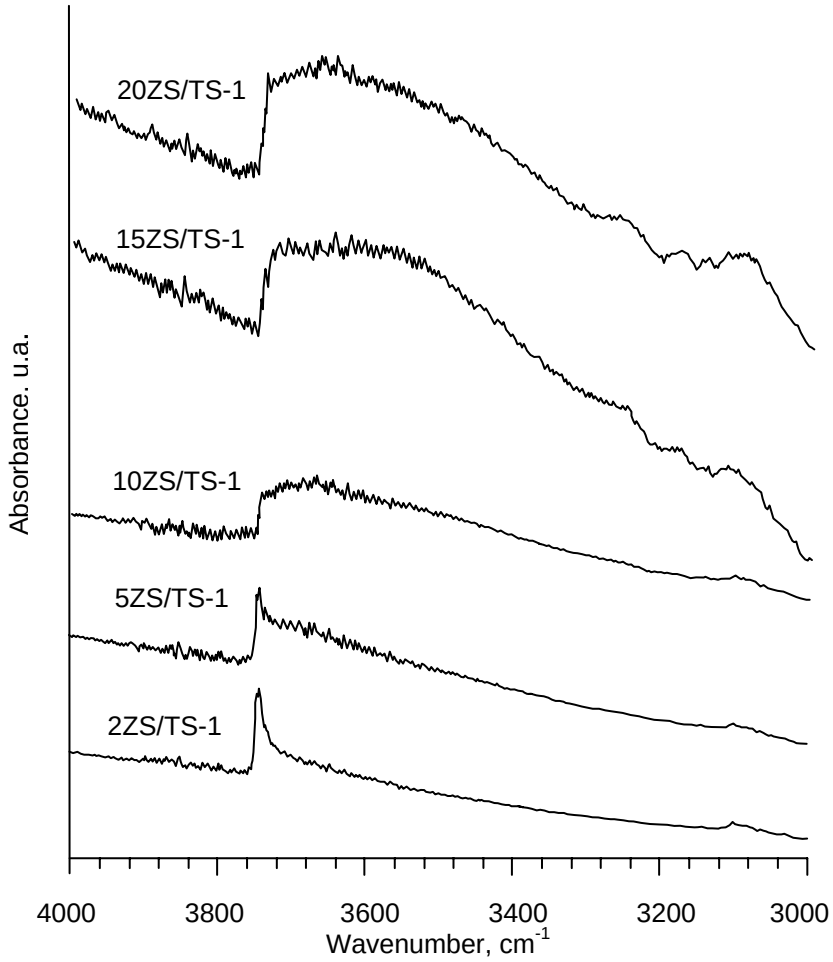

Figure 5. FTIR spectra of the ZS/TS-1 samples after pyridine adsorption and evacuation at 150^{o}C for 1 h. in the hydroxyl region

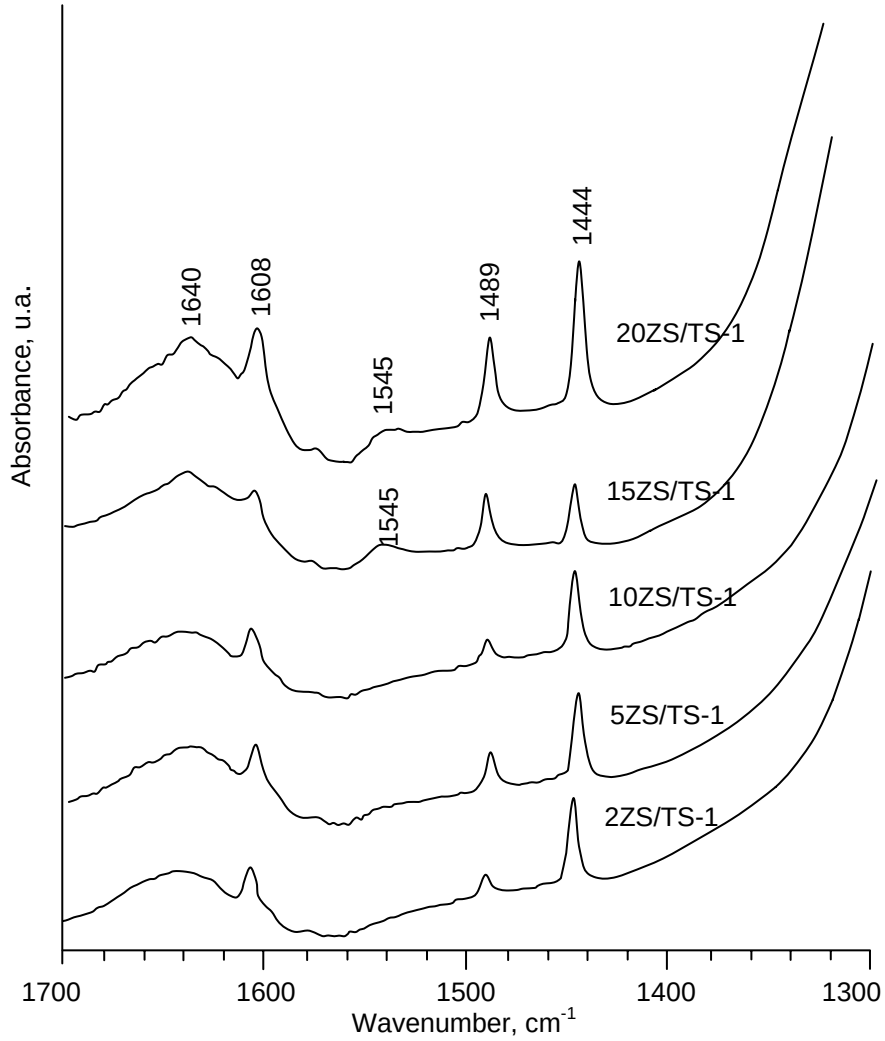

Figure 6. FTIR spectra of the ZS/TS-1 samples after pyridine adsorption and evacuation at 150°C for 1 h. in the pyridine and sulfate regions

The amount of acid sites are calculated based on the area under the peak at 1545 and 1444 cm^{-1} characteristic for Brønsted and Lewis acid sites, respectively (Figure 7). For sample 15ZS/TS-1 and 20ZS/TS-1, the amount of Brønsted acid sites is found to be insignificantly increased with the increase of ZS loading. This finding suggests that the Brønsted acid site is only correlates with the formation of double layer of zirconium, but not directly corresponds with the amount of zirconium loading. Meanwhile, samples 2ZS/TS-1, 5ZS/TS-1 and 10ZS/TS-1 have similar amount of Lewis acid sites. By comparing with the first three samples, sample 15ZS/TS-1 has shown lower amount of Lewis acid sites, while sample 20ZS/TS-1 has slightly higher amount of Lewis acid. These results indicate that for the samples containing less than double layer of zirconium, no correlation can be deduced between zirconium concentration and the amount of Lewis acid sites. However, for sample containing double layer of zirconium, the Lewis acid sites increased significantly as the ZS loading increased. Therefore, the high loading of ZS is also responsible for the formation of Lewis acid sites on the sample.

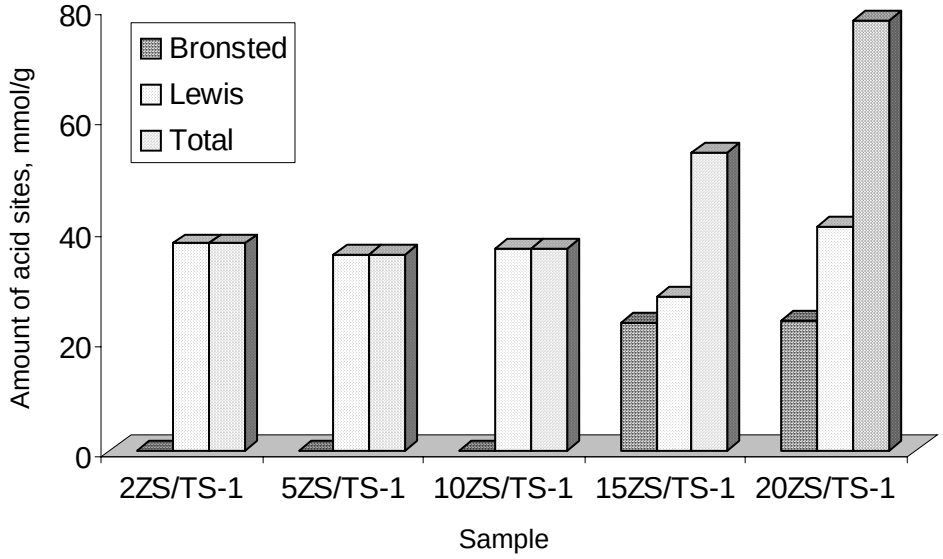

Figure 7. Amount of Brønsted and Lewis acid sites of the samples ZS/TS-1 calculated based on the pyridine peak after evacuation at 150°C for 1 h.

The strength of Brønsted and Lewis acid sites was monitored by evacuation of the pyridine-adsorbed on sample ZS20/TS-1 at different temperatures, i.e. 150, 300, and 400°C for 1 hr. under vacuum. Figure 8 shows the FTIR spectra of the sample after evacuation at different temperatures, taken at room temperature. Generally, the amount of Brønsted and Lewis acid sites decreased as evacuation temperature increased, showing that the sample contains different strength of both acid sites. However, both Brønsted and Lewis acid sites are still present in the sample after evacuation at high temperature, 400°C, indicating that the sample contains high strength of acid sites.

Conclusions

Surface characterization of zirconium sulfate loaded TS-1 catalysts using FTIR spectroscopy technique with pyridine as probe molecule showed that Bronsted acid sites are only present at the samples containing zirconium higher than double layer of surface coverage ca. >1.3 Zr^{4+}/nm^2 TS-1.

Acknowledgements

We gratefully acknowledge funding from The Ministry of Science Technology and Environment Malaysia, under IRPA grant no: 09-02-06-0057 SR0005/09-03 and Ibnu Sina Institute for Fundamental Science Studies, UTM.

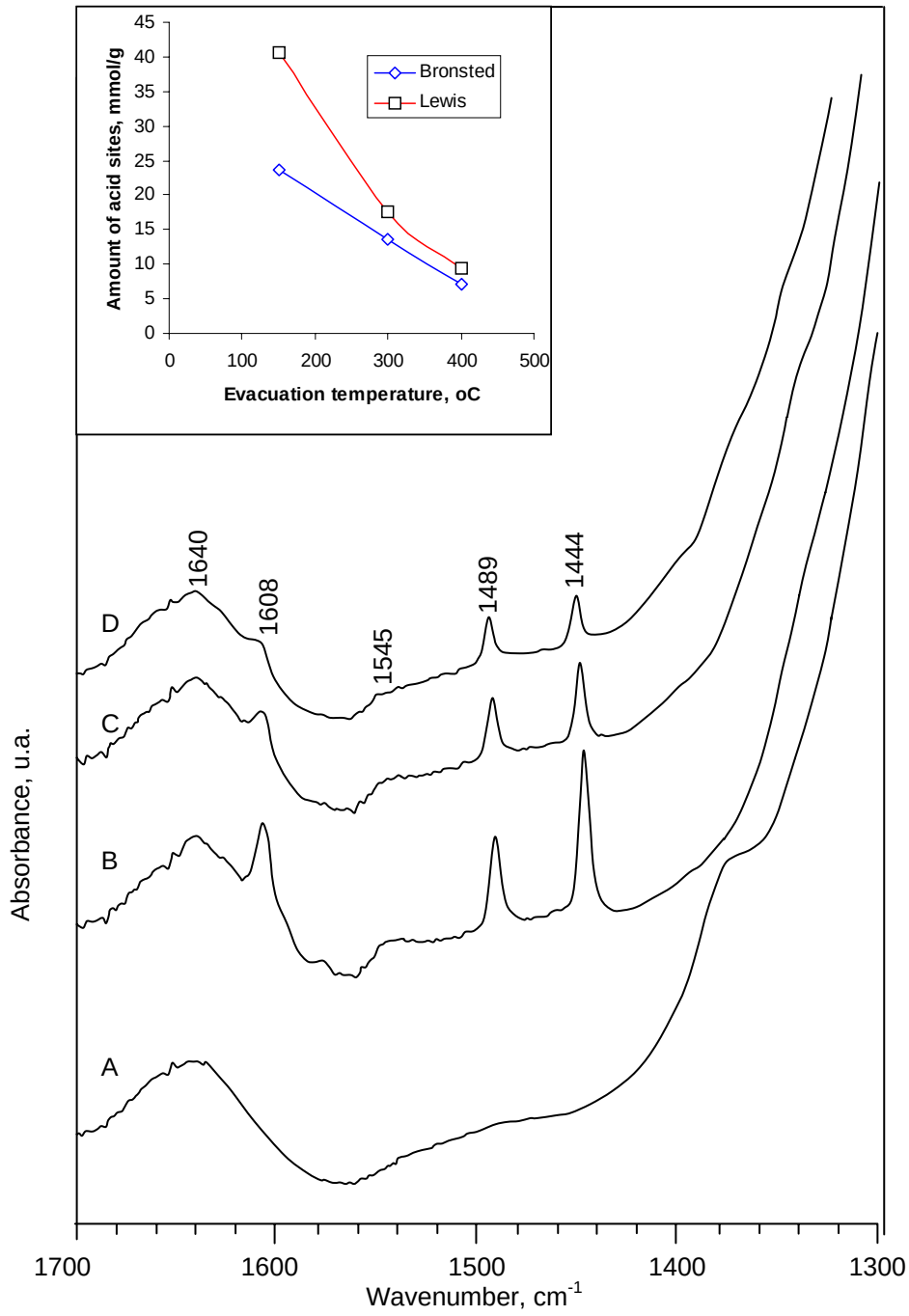

Figure 8. FTIR spectra of sample 20ZS/TS-1. (A). after evacuation at 400°C for 6 hrs., (B). after pyridine adsorption and evacuation at 150°C for 1 h., (C). after evacuation at 300°C, and (D). after evacuation at 400°C

References.

1. M. Hino, S. Kobayashi, and K. Arata, (1979). Solid catalyst treated with anion. 2. Reactions of butane and isobutane catalyzed by zirconium oxide treated with sulfate ion. Solid superacid catalyst. *J. Am. Chem. Soc*. **101**: 6439-6441.
2. B. H. Davis, R. A. Keogh, and R. Srinivasan, (1994). Sulfated zirconia as a hydrocarbon conversion catalyst. *Catal. Today*. 20: 219-256.
3. C. Y. Hsu, V. K. Patel, D. H. Vahlsing, J. T. Wei, and H. K. Myers, Jr., (1991). Liquid phase isomerization of alkanes. *United States Patent* 5,019,671.
4. G. D. Yadav, and J. J. Nair, (1999). Sulfated zirconia and its modified versions as promising catalysts for industrial processes, *Microporous and Mesoporous Mater.* 33: 1-48.
5. S. Damyanova, P. Grange, and B. Delmony, (1997). Surface Characterization of Zirconia-Coated Alumina and Silica Carriers. *J. Catal*. **168**: 421-430.
6. Y.Y.,Huang, B.Y. Zhao, and Y.C. Xie, (1998). A new method to prepare silica- or alumina-supported sulfated zirconia. *Appl. Catal. A: General.* **173**: 27-35.
7. T. Lei, J. S. Xu, Y. Tang, W. M. Hua, and Z. Gao, (2000). New solid superacid catalysts for *n*-butane isomerization: γ-Al_2O_3 or SiO_2 supported sulfated zirconia. *Appl. Catal. A: General.* **192**: 181-188.
8. J.R. Sohn and D.H Seo,. (2003). Preparation of new solid superacid catalyst, zirconium sulfate supported on γ-alumina and activity for acid catalysis. *Catal. Today.* **87**: 219-226.
9. M. Taramasso, G. Perego, B. Notari, (1983) Preparation of porous crystalline synthetic material comprised of silicon and titanium oxides. *United States Patent* 4,410,501
10. Y. Wang, Q. Chen, W. Yang, Z. Xie, W. Xu, D. Huang, (2003) Effect of support nature on WO_3/SiO_2 structure and butene-1 metathesis**.** *Appl. Catal. A: General* **250,** 25-37**.**
11. F. Babou, G. Coudurier and J. C. Vedrine. (1995). Acidic Properties of Sulfated Zirconia: An Infrared Spectroscopic Study, *J. Catal.,* **152**: 341-349.
12. E. E Platero, M. P. Mentruit, C. O. Areán and A. Zecchina. (1996). FTIR Studies on the Acidity of Sulfated Zirconia Prepared by Thermolysis of Zirconium Sulfate, *J. Catal.,* 162: 268-276**.**

Malaysian Journal of Analytical Sciences, Vol.9, No. 3(2005): 523 - 556

DETERMINATION OF ACTIVE INGREDIENTS IN PESTICIDE FORMULATIONS BY GAS CHROMATOGRAPHY WITH AN ELECTRON CAPTURE DETECTOR

Chai Mee Kin[1], Tan Guan Huat[2] and Asha Kumari[3]

[1]Dept. of Science and Mathematics, College of Engineering,Universiti Tenaga Nasional, Km 7, Jalan Kajang-Puchong, 43009 Kajang, Selangor.
Mkchai@uniten.edu.my Fax:03-89263506

[2,3]Dept. of Chemistry, Faculty of Science,Universiti Malaya, Lembah Pantai,50603 Kuala Lumpur.

ABSTRACT

A fast, reliable and effective method for direct determination of two active ingredients namely Chlorpyrifos, and Quinalphos in two pesticide formulations has been established by using Gas Chromatography – Electron Capture Detector (GC-ECD) with the internal standard method. A pure standard solution spiked with internal standard in methanol was sonicated to homogenise the solutions. 2 μL volume of a standard solution was injected. A six point calibration curve that demonstrated a linear range was established for each target compound. The concentration of active ingredients in pesticide formulations was calculated from peak area values at a retention time interpolated in a calibration graph was prepared. Analytical results obtained 36.91 ± 0.52 % of Chlorpyrifos and 10.59 ± 1.07 % of Quilnalphos were within specification for both commercial pesticide formulations.

Keywords: GC-ECD, pesticide formulation, Chlorpyrifos, Quinalphos

INTRODUCTION

Nowadays, organophosphorus (OP) pesticides are employed as an alternative to the inorganic and organochlorine (OC) pesticides because they are nonpersistent. Most of them have a short residue activity, which is desirable in keeping down residues in food crops. Chlorpyrifos and Quinalphos are two popular OP pesticides that are being used in Malaysia.

Chlorpyrifos (Chor; o,o-diethyl o-3,5,6-trichloro-2-pyridyl phosphorothioate) is a very popular pesticide against household pests such as mosquitoes, parasites in cattle and sheep, crop pests and termites as it has a broad range of insecticidal activity and is effective by contact, ingestion and vapor action, but it is not systemic [1]. The total amount of this pesticide imported in Malaysia from 1998 to 2001 was 1410,940 kg showing the widespread use of products containing Chlorpyrifos [2]. Chlorpyrifos is moderately toxic to humans. Poisoning from Chlorpyrifos may affect the central nervous system, the cardiovascular system and the respiratory system. It is used as an insecticide on grain, cotton, field, fruit, nuts and vegetable crops as well as on lawns and ornamental plants [1]. Chlorpyrifos is effective in controlling cutworms, corn rootworms, grubs, flea beetle, termites, fire ants and lice. Hence, the residue problem of Chlorpyrifos is one of the major issues nowadays.

Quinalphos (QP; o,o-diethyl, o-2 quino xalinyl phosphorothioate) is an organophosphorus insecticide and acaricide [3]. The imported OP amounts as an active ingredient in Malaysia from 1998 to 2001 was approximately 61,153 kg [2]. While pure QP is a colorless crystalline solid, the technical material is a liquid. The pure compound is stable at 20 ^{o}C for 1 year. The formulations are stable for 2 years. QP is used on vegetables, fruits, cotton, groundnuts, cereals and rice. It is rapidly metabolized in plants, animals and soil. QP is highly toxic to mammals with oral LD_{50} values ranging from 14 to 137 mg/kg in rats [3].

The accurate, reliable analysis of all components in pesticide formulations is important to public health because of their many field applications and the non-pesticidal components can facilitate pesticide dermal absorption, the major route of exposure, as well as permeation through protective materials [4]. Most studies regarding the separation and its determination in consumer products or the environmental samples by GC-ECD have been

reported [5-10]. Other procedures have been proposed for active ingredient determination in pesticide formulation using Fourier Transform Infrared Spectrometry[11-12], Liquid Chromatography [13-14], Derivative-Spectrophotometry [15], Gas Chromatography – Mass Spectrometry [4]. But very few studies have been performed on quantitation of active ingredients in pesticide formulation by using GC-ECD with the internal standard method.

The aim of this work is the development of a GC-ECD procedure for fast and accurate determination of Chlorpyrifos and Quinalphos in commercial formulations containing these two active ingredients.

Table 1 : The technical details of Chlorpyrifos and Quinalphos

Common Name	Chlorpyrifos	Quinalphos
Chemical Name	o,o diethyl o (3,5,6-trichloro-2-pyridyl) Phosphorothioate	o,o diethyl o-2-Quinoxalinyl phosphorothioate
Empirical Formula	$C_9H_{11}C_{13}NO_3PS$	$C_{12}H_{15}N_2O_3PS$
Molecular weight	350.6	298.3
Physical state	White to pale yellow granular solid	Colorless crystalline solid
Water solubility	2 ppm at 25 ^oC	22 ppm at 24 ^oC
Solubility in organic solvents	Methyl alcohol 45%, Iso-octane 75%, soluble in most organic solvents	Soluble in methanol, ethanol, ether, ketones, aromatic solvents.
Oral LD50 in rats	95-270 mg/kg	14 to 137 mg/kg

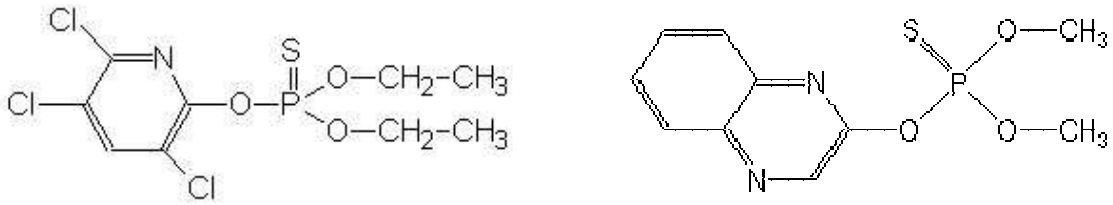

Chlorpyrifos Quinalphos

Figure 1 : The structure of Chlorpyrifos and Quinalphos

EXPERIMENTAL

Reagents

Two commercial formulations, Chlorpyrifos (37.10 % w/w) and Quinalphos (10.90 % w/w) were obtained from the Pesticide Control Division, Department of Agriculture. Pesticide standards of 100 % purity in methanol solution (100 µg/mL) were purchased from Accustandard Inc. New Haven CT. USA. The methanol solvent (HPLC grade) was obtained from Fisher Scientific, Loughborough, USA and was filtered through a 0.45 µm filter from Millipore.

Instrument

A Shimadzu GC-17A fitted with an Electron Capture Detector (ECD) – ECD 17 ver. 2 was used. Nitrogen (99.9999 % purity) was used as the carrier gas in the GC. Analyses were carried out with a SGE 30m QC2/BPX5 capillary column where BPX5 is 5% phenyl equivalent modified siloxane of 30 m long x 0.32 mm ID. The integrator used is a Shimadzu C-R6A Chromatopac. Isothermal condition was applied in this study. Nitrogen carrier gas flow was established at 33 cm/sec linear velocity and the oven temperature was 230 ^oC. The injection volume was 2 µL with the split mode ratio of 1:36. The injector temperature was 250 ^oC and the detector temperature was 300 ^oC.

Procedure

For the internal standard calibration, a series of standard Quinalphos solutions containing 6 concentration levels were prepared by serially diluting with methanol. To each calibration standard, a known constant amount of

internal standard (0.5 ppm Chlorpyrifos) was added. For the analysis of the active ingredient in the commercial formulation, 1.00 g of Quinalphos commercial pesticide formulation was accurately weighted into a 10 mL volumetric flask and dissolved with methanol. The solutions were serially diluted with methanol and a known constant amount of internal standard was added. The solutions were sonicated for 5 minutes in an ultrasonic water bath to homogenize the sample solutions [12]. 2 µL was injected into a gas chromatograph fitted with an ECD. This procedure was repeated for the determination of Chlorpyrifos using Quinalphos (20ppm) as the internal standard.

Determination

First, the response of peak area against concentration of standard solutions and internal standard was tabulated. The Response Factor (RF) for each analyte was calculated using the following equation. The RF is a unitless value [16].

$$RF = \frac{(A_S)\,(C_{IS})}{(A_{IS})\,(C_S)}$$

Where A_S = Response for the analyte to be measured
A_{IS} = Response for the internal standard
C_{IS} = Concentration of internal standard
C_S = Concentration of the analyte to be measured

If the RF value within the working range is constant (20% RSD or less) the average RF can be used for the calculation. Alternatively, the result can be used to plot a calibration curve of response ratio (A_S/A_{IS}) vs C_S [16]. Then the concentration of the active ingredient in the commercial formulations was calculated from peak area value at a retention time, interpolated in a calibration graph prepared for pure standards spiked with the internal standard and using the response ratio data for each injection. The repeatability of each peak area measurement was evaluated for 10 consecutive injections. 8 out of 10 results were used for the calculation.

RESULTS AND DISCUSSION

The chromatogram of the standard solution determined by using the GC-ECD with internal standard method is shown in Figure 1. Baseline resolution of the compound and internal standard is achieved in 14 minutes.

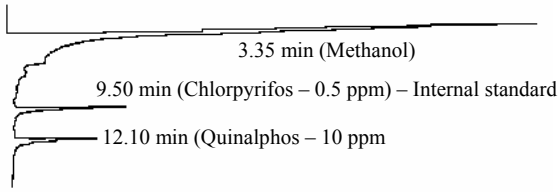

Figure 1a : Chromatography of the Quinalphos Standard Solution

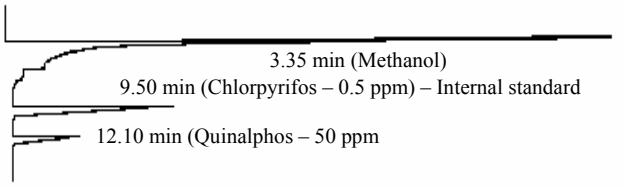

Figure 1b : Chromatography of the Quinalphos Commercial Pesticide Formulation

Retention times observed for Chlorpyrifos and Quinalphos were 9.5 minutes and 12.10 min respectively. From the chromatograms obtained, it is clear that the ECD is extremely sensitive to molecules containing highly electronegative functional groups such as chlorine since the peak area of the Chlorpyrifos at 0.5 ppm is much higher than that of Quinalphos at 10ppm.

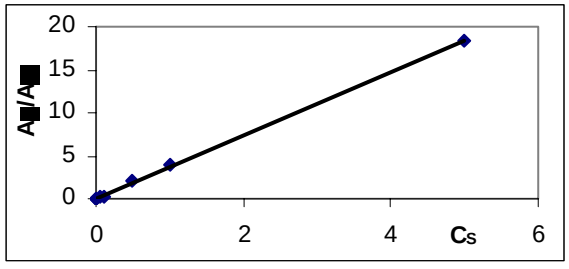

Figure 2a: Calibration Curve of Chlorpyrifos Standard Solution.

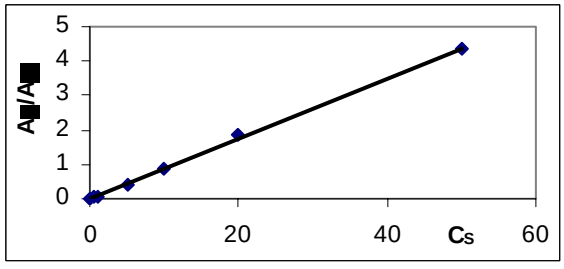

Figure 2b: Calibration Curve of Quinalphos Standard Solution.

A six point calibration curve was constructed using the ratio of peak area of the investigated pesticide against internal standard and concentration of the respective pesticide standard solution (Figure 2). Excellent statistical parameters of the calibration were obtained which are summarized in Table 2 together with the result of the formulation. The relative standard deviation (RSD) obtained were below 2%. The agreement was good between the actual formulation amount and the amount quantitated.

Table 2 : Statistical Parameters of Calibration and Results of Formulation

Compound	Chlorpyrifos	Quinalphos
Calibration Curve	Y = 3.6494 x + 0.0848	Y= 0.0875 x + 0.002
Corre. Coefficients (R^2)	0.9995	0.9994
Mean content in formulation (x ± RSD%)	36.91 ± 0.52 %	10.59 ± 1.07 %
Actual formulated amount	37.10 %	10.90 %

It should be stressed that by using the internal standard method, the error due to sample manipulation was eliminated and especially when taking extremely small sample volumes (2μL). The manual injection technique was applied in this study to introduce liquid samples into the GC system. This method has significant discrimination since the uneven injection volume and injection speed will directly affect the outcome and also the precision of the results. By using the internal standard method, the problem of these inconsistent injection can be eliminated or minimized

CONCLUSION

By using the GC-ECD with the internal standard method, the direct determination of Chlorpyrifos and Quinalphos in commercial pesticide formulations can be carried out without any pre-treatment of samples with good reproducibility and accuracy, in addition to saving time and reducing the volume of organic solvents employed in the analysis. So, the proposed procedure is an environmentally friendly method for quality control analysis of formulated pesticides. Furthermore, it can solve the problems, which are caused by manual injection. This study also demonstrates that this internal standard method is sensitive, selective, rapid and is an excellent choice of confirmation analysis of active ingredients in commercial pesticides.

ACKNOWLEDGEMENTS

The authors acknowledge the financial support of Universiti Malaya and also Universiti Tenaga Nasional. The authors would also like to thank the Department of Agriculture for providing the commercial samples and their kind assistance.

REFERENCES

[1] Chlorpyrifos, Extension Toxicology Network, Pesticide Information Profiles. June 1996.

[2] Report of Imported Pesticide Amounts as an Active Ingredient in Malaysia at 1998 to 2001, Dept. of Agriculture, Malaysia. 2 July 2003.

[3] L.P. Srivastava, R. P. Singh and R. B. Raizada (1999). "Phototoxicity of Quinalphos under Sunlight in Vitro and in Vivo." *Food and Chemical toxicology*, **37**, 177-181

[4] Yu-Wen Lin, Shane S. Que Hee (1998). "Simultaneous gas chromatographic-mass spectrometric quantitation of the alkylbenzene inert components, pesticide manufacturing by products and active ingredient in two Malathion formulations." *J. of Chromatography A*, **814**, 181-186.

[5] M.C. Lopez-Blanco, B. Reboreda-Rodriquez, B. Cancho-Grande (2002). "Optimization of solid-phase extraction and solid-phase microextration for the determination of α- and β-endosulfan in water by gas chromatography-electron-capture detection." *J. of Chromatography A*, **976**, 293-299.

[6] Ch. Lentza-Rizos, E.J. Avramides, E. Visi (2001). "Determination of residue of endosulfan and five pyrethroid insecticides in virgin olive oil using gas chromatography with elecron-capture detection." *J. of Chromatography A*, **921**, 297-304.

[7] Arunee Therdteppitak and Kittima Yammeng (2003). "Determination of organochlorine pesticides in commercial fish by gas chromatography with electron capture detector and confirmation by gas chromatography-mass spectrometry." *ScienceAsia*, **29**, 127-134.

[8] A. Colume, S. Cardenas, M. Gallego, M. Valcarcel (1999). "Semiautomatic method for the screening and determination of 23 organochlorine pesticide in horticultural sample by gas chromatography with electron-capture detection." *J. of Chromatography A*, **849**, 235-243.

[9] Natalia Fidalgo-Used, Giuseppe Centineo, Elisa Blanco-Gonzalez (2003). "Solid-phase microextraction as a clean up and preconcentration procedure for organochlorine pesticides determination in fish tissue by gas chromatography with electron capture detection." *J. of Chromatography A*, **1017**, 35-44.

[10] Xie Quan, Shuo Chen, and Bernhard Platzer (2002). "Simultaneous determination of chlorinated organic compounds from environmental samples using gas chromatography coupled with a micro electron capture detector and micro-plasma atomic emission detector." *Spectrochimica Acta*, Part B, **57**, 189-199.

[11] Guillermo Quintas, Sergio Armenta, Asuncion Morales-Noe (2003). "Simultaneous determination of Folpet and Metalaxyl in pesticide formulations by flow injection fourier transform infrared spectrometry." *Analytica Chimica Acta*, **480**, 11-21.

[12] Guillermo Quntas, Asuncion Morales-Noe, Sergio Armenta (2004). "Fourier transform infrared spectrometric determination of Malathion in pesticide formulations." *Analytica Chimica Acta*, **502**, 213-220.

[13] Jose A. Jimena Garcia, Jose Gimenez Plaza, Jose M. Cano Pavon (1996). "Determination of active components in insecticide formulations by liquid chromatography and resolution of overlapped peaks by multivariate analysis and derivative spectrophotometry." *Analytica Chimica Acta*, **321**, 273-278.

[14] Rodney J. Bushway, L. Brian Perkins and Joan M. King (1988). "Simultaneous determination of Diazinon and Chlorpyrifos pesticide formulations by liquid chromatography." *J. Assoc. Off. Anal. Chem*, Vol **71**, No2, 321-323.

[15] Kazimierz Wrobel-Zasada, Katarzyna Wrobel-Kaczmarczyk, Pedro Luis (1996). "Application of internal standard for derivative-spectrophotometric determination of azinphos-methyl in commercial formulations." *Talanta*, **43**, 1055-1060.

[16] US Environmental Protection Agency, (1995). "Method 508-Determination of chlorinated pesticides in water by gas chromatography with an electron capture detector." Revision 3.1, Edited by J. W. Munch.

Malaysian Journal of Analytical Sciences, Vol.9, No. 3(2005): 557 - 565

SINTESIS BERENZIM LIPID BERSTRUKTUR MENGGUNAKAN MINYAK SAWIT TERBENDALIR DAN ASID ARAKIDIK

***Nur Zamzarina Ahmad Zawawi, Mamot Said, Jumat Salimon dan Nazaruddin Ramli**

Pusat Pengajian Sains Kimia dan Teknologi Makanan, Fakulti Sains dan Teknologi, Universiti Kebangsaan Malaysia (UKM), 43600 Bangi
Email: nr_ina@yahoo.com

ABSTRAK

Penghasilan lipid berstruktur (SL) yang mengandungi asid lemak rantai panjang melalui tindak balas asidolisis berenzim minyak sawit terbendalir dan asid arakidik telah dikaji. Lipase daripada *Thermomyces lanuginose (TL)* dan *Rhizomucor miehei (RM)* digunakan dalam tindak balas asidolisis ini. Parameter optimum sintesis lipid berstruktur ini ditentukan menggunakan perisian Design-Expert 6.0.10. Empat parameter telah terpilih dalam kajian ini iaitu peratus kandungan substrat (Sr), peratus enzim (E_1), suhu (T_e) dan masa (t_r). Julat setiap parameter telah ditentukan seperti berikut : S_r = 1-10%; E_1 = 1-10%; T_e = 45-65°C dan t_r = 8-72 jam. Parameter yang memberi nilai kemasukan asid arakidik tertinggi selepas dianalisis menggunakan kromatografi gas ialah pada S_r = 10.5%; E_1 = 5.5%; T_e = 55°C dan t_r = 42 jam bagi asidolisis yang menggunakan kedua-dua enzim iaitu *Thermomyces lanuginose(TL)* dan *Rhizomucor miehei (RM)* sebagai pemangkin. Sampel yang terpilih tersebut ditentukan takat leburnya dengan menggunakan kalorimeter pengimbas perbezaan (DSC) dan kandungan lemak pejal menggunakan resonan magnetik Nuklear denyutan (pNMR). Perbezaan dilihat amat ketara pada takat lebur di antara kawalan dan sampel yang dianalisis. Contohnya bagi suhu awal, sampel 7 yang menggunakan enzim RM sebagai pemangkin mempunyai suhu awal 8.23 ± 0.13ºC berbanding kawalan iaitu 2.56 ± 0.11ºC dan suhu akhir sampel tersebut ialah 26.35 ± 0.01ºC berbanding kawalan 13.64 ± 0.12 ºC. Daripada analisis yang telah dilakukan didapati peratus kandungan lemak pejal sampel selepas asidolisis lebih rendah daripada sampel kawalan.

ABSTRACT

Production of structured lipid containing long-chain fatty acids by enzymatic acidolysis reaction of fluidized palm oil and arachidic acid were studied. Lipase from *Thermomyces lanuginose (TL)* and *Rhizomucor miehei (RM)* were used as catalysts. The optimal parameters for synthesis of structured lipid were obtained by Design Experts 6.0.10 using Response Surface Design. Four important parameters for the reaction were chosen: Substrate ratio (S_r), Enzyme load (E_1), Reaction temperature (Te) and Reaction time (t_r). The range of each parameter was selected as follows: Sr = 1-10%; E_1 = 2-10%; Te = 45-65ºC and t_r = 8-72 hour. The optimum reaction conditions for the incorporation of arachidic acid into fluidized palm oil using both of enzyme as catalysts were Sr = 10.5%; E_1 = 5.5%; Te = 55ºC and t_r = 42 hour. The melting profiles of chosen samples were obtained from Differential Scanning Calorimeter (DSC) and solid fat content (SFC) was obtained from pulsed Nuclear Magnetic Resonans (pNMR) analyses. The results showed the different melting profile between samples and control. For example sample 7 using lipase *Rhizomucor miehei (RM)* had initial peak 8.23 ± 0.13ºC compared to the control at 2.56 ± 0.11ºC and second peak was 26.35 ± 0.01ºC compared to control at 13.64 ± 0.12ºC. Generally, the interesterified blends had lower SFC than the non-interesterified blends at all ratios analyzed.

Structured lipid, Acidolysis, Arachidic Acid, Lipase and Physicochemical Characteristics.

PENGENALAN

Lipid berstruktur adalah triasilgliserol yang mengandungi asid lemak rantai pendek dan/atau asid lemak rantai sederhana dan asid lemak rantai panjang dengan kedudukan yang spesifik pada tulang belakang gliserol (Dequan et al. 2001). Lipid berstruktur yang mengandungi asid lemak rantai panjang (C14 – C22) dan asid lemak rantai sederhana (C8 – C12) yang terletak pada kedudukan spesifik sn-2 atau sn-1 dan sn-3 telah menarik minat para penyelidik tentang keistimewaan ciri-ciri fizikokimia serta nilai pemakanannya (Xuebing et al. 2000). Kaedah yang paling sesuai untuk pengubahsuaian kedudukan pada triasilgliserol ialah penginteresteran yang dapat mengelakkan pembentukan asid lemak trans yang boleh menyebabkan punca kepada penyakit jantung (Berger 1993).

Penginteresteran boleh dijalankan sama ada secara kimia atau berenzim yang menggunakan mangkin kimia seperti sodium metoksida dan enzim iaitu lipase. Penginteresteran secara kimia memerlukan suhu yang tinggi iaitu lebih daripada 100°C dan menggunakan mangkin bukan organik yang boleh menyebabkan penghasilan bendasing yang boleh menjejaskan kualiti produk akhir (Bhattacharyya 1996). Oleh itu, penginteresteran berenzim dipilih dengan menggunakan enzim lipase sebagai pemangkin. Enzim adalah spesifik di dalam tindak balasnya di mana ia dapat mengelakkan pembentukan asid lemak trans pada produk akhir serta kualiti produk akhir dapat dikekalkan memandangkan tindak balas yang berlaku adalah sederhana dan tidak memerlukan suhu yang tinggi berbanding penginteresteran kimia (Macrae 1983). Sesetengah enzim juga boleh memasukkan asid lemak pada kedudukan sn-1 dan/atau sn-3 pada molekul triasilgliserol bergantung pada ciri-ciri spesifik yang dikehendaki bersesuaian dengan produk yang akan dihasilkan.

Dalam kajian ini, minyak sawit terbendalir telah digunakan sebagai substrat untuk penginteresteran berenzim bagi menghasilkan produk yang mempunyai ciri-ciri yang sama dengan lemak koko. Minyak sawit terbendalir adalah minyak goreng yang terhasil daripada tindak balas pemeringkatan pada suhu tertentu, iaitu daripada bahagian cecair yang lebih dikenali sebagai minyak olein. Minyak ini telah dilakukan proses lanjutan untuk mendapatkan ciri-ciri minyak goreng. Sifat fizikal minyak ini berbeza kerana bersifat separa pepejal pada suhu bilik berbanding olein sawit yang bersifat cecair sepenuhnya. Ia mempunyai kelebihan sebagai minyak goreng iaitu mudah dikendalikan kerana sifat fizikalnya, memberikan kestabilan penggorengan yang lebih baik disamping memberi lebih rasa kerangupan dan dapat memanjangkan jangka hayat produk tersebut. Selain itu, minyak ini juga kurang penyerapan minyak apabila penggorengan dilakukan dan ini menghasilkan produk yang kurang berminyak dan lebih banyak produk boleh digoreng daipada penggunaan minyak masak biasa. Penggunaan minyak ini dalam pembuatan kek dan roti juga akan memberikan produk lebih halus dan lembut teksturnya (Golden Jomalina, 2003).

Dalam kajian ini, minyak sawit terbendalir akan ditindak balas secara asidolisis dengan asid arakidik tulen menggunakan enzim *Thermomyces lanuginose (TL)* dan *Rhizomucor miehei (RM)* untuk menghasilkan lipid berstruktur yang boleh dijadikan sebagai agen pencegah bebunga lemak dan kemungkinan bahan pengganti lemak koko. Kaedah Respons Permukaan (Response Surface Methodology, RSM) daripada Design Expert telah digunakan untuk mendapatkan parameter yang optimum bagi mendapatkan hasil yang optimum. Empat faktor telah dipilih dalam kajian ini iaitu substrat (%), kandungan enzim (%), suhu (°C) dan masa (Jam). Bagi menentukan kesesuaiannya sebagai pengganti lemak koko, analisis takat peleburan dan pengkristalan, kandungan asid lemak dan kandungan lemak pejal telah dilakukan.

BAHAN DAN KAEDAH

Bahan: Minyak sawit terbendalir (FPO) diperolehi daripada Golden Jomalina Food Industries Sdn. Bhd., asid arakidik (C20:0) daripada Sigma Chemical Co., enzim lipase iaitu *Rhizomucor miehei* (RM 1M) dan *Thermomyces lanuginose* (TL 1M) dari Novozymes A/S Sdn. Bhd. dan n-Hexane serta bahan-bahan kimia lain diperolehi daripada Merck Sdn. Bhd. atau Fisher Scientific (Norcross, GA).
Rekabentuk eksperimen: Dalam kajian ini, sebanyak empat parameter dikaji iaitu substrat (%), enzim (%), suhu (ºC), dan masa (jam) menggunakan *Design-Expert Version 6.0.10* daripada Stat-Ease Inc. seperti pada Jadual 1 (kod) dan Jadual 2 (nilai sebenar). Dalam rekabentuk eksperimen ini, sebanyak 60 analisis dijalankan iaitu 50 titik faktor dan 10 titik tengah termasuk duplikat bagi setiap enzim iaitu lipozim TL dan lipozim RM.

Jadual 1: Nilai kod untuk kaedah respons permukaan (RSM)

No.	Parameter			
	Subsrat (%)	Enzim (%)	Suhu (ºC)	Masa (Jam)
1	0	0	-2	0
2	-1	-1	-1	-1
3	1	-1	-1	-1
4	-1	1	-1	-1
5	1	1	-1	-1
6	1	-1	-1	1
7	1	1	-1	1
8	-1	-1	-1	1
9	-1	1	-1	1
*10	0	0	0	0
*11	0	0	0	0
*12	0	0	0	0
*13	0	0	0	0
*14	0	0	0	0
15	2	0	0	0
16	0	-2	0	0
17	-2	0	0	0
18	0	2	0	0
19	0	0	0	0
20	-1	1	1	1
21	-1	-1	1	1
22	1	1	1	1
23	1	-1	1	1
24	0	0	0	-2
25	1	1	1	-1
26	1	-1	1	-1
27	-1	-1	1	-1
28	-1	1	1	-1
29	0	0	2	0
30	0	0	0	2

- titik tengah

Jadual 2: Nilai sebenar bagi kaedah respons permukaan (RSM)

Parameter	-2	-1	0	1	2
Substrat (%)	0.5	3.0	5.5	8.0	10.5
Enzim (%)	0.5	3.0	5.5	8.0	10.5
Suhu (ºC)	35	45	55	65	75
Masa (Jam)	6	24	42	60	78

Asidolisis berenzim: tindak balas dilakukan dengan mencampurkan minyak sawit terbendalir (FPO), asid arakidik dan enzim lipase (TL 1M atau RM 1M) serta heksana sebagai pelarut. Nisbah bahan-bahan tersebut berpandukan pada Jadual 1 dan Jadual 2. Kemudian, sampel akan diletakkan di dalam kukus air bergoncang dengan putaran 250 rpm pada suhu dan masa yang telah ditentukan.

Analisis kromatografi gas: Kandungan asid lemak ditentukan melalui kaedah yang dilakukan oleh Timms (1978) dengan sedikit pengubahsuaian. Ia dilakukan setelah sampel lemak ditukarkan kepada ester metil asid lemak (FAME) melalui langkah pemetilan. Sebanyak 5.4g serbuk sodium metoksida dilarutkan ke dalam 100 ml metanol atau larutan tersebut mencapai kepekatan 3.75%. pemetilan dilakukan dengan menambahkan 1ml heksana, 1ml larutan sodium metoksida dan 0.1 ml sampel. Sampel kemudiannya dihomogenkan dengan menggunakan *vortex mixer*. Setelah pemendakan (natrium gliserolat) berlaku, bahagian supernatant yang jernih diasingkan untuk disuntik sebanyak 1µl menerusi kolum kapilari silika (SGE BPX 70, 60cm × 0.32µm) dibekalkan oleh Servco Services Sdn.Bhd, Kelang. Profil kandungan asid lemak dikesan melalui kromatografi gas (Algilent) yang dilengkapi sisten pengionan nyala (FID) dan alat integrasi (C-R 6A Chromatopac). Suhu pengesan ialah 280ºC manakala suhu penyuntik ialah 240ºC. Suhu oven pula ialah 120ºC sehingga 180ºC dengan kadar pemanasan 4ºC/min. Pemanasan diteruskan kepada suhu 210ºC pada kadar pemanasan 1ºC/min. Kadar gas pembawa (nitrogen) ialah 1.5 ml/min,

pada tekanan 3.2 psi. Faktor pembetul tindak balas (CRF) untuk setiap ester metil asid lemak ditentukan melalui analisis campuran metil ester asid lemak piawai.

Kandungan lemak pejal ditentukan menggunakan resonan magnetik nuklear denyutan (pNMR) bagi sampel-sampel lemak yang telah dilakukan tindak balas asidolisis. Sampel dalam tiub pNMR dicairkan pada suhu 70ºC selama 30 minit, kemudian sampel tersebut disejukkan pada suhu 0ºC selama 90 minit. Setelah itu, bacaan di ambil pada suhu 0, 5, 10, 15, 20, 25, 30, 35 dan 40ºC (PORIM p4.9).

Kelakuan peleburan: Takat lebur dan pengkristalan ditentukan menggunakan Kalorimeter pengimbas perbezaan (DSC), Model Mettler-ToledoV7.0 (Schwerzenbach, Switzerland). Melalui analisis ini, dua sifat terma utama iaitu puncak peleburan (Tp) dan entalpi peleburan (Ep) dapat dikenalpasti. Alat ini dilengkapi perisai sistem analisis terma Model 1020 dengan jenama yang sama. Kalibrasi dilakukan dengan menggunakan n-dekana (takat lebur: -29.66ºC; ΔHf: 202.09 J/g) dan indium (takat lebur: 156.6ºC; ΔHf: 28.45 J/g). Sebanyak 3-5 mg (±0.005) sampel minyak dileburkan pada piring aluminium pada suhu 70ºC selama 30 minit sebelum disimpan sejuk selama 90 minit. Kemudian, sampel ditetapkan suhu awal 0ºC dan diturunkan -40ºC selama 5 minit. Keluk peleburan DSC dicatatkan kadar pemanasannya pada 5ºC dari -40ºC hingga 40ºC. Piring aluminium kosong dijadikan rujukan (Thomas & Dimick 1989).

HASIL DAN PERBINCANGAN

Rajah 1(a) dan (b) menunjukkan kandungan asid oleik (C18:1) dan asid arakidik (C20:0) dalam sampel sebelum dan selepas asidolisis menggunakan enzim *Thermomyces lanuginose (TL)* dan *Rhizomucor miehei (RM)* masing-masing. Nilai tertinggi asid oleik yang terhasil selepas asidolisis ialah sampel 6 (substrat 8%, enzim 3%, suhu 45ºC dan 60 jam) iaitu 59.82 ± 0.59% bagi enzim RM sebagai pemangkinnya. Manakala sampel yang menggunakan enzim TL sebagai pemangkin, nilai asid oleik tertinggi ialah pada sampel 8 (substrat 3%, enzim 3%, suhu 45ºC dan 60 jam) dengan nilai 55.57 ± 7.40%.

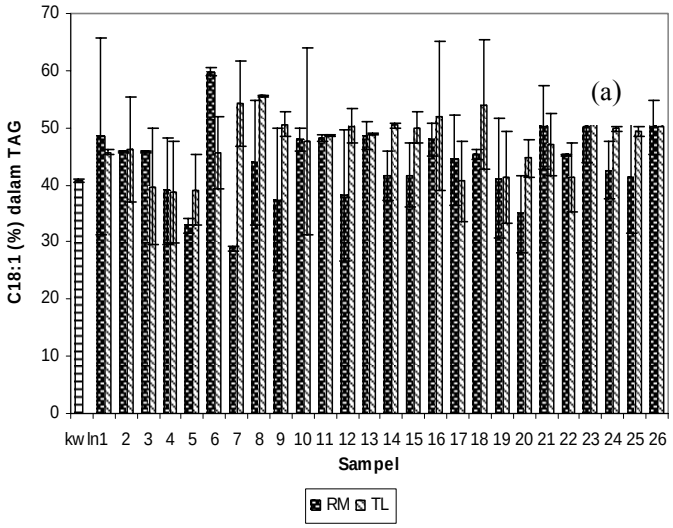

(a)

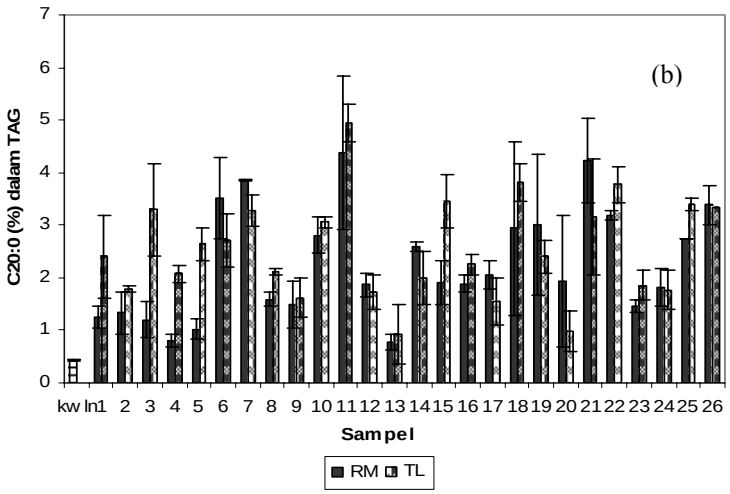

Rajah 1: Kandungan asid oleik (C18:0) (a) dan asid arakidik (C20:0) (b) dalam sampel sebelum dan selepas asidolisis menggunakan enzim *Rhizomucor miehei (RM) Thermomyces lanuginose (TL)*. Kod sampel adalah seperti pada jadual 1 dan 2.

Bagi asid arakidik, nilai tertinggi yang terhasil selepas asidolisis ialah pada sampel 11 (substrat 10.5%, enzim 5.5%, suhu 55ºC dan 42 jam) bagi kedua-dua enzim iaitu enzim RM dan TL dengan nilai 4.38 ± 1.46% dan 4.94 ± 0.01% masing-masing. Menurut Yankah & Akoh (2000), enzim yang digunakan sebagai pemangkin dalam tindak balas penginteresteran adalah faktor utama yang mempengaruhi komposisi dan produk akhir yang terhasil.

Rajah 2(a), (b), (c) dan (d) menunjukkan perubahan profil peratus kandungan lemak pejal bagi sampel minyak sawit terbendalir sebelum dan selepas asidolisis di antara suhu 0 hingga 40ºC menggunakan enzim *Thermomyces lanuginose (TL)* dan *Rhizomucor miehei (RM)*, di mana lemak koko (CB) sebagai kawalan untuk perbandingan. Daripada hasil yang diperolehi, didapati sampel T3 (substrat 8%, enzim 3%, suhu 45ºC dan 24 jam), T7 (substrat 8%, enzim 8%, suhu 45ºC dan 60 jam) dan T14 (substrat 5.5%, enzim 10.5%, suhu 55ºC dan 42 jam) bagi enzim TL 1M mempunyai peratus kandungan lemak pejal yang hampir dengan lemak koko. Apabila menggunakan enzim RM 1M, sampel yang terpilih ialah R7 (substrat 8%, enzim 8%, suhu 45ºC dan 60 jam), R8 (substrat 3%, enzim 3%, suhu 45ºC dan 60 jam) dan R12 (substrat 5.5%, 0.5%, suhu 55ºC dan 42 jam).

Daripada rajah tersebut, didapati minyak sawit terbendalir menunjukkan kandungan lemak pejal yang sangat berbeza dengan lemak koko. Lemak koko menunjukkan tahap peleburan yang tajam di antara suhu 20 hingga 35ºC di mana memberi ciri yang unik dan istimewa. Tetapi minyak sawit terbendalir menunjukkan peratus kandungan lemak yang menurun secara seragam dan ini tidak sesuai untuk penghasilan pengganti lemak koko.

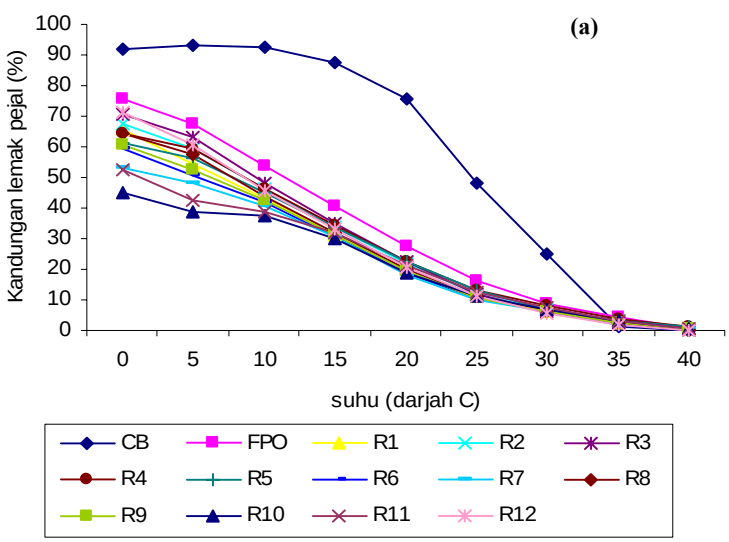
(a)
Kandungan lemak pejal (%)
suhu (darjah C)
CB FPO R1 R2 R3
R4 R5 R6 R7 R8
R9 R10 R11 R12

(b)

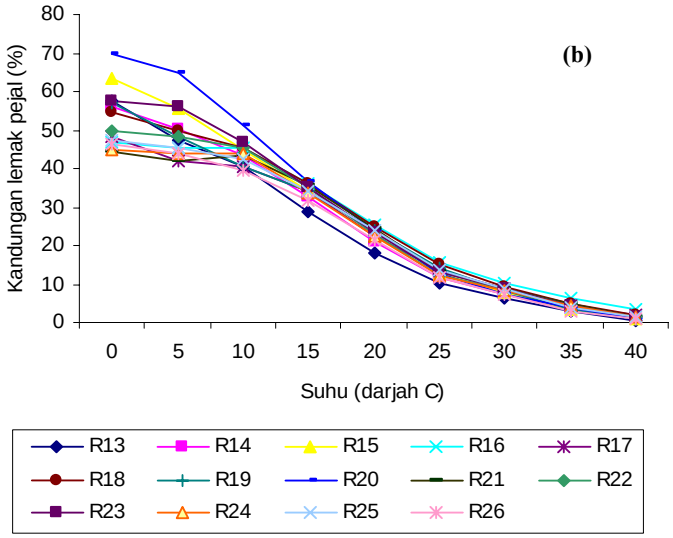
(b)
Kandungan lemak pejal (%)
Suhu (darjah C)
R13 R14 R15 R16 R17
R18 R19 R20 R21 R22
R23 R24 R25 R26

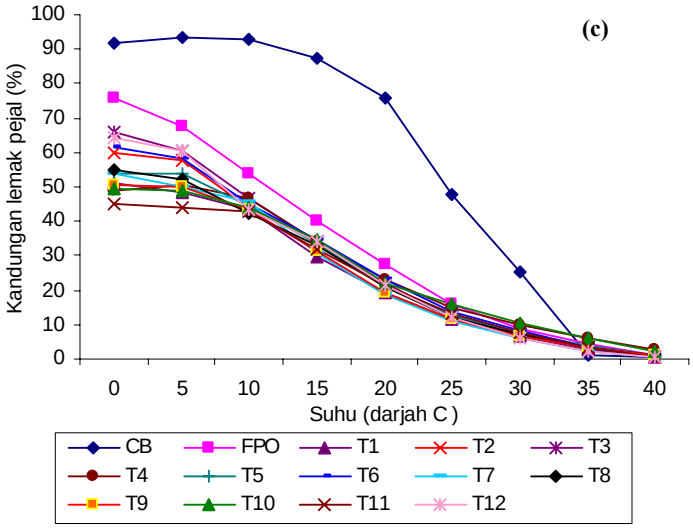
(c)
Kandungan lemak pejal (%)
Suhu (darjah C)
CB FPO T1 T2 T3
T4 T5 T6 T7 T8
T9 T10 T11 T12

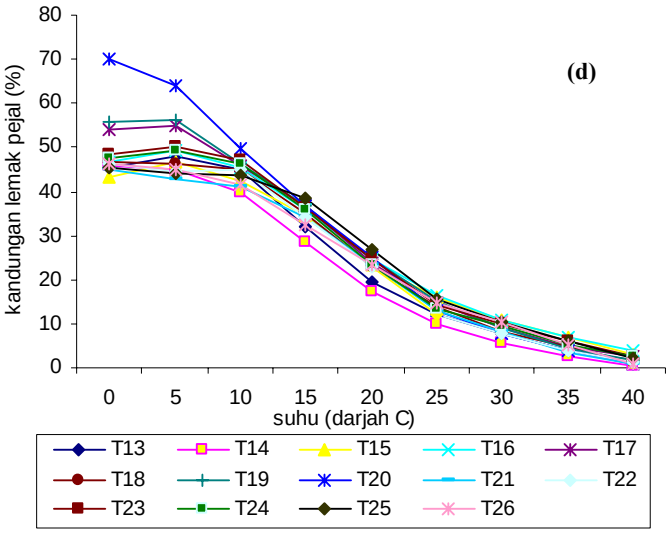

Rajah 2: Graf kandungan lemak pejal (%) melawan suhu bagi *Rhizomucor miehei (RM)* (a), (b) dan *Thermomyces lanuginose (TL)* (c), (d).

Petunjuk:
CB :Lemak koko T1-T26 :Seperti pada Jadual 1 dan 2
FPO:Minyak sawit terbendalir R1-R26 :Seperti pada Jadual 1 dan 2

Walau bagaimanapun, semua sampel yang terpilih mempunyai peratus kandungan lemak pejal yang rendah pada suhu 40ºC dan ini dapat mengurangkan rasa berlilin dalam mulut apabila diaplikasikan dalam produk tertentu (Ming et al. 1999). Daripada Rajah 1 juga didapati peratus kandungan lemak pejal selepas tindak balas adalah lebih rendah daripada sebelum tindak balas. Ini mungkin kerana berlaku penukaran asid lemak tepu kepada asid lemak tak tepu dalam triasilgliserol minyak sawit terbendalir semasa tindak balas asidolisis. Secara umumnya, kandungan lemak pejal bagi minyak campuran bertanggungjawab dalam memberikan ciri-ciri tertentu pada produk termasuklah dari segi bentuk permukaan, kemudahan dalam pembungkusan, keseragaman penyebaran dalam produk, aliran minyak dan ciri-ciri organoleptik (Ming et al. 1998).

Jadual 3 dan 4 masing-masing menunjukkan takat lebur dan takat pengkristalan bagi sampel yang terpilih setelah dinilai peratus kandungan lemak pejalnya yang menghampiri peratus kandungan lemak pejal lemak koko. Hasil menunjukkan perbezaan takat lebur dan takat pengkristalan bagi kedua-dua enzim yang digunakan berbanding dengan kawalan. Perbezaan dilihat amat ketara pada takat lebur di antara kawalan dan sampel-sampel. Bagi suhu awal sampel 7 (substrat 8%, enzim 8%, suhu 45ºC dan 60jam) yang menggunakan enzim RM sebagai pemangkin mempunyai nilai 8.23 ± 0.13ºC berbanding kawalan iaitu 2.56 ± 0.11ºC dan suhu akhir sampel tersebut ialah 26.35 ± 0.01ºC berbanding kawalan 13.64 ± 0.12ºC. Sampel 8 (substrat 3%, enzim 3%, suhu 45ºC dan 60 jam) menunjukkan suhu awal 7.73 ± 0.13 dan suhu akhir 23.18 ± 0.24ºC, manakala sampel 12 (substrat 5.5%, enzim 5.5%, suhu 55ºC dan 42jam) memberikan nilai 8.21 ± 0.13ºC pada suhu awal dan 24.34 ± 0.01ºC bagi suhu akhir.

Bagi sampel yang menggunakan enzim *Thermomyces lanuginose (TL)* sebagai pemangkin, hasil menunjukkan perbezaan yang ketara antara kawalan dan produk tetapi nilai keseluruhannya rendah berbanding penggunaan enzim *Rhizomucor miehei (RM)* pada suhu awal. Sampel 3 (substrat 8%, enzim 3%, suhu 45ºC dan 24jam) memberikan 8.05 ± 0.59ºC berbanding kawalan 2.56 ± 0.11ºC, sampel 7 pula menunjukkan 7.96 ± 0.01ºC dan sampel 14 (substrat 5.5%, enzim 5.5%, suhu 55ºC dan 42jam) dengan 6.29 ± 1.42ºC pada suhu awal. Suhu akhir menunjukkan takat peleburan yang tinggi berbanding menggunakan mangkin *Rhizomucor miehei (RM)* secara keseluruhannya. Sampel 3 memberikan nilai 25.50 ± 1.41ºC berbanding kawalan 13.64 ± 0.12ºC. Sampel 7 dan 14 masing-masing menunjukkan perbezaan suhu akhir yang tidak ketara iaitu 26.25 ± 0.36 dan 26.88 ± 0.71ºC. Dapat dikatakan di sini, nilai bacaan yang berbeza antara sampel sebelum dan selepas asidolisis adalah kerana berlaku penyusunan semula dan berlaku perubahan asil daripada tindak balas asidolisis untuk membentuk kadar peleburan yang rendah dan sederhana dalam rantai triasilgliserol (Chu et al. 2002). Menurut Timms (1984), dalam analisis sifat peleburan,

kaedah penstabilan di bawah suhu peleburan akhir (26ºC) sesuatu lemak adalah perlu bagi pembentukan polimorf yang stabil disamping mengurangkan polimorf yang kurang stabil.

Jadual 3: Takat lebur sampel* sebelum dan selepas asidolisis

Rhizomucor miehei (RM)			*Thermomyces lanuginose (TL)*		
Sampel	Suhu awal (ºC)	Suhu akhir (ºC)	Sampel	Suhu awal (ºC)	Suhu akhir (ºC)
kawalan	2.56 ± 0.11[a]	13.64 ± 0.12[a]	kawalan	2.56 ± 0.11[a]	13.64 ± 0.12[a]
7	8.23 ± 0.13[a]	26.35 ± 0.01[b]	3	8.05 ± 0.59[a]	25.50 ± 1.41[b]
8	7.73 ± 0.13[b]	23.18 ± 0.24[c]	7	7.96 ± 0.01[a]	26.25 ± 0.36[b]
12	8.21 ± 0.13[c]	24.34 ± 0.01[d]	14	6.29 ± 1.42[b]	26.88 ± 0.71[c]

Jadual 4: Takat pengkristalan* sampel sebelum dan selepas asidolisis

Rhizomucor miehei (RM)			*Thermomyces lanuginose (TL)*		
Sampel	Suhu awal (ºC)	Suhu akhir (ºC)	Sampel	Suhu awal (ºC)	Suhu akhir (ºC)
kawalan	17.14 ± 0.35[a]	2.95 ± 0.11[a]	Kawalan	17.14 ± 0.35[a]	2.95 ± 0.11[a]
7	17.78 ± 0.10[ab]	1.93 ± 0.11[b]	3	17.77 ± 1.53[a]	2.11 ± 0.58[a]
8	15.71 ± 0.25[bc]	1.27 ± 0.13[b]	7	20.26 ± 1.28[a]	2.70 ± 0.23[a]
12	16.11 ± 0.60[c]	1.70 ± 0.48[b]	14	20.13 ± 1.02[a]	2.03 ± 0.94[a]

*Nilai dilaporkan sebagai min ± sisihan piawai dan huruf berbeza pada jalur berbeza menunjukkan perbezaan yang beerti ($P<0.05$).

Suhu pengkristalan menunjukkan perbezaan yang tidak terlalu ketara antara kawalan dan sampel-sampel. Sampel 7, 8 dan 12 masing-masing memberikan nilai 17.78 ± 0.10, 15.71 ± 0.25 dan 16.11 ± 0.60ºC pada suhu awal bagi produk yang menggunakan *Rhizomucor miehei (RM)* sebagai pemangkin berbanding kawalan 17.14 ± 0.35ºC. Suhu akhir menunjukkan nilai yang rendah berbanding kawalan iaitu 1.93 ± 0.11, 1.27 ± 0.13 dan 1.70 ± 0.48ºC masing-masing bagi sampel 7, 8 dan 12 berbanding kawalan iaitu 2.95 ± 0.11ºC. Apabila enzim *Thermomyces lanuginose (TL)* digunakan sebagai pemangkin, didapati nilai bacaan selepas asidolisis menunjukkan takat lebur yang lebih tinggi berbanding kawalan pada suhu awal. Sampel 3, 7 dan 14 masing-masing memberikan suhu 17.77 ± 1.53, 20.26 ± 1.28 dan 20.13 ± 1.02ºC masing-masing. Nilai suhu akhir secara keseluruhannya menunjukkan bacaan yang lebih rendah bagi sampel selepas asidolisis berbanding sebelum asidolisis. Sampel 3, 7 dan 14 memberikan nilai 2.11 ± 0.58, 2.70 ± 0.23 dan 2.03 ± 0.94ºC masing-masing berbanding kawalan 2.95 ± 0.11ºC. Dapat disimpulkan di sini, bahawa tindak balas asidolisis lebih mempengaruhi takat lebur sampel berbanding takat pengkristalannya. Ini mungkin kerana berlakunya pertukaran asid lemak semasa tindakbalas asidolisis. Daripada nilai bacaan, dapat disimpulkan bahawa penginteresteran berenzim telah mengubah kadar peleburan dan pengkristalan adunan.

KESIMPULAN

Daripada keputusan yang diperolehi, didapati kandungan asid oleik produk tertinggi selepas asidolisis ialah 59.82 ± 0.59% bagi enzim RM sebagai pemangkinnya. Manakala bagi asid arakidik, produk yang tertinggi ialah dari sampel 11 bagi kedua-dua enzim iaitu enzim RM dan TL dengan nilai 4.38 ± 1.46% dan 4.94 ± 0.01%. Terdapat perbezaan takat lebur dan takat pengkristalan sampel bagi sebelum dan selepas asidolisis untuk kedua-dua enzim yang

digunakan. Peratus kandungan lemak pejal bagi sampel selepas tindak balas asidolisis lebih rendah daripada sebelum asidolisis kerana berlaku pertukaran kedudukan asid lemak pada gliserol dalam rantai triasilgliserol.

PENGHARGAAN

Setinggi-tinggi penghargaan diucapkan kepada Kementerian Sains Teknologi dan Alam Sekitar di bawah peruntukan IRPA 01-02-02-0016 EA 175 dan para pensyarah serta kakitangan Program Sains Makanan, Pusat Pengajian Sains Kimia dan Teknologi Makanan, Fakulti Sains dan Teknologi, Universiti Kebangsaan Malaysia (UKM).

RUJUKAN

1. Berger, K. 1993. Food Product Formulation to Minimize the Content of Hydrogenated Fats. *Lipid Technol*. 5:37-40.

2. Bhattacharyya, S. & Bhattacharyya, D.K. 1996. Utilisation of Mowrah Oil in Edible Fat Products by Fraction, Enzymatic Acidolysis and Their Combination. *J. Oil Tech. Assoc. India* 2:39-41.

3. Chu, B.S., Ghazali, H.M., Lai, O.M., Che Man, Y.B. & Yusof, S. 2002. Physical and Chemical Properties of a Lipase-Transesterified Palm Stearin/Palm Kernel Olein Blend and its Isopropanol-Solid and High Melting Triacylglycerol Fractions. *Food Chemistry.* 76: 155-164.

4. Dequan, Z., Xuebing, X., Huiling, M., Carl-Erik, H. & Jens, A.N. 2001. Synthesis of Structured Triacyglycerols Containing Caproic Acid by Lipase-Catalyzed Acidolysis. Optimization by Response Surface Methodology. *J. Agric.Food Chem.vol* **49**: 5771-5777.

5. Golden Jomalina Food Industries Sdn Bhd. 2003. 9th Mile, Jalan Banting-Klang, 42500 Telok Panglima Garang, Kuala Langat, Selangor. Jomafood@tm.net.my.

6. Macrae, A.R. 1983. Lipase-Catalyzed Interesterification of Oil and Fats. *J. Am. Oil Chem. Soc*. **60**: 243-246.

7. Ming, L.O., Ghazali, H.M. & Let, C.C. 1998. Effect of Enzymatic Transesterification on the Fluidity of Palm Stearin-Palm Kernel Olein Mixtures. *Food Chemistry*. **63**(2): 155-159.

8. Ming, L.O., Ghazali, H.M. & Let, C.C. 1999. Use of enzymatic transesterified palm stearin-sunflower oil blends in the preparation of table margarine formulation. *Food Chemistry*. **64**: 83-88.

9. PORIM Test Methods. 1995. Palm Oil Research Institute of Malaysia, Bandar Baru Bangi. Method P4.9.

10. Thomas, R.D. & Dimick, P.S. 1989. Isolation and Thermal Characterization of High-Melting Seed Crystals Formed During Cocoa Butter Solidification. *J. Am. Oil Chem. Soc*. **66**(10): 1488-1493.

11. Timms, R.E. 1978. Artifact Peaks in the Preparation and Gas-Liquid Chromatography Determination of Methylesters. *Australian Journal of Dairy Technology.* 33: 4-6.

12. Timms, R.E. 1984. Phase Behavior of Fat and Their Mixtures. *Prog. Lipid Res.* **23**: 1-38.

13. Xuebing, X., Lydia, B.F., & Akoh, C.C. 2000. Modification of Menhaden Oil by Enzymatic Acidolysis to Produce Structured Lipid : Optimization by Response Surface Design in a Packed Bed Reactor. *J. Am. Oil Chem. Soc*. **77**(2): 171-176.

14. Yankah, V.V & Akoh, C.C. 2000. Lipase – Catalyzed Acidolysis of Tristearin with Oleic or Caprylic Acids to Produce Structured Lipids. *J.Am. Oil Chem.* **77**(5): 495-500.

Malaysian Journal of Analytical Sciences, Vol.9, No. 3(2005): 566 - 570

Profiling of Biogenic Silica in the Marine Pore Water of Peninsular Malaysia

Che Abd Rahim Mohamed and Law Kok Keong

Program of Marine Science
Pusat Pengajian Sains Sekitaran & Sumber Alam
Fakulti Sains & Teknologi
Universiti Kebangsaan Malaysia
43600 Bangi, Selangor

E-mail: carmohd@pkrisc.cc.ukm.my

Abstract

Sediment cores were collected using gravity core at Pulau Redang (Terengganu), Kuala Selangor and Kapar (Selangor) for determine contents of biogenic silica (Opal) in the marine pore water. Each layer of sediment had been centrifuged by centrifuge machine for extract pore water from the sediments. The concentration of opal was determined using Spectrophotometer methods. The concentrations of opal at Kapar, Kuala Selangor and Pulau Redang were ranging from 0.10 ppm to 0.66 ppm, < 0.10 ppm to 1.80 ppm and 0.57 ppm to 1.05 ppm, respectively. Generally, vertical profile concentration of opal in the pore water was slightly increased with increasing thickness of sediment especially for station located at Kuala Selangor and Kapar areas.

Abstrak

Teras sedimen dikutip di Pulau Redang (Terengganu), Kuala Selangor dan Kapar (Selangor) dengan menggunakan teras gravity untuk penganalisaan kandungan biogenik silika (Opal) dalam air pori marin. Setiap lapisan sedimen di sentrifuge oleh mesin sentrifuge untuk mendapatkan air pori dari sedimen. Kepekatan opal diukur dengan menggunakan kaedah spekrofotometer. Kepekatan opal di Kapar, Kuala Selangor dan Pulau Redang adalah masing-masing berjulat dari 0.10 ppm ke 0.66 ppm, < 0.10 ppm ke 1.80 ppm dan 0.57 ppm ke 1.05 ppm. Umumnya, profil menegak kepekatan opal dalam air pori adalah meningkat dengan peningkatan ketebalan sediment terutama bagi kawasan yang terletak di Kuala Selangor dan Kapar.

Keyword: Opal, sediment core, pore water, Peninsular Malaysia

Introduction

Biogenic silica as nutrients element in marine environment formed from Si and O_2 for develop SiO_2. Marine phyto-zooplanktons such as diatom, radiolarian and sponge spicules are also important during forming process of biogenic silica (Opal). They are deposit onto the seafloor as marine sediments. The contents of opal in marine sediment especially in pore water are always fluctuated from surface to bottom layers. The fluctuations of opal contents in pore water are usually reflected to the chemical properties such as nitrate, phosphate, pH and dissolve oxygen in sediment column [1]. The purpose of this study is to elucidate and determine the concentration profile of opal in pore water at open sea as Pulau Redang, and enclosed system as Kuala Selangor and Kapar.

Sampling and Methodology

Pore water samples were collected from four stations, three stations and three stations at Pulau Redang, Kuala Selangor and Kapar, respectively (Figure 1). The biogenic silica content of these segments was determined by sequential extraction [2] applying an alkaline leaching solution of pH 12.5 with accuracy of the alkaline extraction method is better than 10% [3]. Then the concentrations of opal in marine pore water were analyzed using Spectrophotometer methods.

Results and Discussion

Distribution of opal in pore water

In general, the concentrations of opal in pore water were fluctuated from surface to the deeper layers in all sampling stations (Figure 2). This maybe affected by the chemical properties and dead organisms in the sediments [3]. The highest concentration of opal found at Kuala Selangor in Station 2 was about 1.8 mg/L. Meanwhile, the concentrations of opal in sediment-water interface were not detected in Station 1 at Kuala Selangor because the mixing process was occurred during sampling between sediment-water interfaces with water column. The concentration of opal obtained at Kapar and Pulau Redang stations was ranging from 0.1 mg/L to 0.66 mg/L and from 0.57 mg/L to 1.05 mg/L, respectively (Table 1).

Table 1. Range concentration of opal in pore water obtained at sampling stations

Location	Opal (mg/L)
Pulau Redang	
Stesen 1	0.66-0.96
Stesen 2	0.57-0.95
Stesen 3	0.63-0.94
Stesen 4	0.73-1.05
Kuala Selangor	
Stesen 1	0.00-0.37
Stesen 2	0.55-1.80
Stesen 3	0.73-1.49
Kapar	
Stesen 1	0.10-0.57
Stesen 2	0.15-0.66
Stesen 3	0.23-0.62

At study stations in the Pulau Redang, Kapar or Kuala Selangor were apparently lacking relationship between rain rate of biogenic components to the seafloor and water depth may be caused by the considerable temporal variations of the monsoon seasons (Figure 3). Then the dynamic of water column conditions are also affected the benthic opal fluxes such as export from the river to the estuary and ocean. Therefore, pore water in the sediment layer at Kapar area probably received a wide range of low-high rain rates of benthic opal from the factory discharge (i.e., Kapar Electric Power Station), as a result of dynamic fluctuations of water column (Figure 2).

The distribution fluxes of opal in marine pore water may be caused by the intense dissolution of siliceous frustules in the water column, which is related to their degree of silicification. Investigations by [4], suggest the occurrence of more intensely silicified and quickly sinking diatom assemblages in iron-limited environments such as the equatorial Pacific or high-nutrient–low chlorophyll regions of the Southern Ocean. Then in sediments at Peninsular of Malaysia the terrigenous input and chemical properties such as pH and dissolved oxygen are expected important playing role in the desorb process by organic matter in solid phase stage to produce biogenic silica as liquid phase (Figure 4). But we are lacking to observe a significant relation between the rain rates of biogenic silica to the seafloor, e.g., suspended particles distribution or opal export determined by particle traps.

Conclusion

The concentrations of opal in marine pore water at Peninsular of Malaysia varied from surface to the deeper layers were probably related to terrigenous input.

Acknowledgements

The author would like to thank the laboratory assistant from Universiti Kebangsaan Malaysia for the technical support during sampling and sample analysis.

References

[1] Willey, J.D. & Spivack, A.J. 1997. Dissolved silica concentrations and reactions in pore water from continental slope sediments offshore from Cape Hatteras, North Carolina, USA. *Marine Chemistry*, **56**: 227-238.

[2] DeMaster, D.J., 1981. The supply and accumulation of silica in the marine environment. *Geochim. Cosmochim. Acta* **45**, pp. 1715–1732.

[3] Schluter, M. & Rickert, D. 1998. Effect of pH on the measurement of biogenic silica. *Marine Chemistry*, **63**: 81-92.

[4] Hutchins, D.A. and Bruland, K.W., 1998. Iron-limited diatom growth and Si:N uptake ratios in a coastal upwelling regime. *Nature* **393**, pp. 561–564.

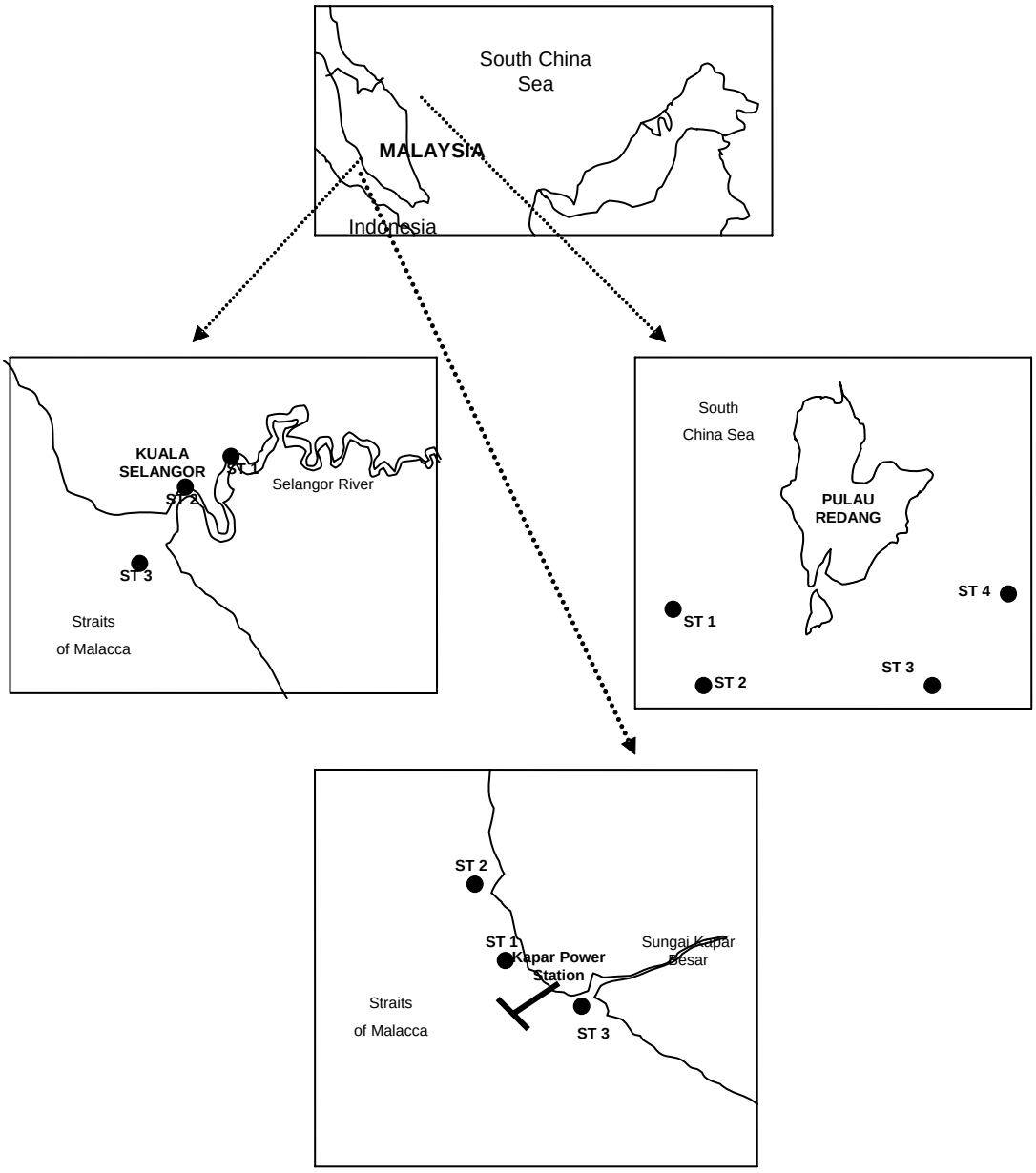

Figure 1. Sampling stations carried out during this study

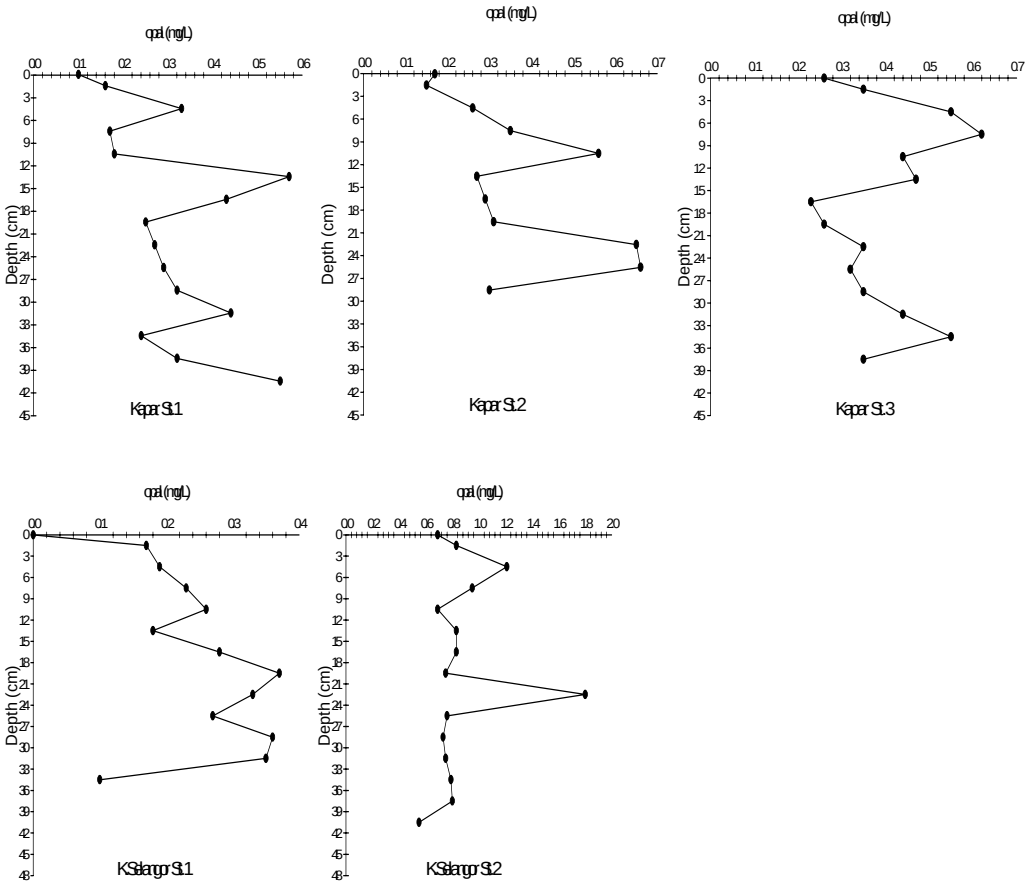
cpal (mg/L)
Depth (cm)
Kapar S1.1
Kapar S1.2
Kapar S1.3
KSelangor S1.1
KSelangor S1.2

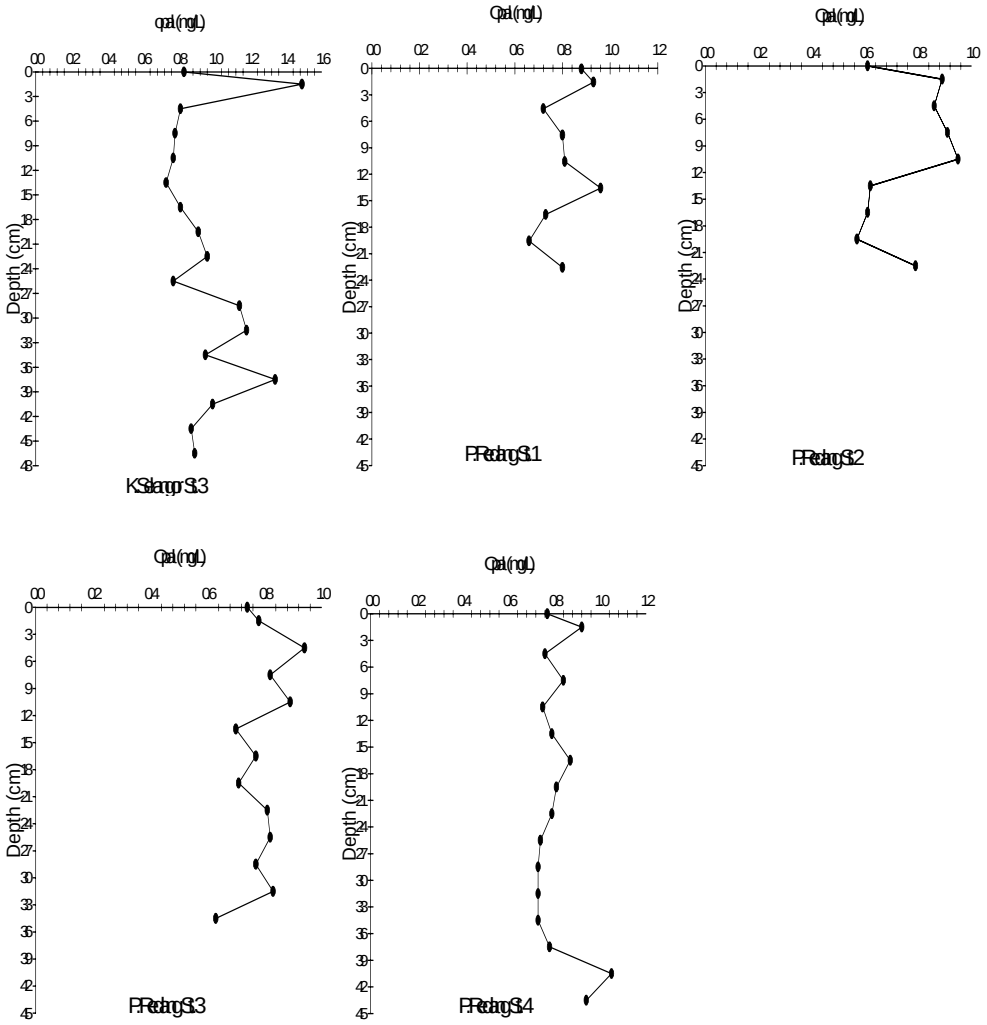

Figure 2. Distribution of opal in pore water obtained at sampling stations

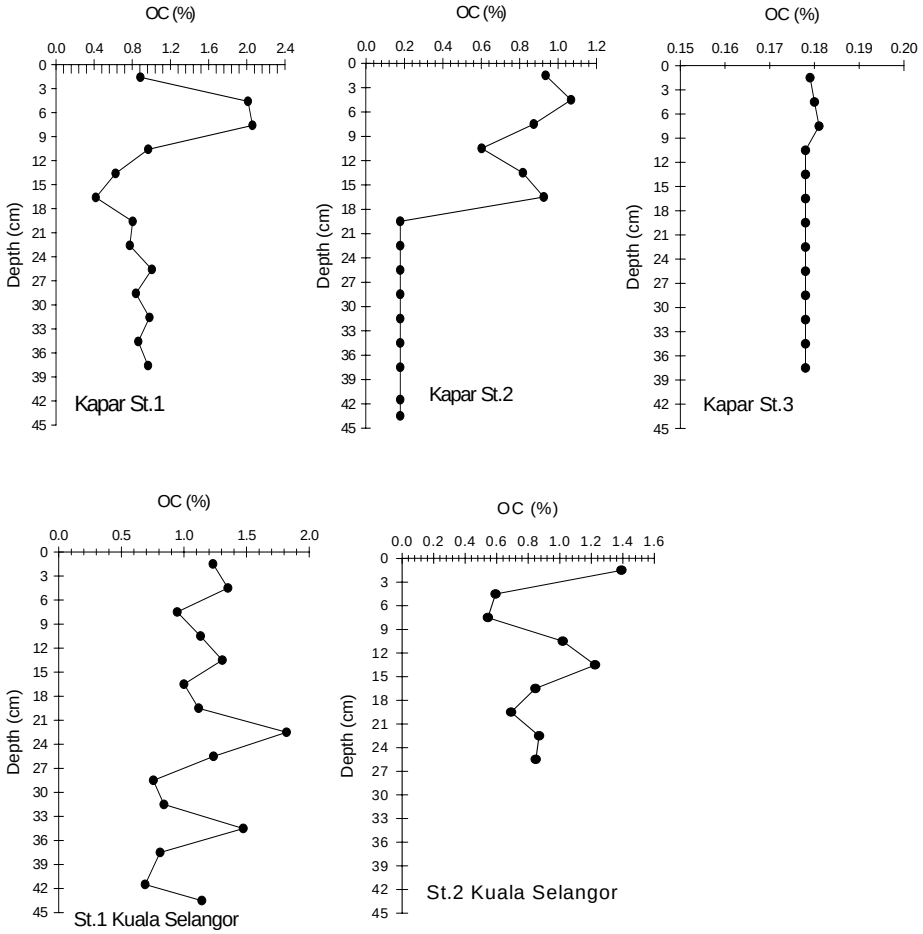
OC (%)
Depth (cm)
Kapar St.1
Kapar St.2
Kapar St.3
St.1 Kuala Selangor
St.2 Kuala Selangor

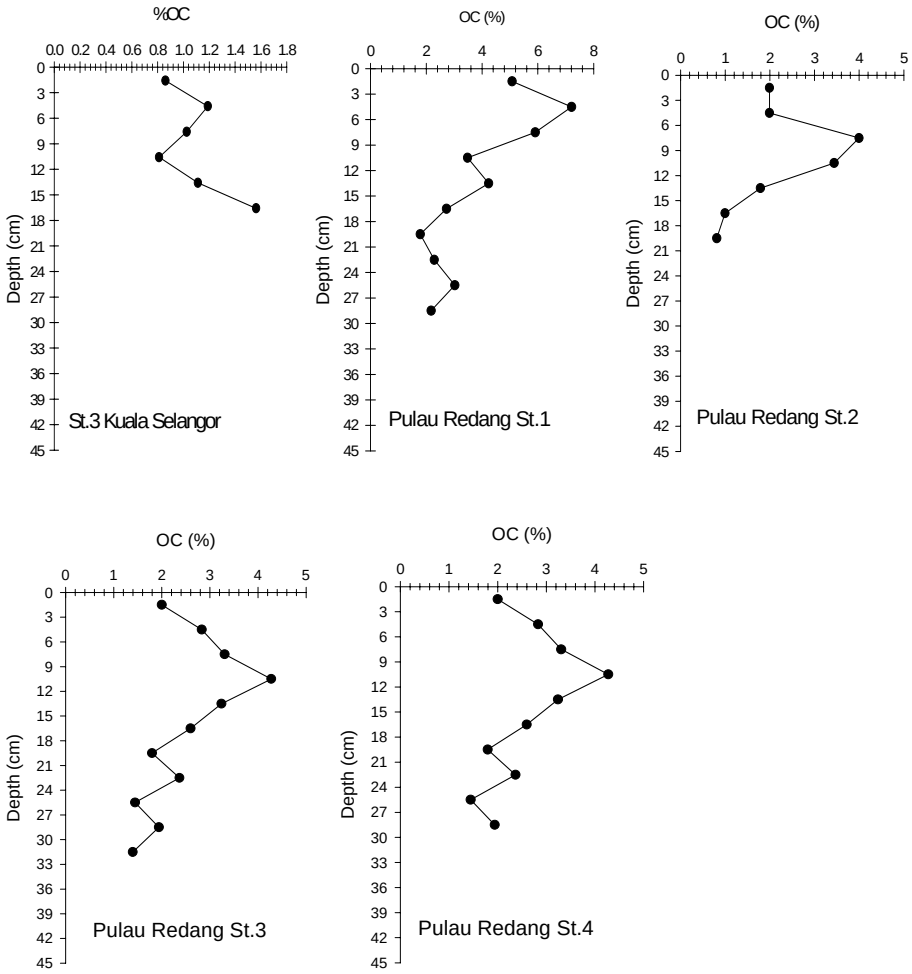

Figure 3. Concentration of organic carbon in the sediment cores obtained during this study

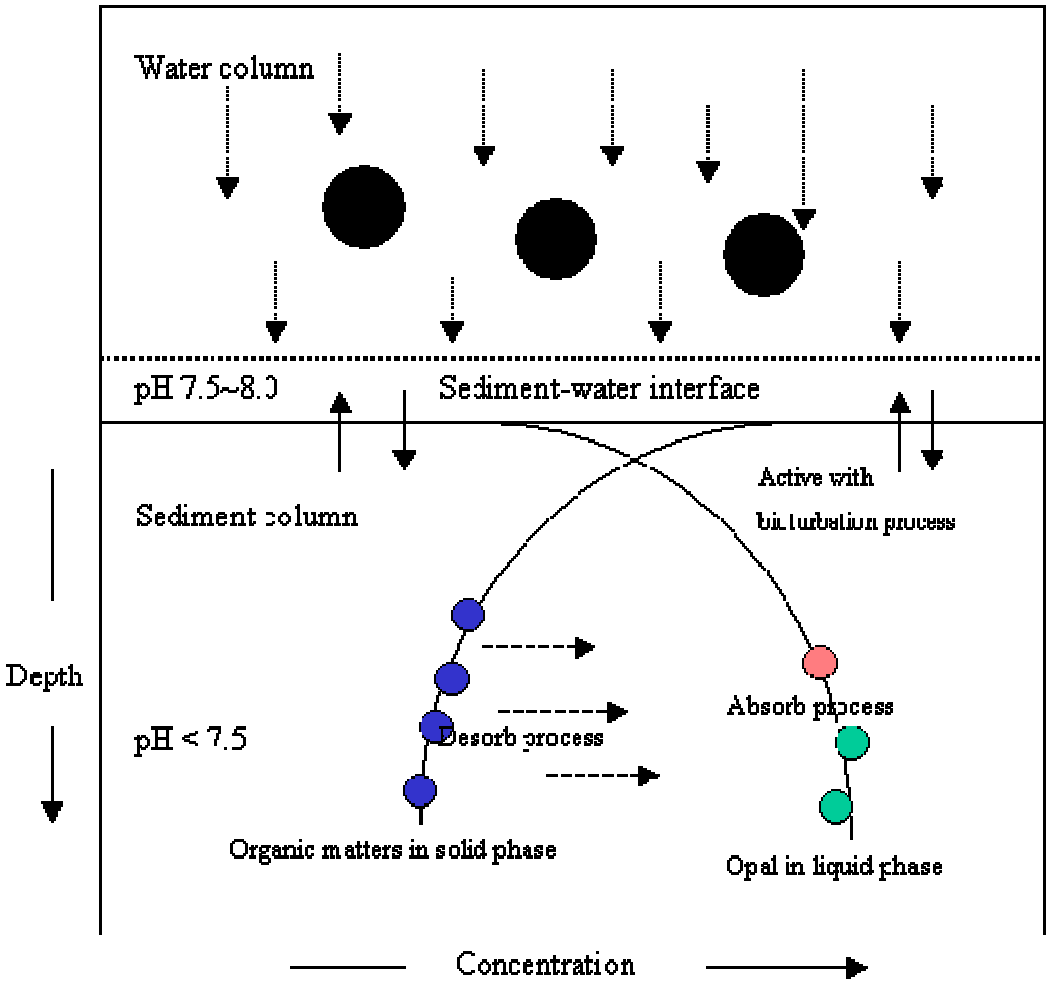

Figure 4. Model deposition and movement process of opal in sediment layer

Malaysian Journal of Analytical Sciences, Vol.9, No. 3(2005): 571 - 581

Composite PVC–Based Electrolytes for Rechargeable Lithium Battery

R.H.Y. Subban and A.H. Ahmad

Faculty of Applied Science, MARA University of Technology, 40450 Shah Alam, Selangor, Malaysia

Abstract

Composite polymer electrolyte films consisting of SiO_2 powders dispersed in poly(vinyl) chloride (PVC)-based electrolytes with $LiCF_3SO_3$ has been prepared and their ionic conductivities studied by impedance spectroscopy. Polymer electrolyte with composition 95 wt % (PVC-$LiCF_3SO_3$)-5 wt % SiO_2 has demonstrated ionic conductivities of 10^{-4} S cm^{-1} at room temperature. The addition of SiO_2 powders increased ionic conductivities due to an increase in the number of charge carriers. The increase in the number of charge carriers is accounted for by vibrational spectroscopy. In $LiCoO_2$/MCMB cells at 32 °C, these composite electrolytes demonstrated high discharge capacity of 118 mA h g^{-1}.

Keywords: PVC, composite polymer electrolyte, ionic conductivity, lithium rechargeable cells

Introduction

Composite polymer electrolytes formed by the incorporation of electrochemically inert inorganic fillers in polymer hosts such as PEO, PVC, PAN, etc. have ionic conductivities in the range between 10^{-5} and 10^{-2} S cm^{-1}. The higher conductivities were reported for composites based on the gel polymer electrolytes and zeolites.

The inorganic fillers used includes ZrO_2 [1], TiO_2 [2], Al_2O_3 [3, 4], γ-$LiAlO_2$ [5], $BaTiO_3$ [6], hydrobpobic fumed silica [7] and SiO_2 [8, 9]. Weston and Steele [10] first demonstrated the idea as a means to increase the mechanical stability of the polymer. It was found that composite formation not only increased the mechanical strength of the electrolyte, it also enhanced the ionic conductivities of the electrolytes leading to their use in lithium batteries [10-12].

Most PVC-based electrolytes reported in the literature are of the gel type and only a few batteries based on them have been reported [13-18]. Although PVC-based composite electrolytes

have been reported in the literature [1], to the best of our knowledge no battery results on PVC-based composite polymer electrolyte system has been reported.

The present paper reports a basic study on the characteristics and cycling performance of a $LiCoO_2$/PVC-$LiCF_3SO_3$-SiO_2/MCMB battery at room temperature for various load currents. Prior to fabricating the battery, the electrolyte was characterised by measuring its ionic conductivity.

Experimental

$LiCF_3SO_3$ and PVC were dissolved separately in tetrahydrofuran (THF) until complete dissolution has taken place. Appropriate amounts of the organic filler, SiO_2 were then added and stirred until the mixture appeared to be homogeneous. The mixture was then cast into different glass dishes and left to dry by evaporation at room temperature.

Electrolyte conductivities were determined from a.c impedance measurements using a computer controlled HIOKI LCR HI TESTER for frequencies ranging from 40 Hz to 1000 kHz. Vibrational spectroscopy were carried out by using FTIR Perkin Elmer Spectrophotometer at a resolution of 1 cm^{-1}.

Composite cathodes were prepared by adding appropriate masses of $LiCoO_2$, activated carbon and suitable resins to form homogeneous slurry by mixing them in a solvent. The slurry was cast onto aluminium grid for use as the cathode. In the case of the anode, a slurry mixture of mesocarbon microbeads (MCMB), activated carbon and suitable resins were prepared and this was casted onto copper grid.

The polymer electrolyte film with the highest room temperature conductivity was used as the separator for the fabrication of the lithium polymer secondary battery. The prepared

electrodes were cut into dimensions of 3.0 x 5.0 cm before stacking them together with the electrolyte in between. The whole set up was packed in an aluminium laminated packaging bag and sealed with a sealing machine in a glove box.

The battery $LiCoO_2$/PVC-$LiCF_3SO_3$-SiO_2/MCMB was subjected to conditioning for 1 cycle by charging it to 4.2 V and discharging it to 2.0 V. After conditioning, the battery was tested by measuring its rate discharge. The battery was charged at 150 mA until it reaches a voltage of 4.2V and then discharged at load currents of 150 mA, 50 mA, 100 mA and 200 mA until a cut-off voltage of 2.0 V. The conditioning and cycling tests were carried out using the battery cycler manufactured by Arbin.

Results and Discussion

The variation of ionic conductivity with SiO_2 content for the polymer electrolytes studied in this work is depicted in Fig. 1. The ionic conductivity was found to reach maximum at 2 wt % SiO_2 after which the conductivity decreases and increases again to reach another maximum at 5 wt % SiO_2. Beyond this concentration a further decrease in conductivity is observed. The plot shown in Fig. 1 is similar to the plot of conductivity-concentration reported by some researchers in the literature [19, 20]. This conductivity behaviour may be explained by the percolation theory [21, 22]. According to this theory, the PVC-$LiCF_3SO_3$-SiO_2 system is considered to be a two-phase system consisting of the ionic conduction phase and the filler phase. The boundary between these two phases (interfacial bonds) makes up the highly conducting bonds which serve as the conducting pathways. When the concentration of filler is small (Region I, Fig.1), there are few highly conducting bonds and so the conductivity is dominated by the normal conducting bonds. As the concentration of filler increases (= 2 wt. %), an infinite network of highly

conducting interfacial bond develops for the first time. This corresponds to the first percolation threshold causing the conductivity to rise. With increasing concentration, some of the existing highly conducting bonds get blocked due to conglomeration of the filler that reduces polymer-filler interface. This causes the conductivity to decrease (Region II). Further increase in concentration of filler causes the highly conducting bonds to increase so that conductivity is governed by the pathways formed by these bonds resulting in a second threshold (= 5 wt. %).

Beyond the second threshold (Region III), the conducting pathways become disrupted due to the blocking and the termination of the formation of the conducting pathways which results in the conductivity decreasing. It is believed that the first percolation threshold corresponding to the first conductivity maximum is due to the mobility of cations and the second percolation threshold corresponding to the second maximum is due to the mobility of the anions. The electrical conductivity of the PVC based polymer electrolyte was optimised for the sample with configuration: 95 wt. % (PVC-$LiCF_3SO_3$)-5 wt. % SiO_2 with a value of 1.15 x 10^{-4} Scm^{-1} which is suitable for battery application [23] and is comparable to the electrolytes used in many work for the fabrication of lithium polymer battery [17, 24-26].

The variation in ionic conductivity with concentration of SiO_2 is supported by FTIR studies. Fig. 2 shows the infra-red spectra of PVC-$LiCF_3SO_3$-SiO_2 samples in the vicinity of the SO_3 symmetric and antisymmetric stretching mode at 1033 and 1263 cm^{-1} respectively. It can be observed that the 1033 cm^{-1} band remains unshifted in the spectra of PVC-$LiCF_3SO_3$-SiO_2 samples; however its relative intensity changes with concentration of SiO_2. The relative intensity of this peak was found to be 33.4, 28.2, 30.4, 22.2 and 31.1 % for filler concentrations of 2, 4, 5, 6 and 8 wt. % respectively. Since the peak at 1033 cm^{-1} is assigned to free ions [27, 28], this means that there exists a concentration of free ions in the polymer system.

Initially, the increase in SiO_2 doping changes the conductivity sharply (Region I, Fig. 1). This is due to the increasing availability of mobile ions on doping with SiO_2. This is proven by FTIR studies where the changes in intensity of the band attributed to free ions at 1033 cm^{-1} was observed to increase to 33.4 % upon addition of 2 wt. % SiO_2. The decrease in conductivity with further increase in the SiO_2 concentration after the first maximum (Region II) could be attributed to ion association which reduces the number of free ions. This has been shown by the decrease in intensity of the band at 1033 cm^{-1} to 28.2 %. Ion association is attributed to the presence of the band at 1263 cm^{-1} which has shifted to 1260 cm^{-1} showing the presence of ion pairs [27, 28]. Beyond 4 wt% SiO_2 concentration, the increasing trend in conductivity could be due to redissociation of ion pairs. At high SiO_2 concentration, redissociation of ion pairs occur giving rise to a larger number of free ions. This is consistent with the increase in intensity of the band at 1033 cm^{-1} to 30.4 % when the concentration of SiO_2 reaches 5 wt. %. The decrease in conductivity after 5 wt. % SiO_2 composition may be explained on the basis that the free ions (redissociated) getting available in this region (Region III) are overcompensated by a decrease in the free mobile ions due to ion-pairing at high SiO_2 concentrations. This is consistent with the decrease in the intensity of the 1033 cm^{-1} band whose intensity decreases to 22.2 % when the concentration of SiO_2 reaches 6 wt%. Beyond 6 wt. % SiO_2 concentration, although the intensity of this band increases to 31.1 %, the conductivity decreases. The decrease could be attributed to the blocking effect due to the presence of a large number of ions.

The voltage profiles for the charge-discharge cycles of the $LiCoO_2$/PVC-$LiCF_3SO_3$-SiO_2/MCMB at room temperature for discharge currents of 150, 200, 100 and 50 mA is shown in Fig. 3. It can be observed that the voltage drop at the initial discharge is higher when the discharge current is increased while the discharge time increases as the discharge current

decreases. This means that the discharge capacity is higher at lower discharge currents. This is supported by the plots of discharge capacity versus cycle number as shown in Fig. 4. From the figure, the average discharge capacity at 50, 100, 150 and 200 mA was found to be 455, 382, 372 and 290 mAh respectively. It is also observed that the discharge capacity decreases as the cycle number increases. This is normal behaviour for Li ion battery and is caused by the higher degree of polarisation at the higher discharge current [29, 30].

Conclusion

Li^+-ion conducting PVC based composite polymer electrolyte with conductivity of 1.15 x 10^{-4} Scm^{-1} has been developed. The cycling of the $LiCoO_2$/PVC-$LiCF_3SO_3$-SiO_2/MCMB battery has demonstrated a room temperature capacity of 118 mAh/g at a discharge rate of 150 mA in the potential range 2.0 to 4.2 V.

Reference

[1] S. Rajendran and T. Uma, Materials Letters 44 (2000) 208
[2] B. Kumar, L.G. Scanlon and R.J. Spry, J. of Power Sources 96 (2001) 337
[3] P.A.R.D. Jayathilaka, M.A.K.L. Dissanayake, I. Albinsson and B.E. Mellander, Electrochim. Acta 47 (2002) 3257
[4] F. Croce, L. Persi, F. Ronci and B. Srosati, Solid State Ionics 135 (2000) 47
[5] F. Capuano, F. Croce and B. Srosati, J. Electrochem. Soc. 138 (1991) 1918
[6] Q. Li, H.Y. Sun, Y. Takeda, N. Imanishi, J. Yang and O. Yamamoto, J. of Power Sources 94 (2001) 201
[7] S.R. Raghavan and S.A. Khan, Electrochemical Society Proceedings Vol. 96-17 (1997) 74
[8] S.S. Sekhon and G.S. Sandhar, European Polym. Journal 34(1998) 435
[9] R.H.Y. Subban and A.K Arof, J. of New Materials for Electrochemical Systems 6 (2003) 197
[10] J.E. Weston and B.C.H. Steele, Solid State Ionics 7 (1987) 75
[11] F. Croce and B. Srosati, J. of Power sources 43 (1993) 9
[12] E. Peled, D. Golodnitsky, G. Ardel and V. Eshkenazy, Electrochim. Acta 40 (1995) 2197
[13] K.M. Abraham and M. Alamgir, Solid State Ionics 70/71 (1994) 20
[14] M. Alamgir and K.M. Abraham, J. of Power Sources 54 (1995) 40

[15] H.T, Kim, K.B. Kim, S.W. Kim and J.K. Park, Electrochim. Acta 45 (2000) 4001
[16] S. Ramesh and A.K. Arof, J. of Power Sources 4120 (2001) 1
[17] N.S. Choi and J.K. Park, Electrochim. Acta 46 (2001) 1453
[18] E.M. Shembel, O.V. Chervakov, L.I. Neduzhko, I.M. Maksyuta, Y.V. Plischuk, D.E. Reisner, P.Novak and D.Meshri, J of Power Sources 96 (2001) 20
[19] B.K. Choi and K.H. Shin, Solid State Ionics 86-88 (1996) 303
[20] N. Srivastava and S. Chandra, European Polymer Journal 36 (2000) 421
[21] J. Maeir, 'Heteregeneous solid electrolytes' in 'Superionic Solids and Solid Electrolytes', Academic Press Inc. 1989 137
[22] Bunde, A., Solid State Ionics 75 (1995) 147
[23] R. Koksbang, I.I. Olsen and D. Shackle, Solid State Ionics 69 (1994) 320
[24] N. Kamarulzaman, Z. Osman, M.R. Muhamad, Z.A. Ibrahim, A.K. Arof and N.S. Mohamed, J. of Power Sources 97-98 (2001) 722
[25] J.Cho and M. Liu, Electrochim. Acta 42 (1997) 1481
[26] S.Ramesh and A.K. Arof, J. of Power Sources 4120 (2001) 1
[27] W. Huang and R. Frech, Polymer 35 (1994), 235
[28] D.R. MacFarlane, P. Meakin, A. Bishop, D. McNaughton, J.M. Rosalie and M. Forsyth, Electrochim. Acta 40 (1995) 2333
[29] H.T, Kim, K.B. Kim, S.W. Kim and J.K. Park, Electrochim. Acta 45 (2000) 4001
[30] D.W. Kim and Y.K. Sun, J. Electrochem. Soc. 145 (1998) 1958

Figure Captions

Fig. 1: Effect of SiO_2 concentration on the ionic conductivity of PVC-$LiCF_3SO_3$- SiO_2 systems

Fig. 2: FTIR spectra of (a) $LiCF_3SO_3$ (b) PVC (c) SiO_2 (d) (PVC-$LiCF_3SO_3$)-SiO_2 (98 wt%-2 wt %) (e) (PVC-$LiCF_3SO_3$)-SiO_2 (96 wt%-4 wt %) (f) (PVC-$LiCF_3SO_3$)-SiO_2 (95 wt%-5 wt %) (g) (PVC-$LiCF_3SO_3$)-SiO_2 (94 wt%-6 wt %) (h) (PVC-$LiCF_3SO_3$)-SiO_2 (92 wt%-8 wt %) in the 1000-1450 cm^{-1} spectral region

Fig. 3: Discharge characteristics of the $LiCoO_2$/PVC-$LiCF_3SO_3$-SiO_2/MCMB cell at 50 mA, 100 mA, 150 mA and 200 mA.

Fig. 4: Discharge capacity as a function of cycle number for $LiCoO_2$/PVC-$LiCF_3SO_3$ SiO_2/MCMB cell discharged at (a) 50 mA (b) 100 mA (c) 150 mA and (d) 200 mA.

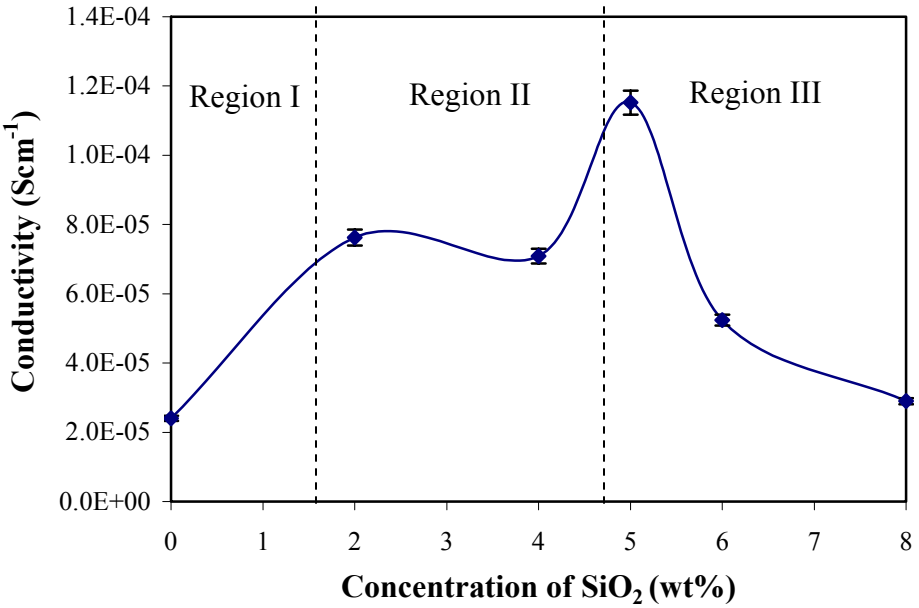
1.4E-04
1.2E-04
1.0E-04
8.0E-05
6.0E-05
4.0E-05
2.0E-05
0.0E+00
Conductivity (Scm-1)
Region I
Region II
Region III
0
1
2
3
4
5
6
7
8
Concentration of SiO2 (wt%)

Fig. 1

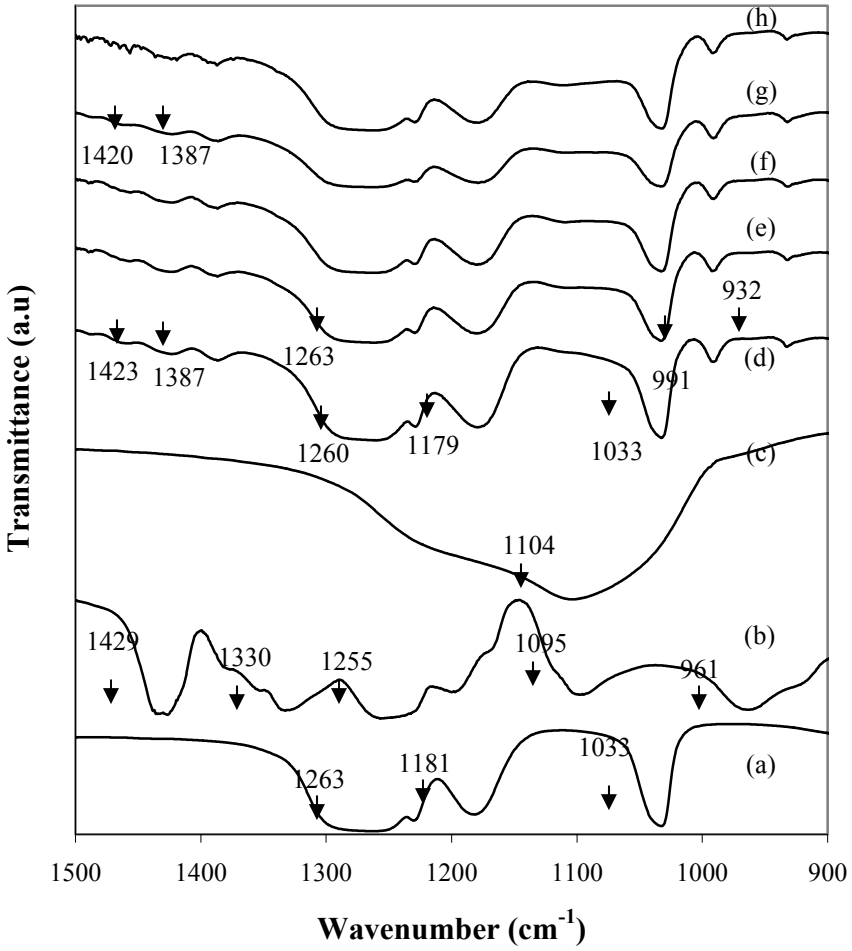
(h)
(g)
1420
1387
(f)
(e)
932
1423
1387
1263
991
(d)
1260
1179
1033
(c)
1104
1429
1330
1255
1095
961
(b)
1263
1181
1033
(a)
Transmittance (a.u)
1500
1400
1300
1200
1100
1000
900
Wavenumber (cm-1)

Fig. 2

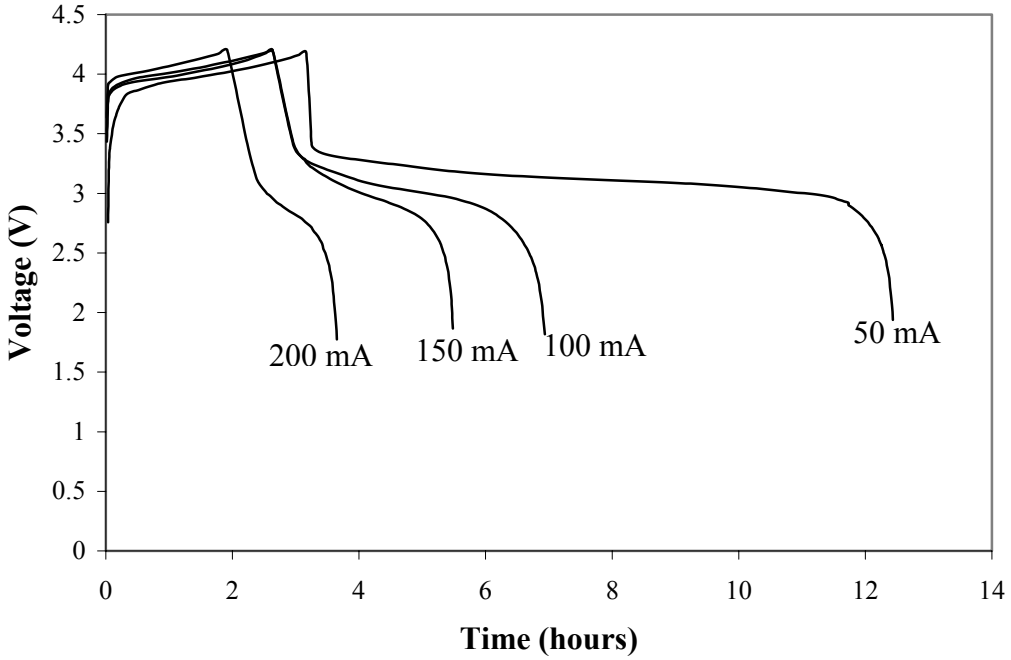
Voltage (V)
Time (hours)
200 mA
150 mA
100 mA
50 mA

Fig. 3

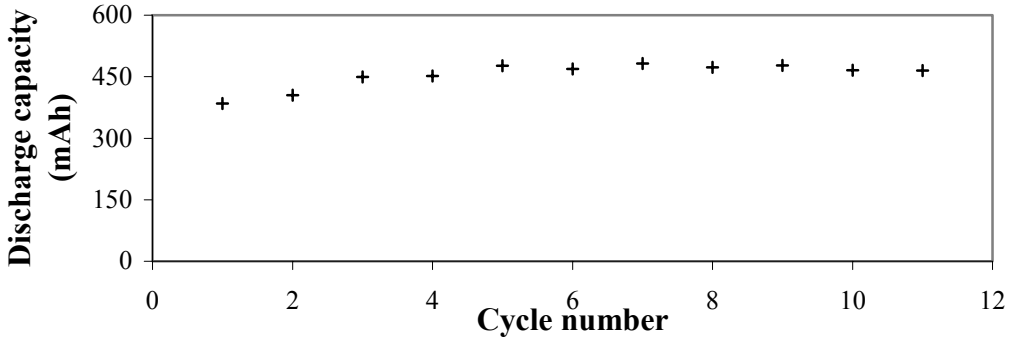
Discharge capacity (mAh)
Cycle number

(a)

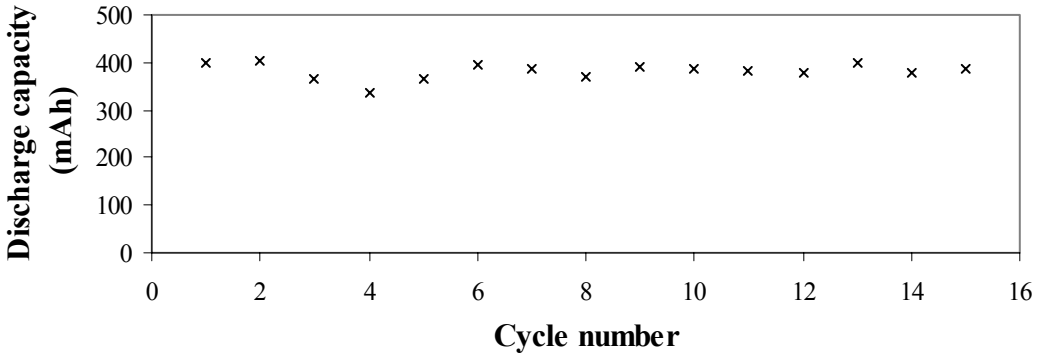
Discharge capacity (mAh)
500
400
300
200
100
0
0
2
4
6
8
10
12
14
16
Cycle number

(b)

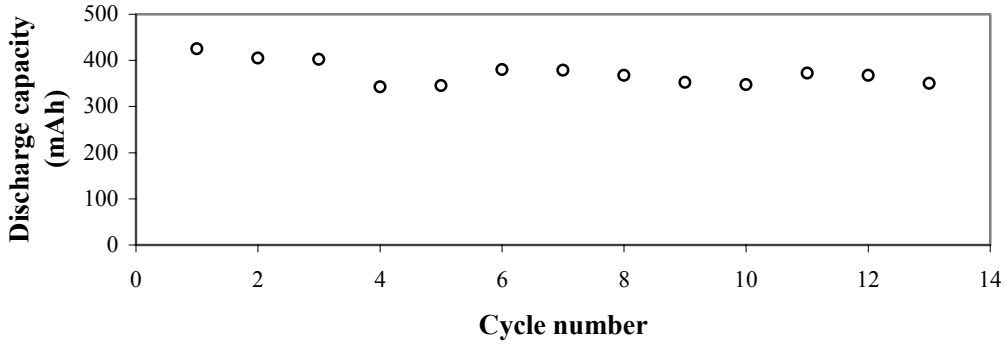
Discharge capacity (mAh)
500
400
300
200
100
0
0
2
4
6
8
10
12
14
Cycle number

(c)

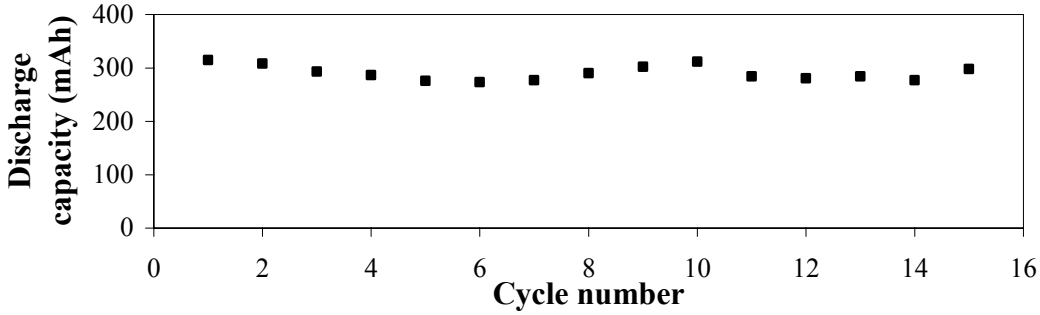
Discharge capacity (mAh)
400
300
200
100
0
0
2
4
6
8
10
12
14
16
Cycle number

(d)

Fig. 4

Malaysian Journal of Analytical Sciences, Vol.9, No. 3(2005): 582 - 585

Solid-phase Extraction (SPE) of Sterols from Water

Dayang Ratena Sari Abg Spian, Nor'ashikin Saim and Rozita Osman

Fakulti Sains Gunaan, Universiti Teknology MARA 40000 Shah Alam Selangor

Abstract

Extraction and preconcentration method for the analysis of cholesterol, coprostanol, and stigmasterol in water sample by solid-phase extraction (SPE) was developed. To establish the suitable extraction conditions, several types of absorbents and eluting solvents for the extraction were evaluated. Recoveries ranging from 99% - 103% were obtained by extraction using SPE C_{18} with methanol:dichloromethane (90:10 v/v) as eluent and pH of sample adjusted to 2. The extracted sterols were derivatised using bis(trimethylsilyl)trifluoroacetamide (1% TMCS) and quantitation were performed using gas chromatography with flame ionization detector (GC-FID).

Keywords: solid-phase extraction, fecal sterols

1.0 INTRODUCTION

Solid-phase extraction (SPE) is an active area of research since this technique has several advantages over the conventional liquid-liquid extraction in terms of its simplicity, reliability and selectivity [1]. Method development in SPE, which involves choosing a suitable sorbent and eluent, is the key factor in SPE technique. The selectivity of SPE depends not only on the properties of the analytes of interest but also on the choice of sorbents and eluting solvents [2-3]. In this study, the suitability of several sorbents, eluents as well as the necessity to adjust the pH of the sample were studied for the analysis of sterols in water.

2.0 MATERIAL AND METHODS

All solvents were of high purity (pesticide grade or HPLC grade). SPE cartridges (C_{18}, C_8 and EVT) were supplied by Jones Chromatography. Individual sterol standards and internal standard (5-α cholestane) were supplied by Sigma-Aldrich Co, USA.

Spiked sample

Spiked water sample was prepared at concentration levels of 6 and 10 ppm. Adjustment of pH of was achieved using HCl.

SPE procedure

SPE cartridges were conditioned with 5 mL of methanol followed by ultrapure water (3 mL x 5 mL) at the rate of 1-2mL/min. Water sample (250 mL) was loaded into the SPE cartridge and cartridges were then dried under vacuum for 30 min. The sterols were eluted from using 5 mL of solvent. The extract was blown down to 1 mL under a gentle flow of nitrogen and derivatized using 100 µL of BSTFA (1% TMCS) at 60^{o}C for 1 hour. Internal standard (5 ppm) was added to the sterol esters and the volume was again reduced to 1 mL under nitrogen prior to GC analysis.

GC-FID Analysis

Gas chromatographic separation and identification of the sterols was performed on an Agilent Technologies 6890N with flame ionization detector (GC-FID). A 25 m x 0.25 mm (i.d) x 0.25 µm film thickness fused silica capillary column HP-5 MS (Agilent Technologies) was used to achieve separation with the following temperature program: initial column temperature, 227 ^{o}C; hold for 2; increase at 8 ^{o}C/min to 305 ^{o}C; hold for 13 min. The detector temperature was set at 290 ^{o}C. Figure 1 shows the chromatogram of sterols after SPE extraction.

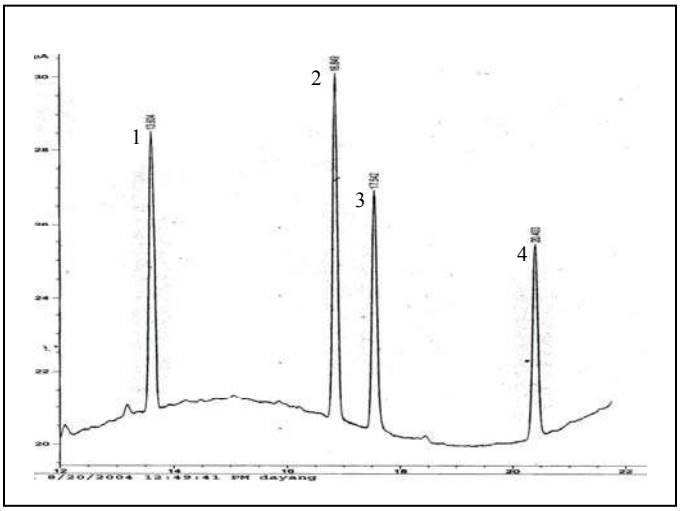

Figure 1. GC/FID chromatogram of sterols after SPE extraction. Peaks: 1. Internal standard (5α- Cholestane); 2. Coprostanol; 3. Cholesterol; 4. Stigmasterol.

3.0 RESULTS AND DISCUSSION

Recovery studies were performed by extracting three sterols, cholesterol, coprostanol and stigmasterol from 250 mL spiked sample of concentration 10.0 ppm. Initial studies done in comparing the efficiencies of two non-polar SPE cartridges, C_{18} and C_8 using several eluting solvents showed that in most cases, the use of C_8 sorbent resulted in low recoveries. Therefore, further investigations on the suitability of eluting solvents/solvent mixtures (methanol, dichloromethane and t-butyl methyl ether) were carried out using C_{18} cartridges (500 mg and 1000mg). It was found that only 75% of sterols were recovered using 500 mg C_{18} cartridge and a significant change in recoveries were observed using 1000 mg C_{18}. Recoveries increased to 99% for stigmasterol and up to 103% for cholesterol and coprostanol. Figure 2 shows the recoveries of sterols using SPE C_{18} cartridge under several selected conditions.

The choice of solvent is a crucial factor in solid phase extraction. The selection of solvent depends on the solubility of analytes. The solvent used must not too strong or too weak for elution step. It was found that a solvent mixture of methanol and dichloromethane of ratio ranged from 90:10 (v/v) to 70:30 (v/v) resulted in higher recoveries compared to other solvent/solvent mixtures. There were no significant differences in the recoveries of sterols using these solvent ratios. A mixture of methanol and dichloromethane (90:10 v/v) was chosen because of better precision.

In SPE, it may be necessary to adjust the pH of the sample to ensure that the analyte is in the appropriate form to achieve the efficient retention by the solid phase [4]. Recommended pH values are between 2 and 8 as extreme pH values can change the nature of the bonded phases. In this study, pH of sample significantly affects the efficiency of C_{18} sorbent. Recoveries increased from 30%-60% to more than 70% with pH of sample adjusted to 2.

Based on this study, 1000 mg C_{18} sorbent can efficiently extract sterols in water using mixture of methanol and dichloromethane (90:10 v/v) as eluent with pH of the sample adjusted to 2.

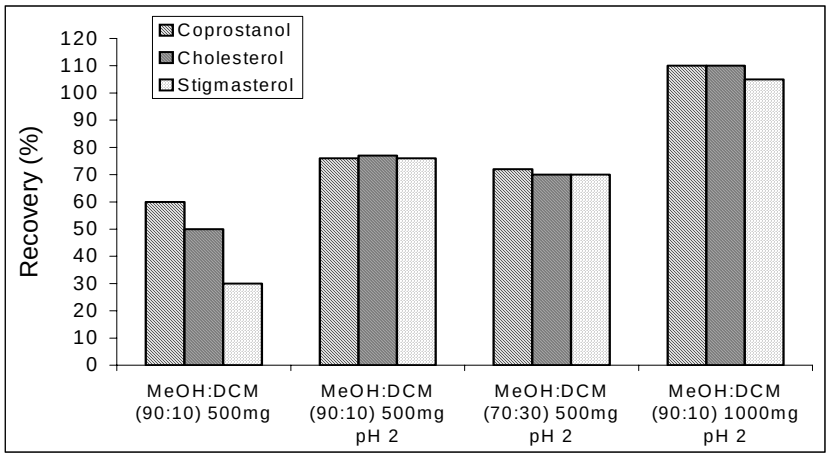

Figure 2. Recoveries of sterols using SPE C_{18} cartridge under various conditions

The optimum SPE conditions were used in extracting sterols at 2 levels of concentrations, 6 ppm and 10 ppm. As shown in Table 1, excellent recoveries with result ranging from 99%-103% were obtained.

Table 1. Recovery of sterols extracted using 1000 mg C_{18} and mixture of methanol and dichloromethane (90:10 v/v) as eluent with pH of the sample adjusted to 2.

Concentration of spiked sample	Sterol	Recovery (%)
6 ppm	Cholesterol	101.7 ± 3.0
	Coprostanol	100.0 ± 6.6
	Stigmasterol	101.7 ± 8.3
10 ppm	Cholesterol	98.7 ± 2.1
	Coprostanol	103.0 ± 6.0
	Stigmasterol	103.0 ± 6.0

The precision of the developed SPE method was established by repeated determinations (n=3) using contaminated water samples. The use of 1000 mg C_{18} SPE cartridge allowed a good repeatability as shown in Table 2.

Table 2. Analysis of sterols in contaminated samples

	Sample 1	Sample 2	Sample 3	Sample 4	Sample 5
Total sterols (ppm)	106.4 ± 0.04	133.7 ± 0.04	160.2 ± 0.04	198.9 ± 0.04	226.8 ± 0.04

The developed SPE technique was compared to liquid-liquid extraction technique in the extraction of 10 ppm spiked sample. As shown in Table 3, the two methods gave comparable results.

Table 3. Recovery of sterols using SPE and Liquid-Liquid Extraction

Sterol	Recovery (%)	
	SPE	Liquid-liquid extraction
Cholesterol	98.7 ± 2.1	100.5 ± 1.6
Coprostanol	103.0 ± 6.0	104 ± 6.1
Stigmasterol	103.0 ± 6.0	103.2 ± 3.0

4.0 CONCLUSION

On the basis of the obtained results, SPE method with C_{18} 1000 mg cartridge with methanol:dichloromethane (90:10 v/v) as eluent and sample pH adjusted to 2 is an effective method for the extraction of sterols in water.

ACKNOWLEDGEMENT
We would like to thank MOSTE for funding this project (IRPA Project number: 09–02–01–0002-EA002).

REFERENCES

1. Fritz, J.S, Dumont, P.J. and Schmidt, L.W. (1995) *J. Chromatography A*, 691, 133-140.
2. Weigel, S., Kallenborn, R. and Hühnerfuss, H. (2004) *J. Chromatography A*, 1023, 183-195.
3. Liu, R., Zhou, J.L. and Wilding, A. (2004) *J. Chromatography A*, 1022, 179-189.
4. Font, G., Manes, J. Molto, J.C. and Pico, Y. (1993) *J. Chromatography*, 642, 135-161.

Malaysian Journal of Analytical Sciences, Vol.9, No. 3(2005): 586 - 588

KAJIAN HUBUNGAN KUANTITATIF STRUKTUR-AKTIVITI (QSAR) KETOKSIKAN SEBATIAN TERBITAN BENZENA

Mohd Zuli Jaafar[1], Mohamed Noor Hasan[2]

[1] *Universiti Teknologi MARA, mohdzuli@nsembilan.uitm.edu.my*
[2] *Universiti Teknologi Malaysia, mnoor@kimia.fs.utm.my*

Abstract

Hubungan kuantitatif struktur-aktiviti (*quantitative structure-activity relationships*, QSAR) bagi suatu set sebatian kimia daripada deskriptor adalah penting untuk mendapatkan korelasi aktiviti biologi dan sifat fizikokimia. Aktiviti biologi sesuatu sebatian kimia termasuklah ketoksikan kepada manusia dan persekitaran terutamanya hidupan air. Menerusi kajian ini, hubungan struktur-aktiviti (*structure-activity relationships*, SAR) bagi sebatian terbitan benzena dengan ketoksikan terhadap sejenis alga hijau *Scenedesmus obliquus* dan ikan *Pimephales promelas* telah ditentukan. Kemajuan dalam kaedah pengkomputeran dan kimia digunakan untuk menjana deskriptor molekul yang mengambil kira kesan sterik, elektronik dan termodinamik. Deskriptor tersebut menjadi pemboleh ubah tidak bersandar untuk membina model ramalan ketoksikan melalui kaedah regresi multivariat seperti regresi linear berganda (*multiple linear regression*, MLR) dan regresi kuasa dua terkecil separa (*partial least square regression*, PLS).

Key words: Quantitative structure-activity relationship, descriptor, Multivariate Linear regression, Partial Least Square Regression

Pengenalan

Kemajuan perindustrian menyebabkan sejumlah besar bahan kimia digunakan dan memasuki kitaran hidup manusia. Setiap tahun berjuta tan bahan kimia dihasilkan untuk tujuan industri dan bilangan bahan kimia baru yang disintesis semakin bertambah. Terdapat lebih 11 juta bahan kimia yang diketahui dan lebih 700,000 bahan kimia baru dilaporkan setiap tahun [1]. Menurut laporan Agensi Pengawalan Alam Sekitar Amerika Syarikat (*United States Environmental Protection Agency*, USEPA), terdapat lebih 2800 bahan kimia yang dihasilkan dalam jumlah yang tinggi (*High Production Volume Chemicals*, HPVC) [2]. HPVC yang banyak menjadi penyumbang pencemaran alam sekitar terutama ketoksikan kepada hidupan akuatik dan seterusnya kepada manusia melalui kitaran makanan. Menyedari hakikat ini, satu kaedah penilaian ke atas ketoksikan perlu dibuat ke atas bahan kimia terbitan benzena yang banyak dan memahami aktiviti molekul berdasarkan struktur molekul tersebut yang menyebabkan ketoksikan.

Hansch *et.al.* adalah antara penyelidik yang mula-mula menjalankan eksperimen yang memperlihatkan korelasi yang baik antara aktiviti biologi dengan stuktur molekul bahan kimia pada tahun 1960an [3, 4]. Eksperimen mereka berjaya menunjukkan korelasi antara sifat-sifat fizikokimia dengan stuktur molekul menggunakan kaedah regresi linear. Persamaan yang memberikan korelasi tersebut pada masa ini lebih dikenali sebagai persamaan hubungan kuantitatif struktur aktiviti (*quantitative structure-activity relationships*, QSAR). Pada masa ini antara 15 hingga 20 ribu aktiviti bahan kimia yang dikaji melalui QSAR telah diterbitkan, sementara itu terdapat lebih 6000 persamaan biologi QSAR telah dibangunkan [1]. QSAR adalah dilihat sebagai satu cabang yang penting dalam bidang Kimometrik. Melalui QSAR, pemahaman kepada beberapa tindak balas kimia dan aktiviti molekul boleh dicapai.

Contoh penggunaan QSAR dalam bidang farmasi iaitu untuk meramalkan tindakan sesuatu bahan kimia ke atas manusia dan bagaimana mod tindakan boleh dikenalpasti termasuk atom yang bertanggung jawab kepada aktiviti molekul ke atas penilaian risiko kanser [5].

Kaedah

Data ketoksikan iaitu aktiviti molekul yang digunakan dalam kajian ini diambil dari beberapa sumber. Set data yang pertama terdiri daripada ketoksikan bagi 40 sebatian terbitan benzena terhadap sejenis alga hijau *Scenedesmus obliquus* menurut eksperimen yang dijalankan oleh Lu *et.al*. [6]. Prinsip kaedah ujian adalah mengenai bagaimana pertumbuhan secara eksponen alga dipengaruhi oleh kepekatan bahan kimia yang tertentu di bawah keadaan eksperimen yang ditetapkan. Unit ketoksikan adalah $\log(1/EC_{50})$ dengan kepekatan dalam mol/L.

Set data yang kedua pula ialah ketoksikan bagi 69 sebatian benzena dan terbitannya terhadap sejenis ikan *Pimephales promelas* yang dilaporkan oleh Hall *et.al.* [7] dengan unit ketoksikan adalah $\log(1/LC_{50})$. Dua set data ini dipilih kerana sebatian benzena dan terbitannya digunakan bersesuaian dengan matlamat kajian mendapatkan model bagi sebatian terbitan benzena. Kumpulan penukarganti dalam data tersebut adalah amino, bromo, kloro, hidroksil, metil, metoksi dan nitro. Kaedah pembangunana model ramalan terdapat pada rajah 2.1 berikut.

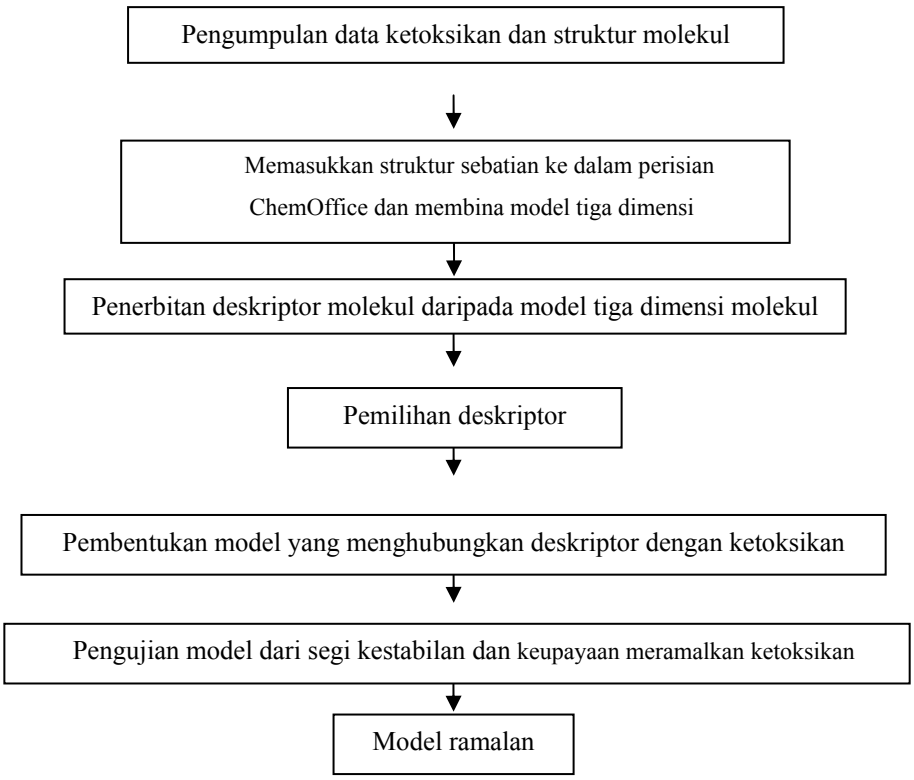

Rajah 2.1: Kaedah mendapatkan model ramalan QSAR

Keputusan dan Perbincangan

Pendekatan QSAR yang telah digunakan dalam kajian ini berjaya membangunkan model yang baik bagi ketoksikan sebatian terbitan benzena terhadap alga hijau *Scedesmus obliquus* dan ikan *Pimephales promelas*. Sementara itu, kaedah pemilihan deskriptor oleh GA memberikan pemboleh ubah yang baik untuk membangunkan model regresi MLR dan PLS. Deskriptor yang digunakan dalam pembinaan model MLR dan PLS ditunjukkan dalam Jadual 4.1.

Jadual 4.1: Deskriptor model MLR dan PLS

Data	Deskriptor	Regresi	Kaedah
Lu	ElcE, Mass dan MR	MLR	Langkah demi langkah,
	ElcE, Lumo, ClogP, SEV, Mass	MLR	GA,
	ElcE, Lumo, Mass dan MW	PLS	GA
Hall	Esb, ElcE, Mass, MW, dan E	MLR	Langkah demi langkah
	ElcE, Lumo, Eb, Ev, Esb, MR, ClogP, SAS, MW, Ovality	MLR	GA
	Lumo, NRE, TotE, Ev, Es, Et, E, MR, SAS, SEV, Ovality	PLS	GA

Penghargaan

Penghargaan ikhlas kepada penyelia tesis, Prof. Madya Dr. Mohamed Noor Hasan atas bimbingan dan nasihat yang diberikan sehingga penyelidikan ini sempurna. Terima kasih yang tidak terhingga atas kerjasama daripada semua pihak di Jabatan Kimia, Fakulti Sains, Universiti Teknologi Malaysia terutamanya Prof. Madya Dr. Umi Kalthom Ahmad dan En. Ibrahim Tintom. Terima kasih juga kepada pihak Universiti Teknologi MARA yang membiaya geran penyelidikan ini.

Rujukan

1. Hansch, C., Hoekman, D., Leo, A., Zhang, L. and Li, P. (1995). "The expanding role of quantitative structure-activity relationship (QSAR) in toxicology." *Toxicology Letters*. **79**. 45-53.
2. Gute, B.D. and Basak, S.C. (2001). "Molecular similarity-based estimation of properties: a comparison of three structure spaces." *Journal of Molecular Graphics and Modelling*. **20**. 95-109.
3. Hansch, C., Maloney, P.P., Fujita, T., Muir, R., (1962). "Correlation of biological activity of phenoxyacetic acids with Hammet substituent constants and partition coefficients," Nature (London) **194**.178-180
4. Hansch, C.and Fujita, T. (1964). "ρ-σ-π Analysis. A methods for the correlation of biological activity and chemical structure." *Journal of American Chemical Society*. **86**. 1616-1626.
5. Andersen, M.E. (1995). "Development of physiologically based pharmacokinetic and physiologically based pharmacodynamic models for applications in toxicology and risk assessment." *Toxicology Letters*. **79**. 35-44.
6. Lu, G.H., Yuan, X., Zhao, H.Y., (2001). "QSAR study on the toxicity of substituted benzenes to the algae (*Scenedesmns obliquus*)." *Chemosphore*. **44**. 437-440.
7. Basak S.C, Gute B.D, Lucic B., Nikolic S, Trinajstic N. (2000). "A comparative QSAR study of benzamidines complement–inhibitory activity and benzene derivatives acute toxicity." *Computers and Chemistry*. **24**. 181–191.